USING GROUND-FAILURE FEATURES FOR PALEOSEISMIC ANALYSIS

Stephen F. Obermeier and Randall W. Jibson, editors

USING LIQUEFACTION-INDUCED FEATURES FOR PALEOSEISMIC ANALYSIS

Chapter A, by Stephen F. Obermeier

USING LANDSLIDES FOR PALEOSEISMIC ANALYSIS

Chapter B, by Randall W. Jibson

U.S. Geological Survey Open-File Report 94-663

ACKNOWLEDGMENT

Funding for much of the research required for this report was provided by the Earthquake Hazards and Landslide Hazards Programs of the U. S. Geological Survey, as well as by grants from the U. S. Nuclear Regulatory Commission.

The Charter A manuscript recieved constructive reviews from John Sims, Alan Nelson, Tom Holzer, Randall Jibson, and Eugene Schweig of the U. S. Geological Survey, from T. Leslie Youd of Brigham Young University, and from Martitia Tuttle of the University of Maryland. Chapter B recieved helpful reviews from Robert Schuster of the U. S. Geological Survey, and from Jim McCalpin of GEO-HAZ, Inc.

PREFACE

Faults are not exposed at the ground surface or are unavailable for study in many tectonic environments. Therefore other types of geologic evidence are required to reconstruct the prehistoric seismic record of an area. Seismic shaking can produce many different types of ground deformation that can be preserved in the geologic record. Many of the types are discussed in the two papers following, but the papers focus primarily on (1) seismically induced liquefaction features and (2) landslides that move as coherent blocks (slumps and block slides) during seismic shaking. Analysis of both liquefaction-induced features and coherent landslides permits quantitative estimation of levels of prehistoric shaking in many field situations. Most other types of deformations permit only crude estimates of shaking levels.

Liquefaction-induced features such as sand-filled fissures are also important because they form only in fairly high levels of seismic shaking: the minimum moment magnitude is about 5.5-6.0 in most geologic environments. Presence of the sand-filled fissures indicates earthquakes that would have damaged built structures. For landslides, the minimum magnitude is somewhat smaller, about 4.5-5.0 for many types of landslides.

Proving a seismic origin for liquefaction-induced features is not very difficult in many geologic environments, particularly where past seismic shaking has been very strong. Independent lines of evidence generally are not required for a definitive assessment of origin. Demonstrating a seismic origin generally involves excluding only a few possible alternate sources for fluidizing sediments, and criteria for doing so have been developed that can be applied to many field situations. Determining a seismic origin for landslides is much more difficult because of the broader range of conditions that can lead to slope failure. Thus, for landslides, multiple, independent lines of evidence of seismic origin generally are required.

Paleoseismic ground-failure studies differ fundamentally from paleoseismic fault studies. Whereas fault studies seek to characterize the movement history of a specific fault, ground-failure studies characterize the shaking history of a site or region irrespective of the earthquake source. In regions that contain multiple seismic sources and in regions where faults cannot be studied in detail, which are the norm, paleoseismic ground-failure studies can be particularly valuable tools in hazard and risk assessments.

The approaches discussed in these two papers have evolved largely within the past 10 years. The techniques have already been instrumental in greatly advancing the status of knowledge about prehistoric seismicity in diverse regions and geologic settings. In addition, the techniques permit estimation of prehistoric levels of shaking and earthquake magnitude in some cases, which can make the techniques at least as useful as fault studies for gleaning information about paleoseismicity.

Stephen F. Obermeier and Randall W. Jibson, editors

CHAPTER A

USING LIQUEFACTION-INDUCED FEATURES FOR PALEOSEISMIC ANALYSIS

STEPHEN F. OBERMEIER

U. S. GEOLOGICAL SURVEY

OPEN-FILE REPORT 94-663

CHAPTER A CONTENTS

CHAPTER A

USING LIQUEFACTION-INDUCED FEATURES FOR PALEOSEISMIC ANALYSIS

STEPHEN F. OBERMEIER

U. S. Geological Survey
922 National Center
Reston, Virginia, 22092

ABSTRACT

Liquefaction features can be used in many field settings to estimate the recurrence interval and magnitude of strong earthquakes through much of the Holocene. The relatively high shaking level required for their formation makes them particularly valuable as records of strong paleo-earthquakes.

This state-of-the-art summary for interpretation and analysis of liquefaction effects takes into account input from both geologic and geotechnical engineering perspectives. Discussed are an overview of the processes involved in formation of the features, criteria for determining whether sediments have been deformed by seismically induced liquefaction, case studies in various geologic settings, and description of the methods for estimating magnitude of prehistoric earthquakes. Also discussed are some types of sediment deformations that can be misinterpreted as having a seismic origin.

1. INTRODUCTION

This text focuses on the methodology for determining whether observed sediment deformation had a seismic shaking origin or a nonseismic origin. Emphasis is placed on the process of liquefaction, which is the transformation of a granular material from a solid state into a liquefied state as a consequence of increased pore-water pressures (Youd, 1973). The discussion encompasses various manifestations of liquefaction-induced deformation in fluvial and nearshore-marine deposits, and the application of criteria for establishing an earthquake origin.

The systematic study of paleoliquefaction is a young discipline. Accordingly, some of the physical parameters that control effects of liquefaction in the field are not completely understood. Still, the principles and methodology for conducting paleoliquefaction studies are sufficiently advanced to warrant their routine application in paleoseismic studies. The method in this text for conducting paleoliquefaction studies was developed largely out of necessity in the United States, where the historic seismic record is particularly short.

Paleoliquefaction studies are useful to engineers and planners because of the high shaking threshold required to develop liquefaction features. The threshold is a horizontal acceleration on the order of 0.1 g for strong earthquakes, even in highly susceptible sediment (National Research Council, 1985, p. 34; Ishihara, 1985, p. 352). Worldwide data on

historical earthquakes show that features having a liquefaction origin can be developed at earthquake magnitudes as low as about 5, but that a magnitude of about 5.5 to 6 is the lower limit at which liquefaction effects become relatively common (Ambraseys, 1988). (Earthquake magnitude, M, is used rather loosely as either moment magnitude or surface-wave magnitude, whichever is larger.)

Liquefaction has been severe and widespread in many worldwide earthquakes. Effects of liquefaction have many manifestations. Some noteworthy reports discuss the effects in the region of the 1811-12 New Madrid, Missouri, earthquakes (Fuller, 1912), in the region of the 1886 Charleston, South Carolina, earthquake (Dutton, 1889), in northern California (Youd and Hoose, 1978), in the vicinity of the 1964 Alaska earthquake (U.S. Geological Survey Prof. Papers 542 through 545), various earthquakes in Japan (O'Rourke and Hamada, 1989), and the earthquake of 1897 in India (Oldham, 1899). Only exceptionally are the deformational effects of liquefaction illustrated and discussed in vertical section, as in this chapter, which is the view most useful for paleoliquefaction studies. Noteworthy accounts of the vertical view are reported by Amick et al. (1990), Audemard and de Santis (1991), Clague et al. (1992), Tuttle and Seeber (1991), Tuttle et al. (in press), Sims and Garvin (in press), Sieh (1978), and Wesnousky and Leffler (1992). Findings of exceptional interest in these reports are discussed herein where appropriate. The principal basis for this text is the author's observations of liquefaction effects at widely diverse geologic and geographic settings.

The liquefaction effects described in this text are caused mainly by cyclic shaking of level or nearly level ground. Primary seismological factors contributing to liquefaction are the amplitude of the cyclic shear stresses and the number of applications of the shear stresses (Seed, 1979). These factors, respectively, are related to field conditions of shaking amplitude (that is, peak acceleration) and duration of strong shaking. Both peak acceleration and duration generally correlate with the earthquake magnitude. Analytical engineering methods for evaluating variable and irregular cyclic stress applications typical of real earthquakes are well developed and yield results acceptable for engineering analysis (Seed et al., 1983), providing that shaking amplitude-time records can be reasonably bracketed. In the text there is a brief discussion of how to set limits for the strength of prehistoric shaking.

Pseudonodules and other such features caused by the plastic deformation or flowage of very soft muds and freshly deposited cohesionless sediments (often referred to as 'syndepositional features' or 'soft-sediment deformations') are discussed briefly. Liquefaction is not required to deform muds and extremely loose, freshly deposited cohesionless sediments, although a high pore-water pressure can be involved. The geologic literature is replete with articles attributing an earthquake origin to deformed muds and convoluted sands. It must be kept in mind, however, that very weak sediments also are commonly deformed as a result of other geologic processes such as loading during rapid sedimentation, localized artesian conditions, or slumping. In addition, soft-sediment deformations often form at such low levels of seismic shaking that the shaking poses no hazard. Thus the usefulness of these features for hazard assessment normally is more limited, and interpretations of origin often are equivocal. Interpretation of the origin of suspected liquefaction features usually is much more straightforward and reliable than for soft-sediment deformations. Still, in field situations where it can be proven that the soft-sediment structures formed synchronously at widespread locations, an earthquake origin can sometimes be attributed. An exemplary study

by Ringrose (1989) made use of soft-sediment deformations scattered throughout a large glacial lake.

This text also contains discussion of features formed by chemical weathering and of features deformed by a periglacial environment, but which mimic those of earthquake origin. Tests are suggested for interpretation of origin.

2. OVERVIEW OF THE FORMATION OF LIQUEFACTION-INDUCED FEATURES

It is the application of shear stresses that causes a buildup of pore-water pressure, which in turn leads to liquefaction of saturated cohesionless sediment. For seismically induced liquefaction, these shear stresses are due primarily to the upward propagation of cyclic shear waves. Sediment on level ground undergoes loading conditions as depicted in Figure 1, with the shear stress applications being somewhat random but nonetheless cyclic. Cohesionless sediments that are loosely packed tend to become more compact when sheared. Continued cyclic shearing can cause the pore-water pressure to increase suddenly to the static confining pressure, leading to large strains and flowage of the water and sediment. No appreciable change in volume of the deposit is required for this change in state from a solid-like to a viscous, liquid-like material (i.e., liquefaction). The process is driven by breakdown of the packing arrangement of grains (Fig. 2).

Liquefaction during earthquake shaking most commonly originates at a depth ranging from a few to about 10 m. Liquefaction takes place only where the sediment is completely saturated. The zone of liquefaction during shaking depends on the relationship between the cyclic shear stresses generated by the earthquake and the stress required to initiate liquefaction in the sediment (Fig. 3).

Sediment vented to the ground surface is the most conspicuous evidence of liquefaction at depth. Water from the zone of high pore-water pressure must escape upward to cause venting. A water-sediment mixture commonly erupts suddenly and violently to the surface, probably mainly through pre-existing holes or through fractures opened in the capping material by the process of hydraulic fracturing and oscillating surface shaking. In exceptional situations the mixture spouts as high as 6 to 7 m, especially where flow is concentrated into holes and cracks through an overlying finer grained cap (Dutton, 1889; Fuller, 1912; Housner, 1958). Water, sand, and silt can continue to flow to the surface as 'sand volcanoes' for hours after earthquake shaking has stopped. Sediment is left behind on the ground surface in the form of cones, often called 'sand blows' or 'sand boils' (Fig. 4). The cones of sand can be as much as a meter in height and tens of meters in width.

The increased pore-water pressure during ground shaking can be manifested in other ways. The high pore-water pressure decreases the shear strength of granular strata at depth. These strata can then fail in shear even where the ground surface is inclined as gently as 0.1 to 5 percent (Youd, 1978; Youd and Bartlett, 1991). Huge masses of overlying soil can shift horizontally in the form of laterally moving landslides (called lateral spreads; Fig. 5). Separation between individual blocks is commonly as much as 2 to 3 m where shaking has been especially strong. This separation tends to be largest near stream banks or scarps in alluvium, even if only a few meters in height, because these breaks in slope are where there is less resistance to lateral movements. Figure 6 illustrates a variation of lateral spreading that can take place on level ground far from breaks in slope. Here, oscillation of the ground above the zone liquefied can form blocks separated by sand-filled fissures.

Liquefaction of granular deposits normally leads to surface cracking and formation of localized depressions because of densification of liquefied sediment after expulsion of water, even where there is no evidence of venting of sand and water to the surface. These settlements can be as much as 0.25 to 0.5 m where thick sands liquefy severely (Tokimatsu and Seed, 1987).

On slopes that exceed about 5 percent, severely liquified sediments can cause huge landslides (sometimes called flow failures) that can flow as much as tens to hundreds of meters. Ground disruption can be so severe that it is difficult to establish the pre-failure surface geometry. Strength properties of materials in the failure zone can be changed greatly. Flow failures along banks of streams and hillsides can also originate by static (nonearthquake) mechanisms, however. Determination that prehistoric landslide movement on a steep slope was seismically triggered generally requires complex engineering testing and analysis difficult to perform in the best of circumstances, irrespective of whether liquefaction was involved (Jibson and Keefer, 1993). Therefore, sites on nearly level ground are best for distinguishing a seismic from a nonseismic origin.

Clastic dikes on level to nearly level ground are the primary source of data used for paleoseismic interpretations. Very important factors controlling the development and density of dikes include not only the compactness and thickness of sediment that liquefied, but also cap thickness. Dikes almost certainly form solely in response to hydraulic fracturing of the cap in a great many field situations, but dike development can be enhanced greatly by lateral spreading or by a prolonged duration of strong oscillation shaking at the surface.

2.1 Process of liquefaction and fluidization

The process of seismically induced liquefaction of saturated granular sediments has been studied extensively and is reasonably well understood (Seed, 1979; National Research Council, 1985; Castro, 1987; Dobry, 1989). Figure 7 illustrates the typical field situation on level ground. A liquefiable sand layer is overlain by a thin, nonliquefiable stratum, and the ground-water table is shallow. Earthquake-induced shear stresses propagate through the loose sand and cause shear strain of the sediment structure. (Shear strain is the angle in radians, γ, shown in Fig 7.) Because grains attempt to move into a denser packing arrangement relatively quickly during back-and-forth shear straining, water in the voids does not have time to escape. The pore-water pressure can thereby increase. In loose deposits, stresses at the grain contacts can approach zero, and concurrently the pore-water pressure carries the weight of the overburden. The first time this occurs is often referred to as 'initial liquefaction' (National Research Council, 1985, p. 42). A large loss of strength can take place once this condition is reached. In very loosely packed sand, the strain can increase suddenly, and blocks on slopes can move large distances. The combination of elevated pore pressure with large loss of strength is sometimes referred to as 'complete liquefaction' (Youd, 1973). In more densely packed sand the pore pressure rise is less sudden, and the strength loss is less severe; thus, any increase in strain is less dramatic and is limited. Very densely packed sands may not develop pore-water pressures high enough to cause liquefaction. For the purpose of this text, the condition of highly elevated pore-water pressure with a significant loss of strength is referred to simply as 'liquefaction'. When the term 'initial liquefaction' is used, emphasis is on the elevated pore-water pressure rather than loss of strength.

The cyclic strain in sands that is required to induce liquefaction usually is very small. Ten cycles of back-and-forth shearing generally suffice if the shear strain exceeds 0.3 percent. For earthquakes having long durations and many cycles, the critical shear strain can be as low as 0.04 percent (Dobry, 1989). Following liquefaction, densification can occur after water is expelled from the sediment. The vertical settlement caused by sediment densification often is quite small, being less than 2 to 3 percent of the height of the stratum that liquefied (Castro, 1987, p. 175).

Only minor disturbance to original stratification may take place in that portion of the stratum where only initial liquefaction has occurred. The effects to bedding are often virtually indistinguishible to the unaided eye. Closer inspection may show that platy minerals such as mica and clay are reoriented from their original flat-lying position (and can form structures known as 'dishes', shown in Fig. 32), and thin laminations of finest constituents are warped. Small, steeply inclined, flame-like sand-rich structures known as 'pillars' (see Fig. 33) can form where water collects beneath a slightly less permeable lamina and then locally penetrates through the lamina to winnow out silt and other very fine constituents. This winnowing takes place by a process often referred to as 'fluidization.'

Fluidization occurs when flowing water exerts sufficient drag or lift to momentarily suspend grains of sediment. When a fluid is forced vertically through a layer of cohesionless sediment at a rate sufficiently high to cause fluidization, the layer expands rapidly, porosity increases, and the sediment ceases to be grain supported and becomes fluid supported. Fluidized flow typically destroys original bedding and structures, at least locally. Fluidization can result from a number of mechanisms, including seepage caused by compaction of underlying sediments, seepage from springs, or seepage from deposits liquefied either from static or earthquake forces.

Reoriented minerals and small deformation structures similar to those caused by liquefaction-induced fluidization occur as syndepositional features in many environments (e.g., see Lowe and LoPiccolo, 1974; Lowe, 1975; and van Loon, 1992), which makes interpretation of a seismic or nonseismic origin uncertain. In contrast, larger features caused by fluidization from seismic liquefaction are easier to interpret because, in many field situations, sand-filled dikes whose widths exceed several centimeters and whose heights exceed a meter or so cut weathering horizons or other strata that are obviously much younger than the source zone for the dikes. This relation generally eliminates the possibility of syndepositional processes in formation of the dikes.

Many variables control the formation of large fluidization features caused by seismic liquefaction. The influence of some of the most important variables is fairly well understood. The main elements are illustrated in Figure 7. Assume stratum H2 liquefies. Water tends to flow upward by two mechanisms, relief of the high pore-water pressure and reconsolidation. Reconsolidatoin tends to cause densification as it progresses from the bottom of stratum H2 upward (Scott, 1986). Water expelled from the zone that liquefied during shaking tends to accumulate beneath a low-permeability capping layer to form a water-rich zone (Fiegel and Cutter, 1994; Liu and Qiao, 1984; Dobry and Liu, in press; Elgamal et al., 1989); this zone in turn probably supplies much of the water and sand that vents to the surface through breaks in the cap. Sediment may also be vented to the surface from greater depth, where liquefaction first developed. Venting can occur during the time of strong shaking or be delayed by as much as a few minutes following very strong shaking (Kawakami and Asada,

1966). Where the cap is thin (< 1-2 m) is the locale where the increased pore-water pressure in the underlying sand-water mixture can most easily break through to the surface. Alternatively, the same pore-water pressure increase may not be large enough to breach entirely through a thicker cap. Characteristics of the lower layer that enhance the liquefaction-fluidization process are (1) a thick, loose sand that, once liquefied, provides a large volume of water available for upward flow, and (2) a permeability that is high enough to allow water to flow quickly to the base of the cap, but that is not so high as to dissipate excess pore pressures between seismic cycles of shearing (Castro, 1987, p.177-179; Dobry, 1989). This simple model fully explains most field observations. However, seemingly contradictory manifestations of the liquefaction and fluidization process also are encountered in the field. For example, sand dikes cutting gravel layers that are much more permeable than the sand dikes have been reported by Tuttle et al. (1992). Numerous field examples of the influence of the physical setting on liquefaction-induced structures are discussed below.

2.2 Factors affecting liquefaction susceptibility and effects of fluidization

The most important factors controlling development of liquefaction-induced dikes and sills are considered in this section.

2.2.1 grain size

Both field and laboratory data show that loosely packed, cohesionless sands that are clean (i.e., with no clay or bonding of grain-to-grain contacts) can readily liquefy and form great numbers of clastic dikes, sills, and sand blows. Figure 8 shows often-cited curves with size boundaries for fine- and medium-grained sands that liquefy most easily and form large fluidization features. On the basis of my field observations of effects of the 1811-12 New Madrid earthquakes and the 1886 Charleston earthquake, for these sand sizes, a nonliquefiable cap of only slightly lower permeability can still provide adequate confinement to form large sand blows.

Deposits of sand and gravel containing more than 30 to 50 percent gravel can liquefy, but liquefaction-induced features in such coarse deposits are sparse in comparison to sands. Such diminishment results from a number of reasons. The high gravel content increases the internal friction resistance, making initial liquefaction more difficult. In addition, gravel-rich deposits are generally more densely packed than sands in field situations. This increased resistance to shearing combined with the high permeability found in many gravel-rich deposits makes liquefaction much more difficult than for sands (Wong et al., 1975, p. 582). In deposits having only a small percentage of fines (amount smaller than about 0.06 mm), the gravels are in point-to-point contact rather than being encased in a matrix of sand and silt. If more than 80 percent of the sediment is coarser than 0.7 mm in diameter, the permeability may be too high to develop a condition of initial liquefaction if there is no cap to inhibit drainage (National Research Council, 1985, p. 94). However, very gravelly sediments can form large liquefaction-induced features if the source deposits are loose, thick, and capped by a stratum of low permeability. For example, extensive liquefaction occured during the Borah Peak earthquake (M 7.3) where very coarse sediment (Fig.8) was confined by a low-permeability cap (Andrus et al., 1991). Large amounts of gravel-bearing sand were vented onto the ground surface. Significant lateral spreading also occurred. The source strata contained at least 70 percent gravel. Peak earthquake accelerations probably were high at this

site, between 0.3 and 0.35 g (Andrus et al., 1991, p. 257). Corroborating evidence of severe liquefaction in gravel is also provided by a disastrous occurrence in a gravel-rich fan deposit near the epicenter of the Fuku, Japan, earthquake of 1948 (Ishihara, 1985, p. 333). In another example (Meier, 1993), gravels liquefied sufficiently to cause damage to many bridges during the 1964 Alaskan earthquake (M 9.2); Ross et al., (1969) found all these bridge sites were relatively near the zone of major energy release, being within 80 km. Sites of sand and silt causing liquefaction-induced damage extended as far as 130 km.

Only very exceptionally can sediment finer than the lower bound for the "potentially liquefiable" sand in Figure 8 readily liquefy. In general, natural deposits with a large proportion of fines contain a significant amount of clay. The presence of even a small amount of cohesion from clay- or silt-sized material can impede particle rearrangement during cyclic straining and greatly increase resistance to cyclic loading. As little as 5 percent of clay- or silt-sized material in a sand deposit can make liquefaction significantly less likely than for the same sand deposit with no fines (National Research Council, 1985, p. 103).

Engineering data show that clay- or silt-bearing sediment that liquefies and has large strength loss generally has less than 15 percent of the particles finer than 0.005 mm, a liquid limit that is less than 35, and a water content that is nearly equal to or greater than the liquid limit (Seed et al., 1983; Youd et al., 1989). (The liquid limit, expressed as a whole number, is the water content at which a remolded sample has such a soft consistency that the sample is on the semisolid-liquid boundary. Liquid limit is measured in a standardized test described in elementary soil mechanics texts.)

Clay and silt-rich deposits referred to as sensitive or 'quick' clays (because they change to a viscous fluid upon remolding) can breakdown and flow during strong seismic shaking, much as liquified sediments do (Updike et al., 1988). Field situations in which sensitive deposits occur are described in Mitchell (1976).

The ability to form recognizable fluidization features generally is greatly diminished in silt and clayey silt sediment. Even though initial liquefaction may occur, the low permeability may restrict water from escaping quickly enough to form fluidization features that are large enough to be recognized in the field (Castro, 1987). Similarly, even though a very soft clay-rich deposit may have had high pore pressures that developed, the effects may not be recognized in the field. Silty very fine sand is the finest sediment in which large seismically induced liquefaction features commonly form in the field. However, a silt deposit can also produce sizeable sand blows, providing the deposit fulfills the engineering criteria described above (Youd et al., 1989).

2.2.2 relative density

The arrangement or packing of sand grains has a profound effect on a sediment's liquefaction susceptibility. Susceptibility of the same sand can be changed from very high to nonsusceptible simply because of a change in packing. The state of looseness or denseness of cohesionless sediments (also called 'compactness' or 'relative density') is generally measured in-situ by the Standard Penetration Test (SPT) blow-count method (American Society for Testing and Materials, 1978). The SPT method is a standard engineering test used on unconsolidated deposits. The test provides quantitative data for design of bridge and building foundations. A sampling tube is driven into the ground by dropping a 140-lb (63.5-kg) weight from a height of 30 in (176 cm). The penetration resistance is measured as the

number of blows required to drive the sampler 1 ft (30.5 cm). Table 1 shows the relation between blow count and relative density. Terms for relative density in the table are used in this text as a semi-quantitative indication of liquefaction susceptibility. Sands that are moderately dense or looser liquefy in many field situations. Dense sands require exceptionally strong shaking, and very dense sands probably rarely generate residual pore pressures large enough to form fluidization features (Seed et al., 1983).

The geologic environment in which sediment is deposited generally has a major bearing on relative density. Wind-blown sand deposited in dunes is very loose in many places. Rapidly flowing streams tend to form more densely packed sediments, but in locales of quiet water even coarse-grained sediments can be laid down gently in a loose condition. Large quantities of loose sand tend to be deposited where small streams empty into much larger streams or lakes. Deltas are especially favorable sites for thick, very loose deposits. Near the ocean, the transition zone from a rapidly flowing stream to a tidal estuary presents a setting where thick, loose, clean sands can be deposited. In brief, there are many local and widespread geologic environments where susceptible sediment occurs. The field geologist must reconstruct ancient depositional settings to predict locations of susceptible sediment for a paleoliquefaction study.

2.2.3 depth of ground-water table

The depth of the ground-water table has a very strong influence on whether or not liquefaction occurs. The extent of the control is indicated in Table 2, which relates the liquefaction susceptibility in San Fernando Valley (California) both to depth of ground-water table and age of the deposit (from National Research Council, 1985, p. 91). A 'high' susceptibility for this example means that a ground motion with 10 cycles of acceleration at 0.2 g (this is equivalent to shaking by a M~6.5 earthquake) is required to produce sand blows. A 'moderate' susceptibility requires 30 cycles at 0.5 g (M~8). The table shows that lowering the water table as little as a few meters can change the susceptibility from high to moderate. Such a large change in water table both in space and time is not unusual in many field settings.

Liquefaction with extensive venting can also readily occur beneath the water surface. Venting beneath water is characterized by sediment, particularly the finer constituents, forming sand volcanoes that are much wider and thinner than under subaerial conditions.

2.2.4 depth and thickness of strata

Liquefaction during earthquake shaking frequently originates in a zone as shallow as 1.5 to 2 m below the ground surface (Bennett, 1984; Obermeier et al., 1986). Features such as dikes can abound from such shallow source zones. In special field situations the top of the source zone can be much shallower, only a few tenths of a meter (Sims, 1973; Audemard and de Santis, 1991); for such shallow depths, though, liquefaction seems to occur mainly where a thin sand stratum is confined between clay-rich layers, and the evidence for liquefaction generally is the development of features such as recumbent folds along the thin sand layer. The sand layer has served as a failure plane. Evidence for liquefaction at a depth as shallow as a few tenths of a meter is not observed often in paleoseismic studies, perhaps because of destruction by weathering. At the other extreme for depth, the source zone for liquefaction can exceed 20 m (Seed, 1979). The most common depth is a range between a few meters and about 10 m.

A 1-m thickness of sand is generally required to form dikes or sills in much abundance. This also is a minimum thickness to systematically distinguish soft-sediment deformation features from earthquake-induced liquefaction features in many field situations. However, at a small number of sites in coastal Washington and Indiana, the author has observed sand strata as thin as 0.3 m that liquefied and formed dikes whose heights exceed 1 m. No significant horizontal ground displacements occurred at these sites. Here the 0.3-m-thick sand strata graded down abruptly into thick sandy gravel beds that showed no evidence of liquefaction. In an exceptional case, Tuttle and Seeber (1991) report tracing small sand dikes down to a 8-10 cm thick sand source at a depth of 2.5 to 3 m. Very strong shaking may be required to form dikes from such very thin source strata.

Liquefaction of a source stratum less than 0.3 m thick still can lead to major lateral spread or flow slide movements, providing the stratum has large lateral extent (Youd, 1987, p. 1377). Indeed, large horizontal movements may be required to produce recognizeable liquefaction effects wherever the source strata are extremely thin. Strata of fine sand as thin as a few centimeters that liquefied in association with spreading, and also formed scattered small dikes, have been observed in lacustrine deposits in Utah (J.R. Keaton, SHB AGRA, Inc., Salt Lake City, Utah, written comm., 1993). Lacustrine sediments seem to be most favorable for development of liquefaction effects in thin strata, because of the large areal extent of the strata.

Whether or not sand vents to the ground surface, or liquefaction-induced ground rupturing occurs at the surface, commonly depends on the relation of the thickness of the source stratum (stratum H2 in Fig. 7) to the thickness of the overlying cap of nonliquefiable sediment (stratum H1). Guidelines for critical thicknesses of strata H1 and H2 for ground rupturing have been developed on the basis of a limited number of field observations (Ishihara, 1985). The curves are based on behavior during a few strong earthquakes ($M \sim 7.5$) and are suspected by the author to reflect ground fracturing exclusively by the mechanism of hydraulic fracturing. A cap thickness exceeding 10 m prevents ground rupture even in the most favorable circumstances for liquefaction, according to Ishihara (Fig. 9). A cap of 1 m in thickness can be breached whenever accelerations exceed about 0.2 g if the thickness of liquefied sand exceeds 1 m. The curves in Figure 9 doubtlessly do not apply for many field situations. For example, Ishihara (1985) has suggested that the curves are valid only for loose sands (SPT blow counts < 10). Still, the curves of Figure 9 generally are valid in a qualitative sense on level ground, far from any sharp breaks in slope. Observations in the meisoseismal region of the 1811-1812 New Madrid earthquakes show that the density of dike occurence and amount of venting are greatly enhanced where the cap is very thin (Obermeier, 1989). Field situations where the curves of Figure 9 are not applicable, even in a qualitative sense, are noted in the following section.

2.2.5 site effects and nature of seismic shaking

The curves in Figure 9 tend to highly overestimate accelerations at sites of lateral spreading because of enhancement of ground breakage toward streams and toward even slight topographic depressions and streams (T.L. Youd, Brigham Young Univ., written comm., 1993). Figure 10 illustrates the relations normally observed. Increased breakage also tends

to occur where the base of the cap dips toward a stream (Hamada et al., 1986; Amick et al., 1991, p. 28).

Another very important factor in breakup of the cap can be shaking of the cap above liquefied sediment. An oscillating cap that is floating on liquefied sediment intensifies lateral spreading and breakup of the cap, especially for strong shaking of long duration. These effects, therefore, are likely to be of increasing importance with an increasing earthquake magnitude. Reflected and refracted waves along the ground surface may have important roles (Zhong-qi et al., 1983), but documentation of this is very incomplete. Surface (Rayleigh) waves may also be important. Surface oscillations seem to become particularly significant over broad alluvial expanses (T.L. Youd, Brigham Young Univ., oral comm., 1994). Observations in the Wabash Valley (see Fig. 16) suggest widths in excess of a kilometer may be necessary for oscillating ground effects to become important (P. J. Munson, Indiana Univ., oral comm., 1993).

2.2.6 geologic details of the cap

Minor characteristics of the cap also can have a profound influence on the manifestations of flow features. Holes left by decayed roots or dug by crayfish can be used as conduits for venting, and can remain more or less circular where liquefaction has not been severe (Audemard and de Santis, 1991). Vertical, planar dikes normally form where a clay-rich cap is weathered, even slightly, and has pre-existing vertical fractures or planes of weakness (Obermeier et al., 1990). Thick sills tend to form beneath a very flexible, peaty cap (Clague et al., 1992), whereas a very strong, brittle, mechanically isotropic cap, especially if sand-rich, tends to favor formation of large craters (Obermeier et al., 1990). Other important factors are discussed where case histories are presented.

2.2.7 seismic history

Both historical observations and field paleoliquefaction evidence show that liquefaction has a strong tendency to recur at the same site. Such a tendency occurs for earthquakes either closely or widely separated in time (Kuribayashi and Tatsuoka, 1975; Youd and Hoose, 1978; Youd, 1984; Saucier, 1989; Obermeier et al., 1990; Tuttle et al., 1992). It is not unusual for dikes to repeatedly use the same path through the cap as a conduit for venting to the surface, even for earthquakes widely spaced in time.

An apparent contradiction to recurrent liquefaction at the same site is the observation that liquefaction commonly seems to densify sediments. Worldwide engineering measurements before and after occurrences of liquefaction indicate that thick zones (> 10 m) of loosely to moderately compact sands in the zone that liquefied during shaking can be densified substantially, whenever liquefaction has been severe (Koizumi, 1966; Ohsaki, 1970.) However, measurable densification does not always occur, as shown by careful measurements by Holzer (1994). Densification should reduce the liquefaction susceptibility. Still, even where liquefaction has been severe and has occurred repeatedly, engineering data show that sediments can remain susceptible. For example, in the meisoseismal region of the 1811-12 New Madrid earthquakes, where liquefaction was severe, the uppermost meter or so of sand directly beneath the impermeable cap is still moderately susceptible at many places (see engineering boring logs in Obermeier, 1989). This relatively loose zone probably originated because water collected beneath the cap and loosened the sands prior to venting, as

well as emplaced sills of loose sand along the base of the cap. Other well-documented case studies can be cited. In the meisoseismal region of the 1886 Charleston, South Carolina earthquake, source sands beneath a low-permeability, humate-cemented cap remain in a loose condition at sites of abundant sand blows (Martin and Clough, 1990). These South Carolina sites experienced at least three previous episodes of liquefaction during the Holocene; still, there is evidence for some densification caused by repeated liquefaction at the same sites because the crater sizes decrease with younger age. Laboratory model studies on layered sand and clay beds also verify formation of a loosened sand zone along the base of the clay beds (Elgamal et al., 1989; Fiegel and Cutter, 1994).

Data from studies in Japan show that the presence of a cap of low permeability may not be required for sands to maintain the ability to reliquefy. The upward flow of water from a liquefied zone at depth appears to be able to loosen sand at shallow depth where sand extends to the surface. This loosening may occur within 2 to 5 m of the surface (Kishida, 1966, p. 75).

In contrast to densification of loose sand at depth, field data indicate that relatively dense sands may be loosened significantly by an occurrence of liquefaction. Data from Koizumi (1966) and Kishida (1966) suggest this loosening may occur where the dense sand is underlain by a much looser sand that liquefied. An upward flow of water through the dense sand may have caused fluidization and loosening.

In the 1979 earthquake of Imperial Valley, California, a 3-m thickness of source sand for a large lateral spread remained loose beneath the cap (Youd, 1984b). The large shearing associated with the lateral spread movement may have maintained the source sand in a highly susceptible state. During shear, granular soils can either compact or dilate depending on the compactness of the sediment, the confining pressure, and the amount of shear deformation. Except for very dense packings, sands initially tend to become more compact as shear strain is applied. At large shear strains such as those for lateral spreading, all but very loose sands or sands under high confining pressure tend to dilate toward a relatively loose condition (Youd, 1984b).

2.2.8 age and mineralogy of sediments

The age of sediment can have a strong influence on liquefaction susceptibility. At many places in the western United States, sufficient changes occur within 500 years to reduce susceptibility from high to moderate (Youd and Perkins, 1978). In this region, the susceptibility commonly decreases from moderate to low as age increases from 500 years to earliest Holocene. Pleistocene sediment is liquefiable only in exceptional circumstances and no modern occurrences of liquefaction have been observed in pre-Pleistocene sediments.

In the eastern United States, however, Pleistocene sediment remains highly susceptible to liquefaction over large regions. Large liquefaction features formed in loose sediment as old as 200,000 to 240,000 years during the 1886 Charleston earthquake (Obermeier et al., 1990). Apparently a very high ground-water table in combination with weakly acidic (organic acids) ground water has prevented significant bonding in the very quartz-rich source sands. In the central United States, abundant liquefaction features developed in sediments as old as late Wisconsinan (ca. 15,000-20,000 years) during the 1811-12 New Madrid earthquakes. Again, the ground-water table appears to have been very shallow through the Holocene (Wesnousky and Leffler, 1992). The source sands in the New Madrid earthquake

region contain a wide variety of minerals, derived largely from glaciers that passed over terranes of igneous and sedimentary rocks. Thus in the Charleston region and the New Madrid earthquake region, source sands of very different mineralogies have remained quit susceptible to liquifaction for a very long time.

Changes in liquefaction susceptibility through time probably depend strongly on fluctuations in the depth of ground water and on water chemistry. Where the water-table depth fluctuates greatly, bonding can occur as a result of chemical reactions or from an influx of clay. Alternatively, only very minor changes in bonding may develop in sediment much older than Holocene if the ground-water table has remained very shallow.

3. CRITERIA FOR AN EARTHQUAKE-INDUCED LIQUEFACTION ORIGIN

A set of criteria has been developed for determining whether observed sediment deformation was caused by seismically induced liquefaction. A seismic origin can be established if the following conditions are met:

1. The features have sedimentary characteristics that are consistent with an earthquake-induced liquefaction origin; namely, there is evidence of an upward-directed hydraulic force that was suddenly applied and was of short duration.

2. The features preferably have sedimentary characteristics consistent with historically documented observations of the earthquake-induced liquefaction processes, in a similar physical setting. In addition, preferably there is more than one type of feature commonly caused by seismically induced liquefaction. Such features include dikes, sills, vented sediment, and some types of soft-sediment deformations.

3. The features occur in ground-water settings where suddenly applied, strong hydraulic forces of short duration could not be reasonably expected except from earthquake-induced liquefaction. In particular, the possibility of an origin from artesian conditions or nonseismic landsliding must be ruled out.

4. Similar features occur at multiple locations, preferably at least within a few kilometers of one another, in similar geologic and ground-water settings. The regional pattern of size and abundance of features should be consistent with a pattern of shaking associable with an earthquake.

5. The evidence for age of the features supports the interpretation that they formed in one or more discrete, short episodes that individually affected a large area and that the episodes were separated by relatively long time periods during which no such features formed.

Determination of the regional pattern of size and abundance of the suspected liquefaction features may be critical to interpretation of origin. Preferably at least 20 to 30 km of cumulative fresh exposure is examined. Such a regional approach to a paleoliquefaction study helps eliminate the possibility that nonseismic processes are responsible for creating the features, and it helps to develop a sense of the various processes that deform sediments. The next section illustrates application of the five criteria above and presents examples of how an understanding of the local geologic setting is critical to interpretations.

4. HISTORIC AND PREHISTORIC LIQUEFACTION--SELECTED STUDIES

In this section, I describe earthquake-induced liquefaction features in four geologic-geographic settings. These include coastal South Carolina, the New Madrid Seismic Zone, the Wabash Valley Seismic Zone of Indiana and Illinois, and coastal Washington State (all in the USA). The two latter areas have not had historic liquefaction. The discussion emphasizes the role of the local geologic setting in deducing an earthquake origin. Special consideration is given to elimination of artesian springs and nonseismic landsliding as possible sources of observed deformations. Where possible, the magnitudes of the prehistoric earthquakes are estimated by comparison with historical liquefaction-producing earthquakes in the region.

4.1 Coastal South Carolina

The strongest historical earthquake in the southeastern United States took place in 1886 near Charleston, South Carolina. The estimated magnitude is about 7.5 (Johnston, 1992). Clear evidence of seismotectonic conditions in the region is lacking, which prompted searches for prehistoric liquefaction features. Liquefaction evidence has since been found for many prehistoric earthquakes (Obermeier et al., 1987; Amick et al., 1990). Results of the searches are shown on Figure 11. The figure shows the approximate boundary of the 1886 earthquake meisoseismal zone, shows the sites where in 1886 swarms of liquefaction features described as "craterlets" were formed (Dutton, 1889; see Fig. 12), and shows the sites where liquefaction features predating 1886 were found. The prehistoric liquefaction-induced features are mainly ancient craterlets that are now filled.

None of the pre-1886 craters found has an expression on the ground surface that is discernible by on-site surface examination or on aerial photographs. These features are seen only in walls of excavations, typically drainage ditches at least 1.5 m deep. At most sites shown on Figure 11, at least three or four pre-1886 craters are exposed within a few hundred meters of one another.

The physical setting of the region within 50 km of the South Carolina coast is conducive to widespread liquefaction. That region is known locally as the "low country" because it has low local relief (1-3 m) and low elevation (0-30 m), and because vast expanses of swamp and marshland are under water much of the year. Most of the Carolina low country is covered by a 5- to 15-m-thick blanket of unconsolidated Quaternary marine and fluvial deposits, which lies on semilithified Tertiary sediment. The Quaternary deposits primarily occur as a series of well-defined, temporally discrete, interglacial beaches and associated back-barrier and shelf deposits that form belts subparallel to the present shoreline. Increasingly older beach deposits are progressively farther inland and at higher altitudes. Most beach deposits consist of clean, medium- to fine-grained sand. Cutting across these marginal-marine deposits at nearly right angles are major rivers. Bordering these rivers are fluvial terraces, which consist largely of clean sand with a cap of clay.

Figure 11 shows the approximate areal extent of the marginal-marine deposits younger than about 250,000 years. The search for liquefaction features was generally restricted to the deposits younger than about 250,000 years and older than about 80,000 years. Sands in these deposits are loose at many places. Normal depth to the ground-water table in these sediments is about 1 to 2 m, even in topographically elevated regions. Deposits older than about 250,000 years have such a low susceptibility to liquefaction (due to effects of chemical weathering) that the likelihood of their liquefying has been extremely low during the late

Pleistocene and Holocene. Deposits younger than about 80,000 years generally have such a high ground-water table that exposures are very limited.

Most of the craters that were discovered had formed on ancient beaches, where the cap is a humate-enriched sand. Tabular sand dikes were discovered in fluvial terraces and in back-barrier environments where the cap is much richer in clay. Sills were observed only rarely. The following discussion concentrates on the craters, because the section below discussing liquefaction effects in the New Madrid Seismic Zone adequately deals with characteristics of tabular sand dikes and sills, which are the types of liquefaction-induced features normally encountered where there is a thick clay-rich cap.

4.1.1 characterization of craters

The geologic setting most frequently associated with the seismically induced craters is the crest or flank of Pleistocene beach ridges, where a thin surficial cover of highly weathered sand-rich material overlies clean sand. Figure 13 is a schematic cross section through a typical low-country beach ridge containing craters. According to eyewitness observations in 1886, "craterlets are found in greatest abundance in belts parallel with (beach) ridges and along their anticlines" (Peters and Herrmann, 1986, p. 68). Thus the locations of crater sites we discovered are consistent with historical observations.

Almost all craters that predate 1886 have a morphology and size comparable to the 1886 craters of Figure 12 except that the craters are now filled with sediment. Figure 12 shows moderate to large craters produced by the 1886 earthquake. Examination of photographs taken in 1886 shows that surficial sheets of vented sand around crater rims normally had thicknesses of about 15 to 20 cm. Maximum reported thickness of vented sand was 1 m, and the maximum crater diameter was about 6 m (Dutton, 1889).

The crater sites shown Figure 11 are located where weathering has imposed a soil profile on the ancient beaches. Near the surface, a thin (< 10- to 15-cm) A horizon (organic matter and several percent sand) overlies a thin (< 10- to 15-cm), very light gray E (eluviated) horizon; the E horizon overlies a thick (0.5- to 1.5-m), weakly cemented, black Bh horizon (humate-enriched sand containing a few percent clay) that grades down rather sharply into a variably thick (0.1- to 1-m), light-colored B-C horizon (transition zone between B and C horizons). The B-C unit grades down into C-horizon sands (parent material). The craters cut the solum and the C horizon. The source sand beds that liquefied during earthquake shaking generally occur within the depth range of 3 to 10 m.

Figure 14 is a vertical section representative of the prehistoric craters. The soil horizon is cut by an irregular crater, which is filled with well defined zones of sediment. The fill materials are fine- to medium-grained sand and clasts from the Bh, B-C, and C horizons of the host, and there is sand from depths much below the exposed C horizon. Walls of the crater are commonly smooth and sharply defined when viewed closely in vertical section, especially in the lower part of the crater.

The Bh horizon of the filled crater generally is much thinner over the central part than on the sides. The Bh horizon of the laterally adjoining undisturbed host is abruptly thicker. Clay content of the Bh horizon in the crater is much less than in the host. With increasing age of the filled crater, the Bh horizon on the filled crater typically is thicker, is more clay rich, and has better developed soil structure. Craters older than about 5,000 to 10,000 years

have Bh horizons that approach the thickness and development in the host sediment enclosing the craters.

The filled craters are characterized by a sequence of five layers. Layer 5 (Fig. 14) is a structureless, gray, humate-enriched and cemented sand, which overlies a thinly (2- to 3-mm) laminated sequence of alternating light- and dark-colored sands (layer 4). The lamina typically are discontinuous and irregular in thickness. The dark color is imparted mainly by humate staining; the dark lamina can have appreciable amounts of silt and clay. The basal bed of this sequence (layer 4) can be clay rich and is rarely thicker than 1 cm. The basal bed sharply overlies a medium-gray structureless sand (layer 3). Layer 3 contains many small clasts of Bh material, charcoal, and wood. This clast-rich layer grades down into a structureless sand zone (layer 3) containing many intermediate-sized clasts (5- to 20-mm diameter) of Bh material and occasional extremely friable clasts of light-colored sand from the B-C and C horizon of the host. Layer 2 grades down into layer 1, which contains densely packed intermediate-sized (1-5 cm) and large-sized (>5 cm) clasts of Bh material in a structureless sand matrix; the large clasts have diameters exceeding 25 cm in many filled craters. Many of the clasts in layer 1 have their long axes vertically oriented. At and below the thinly stratified sequence (layer 4), the sides of the bowl are sharply defined by a color boundary and by clasts within the bowl. Beneath the bowl are dikes containing clean sand that is structureless when viewed at the outcrop. Sides of the dikes sharply cut bedding in the C horizon. The dikes are tube-like in plan view.

The filled craters are interpreted to have formed in the following phases: (1) a large hole is excavated at the surface by the violent upward discharge of the liquefied mixture of sand and water; (2) a sand rim accumulates around the hole by continued expulsion of liquefied sand and water after the violent discharge; (3) sand, soil clasts, and water are churned briefly in the lower part of the bowl, followed by settling of the larger clasts and formation of the graded-fill sequence of sediment (layers 1-3); and (4) the crater is intermittently filled by adjacent surface materials to form the thin stratified-fill sequence (layer 4) during the weeks to years after the eruption. Layer 5 is in the strongly bioturbated zone and thus has no stratification. The sand blanket ejected from the crater is indistinguishable in the field from the surface and near-surface (A, E, and Bh) soil horizons, because the blanket has been incorporated within these soil horizons.

The presence of friable, angular clasts of B-C, C, and Bh horizon material in the graded-fill portion (layers 1-3) is consistent with a short-lived, churning type of upwelling from the vent. Water commonly flows for a day or so from the vents of earthquake-induced sand blows. The violent, boiling phase is much shorter in duration. Hence, the presence of friable clasts argues against a long-term artesian spring origin for these features; such a spring would abrade, round, and disaggregate the clasts. In addition, springs are very unlikely to form in the topographic-geologic setting at some of the crater sites (Fig. 13).

An earthquake origin for the craters is also supported by the presence of sand-filled tabular fissures, whose overall shape and dimensions strongly suggest that they are "incipient craters." Such fissures as shown in Figure 15 are rather common in the epicentral zone of the 1886 earthquake. The figure shows a V-shaped fissure connecting to a tube-like dike with sand transported upward from depth. The tabular fissures in the V-portion widen with depth until they connect to a single, near-vertical, large, sand-filled tube. The V-shaped

fissures probably represent the early phase of development of craters; upward forces, however, were too weak to excavate the overlying material.

It is possible that liquefaction produced craters because of a fortuitous combination of sediment properties. The source beds that liquefied were exceptionally susceptible to liquefaction; they are loose (engineering sense), fine grained, uniformly sized, and free of clay (Martin and Clough, 1990). These properties would cause the source beds to liquefy abruptly and, once liquefied, the sand-water mixture would flow readily. I suspect that the liquefied sand strata quickly migrated laterally to a hole such as that left by a decayed root. The sudden application of an upward force around the hole caused the formation of a V-shaped crack. The liquefied sand violently vented because of its exceptional ability to flow. The V-shaped cracks developed because overlying sediment is isotropically cemented with humate, has no pronounced planes of weakness, and is very brittle; the process is similar to formation of a conchoidal fracture in an isotropic, brittle medium such as glass, when struck by a rock.

Liquefaction-induced craters are common during earthquakes worldwide. Good examples for various earthquakes in Japan are shown in articles by Kawakami and Asada (1966) and by Iwasaki (1986). Craters were especially prevalent during the M 7.5 Niigata earthquake of 1964; soils around Niigata typically are sand rich all the way to the ground surface (Katayama et al., 1966), much as for the Charleston crater region. The presence of sand at very shallow depth does not seem to be necessary, however, to form craters. Some spectacular craters as much as 10 m in diameter and extremely shallow (25 to 40 cm) formed during the great Alaskan earthquake of 1964, apparently from a source stratum at least 6 m deep (Reimnitz and Marshall, 1965). Some of these very large craters may have formed as sand vented to the surface and undermined a clay-rich cap, thereby forming a circular depression at the surface. In Argentina, Youd and Keefer (1994, p.227-229) have shown that holes through a clay-rich cap prior to an earthquake later led to erosion of large craters in response to liquefaction during a M 7.4 earthquake. Craters also formed in a clay-rich cap in the Nile River Valley during the M 5.9 Dahshur, Egypt, earthquake of 1992 (Elgamal et al., 1993). No mechanism for formation of the craters in Egypt can be demonstrated because of the lack of geologic and geotechnical data at the crater sites. However, the regularity of alignment of the craters suggests that man-made holes led to formation of the craters.

4.1.2 prehistoric seismicity

Some filled craters contain small twigs and bark from trees along the contact of layers 3 and 4. This woody matter obviously fell into the open pits soon after they formed. Radiocarbon dates for the woody material from prehistoric craters in the Charleston area have approximate ages of 600 years, 1,250 years, 3,200 years, 5,150 years, and older than 5,150 years (Amick et al., 1990). Hence, four prehistoric earthquakes are documented in the Charleston area during approximately the last 5,000 years, along with one older event.

An estimate of the magnitude of prehistoric earthquakes is provided by comparison of their liquefaction effects with worldwide observations, and also by comparison with observations of liquefaction in South Carolina in 1886. Data from the 1886 earthquake furnish a data base for the regional development of craters, and for their size and abundance. Worldwide data show that features having a liquefaction origin can be developed at

magnitudes as low as M~5 but that a magnitude of about 5.5 is the lower limit at which liquefaction effects are relatively common (Ambraseys, 1988). The source sands that produced craters in coastal South Carolina commonly are highly susceptible to liquefaction and flow; because of this susceptibility one might suggest that a low-magnitude earthquake could have produced the prehistoric craters. However, numerous prehistoric craters in the Charleston area, many having diameters in excess of 3 m, clearly are too large to have been the result of marginal liquefaction. Such large diameters suggest that the earthquake that produced them was much stronger than M 5 to 5.5. In addition, the prehistoric craters that formed 600 and 1,250 years ago extend along the coast at least as far as the craters produced by the M 7.5 earthquake of 1886.

Interpretations of prehistoric earthquake magnitudes must account for liquefaction susceptibility. Principal variables are water-table depth and the compactness of the source sands. The water table is presently very shallow, being less than 1 to 2 m below the ground surface. Almost certainly the water table has been essentially unchanged for the past few thousand years at many of the crater sites (Amick et al., 1990). Just prior to the 1886 earthquake, the Charleston area was experiencing an extraordinarily wet period, so water-table conditions were optimal for production of liquefaction features (Taber, 1914, p. 126). Standard Penetration Test (SPT) data also show the source sands are so loose as to readily liquefy. It is not unusual that the sand deposits at the liquefaction sites have SPT blow counts as low as 10 or less (Martin and Clough, 1990). It is difficult to conceive of any mechanism that would have made the sands much more compact when the prehistoric earthquakes occurred. In summary, the liquefaction susceptibility was high at many places when the 1886 earthquake struck.

It was previously noted that craters having ages of 600 and 1,250 years extend along the coast at least as far as craters of the 1886 earthquake. A comparison of the size (diameter) of the craters shows that those formed 600 years and 1,250 years ago are larger than the 1886 craters, both in the vicinity of Charleston and far away. Consideration of all factors suggests that these prehistoric earthquakes were at least on the order of the M~7.5 event in 1886.

Paleoliquefaction evidence for the event that took place 3,200 years ago has been found only in the vicinity of Charleston. The existence of abundant, exceptionally large craters for this event might suggest that the earthquake was exceptionally large, but the limited size of the affected area suggests otherwise. The absence of craters far from Charleston might be explained alternatively by a lower water table caused by a lower sea level and a generally drier climate earlier during this part of the Holocene (Amick et al., 1990). Absence of the 3,200-year-old craters far from Charleston might also be explained by an exceptionally shallow earthquake, in which energy attenuates rapidly within a short distance. For craters having an age of 5,000 years or older, there is a greatly diminished chance for preservation of organic material that can be dated with accuracy, so it is difficult to evaluate the magnitude of such old events.

Some of the craters far to the north of the Charleston area, in the vicinity of the South Carolina-North Carolina border (Fig. 11), have ages different from those of craters to the south. This difference suggests that another epicentral region may be located in the vicinity of the state boundary.

4.2 New Madrid Seismic Zone

The 1811-12 sequence of earthquakes in the central United States consisted of four very strong earthquakes (M~7.8 to 8.3) within a 3-month period. Six aftershocks had magnitudes of 6 to 7 (Hamilton and Johnston, 1990). Epicenters of the strongest 1811-12 earthquakes probably were distributed along a fault zone exceeding 100 km in length (McKeown et al., 1990). These epicenters, in combination with continuing seismicity, define the New Madrid Seismic Zone (Fig. 16).

The meisoseismal region for the 1811-12 earthquakes was centered in a huge area of alluvial lowlands. Prominent effects of liquefaction extended over an area of 10,000 km^2 in the lowlands and are plainly visible on the ground today (Figs. 17 and 18). Large areas have more than 25 percent of the surface covered with vented sand more than a meter thick (Obermeier, 1989).

The alluvial lowlands is an area of very low relief, thick strata of fine and medium sand at shallow depth, a very high water table, and a clay-rich cap of lower permeability. The sand strata generally are moderately compact, but still sufficiently loose to be liquefied at many places. The area is quite susceptible to the formation of earthquake-induced liquefaction features during strong shaking. The lowland is made up largely of late Wisconsinan braid-bar terraces that formed in floods of glacial meltwater carrying great quantities of sand. Thickness of sand beneath the terraces generally exceeds 30 m, and at most places the sands are capped with clay-rich strata interbedded with thin sand and silt strata having a total cap thickness of a few meters. The alluvial lowland also is occupied by large areas of Mississippi River meander-belt deposits that were laid down during Holocene time. Most of the meander belt consists of point-bar accretion topography of arcuate ridges and swales, abandoned channels, and natural levees. Many abandoned channels are filled with as much as 30 m of soft clay and silt. A cap of montmorillonite-rich clay at least a few meters thick lies on meander-belt sediments at most places.

Reports made shortly after the 1811-12 earthquakes noted great multitudes of sand blows, linear fissures as deep as 6 m and hundreds of meters long, craters many meters in diameter, and lateral spreads as long as hundreds of meters (Penick, 1976). Individual and coalesced sand blows and some long linear fissures through which sand vented are the only features that are still readily visible on the ground surface. Great numbers of intruded dikes and sills can be seen in walls of deep (>3 to 4 m) drainage ditches.

Also within the 1811-12 earthquakes meisoseismal region are many sedimentary features of unknown or nonseismic origin. Mainly the features formed as nonseismic sand boils, mima mounds, or deformed mud.

4.2.1 characterization of venting and fracturing at the ground surface

Even though sand that was vented to the surface by the earthquakes of 1811-12 is still visible today, most evidence of venting has been obliterated by agricultural practices. However, even small features were abundant at the time of a field study by Fuller (1912). Individual sand blows induced by the 1811-12 earthquakes typically are dome-like accumulations of clean sand on the ground surface. Fuller (p. 79) noted that "the normal blow is a patch of sand nearly circular in shape, from 8 to 15 feet across, and 3 to 6 inches high." Such small sand blows as Fuller described can rarely be found at present. The sand

blows now obvious range from about 0.3 to 0.7 m in height at the center, and thin to a feather edge at a distance of 5 to 20 m from the center.

Sand vented to the surface by the 1811-12 earthquakes is obvious on aerial photographs, where the sand vented onto the dark clay-rich cap. The vented sand dries more rapidly than clay during seasonal drying, making a tonal contrast on the photograph. Figures 18A and 18B illustrate the contrast and also illustrate how venting has taken place at irregular and somewhat erratically spaced intervals. The figure photographs also show that extensive venting took place through approximately linear dikes that are more or less parallel. These patterns of erratic spacing and parallelism generally reflect small differences in site characteristics. One of the most obvious is cap thickness. Typically, venting in point-bar deposits has taken place along the highest, thinnest, part of the meander scroll. Where the cap is thicker, sand blows tend to be less abundant but larger. The wider spacing between dikes apparently causes more concentrated flow to the surface.

Long, linear dikes, commonly with exceptionally large quantities of vented sand, also tend to develop parallel to topographic declivities along streams and scarps. Dikes here have formed in response to lateral spreading movements, which generally take place more readily near the declivities (Fig. 18A). Wide (> 1 m) dikes having lengths of many hundreds of meters are not unusual. Whereas the widest dikes tend to be close to the declivities, they also can develop many hundreds of meters away even where the declivity height is small. Fuller (1912, p. 49) for example states, "In the sand-blow districts the spacing of (lateral spreading) fissures varies from several hundred feet down to less than 10 feet..... In the case of the large (several meters wide) fault-block (lateral spread) fissures the spacing is greater, several hundred feet often intervening between the cracks, while the space between them may be half a mile or more. Isolated cracks of this type are not uncommon."

The direction of shaking during the earthquake probably had a very secondary influence on orientation of the largest dikes at most places in the meisoseismal region of the 1811-12 earthquakes (Obermeier, 1989). It is the local geologic-topographic setting that is of predominant influence. Cap thickness and proximity to stream banks and abandoned meanders are most important. Such important influence of the local setting has also been shown in a report about the 1964 Alaskan earthquake (M 9.2) by McCullough and Bonilla (1970, Fig. 46), and is emphasized by Oldham (1899) for the great earthquake of 1987 in India, so the observed effects in the meisoseismal region of the 1811-1812 earthquakes seems typical. Still, localized extension and compression of the ground surface, which may relate to the direction of strong surface shaking, may be relatively common in response to some earthquakes (Oldham, 1899, p. 99).

The aerial photograph in Figure 18 indicates that there is enough randomness in dike orientation that most vertical exposures will intersect many dikes. This is especially relevant because searches for paleoliquefaction features are often made in banks of ditches or rivers, which may not be oriented optimally to intersect dikes.

4.2.2 characterization of sand blows and dikes in sectional view

Most sand blows of the 1811-12 earthquake have a well-defined set of internal relations and stratigraphy, shown in a somewhat idealized version in Figure 19. The main feeder dike is beneath the central part of the dome. The basal few centimeters of sediment

that vented onto the original ground generally is a fine to medium sand with a slight to moderate amount of silt, containing scattered centimeter-long round to irregular clasts derived from the underlying clay-rich strata cut by the dike. Sediment along the basal few centimeters grades up within a few centimeters to coarser sand with less silt containing numerous irregular 1- to 5-cm-long clay-rich clasts. The clasts are encased in clean, medium- to coarse-grained sand. The clasts are largest and most plentiful near the feeder dike. The basal part of the sand-blow deposit also contains numerous 1- to 3-cm long rounded lignite fragments and other low-density materials vented to the surface. These low-density materials originated from the source sand. Clasts from the cap occur almost exclusively in the lowermost quarter of vented material. Above this in the larger sand blows, away from the vent, is a much thicker zone (tens of cm) of very clean, generally medium- to coarse-grained sand that is nearly structureless except for suggestions of laminations of sediment. Higher yet, the sand grades upward to a mainly medium-sized sand. Here there are weakly to moderately developed planar to wavy laminations of fines and sand generally a few millimeters in thickness, which gently dip down and away from the central part of the sand volcano (Fig. 19A). Where sediment vented into swales on the ground surface, this sequence may be capped by a silt-rich stratum with organic debris, 0.5 to several centimeters thick; this cap may also contain multiple very thin (1-mm-thick) clay-rich layers (Saucier, 1989). The organic matter in the cap consists of small pieces of charcoal and wood. The organic debris and thin clay-rich layers formed in swales located both above the vent (Fig. 19A) and in depressions far from the mound of vented sediment.

Closest to where dikes vented onto the ground surface, there can be well-defined strata that dip steeply into the dike (Fig. 19A). These strata may contain relatively coarse-grained sediment. Next to these strata, in the lower and central part of the sand blow, there may be shearing and disruption that probably were caused by the forceful expulsion and boiling of sediment and water.

The overall fining-upward sequence of vented sediment, from the basal clast-bearing sand to the uppermost organic bearing stratum, represents the transition from the turbulent violent eruption very shortly after initial venting to the final ebbing flow from the vent onto the ground surface. The planar and wavy laminations probably represent weak variations in flow from the dike.

Dikes that formed in the clay-rich cap of the 1811-1812 earthquakes meisoseismal region almost invariably are sand-filled fissures that are steeply dipping (60° to 90°) and are mainly planar. In vertical section, dikes having widths exceeding several centimeters commonly are spaced from several meters to hundreds of meters apart.

Dike widths range from millimeters to several meters. Many of the widest 'dikes' are sand-filled fissures that were almost certainly caused by lateral spreading. Figure 20 shows a feature probably having such an origin; the lignitic silty clay stratum in the sand indicates the location of the top of the sand (S1) that flowed into the opening of the lateral spread. The upper sand (S2) probably was vented later during a following earthquake. (In contrast, often only little or no sand vents to the ground surface from the large space between blocks opened by lateral spreading.) Side-walls of many of the larger sand dikes throughout the 1811-12 earthquakes meisoseismal zone tend to be parallel to one another in vertical section, which also indicates a pulling-apart origin during lateral spreading.

Dikes about 15 cm or less in width are very common. Dikes in this width range normally become more narrow upward as illustrated in Figure 19A. The tapering may represent downwarping of the ground surface in response to sand at depth having been vented to the surface. At almost all places even isolated sand blows have vented through small, vertically planar dikes. The smallest dikes pinch together as illustrated in Figure 19B.

Within the uppermost meter or so, dikes cutting through the weathered portion of the clay-rich cap may branch irregularly upward into many smaller segments (Fig. 19C). Possibly pre-existing weathering planes of weakness cause a single large dike to branch into many small members. The clay cap typically contains a large proportion of montmorillonite. During dry years desiccation cracks extend a meter or more in depth. Pedogenesis has also developed a strong soil structure (pedons) in a thick B horizon near the surface.

Where larger dikes branch extensively (Fig. 19C), there may be only minor evidence of venting onto the ground surface. Apparently this network is effective in dissipating the energy of flow. Locally though, venting has excavated the highly fractured zone, leaving behind a widened dike at the top. This excavated zone may contain many clay clasts mixed irregularly in a matrix of sand.

Dikes that cut through the fine-grained cap generally are filled with a loose mixture of fine and medium sand and a minor amount of silt. Clasts of clay, some as long as 20 cm, may also occur but generally are not abundant. Elongate clasts tend to be parallel to sidewalls. The clasts were derived from the sidewalls and transported up the dike. The mixture of sand, silt, and clasts has a sharply defined contact with the sidewalls. Weak laminations within the sand and silt may parallel the sidewalls. Cross-cutting, vertically oriented zones of sand and silt within the dike are also commonplace. These probably represent episodes of venting either during separate pulses, or venting from different source zones at depth.

The finest constituents (fine sand and silt) have been winnowed from dike fillings at some sites of venting. Winnowed zones within the dike are commonly tubular and as much as several centimeters in width. Locally, winnowing extends several meters down into the dike. This winnowing probably took place by water flowing up through the dike during final phases of expulsion of water, following initial emplacement of the sand in the dike.

Many dikes that pinch together upward have a large proportion of silt and clay mixed with the sand near the top. Often it is unclear whether the silt and clay have invaded the dike by pedogenesis or whether the silt and clay were constituents of the originally intruded sediment. Dikes that taper upward are often of limited usefulness for paleoliquefaction studies, owing to difficulties in determining when the dikes formed.

Many variations of the relations shown in Figure 19 exist. One of the most common is a large amount of downwarping of the cap toward the dike. This downwarping tends to be most pronounced where a large amount of sand has been vented to the surface. It is not unusual that the cap be downdropped by more than 0.5 meters on one or both sides of the dike, and that the cap be otherwise faulted or severly deformed near the dike (e.g., Wesnousky and Leffler, 1992, Figs. 9, 12, and 14). Some scattered small tubular dikes can also be found in clay caps of the 1811-1812 earthquakes meisoseismal region. Holes that originated from decay of tree roots or from excavation by crayfish are ubiquitous, and doubtlessly were used as the conduits for small tubular dikes. These tubular holes through

the cap had a very minor role as conduits for venting, though, as compared to steeply dipping planar dikes. However, these holes possibly were preferred paths during the early phase of venting, and thereby controlled where hydraulic fracturing developed planar dikes. Small holes whose walls are defined by angular breaks, and which have a tortuous upward path, also are commonly observed conduits for sand venting during the 1811-1812 earthquakes. Another field example, in Venezeula, of where venting was localized in tubular (crab) burrows is reported by Audemard and de Santis (1991); this venting occurred in response to limited liquefaction during moderate earthquakes.

The preceding discussion has focused on characteristics of dikes that cut through a clay-rich cap that varies in consistency from very soft to brittle. Excellent descriptions and detailed drawings of tabular dikes that cut interbedded clay and sand strata during the 1989 Loma Prieta, California, earthquake (M 7) are in Sims and Garvin (1994). The dikes and sand blows that they describe generally are much smaller and represent less forceful venting than those of the 1811-12 earthquakes, yet the sediment relations in the dikes and sand blows in both regions are quite similar.

Locally, the cap in the 1811-12 earthquakes meisoseismal region is a very weakly cemented sand containing only a minor amount of silt and clay, with slight bonding from oxides of iron and manganese. The liquefaction features in the areas of weakly cemented sand caps appear to have been mainly large open craters, similar to those of the 1886 Charleston, South Carolina, earthquake.

4.2.3 characterization of sills in sectional view

Combinations of dikes and sills are also common within the nonliquefiable cap. Where sills are abundant, dikes generally are also plentiful. Sills form preferentially at three locales: (1) along the base of the cap, (2) along bedding planes and other horizontal planes of weakness in the cap and (3) beneath exceptionally dense, strong root mats. These three locales are illustrated in Figure 21.

Laterally extensive sills as thick as 0.5 m are commonplace along the base of the cap, especially if the cap is very flexible. An intruding sill can dome up a flexible, clay-rich cap having a thickness of as much as a few meters. Sills are also common within the cap where original horizontal sedimentary structures and planes of weakness have not been destroyed by weathering. Sills especially tend to form irregularly within thin beds of silt or sand sandwiched between clay-rich beds. Small branches from the main sill commonly intrude into the overlying clayey stratum, forming more sills and dikes. Clay-rich clasts may abound within the sill. The clasts have been transported many meters horizontally at many places, but clasts that have simply been detached and foundered vertically several centimeters are also very common (see Fig. 21). The shape of clay-rich clasts in the sills, generally angular, suggests a brittle or shattering mode of fracturing of the stratum from which the clasts were derived. Despite this pattern of fracturing, the clay-rich clasts and their source beds commonly have such a soft consistency as to permit very easy penetration of several centimeters by thumb pressure.

Sills at a depth of about a meter or less in a clay-rich cap can be quite wavy in vertical section. These sills can thin and thicken dramatically within a horizontal distance of a meter or less and produce blister-like bulges on the surface. In plan view, these bulges can

range from circular to very elongate. Sills can be as thick as 0.7 m near the surface. Such large thicknesses are less common at greater depths, except locally along the base of the cap. Sills very close to the ground surface generally seem to have formed beneath root-mats of grass and trees.

Figure 22A shows a commonly observed field example in which near-vertical dikes are connected to a laterally extensive sill. The sill has formed within a clay cap that has only incipient horizons of weakness. The sill is at least 25 m long but is only 10 cm thick. The sill more or less follows a single horizon in sectional view. The type of internal layering seen in this sill is commonplace. Individual laminae are composed of small pieces of lignite or fine-grained sand and silt. (See Figs. 22B and 22C.) Also common at this site and elsewhere are structureless sills containing many clay clasts in a sand matrix, as well as sand with graded bedding of clay clasts concentrated along the base.

Laterally extensive sills also tend to form in the upslope direction along the base of a cap at places where the base dips appreciably. Such sills especially occur along the margin of a clay-filled abandoned channel. A sill typically extends upslope to near the edge of the channel filling, to where the clay-rich cap is thinner, and there feeds into a steeply dipping dike which has vented onto the surface (M. P. Tuttle, Univ. of Maryland, written comm. 1993).

The exposure illustrated in Figure 23 shows another common type of field example in which sand dikes and sills cut the upper liquefied sands and the lower portion of the nonliquefiable cap. In the upper part of the liquefied sand (bed A, Fig. 23A), small dikes branch out from a large dike (feature 1), cut through the basal bed of the cap (bed B) at horizontal intervals of 0.5 to 1 m, and extend upward about 0.5 to 1 m. A few dikes and sills intrude to much higher levels (features 2, 3, and 4). At exposures nearby (not shown) dikes extend to the surface. Sand has vented to the surface to produce many large sand blows in the field adjoining the outcrop of Figure 23.

The dikes and sills shown in Figure 23A as features 1 through 4 contain clean, medium-grained sand. The edges of the intrusions are sharp in clay-rich beds such as beds C, D, and G. Locally, intrusions puncture the very soft clay with sharp angular turns and breaks that follow a haphazard path (features 2 through 3). Edges of intrusions are generally less distinct in beds of clean, permeable sand. Dikes commonly widen and terminate upward as flame-shaped structures (feature 4) in a permeable sand bed (bed H). Clay clasts may be present in lower portions of the structures.

The sill at the base of bed B, at the extreme right side of the figure, has an irregular contact along the top. Here the sill has corraded the base of the friable bed B. Small intact pieces of bed B have sunk into the sill, probably attesting to a very water-rich condition in the sill at the time of its intrusion. Such destruction of friable beds by sills is commonplace throughout the meisoseismal region, especially along the base of the cap. In regions of only marginal development of small dikes, sills along the base of the cap and within the cap are not observed at many places, but where present may help to serve as independent evidence for a seismic liquefaction origin.

Features labeled 1 through 4 in Figure 23 are interpreted to be earthquake-induced because (1) they are widely distributed over tens of kilometers, (2) they contain dikes and sills commonly as wide as 15 cm that suggest intrusion by large volumes of water-saturated sediment, (3) they contain clean, medium-sized sand containing large angular clay clasts

(which is evidence of forceful intrusion), and (4) artesian conditions are unlikely at these sites.

The dike shown as feature 5 has an uncertain origin (Fig. 23A). Three small dikes that were truncated at the contact of beds C and D were exposed in a 25-m section along the ditch but were not found in other nearby exposures of beds C and D. The dikes may represent pre-1811-12 seismic liquefaction. They contain, however, a large proportion of silty fine-grained sand, which does not suggest forceful intrusion at this site. Possibly they resulted from springs that formed near the base of a streambank or as slump-related features that formed soon after initial deposition of the host sediments.

Feature 6 (pseudonodules) is discussed in a following section.

Flame-shaped structures such as those of feature 4 have developed at many places within thick sand beds in the meisoseismal region of the 1811-12 earthquakes. Flame-shaped structures commonly have widths ranging from millimeters to about a third of a meter. Apparently the upper sand beds do not liquefy and, because of their relatively high permeability, perhaps in combination with an unsaturated condition, permit the energy of the pressurized water from beneath to dissipate within the large volume.

A form of a rather uncommon deformation feature (not shown) probably related to seismic liquefaction involves plastic deformation of silt and clay along the base of the cap. The lowermost 10 to 20 cm of the cap contains a convoluted mixture of severely disturbed, plastically deformed silt and clay, intruded by sand. Such convolutions probably take place only where extremely soft silt and clay lie directly on liquefied sand.

4.2.4 paleoliquefaction studies

Systematic paleoliquefaction studies were undertaken only recently thoughout the meisoseismal region of the 1811-12 earthquakes. This region has large terraces of late Wisconsinan and early Holocene age where the water table appears to have been very shallow since the terraces were formed (Wesnousky and Leffler, 1992). Thus, if very strong earthquakes occurred since early Holocene time, liquefaction features should be present in the geologic record. Definitive evidence for liquefaction predating 1811-12 has been found in the northern part of the New Madrid Seismic Zone (see Figs. 16 and 17) near Reelfoot Lake (Russ, 1979) and at a site about 30 km northeast of Reelfoot Lake (Saucier, 1991). Russ found that three earthquakes have induced liquefaction during the past 2,000 years, and on that basis suggested a recurrence interval of 600 years for liquefaction-producing events. Saucier (1991) estimated an average recurrence interval of 470 years for liquefaction-producing events in the past 1,300 years. Further south, in the southern half of the seismic zone, field work has uncovered evidence for three liquefaction-producing events the past 2,000 years (Tuttle and Schweig, in press). Whether or not these more southern episodes are correlative with those further north has not yet been resolved. Therefore, the upper limits for the magnitudes of these prehistoric earthquakes cannot yet be determined. Only the lower limits can be estimated, and these are the threshold values. The threshold magnitude is about M 6.4-6.8, on the basis of historical observations of liquefaction-producing events in the New Madrid Seismic Zone (Obermeier, 1988).

4.3 Wabash Valley Seismic Zone

Many small to slightly damaging earthquakes have occurred throughout the region of the Wabash River valley of Indiana and Illinois in the past 200 years. Seismologists have long suspected that the weakly defined Wabash Valley Seismic Zone (Fig. 16) could be capable of producing earthquakes stronger than the largest of record ($M \sim 5.5$; Hamilton and Johnston, 1990). A search for paleoliquefaction features has revealed good evidence for major prehistoric earthquakes.

The region for the main search was that part of the Wabash River valley along the central axis of the Wabash Valley Seismic Zone. Alluvium generally as thick as 10 to 30 m lies on bedrock. The valley contains expanses of low glaciofluvial terraces of late Pleistocene age. These terraces are mainly braid-bar deposits of gravel and gravelly sand. Inset into the Pleistocene terraces are slightly lower Holocene floodplains of finer point-bar sediment. The sand-gravel deposits of both braid bars and point bars typically are overlain by a 2- to 5-m-thick alluvial cap of sandy silt to clayey silt. Bordering the valley are extensive plains of silt and clay that contain patches of clean sand, laid down in slackwater areas during glaciofluvial alluviation. The water table is presently shallow (<3 m) and appears to have been so over large areas much of the time following glaciofluvial alluviation, on the basis of depth of carbonate leaching and B-horizon soil development in sandy and silty alluvium. This combination of a relatively shallow water table and widespread sand-rich deposits with an overlying fine-grained cap has provided an excellent opportunity for liquefaction features to form throughout much of the Holocene.

4.3.1 characterization of features

Hundreds of dikes have been found. Sills within the cap are sparse, even if thick sills occur along the base. These features occur both in Holocene point-bar deposits and in the late Pleistocene glacial outwash and slackwater deposits. Figure 24 shows the locations searched, sites where dikes were discovered, and sites of exceptionally large (widest) dikes. Virtually all sites shown on the figure have more than one dike and many sites have more than 10. Almost all the liquefaction sites are in actively eroding banks of rivers. The dikes are steeply dipping, tabular, and connect to a sediment source at depth. Many smaller dikes pinch together as they go up, and erosionally truncated dikes are also fairly common. Dikes filled with sand containing some gravel and silt are very common. Mainly sand was vented, though commonly with large quantities of gravel (Fig. 25). Where dikes cut through a thick clay cap without pronounced horizontal planes of weakness, it is not unusual that the dike width does not exceed a centimeter throughout a height of as much as 4 to 5 m. Widths as much as 15 cm or more throughout the height are very common and widespread in the region. Locally, though, in what is interpreted as meisoseismal regions of the prehistoric earthquakes, dikes have widths ranging from 0.7 to 2.5 m. There is generally a fining-upward sequence of coarsest material in the dikes. Within many dikes there are sharply defined, vertically intertwined and intersecting zones containing distinctly different grain sizes. In some places these zones can be traced to different source strata at depth.

Sediment vented to the surface extends as much as 40 m in width. Thicknesses of vented sediment of 0.15 to 0.2 m are not unusual. Most vented sediment fines upward and laterally, especially if gravel was vented. The vented sediment at sites bordering the Wabash

River generally lies on a paleosol and is buried beneath a 1- to 3-m thickness of overbank deposits, as illustrated in Figure 25. On slightly elevated terraces, where flooding has been rare, the vented sediment has been incorporated into the surface soil.

At some sites there is good evidence for more than one pulse of venting. This evidence is best shown at sites near Vincennes where there are large dikes for the event of 6,100 yr b.p. (Fig. 24), and is manifest as two fining-upward sequences of vented sediment. The lower pulse vented sand that fines upward to a thin silt layer; the upper pulse has abundant sand and gravel that fines upward. There is no evidence of a significant hiatus between the upper and lower pulses. Thickness of sediment vented from the lower pulse is much less than for the upper pulse.

The interpretation that sediments was vented from the dikes onto the ground surface rather than intruded as sills is based on several lines of evidence. Sills would cut irregularly across sedimentary horizons at some places (see Figs. 21 and 22), rather than always being confined to a single horizontal layer as in the Wabash Valley. Sills also would tend to follow the contact between sand and clay strata rather than lie on a paleosol, and sills probably would have some dikes branching up.

4.3.2 ages of dikes

On the basis of archaeological and radiocarbon dating, combined with stratigraphic and pedological characteristics of the sites, most of the liquefaction features in Figure 24 near the Wabash River resulted from a single earthquake about 6,100 years ago (Munson et al., 1992, 1994; Obermeier et al., 1993). Very large dikes with extensive sand blows from this earthquake are in the vicinity of Vincennes. Thus the epicenter was probably in the Vincennes area. Radiocarbon ages at widespread sites tightly constrain when the earthquake occurred. Munson et al. (1994) estimate the age of the 6,100 yr b.p. event is accurate within $\pm$ 200 years. Still, the evidence for two pulses of venting admits the possibility of more than one strong earthquake spaced very closely in time. Such close spacing of strong earthquakes happened in the nearby 1811-12 New Madrid earthquakes.

The next strongest earthquake in the Wabash Valley took place about 12,000 years ago. Again the largest dikes are approximately central to the regional distribution. A yet smaller event occurred about 3,000 years ago. Other earthquakes are represented by scattered dikes of late Pleistocene age, but the paucity of exposures having such large age precludes determining any regional pattern of sizes.

Bracketing the time when the dikes west of the Wabash River formed has not yet been done. However, the severity of weathering of vented material and in dikes shows that almost all the dikes have an age extending back thousands of years.

4.3.3 evidence for seismic origin

All aspects of the Wabash Valley dikes can also be observed in the 1811-12 New Madrid earthquakes meisoseismal region, which has a physical setting generally similar to that of the Wabash Valley. An earthquake-induced liquefaction origin is interpreted for the dikes of the Wabash Valley for the following reasons, considered in combination: (1) the dikes widen downward or else have walls that are parallel (agreeing with a lateral spreading origin); (2) dikes are approximately linear in plan view and exhibit strong parallel alignment

in local areas; (3) the dikes vented large quantities of sandy sediment to the surface; (4) material in the dikes fines upward and was transported upward; (5) bedding in some source beds is homogeneous, and the contact of source beds with overlying fine-grained sediment is highly disturbed in some places; (6) flow structures project upward from the source zones into the bottom of the dike; (7) many dike sites are in flat and topographically elevated landforms, located at least several kilometers from any high, steep slopes that might have existed at the time of formation of the dikes, and therefore could not have been induced by nonseismic landsliding; (8) other nonseismic mechanisms such as artesian springs that could produce similar features are not plausible at many dike sites because of the lack of topographic relief and the local geologic setting, (9) the size and abundance of the dikes along the Wabash River, the area where data are most complete, generally decreases with increasing distance from a core region of largest dikes (Fig. 24), and (10) large regions in the same geological setting, with liquefiable sediment, have been searched far north of the Wabash Valley Seismic Zone and have no dikes (Munson et al., 1994). Detailed discussion of these factors is in Obermeier et al. (1993).

Sills within the cap such as those illustrated in Figure 22 are sparse in the Wabash Valley region. I have observed elsewhere a similar lack of sill development in the cap. For example, in the banks of the Chehalis River, near Centralia, Washington (Fig. 26), there are many dikes exposed that doubtlessly were induced by the 1949 earthquake of Olympia, Washington (M 7.1). The field setting is that of a thick (6-8 m) cap of stiff clay with no horizontal planes of weakness that overlies medium sand. The dikes along the Chehalis River have a tabular morphology that strongly resembles many in the Wabash Valley, in that very thin (1 cm) dikes commonly extend upward several meters or more before pinching together.

4.3.4 paleoseismic implications

Historical earthquakes in the Wabash Valley, with magnitudes as high as M~5.5, have not been reported as having caused liquefaction. Undoubtedly the paleoearthquakes in the Wabash Valley far exceeded the magnitude of any historic events because of the large areal distribution of liquefaction effects and the large size of some of the dikes. Magnitude of the 6,100-year-old event is estimated to be M~7.5 (Obermeier et al., 1993). The technique for estimating magnitude is discussed in the section below dealing with paleoearthquake magnitudes.

4.4 Coastal Washington

Tidal marshes buried in coastal Washington and nearby coastal Oregon record episodes of sudden submergence accompanied by tsunamis during late Holocene time; these episodes have been ascribed to great (M~8 to 9) earthquakes on the basis of the large region along the coast that appears to have submerged simultaneously (Atwater, 1987, 1992; Darienzo and Peterson, 1990; Nelson, 1992). They discovered no direct evidence of strong shaking to corroborate that seismic shaking accompanied the episodes of submergence, however. These inferred earthquakes were interpreted to have originated by rupture along the thrust fault where the oceanic (Juan de Fuca) plate is being subducted beneath the continental (North America) plate--the Cascadia subduction zone (Fig. 26).

The possibility of recurrent great subduction earthquakes in coastal Washington and Oregon was first suggested from geophysical comparison of the Cascadia subduction zone with subduction settings worldwide (Heaton and Hartzell, 1987). However, no strong Cascadia earthquake has occurred during the time of written history in the Pacific Northwest, some 200 years. Modern seismicity on the subduction zone is limited to scattered, small earthquakes, none with thrust mechanisms in the region of sudden submergence.

Atwater (1992) inferred at least two times of coseismic subsidence when great earthquakes struck the coast of Washington State, including the region around the Columbia River valley, during the past 2,000 years. Strong evidence indicates that one event was about 300 years ago, and less widespread evidence indicates that another event occurred between 1,400 and 1,900 years ago. The portion of the thrust fault that ruptured and provided energy for seismic shaking was most likely a small distance offshore (few tens of kilometers), on the basis of the location of the subsided zone (Atwater, 1987), heat-flow data (Hyndaman and Wang, 1993), and strain data (Savage and Lisowski, 1991).

The inferred earthquakes would be expected to have caused such strong shaking as to have produced abundant liquefaction features near the coast, even in sediments having moderate to low susceptibility. To verify occurrence of the earthquakes, I initiated a search for liquefaction features in cutbanks of islands in the Columbia River.

4.4.1 Columbia River features

Many large islands were searched between the towns of Astoria and Portland (Fig. 26). These islands originated as braid bars on a grand scale. The islands are flat, poorly drained, and swampy. Large portions are submerged during the highest tides. Strong currents and wave pounding are severely eroding many islands and as a result have sculpted clean, vertical banks as high as 2 meters, which extend from water level to the top of the banks. Significant areas are also being cleaned in plan view by tides.

The banks of the islands between Astoria and Longview expose mainly soft clay-rich silt deposits (Fig. 27). Age at the base of the exposed clay-rich cap is less than 1,000 and more than 600 years on most islands, on the basis of radiocarbon ages of fossil marsh plants (genus Scirpus) found in growth position and now just above the level of low tide.

Regional stratigraphic control of sediments exposed on the islands is excellent. About 1.5 m below the top of the banks is a tan horizon with a thickness of a few centimeters. This horizon is exceptionally rich in volcanic ash. About 10 to 15 cm lower is a blue-grey horizon, generally several centimeters thick, also rich in ash. Very locally, rounded pumice clasts as large as 5 cm in diameter occur in the lower ash horizon. Chemical analysis shows that the ash and pumice have minerals and elements identical with those of an eruption from Mount St. Helens, in A.D. 1480-1482 (C. D. Peterson, Portland State Univ. written comm., 1992). Therefore, the radiocarbon ages on fossil marsh plants and the ash data show that the sediments are old enough to record liquefaction associated with the 300-year-old downdropping event, but probably are not old enough for the event of 1,400 to 1,900 years ago.

At many places sand is exposed immediately beneath the clay cap. Alluvium that makes up the islands, generally thick, fine- to medium-grained sand, probably typically exceeds 100 m in thickness. Conditions on many islands are nearly ideal for formation of

large liquefaction-induced features. Not only is the cap thin, but the ground-water table has almost certainly been within a meter or so of the ground surface since the islands formed. The tidal range at these islands is about 2 to 2.5 m, and high tides inundate parts of the islands and doubtlessly have done so for at least several hundred years.

More than three hundred dikes have been found along 9 km of vertical banks in scattered islands upstream as far as Deer Island (Fig. 26). At some places the tabular nature of the dikes is exposed in plan view. Maximum dike widths and abundance of dikes tend to decrease in the upstream direction. Figure 27 illustrates relations observed at many islands. A thin sand sheet lies on a weakly developed, very soft soil that is about 1 m below the present surface. Locally, the upper few centimeters of the soil is contorted by small (cm-sized) folds and other soft-sediment deformations. The sand sheet is 1 to 4 cm in thickness and is as wide as 10 m. The sheet connects to a nearly vertical, narrow planar dike that widens downward markedly and connects to sand beneath the clayey cap. Width of the uppermost 5 to 15 cm of almost all dikes is only several millimeters or less. Width near the base of the cap is generally less than a few centimeters. Where pits were dug along the bottom of the cap, flow structures in the sand could be observed going into the base of the dikes. Pits also exposed sills as thick as 0.1 m running along the base of the cap. Sills also have intruded into the cap.

All dikes are interpreted to have been caused by the coastal downdropping earthquake event about 300 years ago for the following reasons: (1) the radiocarbon ages of sticks along the surface of venting agree with the 300-year downdropping event; (2) ages of trees (determined from tree rings) rooted in sediment above vented sand have maximum values (about 200 years) that are reasonable for the 300-year old downdropping event; (3) dikes generally increase in abundance toward the coast; and (4) maximum dike sizes (widths) increase toward the coast. The 1-m thickness of silt and clay above vented sand is interpreted to have been deposited following the regional downdropping from the subduction zone earthquake 300 years ago. This 1-m thickness agrees well with the estimates of coastal tectonic submergence (Atwater, 1987; 1992; Darienzo and Peterson, 1990).

The 1- to 4-cm-thick sheet of vented sand may be exceptionally thin because of the tidewater action, or because of subaqueous venting. The surface of venting is submerged at moderate to high tide. Tidewater flows fast in this area, so any large cones of sand initially vented to the surface could have been beveled off and the sand scattered over a large area.

Many dikes are so narrow at the top as to be hardly distinguishable. This same relation can also be observed infrequently in dikes in the Wabash Valley and in dikes in the 1811-12 New Madrid earthquakes' meisoseismal region. The cause for this pinching is not known but may represent venting of a very water-rich mixture of sand and water through an exceptionally soft cap that closes partially after venting. The widest dikes (as much as 30 cm) on the Columbia River islands are interpreted to have formed by lateral spreading, because the sidewalls appear to be parallel.

It has been suggested to me by others that the properties of the soft silt cap on the islands may have prevented dikes from forming far inland; they suggest, instead, that only sills formed as a result of severe liquefaction over large regions. The basis for this suggestion is the presence of numerous, thin, sill-like features along the base of the cap, which have been observed in samples collected in 10-cm diameter tubes. I believe that such

an interpretation is unlikely for two reasons: (1) I have never observed in other geographic-tectonic regions where extensive formation of sills was not accompanied by dikes, and (2) the mechanics of forming sills by severe liquefaction over a large region, without also forming dikes, does not seem plausible. In order to form sills over a large area, the cap must be lifted to provide space for the intrusion. The force required to lift the cap must at least equal the weight of the cap. The simplest of calculations shows that the uplift force to raise a 1-2-m cap is at least an order of magnitude higher than the tensile strength of a soft cap. Therefore, extensive development of dikes should occur. I can envision other mechanisms whereby small sills would form without liquefaction, however, as a result of seismic shaking.

4.4.2 strength of prehistoric shaking

Subduction earthquakes can have very large variations in shaking characteristics, offering the possibility of an especially long duration of shaking at very low frequencies. Such uncertainties cause difficulty in interpretations of the strength of prehistoric shaking. Still, significant conclusions can be drawn for the earthquake of 300 years ago. Small dikes possibly with venting in the Columbia River islands appear to go inland as far as 90 km. These dikes very likely formed at an acceleration level on the order of 0.1-0.2 g (Obermeier, 1994). These accelerations accord with both theoretically and statistically derived accelerations from seismological models for the scenario of a $M \sim 8$ subduction earthquake slightly offshore (Geomatrix, 1994; Youngs et al., 1993), although the uncertainties in the seismological models are relatively large.

The lack of abundant very wide dikes throughout islands of the lower Columbia River valley also supports the seismological models noted above, which predict that exceptionally strong shaking should not extend very far onshore. Even though severe erosion of some islands has probably removed evidence of dikes wider than 30 cm at some places, there are many locales where erosion probably has been slight. (The widest observed dikes, 30 cm, are quite small in comparison to the width of dikes commonly found in the meisoseismal region of the 1811-12 New Madrid earthquakes or in the Wabash Valley.) Another plausible model consistent with observed liquefaction effects in the Columbia River islands is a subduction earthquake having a long duration of shaking at moderate to low peak accelerations and at an exceptionally low dominant vibration frequency (perhaps exceeding a few Hz). The fine sands that underlie the Columbia River islands are so thick and have such a low permeability that pore pressures would not dissipate between cycles of shaking, even at an extremely low frequency. In addition, the thick alluvial deposits of the Columbia River valley probably strongly amplify bedrock accelerations, irrespective of vibration frequency (Dickenson et al., 1994). Therefore the sand deposits of the Columbia River should be especially susceptible to forming liquefaction features during a long duration of shaking, even at low to moderate accelerations and exceptionally low frequencies.

4.4.3 ancient marine terrace features

Many ancient fluidization features have been identified in late Pleistocene marine-terrace deposits. The fluidization features can be seen for a span of 500 km along the coast extending from central Washington to near the California-Oregon boundary (Peterson et al., 1991; Peterson, 1992). These terraces have been variably uplifted as much as a few tens of

meters. The features are well exposed in cliffs cut into the terraces by ocean waves. The features are of particular interest because they admit the possibility of a long continuing record of subduction-zone earthquake shaking near the coast. The methodology for interpretation of an earthquake liquefaction origin is instructive.

Source beds for the fluidization features include beach sands and sandy gravels, and lagoonal sands. The features reported by Peterson include clastic dikes as high as 5 m. Dikes are filled with clean sand or gravelly sand at almost all places. Dikes are as wide as a meter in scattered locales. At a few places dikes have penetrated upward into dune sands or have cut through lagoonal muds and peat. Sills are particularly abundant. Sills commonly extend beneath lagoonal muds and peats; small, steeply dipping dikes branch off from these sills at many places and cut up into thin (less than 0.5 m) strata of low-permeability at the surface. The largest sills are as much as a meter in thickness. Even thin sills can extend far laterally.

The possibility that the fluidization features were caused by wave-action that induced liquefaction must be considered because the terrace deposits were laid down under shallow marine or shoreline conditions. Storm waves can impose significant shear stresses on the ocean bottom sediments, even where the water depth exceeds 60 to 70 m (E.C. Clukey, geotechnical engineer, Exxon Corp., written commun., 1992). Wave-induced cyclic shear stresses are thought to cause liquefaction in sands and granular deposits in a manner analogous to seismically induced liquefaction (Nataraja and Gill, 1983). The action of storm waves pounding on beaches also seems plausible as a mechanism for forming fluidization features. For the fluidization features in the marine terraces of coastal Oregon and Washington, though, the mechanism of wave-related liquefaction probably can be eliminated at some sites because dikes extend up into dune sands where wave action seems unlikely. Additionally, some dikes and sills cut lagoonal deposits at places that probably would have been protected from wave action. Significant artesian pressures at these lagoonal sites also are implausible. Thus a seismic liquefaction origin seem probable for some of the features along the coast.

5. FEATURES GENERALLY OF NONSEISMIC OR UNKNOWN ORIGIN

Features that form in a wide variety of environments are considered in this section. The discussion includes both chemical processes related to weathering, and physical processes as diverse as slumping, freezing behavior, and flowing water.

5.1 Terrestrial disturbance features

A wide variety of ground-disturbance features similar to those caused by seismic liquefaction form above the water table. A hydrological or a geotechnical engineering perspective is often helpful for interpreting origin.

5.1.1 nonseismic sand boils

Features suspected to have a seismic origin should be examined first with the perspective of determining whether artesian conditions were plausible at the site. This is the basic approach that was taken for evaluation of the craters in coastal South Carolina, where it

was shown that nonseismic sand boils were implausible because the craters had formed along the crests of ridges.

Nonseismic sand boils that abound in parts of the meisoseismal region of 1811-12 New Madrid earthquakes are especially instructive. Flooding causes strong artesian flow beneath man-made levees that parallel the Mississippi River. These artesian conditions cause abundant sand boils to form in nearby lowlands every few years (Kolb, 1976). The sand boils are generally restricted to within 0.5 to 1 km of the levees. (It should be noted that natural levees should not cause artesian conditions, because of the many breaks in the levees.)

The cone-shaped external form of the nonseismic sand boils along the levees is similar to that of solitary sand blows of earthquake-induced liquefaction. Internally though, differences occur because artesian flow normally starts slowly and steadily increases, in contrast to the much more sudden, violent flow that typically accompanies early phases of venting of earthquake liquefaction. Evidence for this large difference in flow rates is in the sedimentary record. The basal portion of sediment vented by nonseismic sand boils along the Mississippi River levees typically is significantly finer than that of seismic sand blows. The sand boils generally are underlain by a discrete zone of silt to silty very fine sand that ranges in thickness from a few millimeters to a few centimeters. Going upward in sand boils, there are planar strata of silty sand to clean sand that dip away from the central part of the sand boil; the individual strata are much more discretely defined, more uniform in thickness (typically about 1 cm) and have a more narrow range of grain sizes than sediment vented in response to earthquake liquefaction. Probably the individual layers in sand boils represent variations in the level of flood waters.

Artesian flow beneath levees along the Mississippi River frequently forms sand boils that cut through a thin (generally < 1 m) clay-rich cap. The sand boils have more or less circular vents whose diameters generally range from a few cm to greater than 1 m. Excavations show that numerous small sand-filled fissures and tubes in the cap can connect sand directly below the cap to the main dike of a sand boil; clay clasts derived from sidewalls occur within the dikes. The upper part of the main dikes can contain stratified deposits of sand layered with other materials, as much as 1 m or more below the original ground surface. These stratified deposits probably consist of material that fell from the surface into a hole with water. In contrast to the circular dikes for artesian sand boils, earthquake-induced venting normally takes place through tabular fissures. Therefore, tabular sand-filled fissures that widen downward and extend horizontally for tens to hundreds of meters are probably dikes associable with earthquake-induced liquefaction, although the possibility of a nonseismic landsliding origin (discussed below) must be considered.

Where the cap in the meisoseismal region of the 1811-12 earthquakes is very sand-rich and friable, both nonseismic sand boils and sand blows typically form more or less circular craters at the surface. Craters from both can be as much as a meter in diameter. I am unaware of definitive sediment relations to always ascertain a seismic or nonseismic origin for individual craters. Therefore the regional pattern of occurrence may be critical for interpretations.

5.1.2 streambank landslides

Slumps (of largely rotational movement) are commonplace along streambanks for both seismic and nonseismic conditions. Sliding blocks (of dominantly horizontal movement) can develop in special nonseismic field settings and can resemble seismically induced lateral spreads. I judge that generally it is not worthwhile to attempt to assign seismic or nonseismic origin to prehistoric slumps along actively eroding streambanks; there are too many uncertainties about the physical setting when such an ancient slump formed. For example, questions crucial to interpretation include the initial ground slope and the possibility of a streambank having been undercut by an eroding stream. These questions may be virtually impossible to resolve. Slumps in loose, fine sands are especially difficult to interpret because they may be prone to static liquefaction even on relatively gentle slopes (Lade, 1992).

Very thin sand layers bounded above and below by low-permeability materials can slump whenever river levels drop rapidly (Springer et al., 1985). This same sediment may move as a lateral spread during earthquake shaking. For example, large blocks of clay bedded with thin, laterally continuous sand lenses ruptured as far back as 200 m from a free face during the 1964 Alaska M 9.2 earthquake (Seed, 1968). Seed interpreted the failures to have initiated in the thin sand lenses.

Recent studies show instead that failure at some of the Alaskan sites initiated during the earthquake through sensitive ("quick") clay layers in the blocks (Updike et al., 1988). Large slab-like blocks of sensitive clay also commonly fail under static conditions, however (Karlsrud et al., 1984). Proving a paleoseismic origin for ancient block failures along stream banks in sensitive clays or in clays with thin sand beds has never been done to my knowledge, and probably would be a formidable task.

Large blocks of alluvium that slip nonseismically along buried erosional surfaces on clay-rich shales are not unusual. This type of failure is enhanced where the erosion surface dips toward a deep river. Good examples of this type of failure are located along the Ohio River, where the shales have internal friction angles as low as 7° to 8°. In contrast to the process of earthquake-induced liquefaction, the large blocks seem to move slowly and there is no evidence of sudden or forceful venting of sediment (Obermeier et al., 1993).

Nonseismic sliding blocks can form steeply dipping fissures through a clay-rich cap. These breaks conceivably could be filled with cohesionless sediment that flows into the fissure from beneath the cap, which could resemble dikes formed by earthquake-induced liquefaction. A test for seismic origin is provided, though, if dikes can be found on alluvial plains far from any significant slopes. Another criterion for origin is to place limits on the maximum artesian head; if this head is sufficiently low, a seismic origin is likely (Obermeier et al., 1993).

One more test for landslides of suspected seismic origin is the regional pattern of sizes and ages (Jibson and Keefer, 1988; 1989). Landslides far from active streambanks, in more stable settings, also can be analyzed using geotechnical engineering procedures to interpret the liklihood of seismic triggering (Jibson, companion paper in this document).

5.1.3 ground disturbance by trees

Many Quaternary beach sediments of the southeastern United States contain evidence of ground disturbance by trees. Tree roots commonly penetrate the sand-rich cap to a depth of 2 to 3 m. When the roots decay, large holes develop that later fill with sand. Many now display poorly defined layers of clay-mineral segregation that result from weathering; however, the fill sediment has neither the well-defined laminar bedding nor the underlying graded zone of sediment that characterizes filled seismic craters.

The beach deposits also contain fairly widespread evidence of pits that were excavated by root mats of trees as the trees were thrown down (perhaps by hurricanes). Sediment in these pits typically does not have the orderly progression of clast sizes present in the lower part of the liquefaction-induced craters (Fig. 14). Pits excavated by thrown trees sometimes can be distinguished from liquefaction-induced craters by the absence of feeder dikes or by the absence of sediment from depth in the pit. Verification that sediment has been introduced from depth may require analysis of mineralogical, weathering, and grain-size data (Gelinas, 1986).

Roots from thrown trees can also form tabular breaks in a clay-rich cap. Locally the breaks can be filled with sand, gravel, and other sediment dragged into the break as the root is pulled from the ground. However, the dragged sediment tends to be arranged much more haphazardly and have a much larger range of grain sizes than an intrusion formed by seismic liquefaction.

5.1.4 mima mounds

Mima mounds (sometimes called prairie or pimple mounds) have been interpreted as having a seismic origin in many geographic areas (Berg 1990); however, seismicity has never been observed to have produced features closely resembling mima mounds (Saucier, 1991). Mima mounds occur through a large part of the meisoseismal region of the 1811-12 New Madrid earthquakes. Here the mounds are domes of silt or sand-rich materials that are generally less than 30 m in diameter and 1 m high. In exceptional cases the domes are as much as 1.7 m high but have diameters of only 10 to 12 m. The mounds have essentially the same texture as the underlying sediment. Soil development in the mounds is strong, indicating an age of thousands of years. The origin(s) of the mima mounds in the vicinity of the 1811-12 earthquakes is not known. In many upland areas, though, the mima mounds are formed on nonliquefiable deposits and therefore are not of earthquake origin. Mounds on alluvial lowlands can be identified as not resulting from earthquake liquefaction if excavation shows an absence of vents to connect the mounds to underlying source beds (Fuller, 1912, p. 80).

Mima mounds can usually be distinguished from sand blows on aerial photographs. Mounds typically show regularity of spacing, alignment, and size (Fig. 28). In contrast, sand blows are typically more irregularly spaced, have widely differing sizes (heights and diameters), and are not aligned along such precisely defined curves. Comparison of sand blows formed on point-bar deposits (Fig. 18) with Figure 28 illustrates the contrast.

5.2 Features formed in subaqueous environments

It is not possible in this chapter to describe and discuss a great number of features, mainly syndepositional in origin, that can also be triggered by seismic shaking. Only some of the more common types, mainly formed in fluvial and near-shore marine situations, are discussed herein. For a more complete overview of the myriad possibilities, the reader is referred to Allen (1982), Jones and Preston (1987), Einsele et al. (1991), Reineck and Singh (1980), Mills (1983), Lowe and LoPiccolo (1974), Lowe (1975), van Loon and Brodzikowski (1987), and van Loon (1992).

Four types of features are considered below: (1) load structures in muds; (2) water-escape structures; (3) sheet slumps, warped bedding, and recumbent folding; and (4) bedding caused by turbidity flow. Generally it is impossible to assemble compelling evidence for a seismic versus nonseismic origin for these features.

5.2.1 load structures in muds

Any plastic deformation of mud almost always occurs soon after deposition. The deformation generally is triggered because the rapid deposition of sand above very soft, clay-rich sediments causes buildup of pore-water pressure and gravitational instability (Dzulynski and Walton, 1965; Allen, 1982; Brodzikowski et al., 1987). Plastic deformations seem to be most abundant where rivers carry much sand, silt, and clay; settings where rivers debouch into lakes are also favorable. Montmorillonite-rich clays seem to enhance the deformations, because of the exceptional ability of montmorillite to absorb water and become extremely soft.

Especially commonplace in the geologic record are soft-sediment deformational features known as "load-casted" or simply "load" structures. Load structures are bulbous bodies of sandy or silty material that intrude downward into underlying weaker, finer grained muddy sediment. The severity of deformation is controlled by two factors: the difference in densities between the two adjacent layers, and the weakness of the underlying layer. Sand deposited rapidly over water-saturated, extremely soft mud is ideal for formation of load features. Two types of load structures are prevalent -- pseudonodules and load-casted ripples.

Pseudonodules form when overlying sandy or silty sediment becomes detached and sinks to become isolated kidney-shaped bodies encased in the underlying mud. Pseudonodules generally occur laterally adjacent to other undetached load structures (Allen, 1982, p. 359-360). Pseudonodules have been produced experimentally in the laboratory by hammering a container in which sand overlaid water-saturated, very soft clay (Kuenen, 1958; see Fig. 29). Sims (1975) correlated pseudonodules found in modern lake sediments, similar to those produced by Kuenen, with known earthquake events.

In the case of load-casted ripples, sandy or silty intrusions form because of the unequal loading of migrating ripples of sand on a mud substratum. Load-casted ripples show progressively deformed radial internal lamination caused by the rotation of the ripple cross-laminations as the ripples sink (Dzulynski and Walton, 1965, p. 146-149). The asymmetry reflects current direction, as illustrated in Figure 30. The development of load-casted ripples requires local deformation that is synchronous with deposition of overlying sand, and therefore load-casted ripples cannot likely be related to earthquake events.

The distinction between possible earthquake-induced load structures and those produced by rapid sedimentation is illustrated in a ditch exposure in the meisoseismal region of the 1811-12 New Madrid earthquakes. The section in Figure 31 shows clays interbedded with layers of sand that are apparently related to intermittent deposition in a water-filled swale. Small, delta-like sand bodies formed convex-upward sand lenses containing climbing ripple cross-laminations. The lenses are coarser upward, fine toward the edges, and are laterally adjacent to layers of pseudonodules (25-50 cm long and 5-25 cm wide) made up of similar grain sizes. The base of each sand lens has load structures, including load-casted ripples. The load structures make up a greater percentage of each sand lens as it thins toward the edge (see north-south view of Fig. 31). Detailed discussion of these sedimentary structures is in Obermeier et al. (1990, p. 35-38). The load structures in Figure 31 are interpreted as synsedimentary in origin and not as earthquake induced on the basis of the following criteria: (1) both the pseudonodules and load-casted ripples are gradational into the sand lenses, with the sense of development related to flow direction; (2) several layers of pseudonodules are laterally equivalent to largely undeformed sand lenses; and (3) the recurring conditions of sedimentation (rapid progradational deposition of sand over soft clay) were conducive to this type of soft-sediment deformation. Although load structures such as these may be formed by earthquakes, their vertically repeated occurrence in this sequence (as shown also by Allen, 1982, Figs. 9, 10; or Coleman and Prior, 1980, Figs. 15, 21, 22, and 32) within what was obviously a short time span argues for a depositional origin.

5.2.2 water-escape structures in granular sediments

The water-escape features discussed below, listed in order of generally increasing size, include dish structures, pillars, and convolute laminations, (Pettijohn and Potter, 1964; Lowe and LoPiccolo, 1974). Also included in this class are ball-and-pillow structures in which large pseudonodules of sand have foundered in sand (as shown in Pettijohn and Potter, 1964, Plate 100 A). These features can develop within a time frame either shortly after or long after initial deposition, in response to a generally upward flow of water through granular deposits (Lowe and LoPiccolo, 1974). Laminar flow by seepage may be adequate to form small features such as dishes, but turbulent flow by fluidization is required for many others (Lowe and LoPiccolo, 1974).

In vertical section, dish structures appear as thin, dark-colored, subhorizontal flat to concave-upward laminations (Fig. 32). Individual dishes range from clean sharp lines as thin as a feather's edge to diffuse zones up to 2 mm thick. Widths can be as much as 50 cm (Lowe and LoPiccolo, 1974). Dishes appear to form as upward moving water locally flows beneath laminations of lower permeability and escapes by horizontal flow. The finer grains, such as clay, mica, and organic grains, are filtered out and become trapped within the lower permeability zone.

Pillars are circular columns or sheet-like zones of structureless or swirled sand, sometimes bounded by dark laminations, that cut steeply through sand ranging from structureless to laminated (Fig. 33). These features range from tiny vertical tubes less than a millimeter in diameter to large flame structures more than a meter across and several meters in height (Lowe and LoPiccolo, 1974). These features form from a localized fluidization of the sediment.

Convolute bedding is the name given to a laterally extensive series of more-or-less regular folds (Fig. 34), which are developed either throughout or confined to the upper part of a single sedimentary unit (Allen, 1982). As Allen describes, folds increase in wavelength with increasing thickness of the bed or deformed zone. Strong asymmetry and recumbent folding are rare. Convolute bedding can develop at the top of sand units as thin as 15 cm (Lowe, 1975) and thicker than 5 m (Lowe and LoPiccolo, 1974). The origins of convolute bedding are unclear but probably relate to a variety of mechanisms (Lowe, 1975). Lowe notes that convoluted sediment is typically somewhat finer grained and more clay rich than subjacent sand; formation of convolutions in sand beds may be caused more by instability of the subjacent sand rather than by fluidization of the convolute-bedding zone.

Figure 34 shows field relations commonly observed between dish structures, pillars, and convolute bedding. I have observed all these features and relations in proximity to dikes at sites of earthquake-induced liquefaction.

Ball-and-pillow structures, in which kidney-shaped bodies of sand, locally slightly silty, have foundered into a cleaner sand are abundant in many glaciofluvial deposits. The foundered bodies have lengths ranging from centimeters to tens of centimeters. Clearly the features readily form very soon after deposition of the host sediments. Seismic shaking can also trigger ball-and-pillow features (Ringrose, 1989).

5.2.3 sheet slumps, warped beds, and recumbent folds

Features such as sheet slumps, and warped beds (Allen, 1982) and recumbent folds (Allen and Banks, 1972; Sims, 1973; Owen, 1987) are well represented in the geologic record. Sheet slumps tend to form in thin, laterally extensive deposits of silt and sand interbedded with mud. The mode of failure is mainly translational movement of a sheet-like body down a very gentle slope. Slight to severe warping and local thrusting may develop in the failed sheet. Sheet slumps range in thickness from a few tenths of meters to greater than 100 m (Allen, 1982). Lacustrine and marine deposits normally host the slumps. Studies in modern environments show that huge sheet slumps can develop on subaqueous slopes of one percent or lower (Allen, 1982). Oversteeping or earthquake shocks are often invoked to explain sheet slumps.

Thin beds of alternating mud and cohesionless sediment can also be warped by earthquakes, especially in strata near the surface. Audemard and de Santis (1991) observed that during a moderate earthquake, warping developed within the uppermost 0.2 m where mud overlaid a thin sand stratum. Sims (1973) reported the occurrence of low-amplitude folds in the uppermost 4 to 5 cm of lake sediments (mud with very fine sandy laminae and partings) and interpreted the folds to have developed in response to a Richter magnitude 6.5 earthquake that had occurred locally. Load structures and recumbent folds were also developed in the muds. Sims found similar features in buried strata, and showed that the buried features were synchronous with previous historic earthquakes. Similarity of morphology in the same types of source sediment played an important role in his arguments.

5.2.4 turbidity flow features

A turbidite is a sequence of deposits produced by the flow of a sediment-water mixture known as a turbidity current. Many turbidites are thought to be caused by huge submarine landslides. The model sequence of deposits going upward is (1) a thick bed of structureless sand possibly with some gravel that fines upward, (2) beds of sand with parallel and ripple laminations, and possibly beds with convoluted laminae, (3) thin beds of silt and sand with parallel laminations, and (4) a bed of mud. The many variations found in nature are discussed in Allen (1982).

Widespread turbidites are very common in marine sediments (see numerous articles in the journal edited by Cita and Lucchi, 1984). It is often tacitly assumed that such a distribution strongly suggests a seismic origin to turbidites and warrants the name 'seismites.' Although a widespread synchronous distribution is suggestive of seismicity, other mechanisms such as storm-induced wave trains or tsunamis can be responsible. An excellent example of how turbidites can be used in conjunction with other evidence for tectonism (regional downdropping) is given in Adams (1990). (See accompanying text by Jibson for discussion of seismic versus nonseismic origin of turbidites.)

5.2.5 paleoseismic examples

Data showing the regional pattern of types, sizes, and abundance of features generally is required to develop compelling evidence for a seismic origin for the types of features described in this section. This approach for test of origin is quite similar to the one used for interpreting an earthquake-induced liquefaction origin. Proving widespread development of deformed sediments at the same time in fluvial deposits is extremely difficult; proving such development in lakes, especially deep lakes, can be more tractable.

An illustrative example is given by Ringrose (1989). Features of probable seismic shaking origin were found at widespread locations in sediment in a late Quaternary glacial lake, located in Scotland. The sediment consists mostly of laminated silt and sand. Deformation features developed in two episodes about 10,000 years ago. The features are restricted to well-defined horizons of very large areal extent. The sediments are now drained, exposing sites for detailed viewing of the styles of deformation. Figure 35 shows how the styles vary from most severe (Fig. 35A) to marginal (Fig. 35D). The most severe deformations are centrally located in a geographic sense, and are characterized with the 'fault-grading stratigraphy' of Seilacher (1969). This stratigraphy refers to four-fold sequence, going from the top down: (1) completely fluidized sediment, (2) partially coherent sediment layers, (3) faulted layers, and (4) undeformed sediment. Evidence of deformation in Figure 35D is so slight that beds are only gently warped, and there is very minor evidence for fluidization.

In a study in eastern Canada, Adams (1982) has reported the presence of thin contorted zones within silt and clay varves of early Holocene age. The contorted zones were synchronous at widely scattered glacial lake sites, and there was a crude regional pattern with greatest deformations at the center. Thus, a paleoseismic origin was interpreted.

Morner (1985) has reported a similar type of finding in glacial lake varves of early Holocene age in Sweden; association of deformed varves with tectonic faulting, fracturing, and slumping led to a seismic interpretation.

Seismicity can also cause a short burst in the rate of increasing sedimentation. Doig (1986) has suggested that undeformed silt horizons in widespread lakes were caused by prehistoric earthquakes in eastern Canada. An important element in interpretation was the presence of the silt horizons containing distinctive chemical imprints within normally organic-rich deposits; these same relations were documented for a historic earthquake.

5.3 Features formed by weathering

Distinguishing liquefaction features from those of weathering origin can be difficult where weathering has been severe. A wide variety of features produced by chemical weathering in the southeastern United States mimic those caused by earthquake liquefaction (Obermeier et al., 1990). The discussion below concerns features that are regional in occurrence, but the concepts are applicable to sediments in many subtropical areas. The discussion focuses on the following: (1) E-horizon tongues and (2) BE or fragipan soil horizons.

A loose, clean, white sand blanket covers large regions of the southeastern United States where the ground surface is underlain by sandy sediments of barrier beach and nearshore marine origin, Pleistocene to Tertiary in age. The white sand underlies a 0- to 15-cm-thick, dark-gray A horizon. This white sand resembles vented sand but is a pedogenic E horizon that has formed by severe weathering and leaching of the underlying sandy sediment (Gamble, 1965). Clays and labile minerals have been removed from the E horizon, and weathering products have been deposited in the underlying B horizon. The boundary between the E and B horizons is commonly abrupt and irregular and is characterized by narrow, near-vertical tongues of the white E horizon that penetrate downward into the B horizon. Locally, tongues of E-horizon sand extend more than a meter into a thick, red to brown, clayey B horizon. Tongues of this size and shape can give the impression of fractured and brecciated ground and might be mistaken for liquefaction features unless examined carefully. Pedogenic tongues can range in morphology from tubular (Gamble, 1965) to planar (defining B horizon polygons; Nettleton et al., 1968a). Hence, tongue morphology is tenuous evidence for either pedogenic or earthquake origin.

A very common type of pedogenic tonguing is sketched in Figure 36. The tongue of white sand has a 10- to 30-cm thickness and dips gently downslope. The tongue is surrounded by black to dark-orange, humate and iron-oxide-stained sand. Some of the nearly horizontal parts of the tongue can be traced for distances as much as 7 m. At the upslope end of the tongue, the feature abruptly turns up, breaks through the overlying Bh soil horizon, and flares toward the surface. At the surface, the tongue is continuous with white sand of the E horizon. The downslope end of the tongue (not shown) is terminated by a black- and orange-stained rind that is continuous with the Bh horizon; in other cases the tongue-rind contact becomes diffuse downslope.

Another category of pedogenic feature that might be confused with earthquake-induced liquefaction is the BE' horizon. The horizon is surrounded by leached, clean sand (Fig. 37). Studies of this weathering profile indicate that the clean sand forms from the progressive chemical destruction of a clay-rich Bt (argillic) horizon (Daniels et al., 1966; Nettleton et al., 1968a,b; Steele et al., 1969). Relations illustrated in Figure 37 tend to occur in the area (plan view) between red, oxidized spodosols on beach ridge crests and the area where there

are black, organic-rich spodosols in interridge depressions. For the example shown, the BE' horizon is a zone of pale-brown, clayey sand and white sand. Both above and below the horizon is light-colored, well-sorted, fine- to medium-grained quartz sand. This sand cuts vertically across the clay layer at many places and creates irregular masses of the brown clayey sand. The contacts of the sand and the brown clayey sand are typically sharp with regard to both color and texture. The sand grain sizes in both the leached sand and clayey sand masses are essentially the same. Sharp contacts between the leached quartz sand areas and the pale-gray to pale-brown clayey material may suggest to the uninitiated that this feature formed by some type of ground disruption, possibly ancient liquefaction.

The examples above are but two of many types of confusing features caused by weathering. Other common types resemble shear zones and joints caused by faulting.

5.4 Features formed in a periglacial environment

Two classes of features produced in a periglacial (freezing-melting) environment, loosely defined as (1) involutions and (2) ice-wedge casts, can resemble features that have an earthquake-induced origin. Both classes are discussed below. Involutions are surficial manifestations of frost-related stirring (cryoturbation) and are generally characterized by distortion and mixing of the uppermost meter or so of the ground. Ice-wedge casts are downward-pinching, planar, nearly vertical features that originated as a result of thermal contraction of frozen ground.

Not discussed are sediment deformations caused by the weight or movement of glaciers. Such deformations, called 'glacitectonic', are extensively referenced in van Loon and Brodzikowski (1987).

5.4.1 involutions

Involutions are level-ground perturbations of surficial sediments caused by freezing or thawing action (see examples in Fig. 38). This action can also cause localized development of excess pore-water pressure. Involutions frequently show effects of fluidization (Fig. 38B). Involutions very commonly have boundaries and convolute bedding that point to a predominantly plastic mode of deformation. Involutions can be especially abundant where an eolian silty or fine-sand deposit is at the surface. Beneath the uppermost deposit there may be sediment ranging in size from gravel- to silt-rich (see Fig. 38; van Vliet-Lanoe, 1988, Fig. 11).

The morphological range is large. Vandenberghe (1988, p. 182) lists six types in terms of symmetry, amplitude-wavelength ratio, and pattern of occurrence. The features range from individual folds of small amplitude and large wavelengths (resembling slightly warped bedding caused by earthquake shaking) to intensely convoluted forms having amplitudes generally between 0.6 and 2 m (again resembling earthquake-induced convoluted bedding); load structures, diapirs, and dikes are also common. The genesis of involutions is probably related to three main process categories: load casting during melting, pressures in water trapped between freezing fronts, and pressures and heaving caused during freezing (Vandenberghe, 1988).

Features caused by load casting during melting (mainly bulbous downward intrusions and detachments of sediment going into a host) are similar in form to soft-sediment

deformation features described in a previous section. One important difference, though, is that frost-related load features are independent of the vertical lithological composition of the sediment. Even lithologically homogeneous sand can host load structures. Low-density, organic-rich sediments can also sink into denser sand (Harry and Gozdzik, 1988, p. 48-49).

Permanently frozen ground beneath a zone of thawing commonly leads to formation of involutions along the contact. Involutions are also thought to form as a result of high pressure in water trapped between freezing fronts. Such a pressure may develop between two impermeable layers, in which the basal layer is permafrost and the upper layer is the seasonal freezing front. Small mud volcanoes (Shilts, 1978), as large as 3 m in diameter, are thought to be caused by this process. Different susceptibilities to frost heaving and ice lensing may also explain some involutions. Small differences in grain-size properties may be significant.

In summary, many involutions are so similar to earthquake-induced features that assigning an unequivocal origin may not be possible. Involutions commonly are associated with ground patterned by freezing ('patterned ground') and ice-wedge casts, however, which helps in interpretation.

5.4.2 ice-wedge casts

The types of features that are included in this category are variously described as ice-wedge casts (Black, 1976), ground-wedge pseudomorphs (Harry and Gozdik, 1988), or other names based on morphological variations. All result from ground cracking caused by contraction of frozen ground. These contractions often fracture the ground in a polygonal network, in plan view. Wedges of ice then form in the cracked ground. The ice wedges grow wider through time. Later, when permafrost melts, host sediment slowly replaces the melting ice. Eolian sediment may also be blown into the depression.

Figure 39 shows a cross section of an ice-wedge cast of a type commonly seen in the northeastern United States. The cast is the downward-pinching body of sediment. Slump structures are in the cast, and edges of the host are shown upturned. The slump structures represent where sediment fell into or moved down the fissure as ice melted. Upturned edges of the host were formed by horizontal pressures as the ice wedge grew in width. The cast can have a width much exceeding a meter and a depth of as much as 10 m (Flint, 1971). Commonly, though, in the central and eastern United States, widths at the top are on the order of 0.5 to 1 m and depths are 3 to 4 m (see sketches in Johnson, 1990, and Stone and Ashley, 1992). Ice-wedge casts are common and widespread in clean granular deposits such as glaciofluvial sands and gravelly sands that have been subjected to permafrost conditions (Svensson, 1988; an excellent photograph is in Flint, 1971, p. 279). Casts are also widespread in glacial till (Svenson, 1988; Johnson, 1990) but tend to be more faintly delineated.

An earthquake-induced origin can be incorrectly deduced for ice-wedge casts, especially in clean granular deposits. However, with careful field study, an earthquake hypothesis can be tested. Field studies (Stone and Ashley, 1992) for the example of Figure 39 show that the uppermost meter of the cast is composed of fine sand and silt, including pebbles polished by wind abrasion, rather than sediment from depth vented to the surface. Stone and Ashley also showed that air photographs reveal a well-developed polygonal

network of the wedge structures in plan view. Therefore, evidence is very strong that the wedge structures were the result of permafrost.

Many ice-wedge casts in granular materials in the northeastern United States show little or no evidence of upturning of strata in host deposits. The upturned deformation is probably destroyed whenever the uppermost portion of host material moves into the void left by melting ice. Host material moves by sloughing, creep, and localized normal faulting. Strong vertical alignment of infilling sediment commonly takes place, especially in narrow casts. This vertical alignment superficially resembles effects of upward flowing water such as winnowing out of fine grain sizes and fluidization. However, a liquefaction origin is almost unequivocally eliminated if there are no feeder dikes going from the host to sediment in the cast. Features in glaciofluvial deposits described by Black (1976) as pseudo-ice-wedge casts (Fig. 40) can very closely resemble ice-wedge casts. The features probably develop as nearly vertical, open tension fractures, which form in response to any number of nonfrost-related mechanisms. Possibilities include loss of lateral support or differential settlement of underlying sediments. Such mechanisms can occur thousands of years after the host sediment was laid down. Simply lowering the water table can cause large differential settlements and crack the ground at places where the glaciofluvial deposits are underlain by thick, soft silts or clays.

6. ESTIMATION OF STRENGTH OF PALEOEARTHQUAKES

Interpretations of the strength of paleoearthquakes can be made using independent techniques. Only a crude association exists between severity of shaking, as measured by the Modified Mercalli Intensity scale, with threshold for formation of liquefaction effects and some soft-sediment deformations such as pseudondules and small recumbent folds. Using another approach (magnitude bound method) in field situations where the regional extent of liquefaction from a paleoearthquake can be estimated, a probable minimum magnitude can be determined. Using yet another method (method of Seed and Idriss) limits can be placed on accelerations that formed the liquefaction features, in terms of probability; these accelerations can then be compared with estimates of accelerations from seismological models for assessing magnitude. A method with much promise makes use of dike width as a measure of the severity of lateral spreading, and thereby the strength of shaking. Such a method is a variation of the Liquefaction Severity Index of Youd and Perkins (1987) and it's updated version (Bartlett and Youd, 1992). Yet another method with great promise for paleoseismic analysis uses an energy approach for assessing liquefaction potential (Law et al., 1990).

The methods discussed below for estimating prehistoric earthquake magnitude require locating the epicentral region. I suggest using the regional pattern of maximum dike widths to deduce this location. Where field data are adequate, though, a measure of the sum of dike widths is preferable. Dike width is used rather than density of dikes (number of dikes in plan view or sectional view, per unit of measure), because the density generally is highly sensitive to cap thickness (Fig. 9; Obermeier, 1989). Alternatively, the amount of lateral spreading, which normally is the prime factor in controlling dike width, is so insensitive to cap thickness as to not be used as a parameter for the Liquefaction Severity Index.

6.1 Association with Modified Mercalli Intensity

The Modified Mercalli Intensity (MMI) value is a qualitative measure of earthquake-induced damage (Wood and Neumann, 1931). The scale ranges from I to XII, with I representing the level at which shaking may be felt slightly and XII representing total destruction. MMI of about VI is the threshold for widespread development of small-scale soft-sediment deformation features such as folds, pseudonodules, contorted laminations, and recumbent folds (Sims, 1975).

Although liquefaction effects have occurred at MMI values as low as V and VI (Keefer, 1984), the lowest intensity at which liquefaction-induced features can become common is a value of VII, if highly susceptible deposits are present (National Research Council, 1985, p. 34). Values of VIII to IX are generally required before liquefaction-induced ground failure becomes severe enough to cause damage to buildings. A shortcoming of the use of MMI values as a measure of the strength of shaking of prehistoric earthquakes is that only a very crude association exists with ground failure effects.

6.2 Magnitude bound

Figure 41 shows the distance from the epicenter to the farthest observed liquefaction effect at the ground surface (plan view), such as venting of sand or ground fissuring. The data are from worldwide earthquakes in a wide variation of tectonic and alluvial settings. The sites of liquefaction range from having thin to thick alluvium. Amplification of bedrock shaking is probably small for thin alluvium, whereas for thick alluvium the amplification is undoubtedly as high as 2 to 2.5 at many places (Idriss, 1990). Liquefaction susceptibility is also doubtlessly very high at many of the farthest sites. Therefore, using the bound in the figure should provide a minimum estimate of magnitude of paleoearthquakes, especially in regions where conditions are less than optimal for forming liquefaction effects.

The farthest sites of liquefaction effects on the ground surface (in plan view) almost certainly cannot be expected to be found in a paleoliquefaction search (normally in section view). However, it has been my experience that this farthest distance can be reasonably approximated if adequate outcrop is searched in sectional view. A lower limit magnitude thus can be established by using the plot in Figure 41. Two illustrative examples are given based on my field experience, one for the Charleston earthquake of 1886 and the other for the New Madrid earthquakes of 1811-12. Both examples are regions of widespread moderate to high liquefaction susceptibility and probably at least moderate amplification of bedrock accelerations. Using the farthest liquefaction effects observed (90 - 100 km) at the time of the 1886 Charleston earthquake as a point on the outer bound of Figure 41 yields an estimated minimum magnitude of about M 6.8; actual magnitude was M~7.5. I have found small liquefaction features (unweathered dikes extending almost to the surface) almost certainly caused by the 1886 earthquake, as far as 100 km from the epicenter. In a similar vein for the 1811-12 New Madrid earthquakes, I have found liquefaction features (unweathered dikes extending nearly to the surface) in widely spaced regions as far as 250-275 km from the epicenter of the M~8.3 event. Farthest effects observed in 1811-12 were the same distances in these widely spaced regions. Using Figure 41 yields M 7.5-7.7. What these findings suggest is that if effects of liquefaction are observed at the surface at the time of the earthquake, in the same region there should be an abundance of dikes that pinch

together only slightly below the ground surface -- and that some could be found in a search for liquefaction features. (It must be kept in mind though, that small, pinching up dikes that do not approach the surface may extend much further from the meisoseismal region.) In summary, my experience for the two earthquakes above, based on farthest discovered paleoliquefaction features that approach the ground surface (within 1-2 m), indicates that the estimates of magnitude using Figure 41 are not outrageously lower than actual values providing field conditions are favorable for liquefaction.

The outer bound line in Figure 41 can sometimes be adjusted to account for influence of the local setting on farthest development of liquefaction effects, in regions of historic liquefaction. Such an example is given in Obermeier et al. (1993).

6.3 Method of Seed and Idriss

The method of Seed and Idriss (1971) provides an estimate of the shaking threshold required to produce minor effects of liquefaction during future earthquakes (Fig. 42). The minor effects are widely scattered occurrences of limited venting, and only limited venting, or small ground openings (several cm) caused by lateral spreading. The method is a standard technique used by engineers to approximate the threshold (minimum) level of shaking to cause these minor effects. The most recent version is based on worldwide occurrences of liquefaction during many earthquakes, supplemented with theoretical studies (Seed et al., 1983). The method applies to level ground and nearly level ground conditions (slopes on the order of 5 percent or less). The method can be adapted to paleoseismologic studies, in terms of probabilistic accelerations.

The properties of the source deposits are evaluated by in-situ testing using the Standard Penetration Test (SPT) method (discussed previously). The SPT blow count value (N_1), corrected for site conditions of depth of the water table and static stress conditions of the source stratum, is then related to the shaking required to cause venting. Figure 42 shows the boundary curves for different earthquake magnitudes. The curves relate the N_1 value in clean sands to the field cyclic stress ratio. This is the ratio, on an element in the sand layer, of the average earthquake-induced horizontal cyclic shear stress ($\tau_{h\,avg}$) to the static effective stress (σ_o'). The field cyclic stress ratio due to earthquake shaking is computed from the following equation (Seed et al., 1983):

$$\tau_{h\,avg}/\sigma_o' = (0.65\ A_{max}\ \sigma_o\ r_d)/(\sigma_o' g)$$

where A_{max} is the peak horizontal acceleration at the ground surface, σ_o is the total overburden stress on the sand under consideration, σ_o' is the initial effective overburden stress (total stress minus pore-water pressure) on the sand layer under consideration, r_d is the stress reduction factor ranging from a value of 1 at the ground surface to a value near 0.9 at a depth of about 10 m, and g is the acceleration of gravity.

The curves of Figure 42 for various magnitudes are based on the premise that the expected duration (i.e., number of cycles) of strong shaking is longer for increasingly higher magnitudes. The curves define where the probability of minor liquefaction (venting or significant ground cracking) is about 25 percent (Liao et al., 1988), as shown in Figure 43A. That is, venting or significant ground cracking occurs in about 25 percent of the cases for field cyclic stress ratios in Figure 42 that lie on a curve for a given magnitude. Increasing the ordinate by 25 percent raises the probability to about 60 percent. Raising the ordinate to

50 percent probability means there is an equal liklihood that stronger or weaker seismic shaking is required.

It should be noted that the curves of Figure 42 do not fully account for field conditions that are not conducive to venting, such as the presence of a very thick cap or a mat of peat at the surface. Elimination of sites having these unfavorable conditions would probably significantly increase the probability.

A misconception among many geologists is that the strength of clay- or silt-rich sediment in the cap has a major bearing on whether or not venting occurs. However, the pore-water pressure that develops along the base of the cap, where there is even marginal liquefaction of a thick source bed, normally greatly exceeds the tensile strength of the sediment in the cap; thus, hydraulic fracturing of the cap should occur. Even where the cap is very soft, a brittle mode of fracturing typically occurs rather than formation of plastic intrusions. Experience shows, though, that a field situation where venting may be significantly inhibited is where the cap has sufficient roots to greatly increase the tensile strength. For this situation, abundant sills can form. Laterally extensive sills may also form in abundance where a thin (1-2 m), very soft, and thereby very flexible cap exists, but I believe that dikes should also form within the area unless some special condition exists, such as a free face where the sill can vent. Careful study is required to the locate the source bed of a sill that extends far laterally.

Figure 42 can be modified to account for the fact that a high fines content in source sediment diminishes the effects of liquefaction. Corrections have been developed for silty sands, for silts, and for sands containing a small amount of clay (National Research Council, 1985). Figure 43B shows the effect of fines in terms of probability. The curves of Figure 41 can also be used to estimate susceptibility for some gravel-rich deposits (Andrus and Youd, 1987).

In order to use the method of Seed and Idriss for estimating the strength of paleoseismic shaking, bounds must be placed on depth of the water table at the time of the earthquake, and an estimate must be made for the SPT blow counts of the source beds. Maximum depth to the water table sometimes can be bracketed by observing the highest regional level at which dikes cut the base of the cap. The water level almost certainly was at least this high; if the water level had been lower, the excess pore-water pressure probably would have been dissipated into granular, permeable sediment along the base of the cap.

The SPT blow count (N_1 value) of a source stratum can be increased (generally a small amount) by earthquake shaking even if the shaking is not strong enough to cause liquefaction (Castro, 1987). An occurrence of severe liquefaction may more than double the blow count of the source stratum (see data in Kawakami and Asada, 1966, Fig. 4; Chameau et al., 1991, Figs. 4 and 6); it is not known how severe liquefaction must be to cause such a significant change, or the field settings conducive to such a significant change. Alternatively, sites showing field evidence for strong liquefaction may not show evidence for measurable changes in the source stratum (Holzer, 1994). At sites of marginal liquefaction effects, though, changes caused by an occurrence of liquefaction are likely to be small. Even this hypothesis should be tested where possible. In some geographic regions a sense of likely changes may be gotten by statistical comparison of blow counts in sediments that pre- and post-date the earthquake. Liquefaction during the paleoearthquake should have been most

severe at sites of lowest blow counts, in a statistical sense. Large differences in lowest blow counts in sediments that pre- and post-date the earthquake could indicate changes caused by liquefaction.

It is obvious that the curves in Figure 42 do not yield a unique solution to both acceleration and magnitude. Only possible combinations can be determined. The estimate of magnitude preferably should be based on estimates of accelerations from seismological models or statistical studies, in conjunction with an estimate of magnitude based on the observed areal distribution of the paleoliquefaction features.

6.4 Overview of estimates of magnitude

Factors that control the regional extent (span) of liquefaction features and sizes of liquefaction features include liquefaction susceptibility and amplification of bedrock shaking, as well as seismological factors of focal depth and shaking frequency of the earthquake, and stress change (drop) in the rock of the rupture zone at the time of the earthquake. Possible shaking characteristics are myriad. A shallow hypocentral depth can result in more severe shaking in the meisoseismal area than that caused by a deeper earthquake. Far from the meisoseismal area, however, shaking may be less severe for the more shallow earthquake than for a deeper one. A higher stress drop should cause accelerations to be higher both in the meisoseismal area and far away. Clearly, any interpretation of prehistoric magnitude needs to be calibrated as much as possible to the local tectonic setting in order to select the most reasonable parameters.

An accounting for all the factors above was implicit in the analysis of prehistoric liquefaction features centered about Charleston, South Carolina, discussed previously. There I concluded that some prehistoric earthquakes were at least equal in strength to the 1886 earthquake (M~7.5). Seismological factors were indirectly considered by showing that the size and span of features predating 1886 exceeded those of the 1886 event, both in the meisoseismal region of the 1886 earthquake and far away. In addition, near Charleston, the features that predate 1886 are more abundant and larger than elsewhere, which helped to define the region of strongest shaking.

The South Carolina example, where one can compare historical and prehistoric liquefaction effects to estimate past earthquake magnitudes, is exceptional. At most places such extensive historic liquefaction data from a very strong earthquake do not exist for the same seismotectonic setting. Estimates of magnitude elsewhere must be based on a more numerical analysis. Such an approach was used for analysis of liquefaction features in the Wabash Valley (Obermeier et al., 1993). Here historic liquefaction-producing earthquakes in the years 1811-12 and 1895 occurred in the New Madrid Seismic Zone, some 100 km southwest of the Wabash Valley. Seismotectonic setting of the two areas is likely similar. Thus the factors of hypocentral depth, stress drop, and frequency characteristics, can be assumed to be similar as a first approximation. The geologic and ground-water settings (i.e., liquefaction settings) are also similar between the sites of historic liquefaction and the Wabash Valley. Accounting for differences in amplification of bedrock shaking permitted definition of a curve parallel to the bound in Figure 41, and thereby an estimate of magnitude.

In regions of no strong historic earthquakes, theoretical geophysical models and statistically based estimates for acceleration-magnitude relations must be relied on heavily for making estimates of prehistoric magnitude.

6.5 Negative evidence

The absence of liquefaction features (negative evidence) also plays an important role in assessing prehistoric earthquakes. Where location of the water table can be bounded through time, and the susceptibility of potential source deposits can be estimated, the lack of liquefaction effects can be used to place limits on the maximum levels of prehistoric ground shaking. There is no well-defined procedure for determining the amount of outcrop that must be searched for liquefaction features to support such a negative conclusion. Some uncertainty arises because strong shaking probably attenuates from the energy source as a somewhat variable (stochastic) function rather than in a smooth manner. Many observations of damage to buildings caused by earthquakes show that large variations in ground response probably are commonplace within both short and long distances from the meisoseismal area. These variations often have no readily identifiable basis. Similarly, both the size and abundance of liquefaction-induced features can have large variations within a local area. For example, in the meisoseismal area of the 1811-12 New Madrid earthquakes, within a given length of outcrop there may be hundreds of dikes and sills of all sizes. Yet, in an outcrop of the same length nearby, where conditions for liquefaction appear to be about the same, an order of magnitude fewer features can be found.

I suggest that where there is any doubt that the source sediments have been at least moderately susceptible to liquefaction through time, ten or more kilometers of fresh outcrop must be searched in order to find effects of accelerations as low as 0.1 to 0.2 g. Preferably the contact of the base of a fine-grained cap with potentially liquefiable sand can be observed at many places. The search is best conducted when the stream level is very low, if streambanks are searched.

References Cited

Adams, J., 1982, Deformed lake sediments record prehistoric earthquakes during the deglaciation of the Canadian Shield [abs.]: EOS, Transactions, American Geophysical Union, v. 63, no. 18, p. 436.

Adams, J., 1990, Paleoseismicity of the Cascadia subduction zone: Evidence from turbidites off the Oregon-Washington margin: Tectonics, v. 9, no. 4, p. 569-583.

Allen, J.R.L., 1982, Sedimentary structures--their character and physical basis: The Netherlands, Elsevier Publishing Co., Developments in Sedimentology, 30B, v. 2, 663 p.

Allen, J.R.L., and Banks, N.L., 1972, An interpretation and analysis of recumbent-folded deformed cross-bedding: Sedimentology, v. 19, p. 257-283.

Ambraseys, N.N., 1988, Engineering seismology: Earthquake Engineering and Structural Dynamics, Journal of the International Association for Earthquake Engineering, v. 17, p. 1-105.

American Society for Testing and Materials, 1978, Annual book of ASTM standards, part 19, Designation D 1586-67 (reapproved 1974), standard method for penetration test and split barrel sampling of soils: Philadelphia, Pa., p. 235-237.

Amick, D., Gelinas, R., Maurath, G., Cannon, R., Moore, D., Billington, E., and Kemppinen, H., 1990, Paleoliquefaction features along the Atlantic seabord: U.S. Nuclear Regulatory Commission, Report NUREG\CR-5613, Washington, 146 p.

Amick, D. and Gelinas, R., 1991, The search for evidence of large prehistoric earthquakes along the Atlantic coast: Science, v. 251, p. 655-658.

Andrus, R.D., Stokoe, K.H., and Roesset, J.M., 1991, Liquefaction of gravelly soil at Pence Ranch during the 1983 Borah Peak, Idaho earthquake: Proceedings of the Fifth International Conference on Soil Dynamics and Earthquake Engineering, Karlsruhe, Germany, p. 251-262.

Andrus, R.D., and Youd, T.L., 1987, Subsurface investigation of a liquefaction-induced lateral spread, Thousand Springs Valley, Idaho: U.S. Army Waterways Experiment Station Miscellaneous Paper GL-87-8, 106 p.

Atwater, B.F., 1987, Evidence for great Holocene earthquakes along the outer coast of Washington State: Science, v. 236, p. 942-944.

Atwater, B.F., 1992, Geologic evidence for earthquakes during the past 2,000 years along the Copalis River, southern coastal Washington: Journal of Geophysical Research, v. 97, no. B2, p. 1901-1919.

Audemard, A., and de Santis, F., 1991, Survey of liquefaction structures induced by recent moderate earthquakes: Bulletin of the International Association of Engineering Geology, no. 44, p. 5-16.

Bartlett, S.F., and Youd, T.L., 1992, Empirical analysis of horizontal ground displacement generated by liquefaction-induced lateral spreads: Technical report NCEER-92-0021, State University of New York at Buffalo.

Bennett, M.J., 1984, Quaternary geology of ground failure sites in Long Valley and Little Antelope Valley; in Sintz, J. ed., Western Geological Excursions: 1984 Annual

Meeting of the Geological Society of America, Reno, v. 2, p. 67-72.
Berg, A.W., 1990, Formation of mima mounds: A seismic hypothesis: Geology, v. 18, p. 281-284.
Black, R.F., 1976, Periglacial features indicative of permafrost; ice and soil wedges: Quaternary Research, v. 6, p. 3-26.
Brodzikowski, K., Haluszczak, A., Krzyszkowski, D., and Van Loon, A., 1987, Genesis and diagnostic value of large-scale gravity-induced penecontemparaneous deformation horizons in Quaternary sediments of the Kleszcyow Graben (central Poland); in Jones, M.E., and Preston, R.M.F., eds., Deformation of Sedimentary and Sedimentary Rocks: Geological Society of America Special Publication No. 29, 287-298.
Carroll, M.T., 1979, A model for karst-like development in calcareous outwash deposits: M.S. thesis, University of Illinois, Urbana-Champaign, Ill., 130 p.
Castro, G., 1987, On the behavior of soils during earthquakes; in Cakmak, A.S., ed., Developments in Geotechnical Engineering, v. 42, Soil Dynamics and Liquefaction: Elsevier Publishing Co., p. 169-204.
Chameau, J.L., Clough, G.W., Reyna, F., and Frost, J.D., 1991, Liquefaction response of San Francisco bayshore fills: Bulletin of the Seismological Society of America, v. 81, no. 5, p. 1998-2018.
Cita, M.B., and Lucchi, F.R., eds., 1984, Special Issue, Seismicity and Sedimentation: Marine Geology, International Journal of Marine Geology, Geochemistry, and Geophysics, v. 55, nos. 1 and 2, 151 p.
Clague, J.J., Naesgaard, E., and Sy, A., 1992, Liquefaction features on the Fraser delta: evidence for prehistoric earthquakes: Canadian Journal of Earth Sciences, v. 29, no. 8, p. 1734-1745.
Coleman, J.M., and Prior, D.B., 1980, Deltaic sand bodies: A 1980 short course, education course note series no.15, American Association of Petroleum Geologists, 171 p.
Coulter, H.W., and Migliaccio, R.R., 1966, Effects of the earthquake of March 7, 1964 at Valdez, Alaska: U.S. Geological Survey Professional Paper 542-C, 36 p.
Daniels, R.B., Nettleton, W.D., McCracken, R.J., and Gamble, E.E., 1966, Morphology of soils with fragipans in parts of Wilson County, North Carolina: Soil Science Society of America Proceedings, v. 30, p. 376-380.
Darienzo, M.E., and Peterson, C.D., 1990, Episodic tectonic subsidence of Late Holocene salt marshes, northern Oregon central Casadia margin: Tectonics, v. 9, no. 1, p. 1-22.
Dickenson, S.E., Obermeier, S.F., and Roberts, T.H., 1994, Constraints on earthquake shaking in the lower Columbia River region of Washington and Oregon, during late Holocene time: Proceedings of the Fifth U.S. National Conference on Earthquake Engineering at Chicago, Illinois, Earthquake Engineering Research Institute, El Cerrito, Calif., in press.
Dobry, R., 1989, Some basic aspects of soil liquefaction during earthquakes: Proceedings of Conference on Earthquake Hazards and Design of Constructed Facilities in the Eastern United States, Annals of the New York Academy of Sciences, v. 558, p. 31-38.
Dobry, R., and Liu, in press, Centrifuge modeling of soil liquefaction: Proceedings of the

Tenth World Conference on Earthquake Engineering, Madrid, Spain, July 19-24, 1992.

Doig, R., 1986, A method for determining the frequency of large-magnitude earthquakes using lake sediments: Canadian Journal of Earth Sciences, v. 23, no. 7, p. 930-937.

Dutton, C.E., 1889, The Charleston earthquake of August 31, 1886: U.S. Geological Survey Ninth Annual Report 1887-88, p. 203-528.

Dzulynski, S., and Kotlarczyk, J., 1962, On load-casted ripples: Annales de la Societe Geologique de Pologne, v. 32, p. 148-159.

Dzulynski, S., and Smith, A.J., 1963, Convolute lamination, its origin, preservation, and directional significance: Journal of Sedimentary Petrology, v. 33, p. 616-627.

Dzulynski, S., and Walton, E.K., 1965, Sedimentary features of flysch and greywackes: Developments in Sedimentology, v. 7, Elsevier, 274 p.

Einsele, G., Ricken, W., and Seilacher, A., eds., 1991, Cycles and events in stratigraphy: Springer-Verlag, 955 p.

Elgamal, A-W.M., Amer, M., and Adalier, K., 1993, Liquefaction during the October 12, 1992 Egyptian Dahshure earthquake: Third International Conference on Case Histories in Geotechnical Engineering, S. Prakash, ed., University of Missouri at Rolla, Vol. III, June 1-4, St. Louis, Mo.

Elgamal, A-W.M., Dobry, R., and Adalier, K., 1989, Study of effect of clay layers oln liquefaction of sand using small-scale models: Proceedings from the Second U.S.-Japan Workshop on Liquefaction, Large Ground Deformation and Their Effects on Lifelines, Technical Report NCEER-89-0032, State University of New York at Buffalo, p. 233-245.

Fiegel, G. L., and Kutter, B.L., 1994, Liquefaction mechanism for layered soils: Journal of Geotechnical Engineering, American Society of Civil Engineers Proceedings, v. 120, no. 4, p. 737-755.

Flint, R.F., 1971, Glacial and Quaternary geology: Wiley and Sons, 892 p.

Fuller, M.L., 1912, The New Madrid earthquake: U.S. Geological Survey Bulletin 494, 119 p.

Gamble, E.E., 1965, Origin and morphogenetic relations of sandy surficial horizons of upper Coastal Plain soils of North Carolina: Ph.D. thesis, North Carolina State University, Raleigh, 254 p.

Gelinas, R.L., 1986, Mineral alterations as a guide to the age of sediments vented by prehistoric earthquakes in the vicinity of Charleston, South Carolina: M.S. thesis, University of North Carolina, Chapel Hill, 304 p.

Geomatrix, 1994, Seismic design mapping State of Oregon: Task 2, Ground Motion Attenuation, report prepared for Oregon Department of Transportation under contract 11688, by Geomatrix Consultants, San Francisco.

Hamada, M . 1992, Large ground deformations and their effects on lifelines, 1964, Niigata Earthquake: Case Studies of Liquefaction and Lifeline Performance During Past Earthquakes, Vol. 1, Japanese Case Studies, NCEER Report 92-0001, State University of New York at Buffalo, 123 p.

Hamilton, R.M., and Johnston, A.C., eds., 1990, Tecumseh's prophecy -- preparing for the next New Madrid earthquake: U.S. Geological Survey Circular 1066, 30 p.

Hamilton, R.M., and Zoback, M.D., 1982, Tectonic features of the New Madrid seismic zone from seismic reflection profiles, in McKeown, F.A., and Pakiser, L.C., eds., Investigations of the New Madrid, Missouri, earthquake region: U.S. Geological Survey Professional Paper 1236-F, p. F55-F82.

Harp, E.L., Wilson, R.C., and Wieczorek, G.F., 1981, Landslides from the February 4, 1976 Guatemala earthquake: U.S. Geological Survey Professional Paper 1204-A, 35 p.

Harry, D.G., and Gozdzik, J.S., 1988, Ice wedges: growth, thaw transformation, and paleoenvironmental significance: Journal of Quaternary Science, v. 3, no. 1, p. 39-55.

Heaton, T.H., and Hartzell, S.H., 1987, Earthquake hazards on the Cascadia Subduction Zone: Science, v. 236, p. 162-168.

Holzer, T.L., 1994, Written comm., Unpublished data for the M 6.6 Superstition Hills, California, earthquake of November, 1987.

Housner, G.W., 1958, The mechanism of sand blows: Bulletin of the Seismological Society of America, v. 58, p. 155-161.

Hyndaman, R.D., and Wang, K., 1993, Thermal constraints on the zone of major thrust earthquake failure: The Cascadia Subduction Zone: Journal of Geophysical Research, v. 98, no. B2, p. 2039-2060.

Idriss, I.M., 1990, Response of soft soil sites during earthquakes: H. Bottom Seed Memorial Symposium Proceedings, v. 2, BiTech Publishers, Ltd., Vancouver, B.C., Canada, p. 273-289.

Ishihara, K., 1985, Stability of natural soil deposits during earthquakes: Proceedings of the Eleventh International Conference on Soil Mechanics and Foundation Engineering, San Francisco, v. 1, p. 321-376.

Iwasaki, T., 1986, Soil Liquefaction studies in Japan: State of the art: Soil dynamics and earthquake engineering, Computational Mechanics Publications, v. 5, no. 1, p. 2-68.

Jibson, R.W., and Keefer, D.K., 1988, Landslides riggered by earthquakes in the Central Mississippi Valley, Tennessee, and Kentucky: U.S. Geological Survey Professional Paper 1336-C, 24 p.

Jibson, R.W., and Keefer, D.K., 1989, Statistical analysis of factors affecting landslide distribution in the New Madrid seismic zone, Tennessee and Kentucky: Engineering Geology, v. 27, p. 509- 542.

Jibson, R.W., and Keefer, D.K., 1993, Analysis of the seismic origin of landslides: Examples from the New Madrid Seismic zone: Bulletin of the Geological Society of America, v. 105, p. 521-536.

Johnson, W.H., 1990, Ice-wedge casts and relict patterned ground in central Illinois and their environmental significance: Quaternary Research, v. 33, no. 1, p. 51-72.

Johnston, A.C., in press, The stable-continental-region earthquake data base, in Coppersmith, K. J., and others, eds., Methods for assessing maximum earthquakes in the central and eastern United States: Project RP-2556-12, Electric Power Research Institute, Palo Alto, Calif.

Jones, M.E., and Preston, R.M.F. (eds.), 1987, Deformation of Sediments and Sedimentary Rocks: Geological Society Special Publication No. 29, Blackwell Scientific

Publications, 350 p.
Karlsrud, K., Aas, G., and Gregersen, O., 1984, Can we predict landslide hazards in soft sensitive clays? Summary of Norwegian practice and experiences: Fourth International Symposium on Landslides, Toronto, v. 1, p. 107-130.
Katayama, S., Fujii, T., and Takahashi, Y., 1966, Damage caused by the Niigata earthquake and the geological features of National Highway in the suburbs of Niigata City: Soils and Foundations, Japanese Society of Soil Mechanics and Foundation Engineering, v. 6, no. 1, p. 54-70.
Kawakami, F., and Asada, A., 1966, Damage to the ground and earth structures by the Niigata earthquake of June 16, 1964: Soils and Foundations, Japanese Society of Soil Mechanics and Foundation Engineering, v. 6, no. 1, p. 14-30.
Keefer, D.K., 1984, Landslides caused by earthquakes: Geological Society of America Bulletin, v. 95, p. 406-421.
Kishida, H., 1966, Damage to reinforced concrete buildings in Niigata City with special reference to foundation engineering: Soils and Foundations, Japanese Society of Soil Mechanics and Foundation Engineering, v. 6, no. 1, p. 71-88.
Koizumi, Y., 1966, Changes in density of sand subsoil caused by the Niigata earthquake: Soils and Foundations, Japanese Society of Soil Mechanics and Foundation Engineering, v. 6, no. 2, p. 38-44.
Kolb, C.R., 1976, Geologic control of sand boils along Mississippi River levees; in Coats, D.R., ed., Geomorphology and Engineering: Halstead Press, p. 99-114.
Kuenen, P.H., 1958, Experiments in geology: Transactions of the Geological Society of Glasgow, v. 23, p. 1-28.
Kuribayashi, E. and Tatsuoka, F., 1975, Brief review of liquefaction during earthquakes in Japan: Soils and Foundations, Japanese Society of Soil Mechanics and Foundation Engineering, v. 15, no. 4, p. 81-91.
Lade, P.V., 1992, Static instability and liquefaction of loose fine sandy slopes: Journal of Geotechnical Engineering, American Society of Civil Engineers Proceedings, v. 118, no. 1, p. 51-71.
Law, K. T., Cao, Y. L., and He, G. N., 1990, An energy approach for assessing seismic liquefaction potential: Canadian Geotechnical Journal, v. 27, p. 320-329.
Liao, S.S.C., Veneziano, D., and Whitman, R.V.,1988, Regression models for evaluating liquefaction probability: Journal of Geotechnical Engineering, American Society of Civil Engineers Proceedings, v. 114, no. 4, p. 389-411.
Liu, H., and Qiao, T., 1984, Liquefaction potential of saturated sand deposits underlying foundation of structure: Proceedings of the 8th World Conference on Earthquake Engineering, San Francisco, v. 3, p. 199-206.
Lowe, D.R., and LoPiccolo, R.D., 1974, The characteristics and origins of dish and pillar structures: Journal of Sedimentary Petrology, v. 44, no. 2, p. 484-501.
Lowe, D.R., 1975, Water escape structures in coarse-grained sediments: Sedimentology, v. 22, no. 2, p. 157-204.
Martin, J.R., and Clough, G.W., 1990, Implications from a geotechnical investigation of liquefaction phenomena associated with seismic events in the Charleston, South Carolina area: Virginia Polytechnic Institute and State University, Blacksburg, Va.,

414 p.
McColloch, D.S., and Bonilla, M.G., 1970, Effects of the earthquake of March 27, 1964, on the Alaska Railroad: U.S. Geological Survey Professional Paper 545-D, 161 p.
McKeown, F.A., Hamilton, R.M., Diehl, S.F., and Glick, E.E., 1990, Diapiric origin of the Blytheville and Pascola arches in the Reelfoot Rift, east-central United States: Relation to New Madrid seismicity: Geology, v. 18, p. 1158-1162.
Meier, L.S., 1993, The susceptibility of a gravelly soil site to liquefaction: M.S. thesis, Virginia Polytechnic Institute, Blacksburg, Va., 71 p.
Mills, P.C., 1983, Genesis and diagnostic value of soft-sediment deformation structures -- a review: Sedimentary Geology, v. 35, no. 2, p. 83-104.
Mitchell, J.K., 19976, Fundamentals of soil behaviour: John Wiley & Sons, Inc., New York, 422 p.
Morner, N., 1985, Paleoseismicity and geodynamics in Sweden: Tectonophysics, v. 117, p. 139-153.
Munson, P.J., Munson, C.A., Bleuer, N.K., and Labitzke, M.D., 1992, Distribution and dating of prehistoric liquefaction in the Wabash Valley of the Central U.S.: Seismological Research Letters, v. 63, no. 3, p. 337-342.
Munson, P.J., Munson, C.A., and Bleuer, N.K. 1994, (in press), Late Pleistocene and Holocene earthquake-induced liquefaction in the Wabash Valley of southern Indiana: U.S. Geological Survey Open-File Report, Summaries of Technical Reports, National Earthquake Hazards Reduction Program, Fiscal Year 1993, v. 36, 5 p.
Nataraja, M.S., and Gill, H.S., 1983, Ocean wave-induced liquefaction analysis: Journal of Geotechnical Engineering, American Society of Civil Engineers Proceedings, v. 109, no. 4, p. 573-590.
National Research Council, 1985, Liquefaction of soils during earthquakes: Washington, D.C., National Academy Press, 240 p.
Nelson, A.R., 1992, Holocene tidal-marsh stratigraphy in South-central Oregon -- evidence of localized sudden submergence in the Cascadia Subduction Zone: Quaternary Coasts of the United States: Marine and Lacustrine Systems, SEPM Special Publication No. 48, p. 287-301.
Nelson, A.R., and Personius, S.F., in press. Great earthquake potential in Oregon and Washington: an overview of recent coastal geologic studies and their bearing on segmentation Holocene ruptures, central Cascadia subduction zone, in Rogers, A.M., ed., Assessing and reducing earthquake hazards in the Pacific Northwest: U.S. Geological Survey Professional Paper.
Nettleton, W.D., McCracken, R.J., and Daniels, R.B., 1968a, Two North Carolina Coastal Plain catenas-I. Morphology and fragipan development: Soil Science Society of America Proceedings, v. 32, p. 577-582.
Nettleton, W.D., Daniels, R.B., and McCracken, R.J., 1968b, Two North Carolina Coastal Plain catenas-II. Micromorphology, composition, and fragipan genesis: Soil Science Society of America Proceedings, v. 32, p. 582-587.
Nuttli, O.W., 1979, Seismicity of the central United States, in Hatheway, A.W., and McClure, C.R., Jr., eds., Geology in the siting of nuclear power plants: Reviews in Engineering Geology, v. 4, p. 67-93.

Obermeier, S.F., 1988, Liquefaction potential in the central Mississippi Valley: U.S. Geological Survey Bulletin 1832, 21 p.

Obermeier, S.F., 1989, The New Madrid earthquakes: An engineering-geologic interpretation of relict liquefaction features: U.S. Geological Survey Professional Paper 1336-B, 114 p.

Obermeier, S.F., 1994, Preliminary limits for the strength of shaking in the Columbia River valley and the southern half of coastal Washington, with emphasis for a Cascadia subduction earthquake about 300 years ago: U.S. Geological Survey Open-File Report 94-589, 40 p.

Obermeier, S.F., Jacobson, R.B., Powars, D.S., Weems, R.E., Hallbick, D.C., Gohn, G.S., and Markewich, H.W., 1986, Holocene and late Pleistocene (?) earthquake-induced sand blows in coastal South Carolina: Proceedings of the Third U. S. National Conference on Earthquake Engineering, Earthquake Engineering Research Institute, v. 1, p. 197-208.

Obermeier, S.F., Jacobson, R.B., Smoot, J.P., Weems, R.E., Gohn, G.S., Monroe, J.E., and Powars, D.S., 1990, Earthquake-induced liquefaction features in the coastal setting of South Carolina and in the fluvial setting of the New Madrid seismic zone: U.S. Geological Survey Professional Paper 1504, 44 p.

Obermeier, S.F., Martin, J.R., Frankel, A.D., Youd, T.L., Munson, P.J., Munson, C.A., and Pond, E.C., 1993, Liquefaction evidence for one or more strong Holocene earthquakes in the Wabash Valley of southern Indiana and Illinois, with a preliminary estimate of magnitude: U.S. Geological Survey Professional Paper 1536, 27 p.

Obermeier, S.F., Weems, R.E., and Jacobson, R.B., 1987, Earthquake-induced liquefaction features in the coastal South Carolina region: U.S. Geological Survey Open-File Report 87-504, 13 p.

Ohsaki, Y., 1970, Effects of sand compaction on liquefaction during the Tokachioki earthquake: Soils and Foundations, The Japanese Society of Soil Mechanics and Foundation Engineering, v. 10, no. 2, p. 112-128.

Oldham, R.D., 1899, Report on the great earthquake of 12th June 1987: Memoirs of the Geological Survey of India, Geological Survey of India, v. 29, 379 p.

O'Rourke, T.D., and Hamada, M., eds., 1989, Proceedings from the Second U.S. Japan Workshop on Liquefaction Large Ground Deformation and Their Effects on Lifelines: Technical Report NCEER-89-0032, State University of New York at Buffalo, 498 p.

Owen, G., 1987, Deformation processes in unconsolidated sands; in Jones and Preston, eds., Geological Society Special Publication No. 29, Deformation of Sediments and Sedimentary Rocks: Blackwell Scientific Publications, Oxford, England, p. 11-24.

Penick, James, Jr., 1976, The New Madrid earthquakes of 1811-12: University of Missouri Press, Columbia, 181 p.

Peters, K.E., and Herrmann, R.B., compilers and eds., 1986, First-hand observations of the Charleston earthquakes of August 31, 1886, and other earthquake materials: South Carolina Geological Survey, Bulletin 41, 116 p.

Peterson, C.D., 1992, Variation in form and scale of paleoliquefaction structures in late Pleistocene deposits of the central Cascadia margin: Abstracts with Programs, Geological Society of America, Cordilleran Section, v. 24, no. 5, p. 74.

Peterson, C.D., Hansen, M., and Jones, D., 1991, Widespread evidence of paleoliquefaction in late-Pleistocene marine terraces from the Oregon and Washington margins of the Cascadia subduction zone: Programs and Abstracts, American Geophysical Union, 1991 Fall Meeting, p. 313.

Pettijohn, F.J., and Potter, P.E., 1964, Atlas and glossary of primary sedimentary structures: New York, Springer-Verlag, 370 p.

Reimnitz, E., and Marshall, N.F., 1965, Effects of the Alaska earthquake and tsunami on recent deltaic deposits: Journal of Geophysical Research, v. 70, no. 10, p. 2363-2376.

Richter, C.F., 1958, Elementary Seismology: San Francisco, W. H. Freeman and Company, 768 p.

Reineck, H.E., and Singh, I.B., 1980, Depositional Sedimentary Environments: Springer-Verlag, Berlin, 551 p.

Ringrose, P.S., 1989, Paleoseismic (?) liquefaction event in late Quaternary lake sediments at Glen Roy, Scotland: Terra Nova, v. 1, no. 1, p. 57-62.

Ross, G.A., Seed, H.B., and Migliaccio, R.R., 1969, Bridge foundations behavior in Alaska earthquake: Journal of Soil Mechanics and Foundation Engineering, American Society of Civil Engineers Proceedings, v. 95, p. 1007-1036.

Russ, D.P., 1979, Late Holocene faulting and earthquake recurrence in the Reelfoot Lake area, northwestern Tennessee: Geological Society of America Bulletin, v. 90, 1013-1018.

Sanders, J.E., 1960, Origin of convoluted laminae: Geology Magazine, v. 97, p. 409-421.

Saucier, R.T., 1989, Evidence for episodic sand-blow activity during the 1811-12 New Madrid (Missouri) earthquake series: Geology, v. 17, p. 103-106.

Saucier, R.T., 1991, Comment on "Formation of mima mounds: a seismic hypothesis": Geology, v. 19, p. 284.

Savage, J.C., and Lisowski, M., 1991, Strain measurements and the potential for a great subduction zone earthquake off the coast of Washington: Science, v. 252, p. 101-103.

Schnabel, P.B., Lysmer, J., and Seed, H.B., 1972, SHAKE: A Computer Program for Earthquake Response Analysis of Horizontally Layered Sites: Report No. EERC 72-12, Earthquake Engineering Research Center, University of California, Berkeley, Calif.

Scott, R.F., 1986, Solidification and consolidation of a liquefied sand column: Soils and Foundations, Japanese Society of Soil Mechanics and Foundation Engineering, v. 26, no. 4, p. 23-31.

Seed, H.B., 1968, Landslides during earthquakes due to soil liquefaction: Journal of the Soil Mechanics and Foundation Engineering, American Society of Civil Engineers Proceedings, v. 94, no. SM 5, p. 1053-1122.

Seed, H.B., 1979, Soil liquefaction and cyclic mobility for level ground during earthquakes: Journal of Geotechnical Engineering, American Society of Civil Engineers Proceedings, v. 105, no. GT2, p. 201-255.

Seed, H.B., and Idriss, I.M., 1971, A simplified procedure for evaluating soil liquefaction potential: Journal of Soil Mechanics and Foundation Engineering, American Society of

Civil Engineers Proceedings, v. 97, no. SM 9, p. 1249-1274.
Seed, H.B., Idriss, I.M., and Arango, I., 1983, Evaluation of liquefaction potential using field performance data: Journal of Geotechnical Engineering, American Society of Civil Engineers Proceedings, Journal of the Geotechnical Engineering Division, v. 109, no. 3, p. 458-482.
Seilacher, A., 1969, Fault-graded beds interpreted as seismites: Sedimentology, v. 13, p. 155-159.
Shilts, W.W., 1978, Nature and genesis of mudboils, central Keewatin, Canada: Canadian Journal of Earth Sciences, v. 15, p. 1053-1068.
Sieh, K.E., 1978, Prehistoric large earthquakes produced by slip on the San Andreas Fault at Pallett Creek, California: Journal of Geophysical Research, v. 83, no. B8, p. 3907-3939.
Sims, J.D., 1973, Earthquake-induced structures in sediments of Van Norman Lake, San Fernando, California: Science, v. 182, p. 161-163.
Sims, J.D., 1975, Determining earthquake recurrence intervals from deformational structures in young lacustrine sediments: Tectonophysics, v. 29, p. 141-152.
Sims, J.D., 1978, Annotated bibliography of penecontemporaneous deformational structures in sediments: U.S. Geological Survey Open-File Report 78-510, 79 p.
Sims, J.D., and Garvin, C.D., in press, Recurrent liquefaction induced by the 1989 Loma Prieta earthquake and 1990 and 1991 aftershocks: implications for paleoseismicity studies: Bulletin of the Seismological Society of America
Springer, F.M., Ullrich, C.R., and Hagerty, D.J., 1985, Streambank stability: Journal of Geotechnical Engineering, American Society of Civil Engineers Proceedings, v. 111, no. GT5, p. 624-640.
Steele, F., Daniels, R.B., Gamble, E.E., and Nelson, L.A., 1969, Fragipan horizons and Be masses in the middle coastal plain of north central North Carolina: Soil Science Society of America Proceedings, v. 33, p. 752-755.
Stone, J.R., and Ashley, G.M., 1992, Ice-wedge casts, pingo scars, and the drainage of glacial Lake Hitchcock; in Robinson, P., and Brady, J.B., eds., Guidebook for Field Trips in the Connecticut Valley Region of Massachusetts and Adjacent States, v. 2: Contribution No. 66, Department of Geology and Geography, University of Massachusetts, p. 305-331.
Svensson, H., 1988, Ice-wedge casts and relict polygonal patterns in Scandinavia: Journal of Quaternary Science, v. 3, no. 1, p. 57-67.
Taber, S., 1914, Seismic activity in the Atlantic Coastal Plain near Charleston, S.C.: Bulletin of the Seismological Society of America, v. 4, p. 108-160.
Terzaghi, K., and Peck, R.B., 1967, Soil mechanics in engineering practice: New York, John Wiley, 566 p.
Thorson, R.M., Clayton, W.S., and Seeber, L., 1986, Geologic evidence for a large prehistoric earthquake in southeastern Connecticut: Geology, v. 14, no. 6, p. 17-35.
Tokimatsu, K., and Seed, H.B., 1987, Evaluation of settlements in sands due to earthquake shaking: Journal of Geotechnical Engineering, American Society of Civil Engineers Proceedings, v. 113, no. 8, p. 861-878.
Tsuchida, H., and Hayashi, S., 1971, Estimation of liquefaction potential of sandy soils:

Proceedings of the Third Joint Meeting, U.S.-Japan Panel on Wind and Seismic Effects, UJNR, Tokyo, May, 1971, p. 91-109.

Tuttle, M. P., and Schweig, E. C., in press, Archeological and pedological evidence for large prehistoric earthquakes in the New Madrid seismic zone, central United States: Geology.

Tuttle, M., and Seeber, L., 1991, Historic and prehistoric earthquake-induced liquefaction in Newbury, Massachusetts: Geology, v. 19, p. 594-597.

Tuttle, M., Cowie, P., and Wolf, L., 1992, Liquefaction induced by modern earthquakes as a key to paleoseismicity: a case study of the 1988 Saguenay event: Proceedings of the Nineteenth Water Reactor Safety Information Meeting, U.S. Nuclear Regulatory Commission, NUREG/CP-00119, v. 3, p. 437-462.

Updike, R.G., Egan, J.A., Moriwaki, Y., Idriss, I.M., and Moses, T.L., 1988, A model for earthquake-induced translatory landslides in Quaternary sediments: Geological Society of America Bulletin, v. 100, p. 783-792.

van Loon, A.J., 1992, The recognition of soft-sediment deformations as early-diagenetic features--A literature review, in Wolf, K.H., and Chilingarian, G.V., eds., Developments in Sedimentology, v. 47: Elsevier, p. 135-189.

van Loon, A.J., and Brodzikowski, 1987, Problems and progress in the research of soft-sediment deformations: Sedimentary Geology, v. 50, . 167-1993.

van Vliet-Lanoe, B., 1988, The significance of cryoturbation phenomena in environmental reconstruction: Journal of Quaternary Science, v. 3, no. 1, p. 85-96.

Vandenberghe, J., 1988, Cryoturbations, in Clark, M. J., ed., Advances in periglacial geomorphology: John Wiley and Sons, p. 179-198.

Veneziano, D., and Liao, S., 1984, Statistical analysis of liquefaction data: Proceedings of the Fourth ASCE Specialty Conference on Probabilistic Mechanics and Structural Reliability, American Society of Civil Engineers, New York, p. 206-209.

Wald, D.J., Helmberger, D.V., and Heaton, T.H., 1991, Rupture model of the 1989 Loma Prieta earthquake from the inversion of strong-motion and broadband teleseismic data: Bulletin of the Seismological Society of America, v. 81, no. 5, p. 1540-1572.

Weems, R.E., and Obermeier, S.F., 1990, The 1886 Charleston earthquake--an overview of geologic studies: Proceedings of the 17th Water Reactor Safety Information Meeting, Document NUREG/CP-0105, U. S. Nuclear Regulatory Commission, Washington, p. 289-313.

Wesnousky, S.G., and Leffler, L.M., 1992, The repeat time of the 1811 and 12 New Madrid earthquakes; a geological perspective: Bulletin of the Seismological Society of America, v. 82, no. 4, p. 1756-1784.

Wong, R.T., Seed, H.B., and Chan, C.K., 1975, Cyclic loading liquefaction of gravelly soils: Journal of Geotechical Engineering, American Society of Civil Engineering Proceedings, v. 101, no. GT6, p. 571-582.

Woods, H.O., and Neumann, F., 1931, Modified Mercalli intensity scale of 1931: Bulletin of the Seismological Society of America, v. 21, p. 277-283.

Youd, T.L., 1973, Liquefaction, flow, and associated ground failure: U.S. Geological Survey Circular 688, 12 p.

Youd, T.L., 1978, Major cause of earthquake damage in ground failure: Civil Engineering,

v. 48, no. 4, p. 47-51.
Youd, T.L., 1984a, Geologic effects - liquefaction and associated ground failure, in Proceedings of the Geologic and Hydrologic Hazards Training Program: U.S. Geological Survey Open-File Report 84-760, p. 210-232.
Youd, T.L., 1984b, Recurrence of liquefaction at the same site: Proceedings of the Eighth World Conference on Earthquake Engineering, vol. 3, p. 231-238.
Youd, T.L., 1991, Mapping of earthquake-induced liquefaction for seismic zonation: Proceedings of the Fourth International Conference on Seismic Zonation, Earthquake Engineering Research Institute, El Cerrito, Calif., v. 1, p. 111-147.
Youd, T.L., and Bartlett, S.F., 1991, Case histories of lateral spreads from the 1964 Alaska earthquake: Proceedings from the Third Japan-U.S. Workshop on Earthquake Resistance to Design of Lifeline Facilities and Countermeasures for Soil Liquefaction, Technical Report NCEER-91-0001, State University of New York at Buffalo, p. 175-189.
Youd, T.L., Holzer, T.L., and Bennett., M.J., 1989, Liquefaction lessons learned from Imperial Valley, California: Twelfth International Conference on Soil Mechanics and Foundation Engineering, Proceedings of Discussion Session on Influence of Local Conditions on Seismic Response, Rio de Janeiro, p. 47-54.
Youd, T.L., and Hoose, S.N., 1978, Historic ground failures in northern California triggered by earthquakes: U.S. Geological Survey Professional Paper 993, 177 p.
Youd, T.L., and Perkins, D.M., 1978, Mapping liquefaction-induced ground failure potential: Journal of Geotechnical Engineering, American Society of Civil Engineers Proceedings, v. 104, no. GT4, p. 433-446.
Youd, T. L., and Keefer, D.K. 1994, Liquefaction during the 1977 San Jose Province earthquake (Ms 7.4): Engineering Geology, v. 37, p. 211-233.
Youd, T.L., and Perkins, D.M., 1987, Mapping of liquefaction severity index: Journal of Geotechnical Engineering, American Society of Civil Engineers Proceedings, v. 113, no. 11, p. 1374-1392.
Youngs, R. R., Chio, S. J., Silva, W. L., and Humphrey, J. R., 1993, Strong ground motion attenuation relations for subduction zone earthquakes based on empirical data and numerical modeling, Seismological Research Letters, Seismological Society of America, v. 64, p. 18 (abstract).
Zhong-qi, W., Hong-qi, F., and Shu-dong, 1983, Macroscopic features of earthquake induced soil liquefaction and its influence on ground damage: Canadian Geotechnical Journal, v. 20, no. 1, p. 61-68.

TABLE 1. Relative density of sand as related to Standard Penetration Test blow counts (Terzaghi and Peck, 1967)

No. of blows (N)	Relative density
0-4	Very loose
4-10	Loose
10-30	Medium or moderate
30-50	Very dense

TABLE 2. Influence of age of deposit and depth of ground-water table on liquefaction susceptibility in the San Fernando valley, California (National Research Council, 1985, p. 91)

	Depth to ground-water table (m)		
Age of deposit	0-3	3-10	>10
Latest Holocene	high	low	nil
Earlier Holocene	medium	low	nil
Late Pleistocene	low	nil	nil

Figure 1. Vertical section showing idealized field loading conditions changing with time as energy propagates upward from hypocenter. Stresses shown represent pre-liquefaction cyclic loading conditions. σ_o^1, initial vertical effective stress; τ_h, earthquake-induced horizontal shear stress.

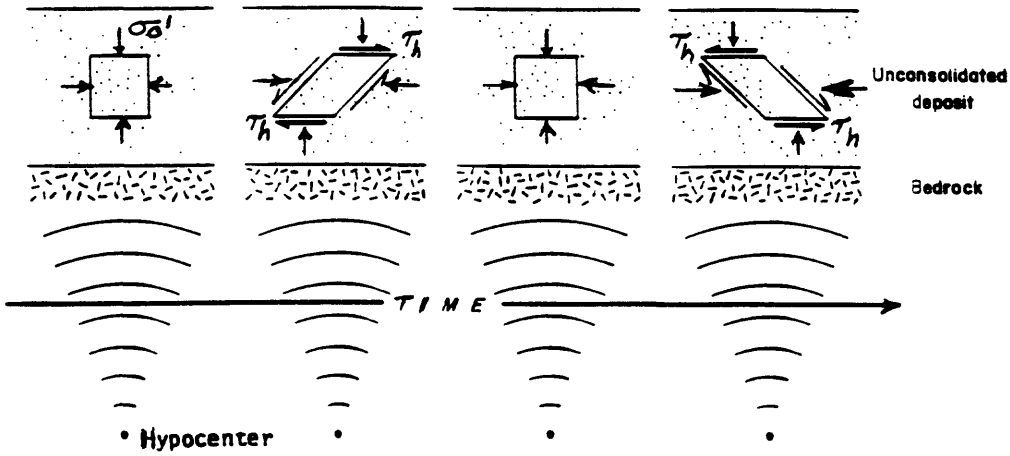

Figure 2. Schematic depiction of changes in packing arrangement caused by liquefaction.

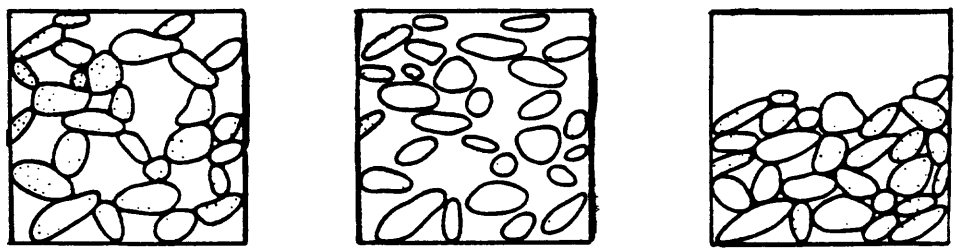

A

Loose depositional packing

B

Packing during liquefaction, with excess pore-water pressure throughout

C

Resedimentation, with layer of water at top

Figure 3. Schematic depiction illustrating location of the zone of liquefaction that is induced during earthquake shaking. C, number of shaking cycles. (From Seed and Idriss, 1971.)

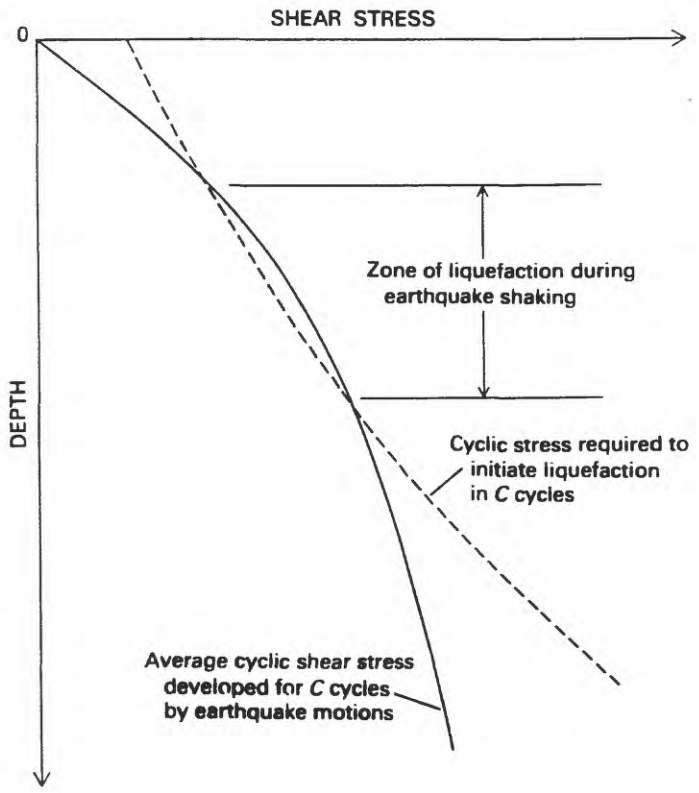

Figure 4. Small sand blows near the town of El Centro from the 1979 Imperial Valley, California, earthquake. The sand blows were produced by a mixture of sand and water that spouted to the surface; they provide evidence of extensive liquefaction at depth. (Photograph courtesy of R.F. Scott.)

Figure 5. Vertical section of lateral spread before and after failure. Liquefaction occurs in the cross-hatched zone. The surface layer then moves laterally down the gentle slope, breaking into blocks bounded by fissures. Sand is vented to the surface through some fissures, but other fissures are only partly filled. The blocks can tilt and settle differentially with respect to one another. (From Youd, 1984.)

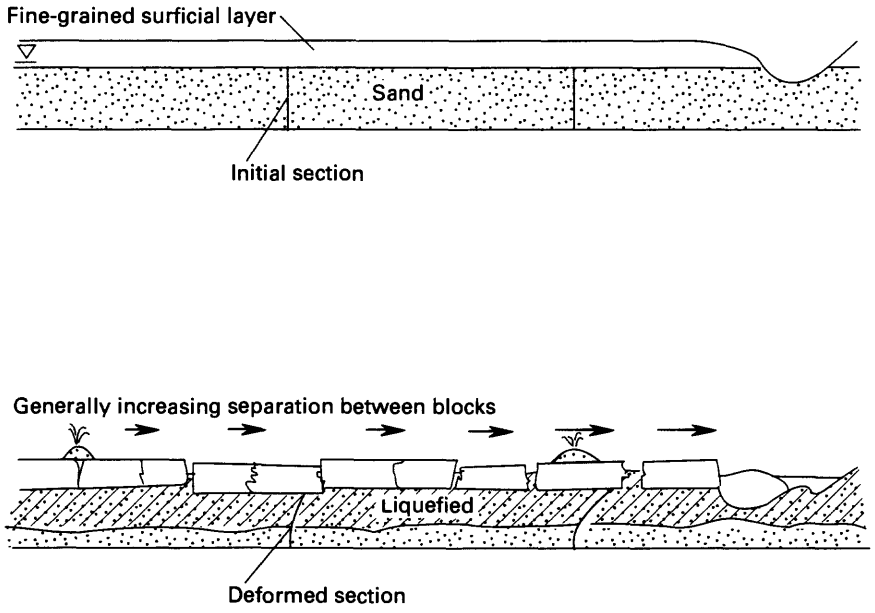

Figure 6. Vertical section showing the mechanism of ground oscillation. Liquefaction occurs in the crosshatched zone, decoupling the surface layer from the underlying firm ground. Vibration of the decoupled layer vibrates in a different frequency than the underlying and surrounding firm ground, which causes fissures to form between oscillating blocks and adjacent firm ground. Traveling ground waves and opening and closing fissures are commonly seen during ground oscillation. (From Youd, 1984.)

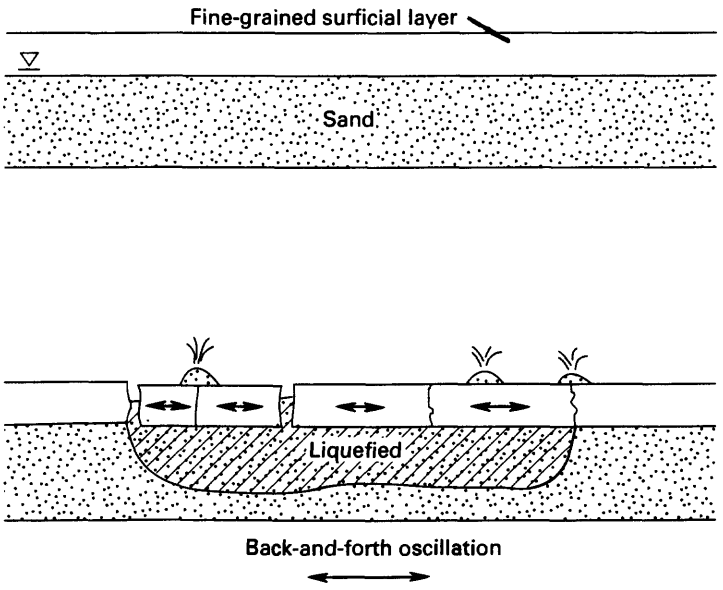

Figure 7. Vertical section showing typical sediment relations, seismic loading condition, and water flow paths involved in formation of sand blows; γ, shear strain (angle in radians); a, horizontal acceleration; τ_h, shear stress induced by horizontal acceleration.

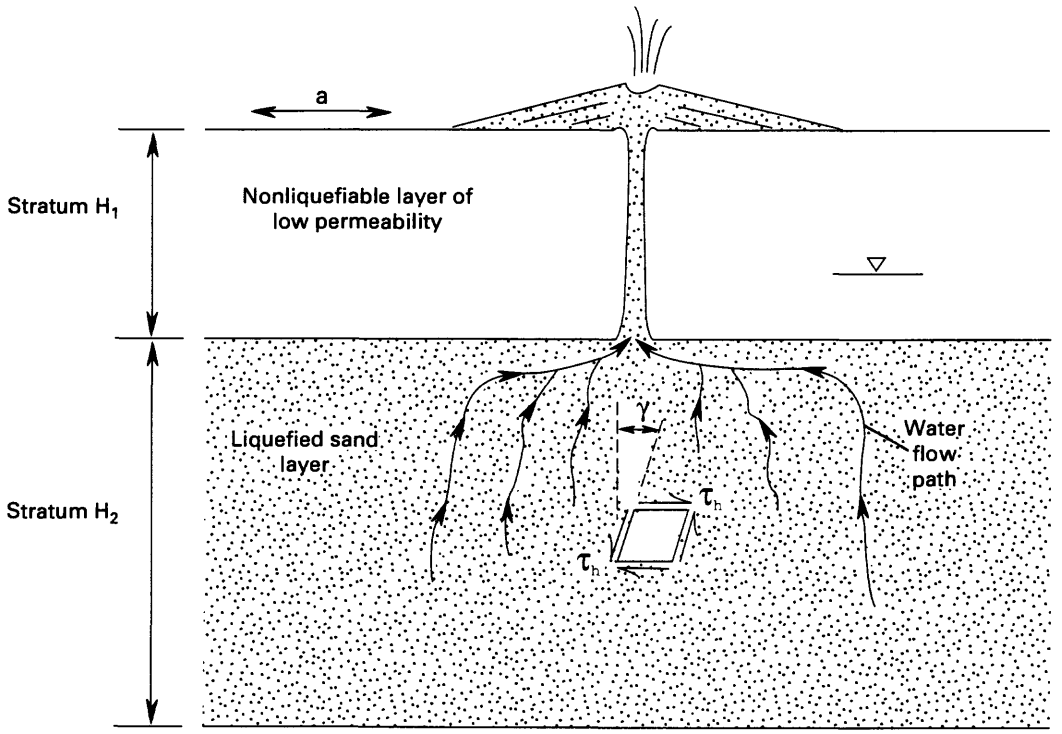

Figure 8. Gradation curves showing grain sizes most susceptible to liquefaction. (From Tsuchida and Hayashi, 1971.) Line for M 7.3 Borah Peak earthquake shows gradation of coarsest natural deposit that is verified to have produced severe liquefaction effects at ground surface. (From Youd and Andrus, 1987.) +, coarsest grain size suspected to be able to develop the condition of initial liquefaction without confinement by a cap of low permeability.

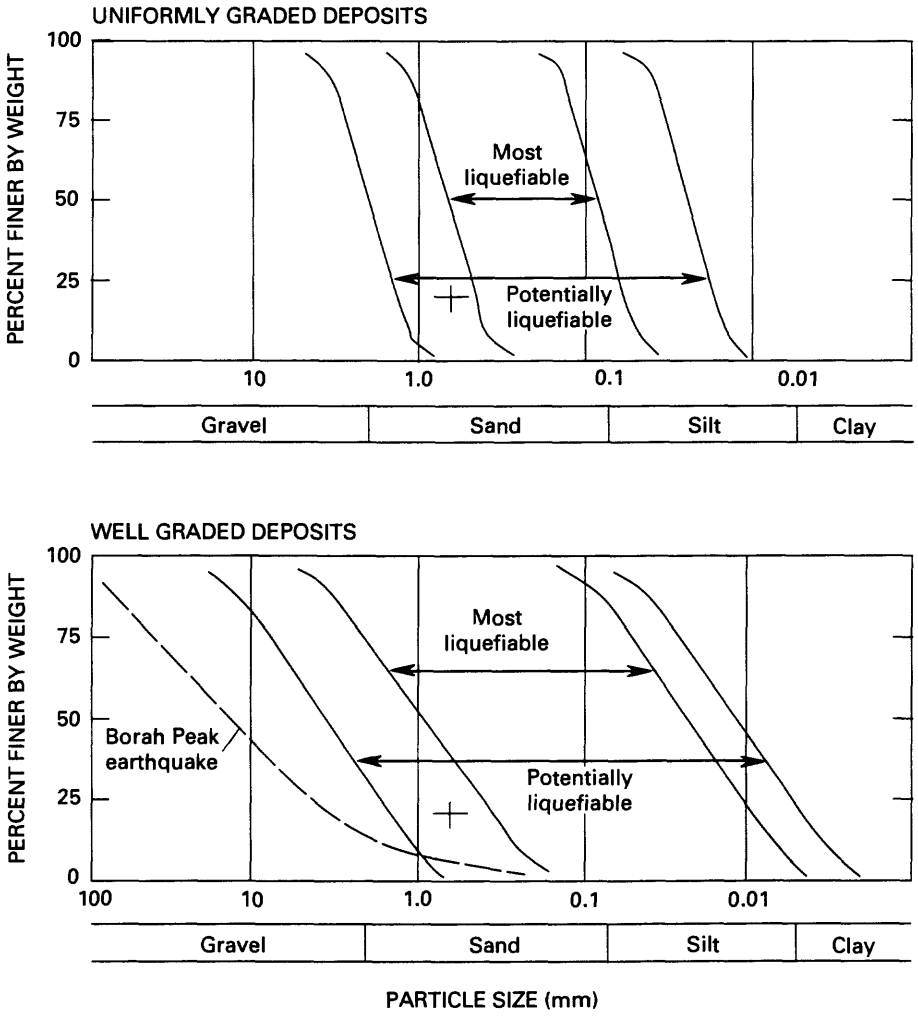

Figure 9. Proposed boundary curves relating thicknesses of nonliquefiable surface layer to thickness of the liquefiable zone, as a function of peak earthquake accelerations required to induce venting or ground rupturing at the surface. (From Ishihara, 1985.)

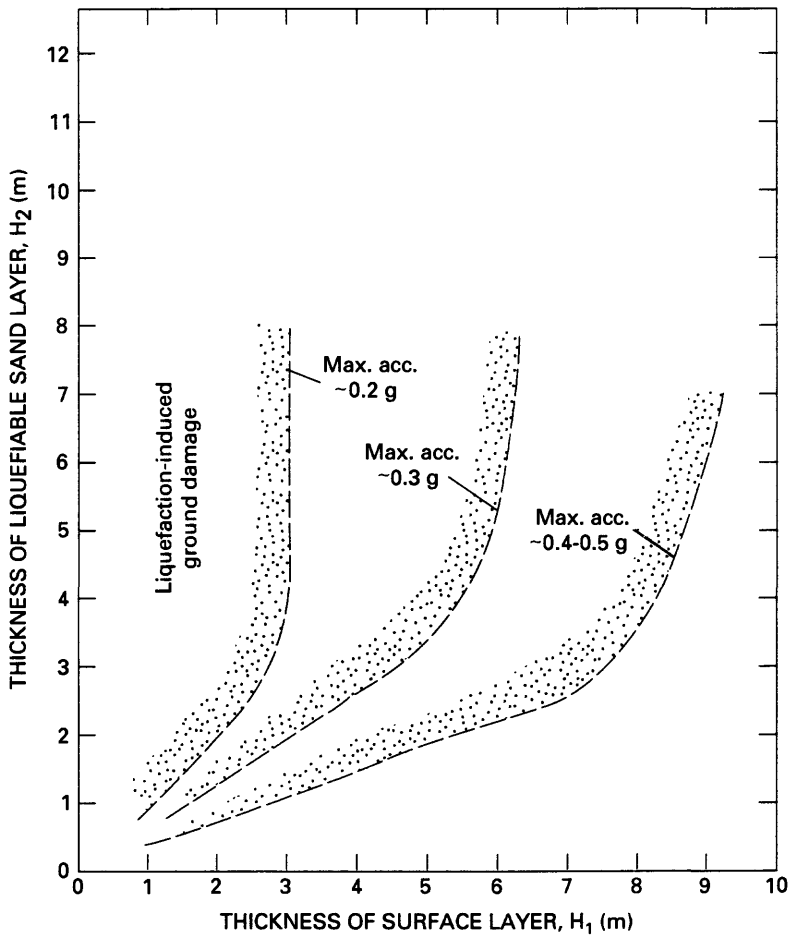

Figure 10. Normal pattern of major ground cracking produced by lateral-spread movements toward a topographic depression. Situation A shows pattern along straight and concave banks. Situation B shows pattern along slightly convex banks. Situation C shows pattern along slightly convex banks. (From McCulloch and Bonilla, 1970).

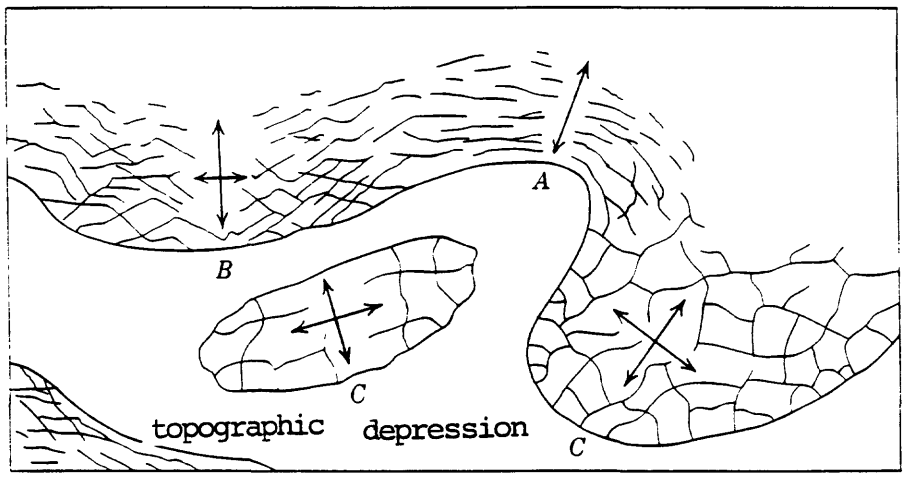

Figure 11. Coastal portion of South and North Carolina containing liquefaction sites. Unshaded onshore region is predominantly marine deposits younger than about 240,000 years. Numerous ancient beach ridges lie in this unshaded region. Shading denotes region of older marine deposits that was not reconnoitered, except locally. Younger fluvial sediments occur locally. All liquefaction sites along the Edisto River are in fluvial sediments. Almost every liquefaction site shown represents an area where numerous liquefaction features are exposed in a network of drainage ditches several kilometers in length. Index map shows coastal region searched.

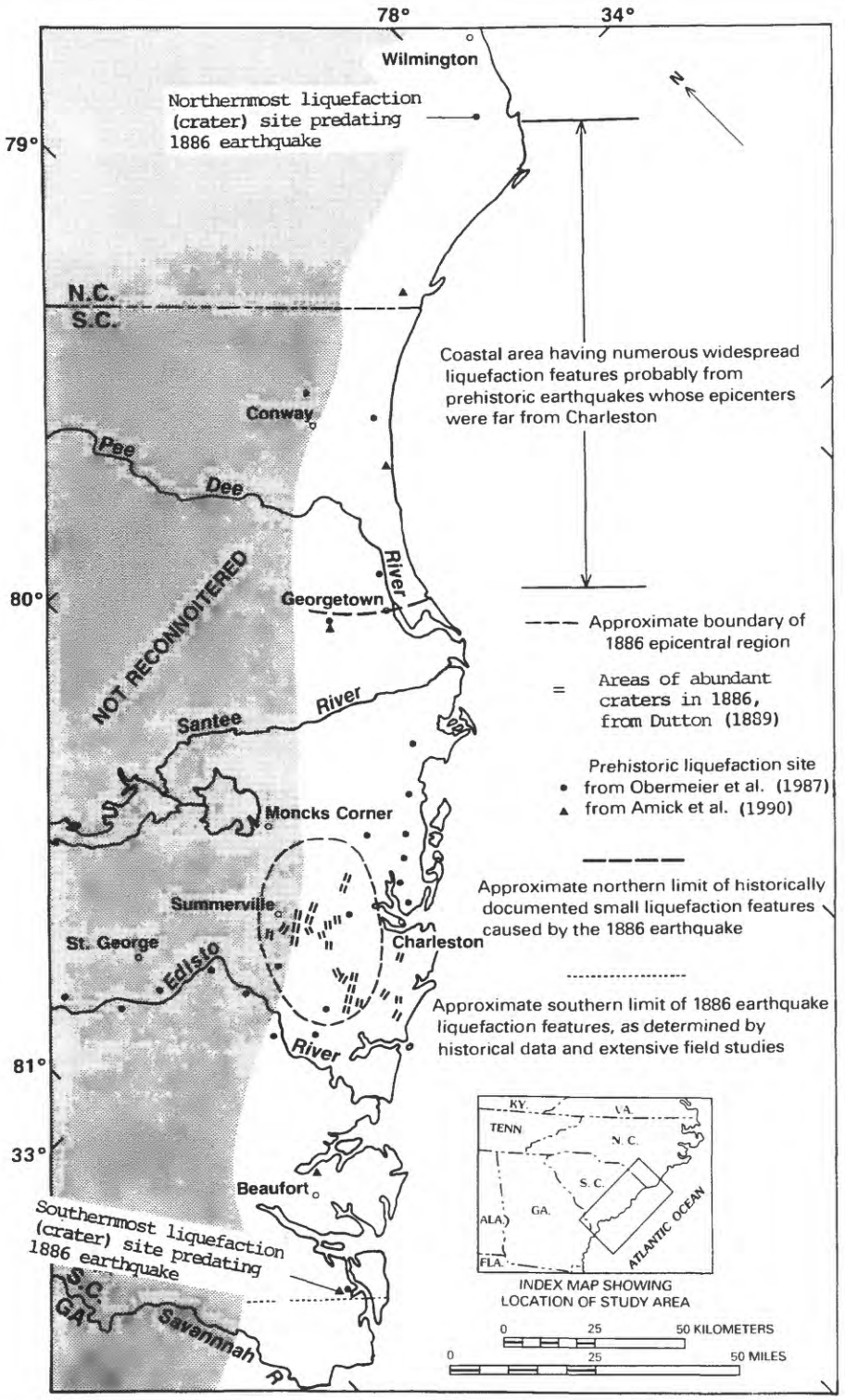

Figure 12. Craters produced by the 1886 Charleston, South Carolina, earthquake. A, Sketch from a photograph of an 1886 crater (sand blow at Ten Mile Hill, near the present Charleston airport). Note that the crater contains sand sloughing toward the lowest parts and that there is a constructional sand volcano located in the right part of the crater (at arrow). The crater is surrounded by a thin blanket of sand partly veneered with cracked mud. B, Photograph of typical crater produced by the 1886 earthquake. Note the thin blanket of ejected sand around the crater and sand and clasts of dark soil within the crater. (Photograph from the archives of the Charleston Museum).

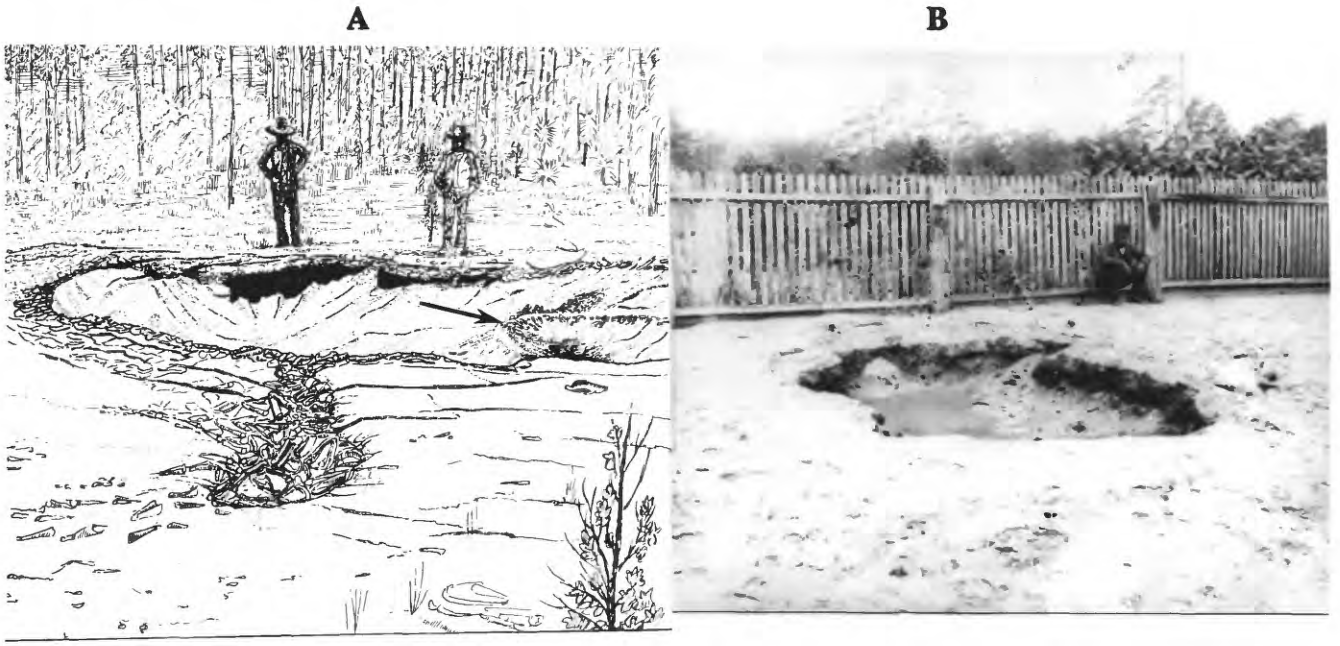

Figure 13. Schematic vertical section of representative barrier showing sediment types, ground-water-table locations, filled craters, and Bh (humate-rich) soil horizons. Modern shoreline is located southeastward. Lagoonal clay deposit at left is younger and lower in elevation than the barrier-bar deposit.

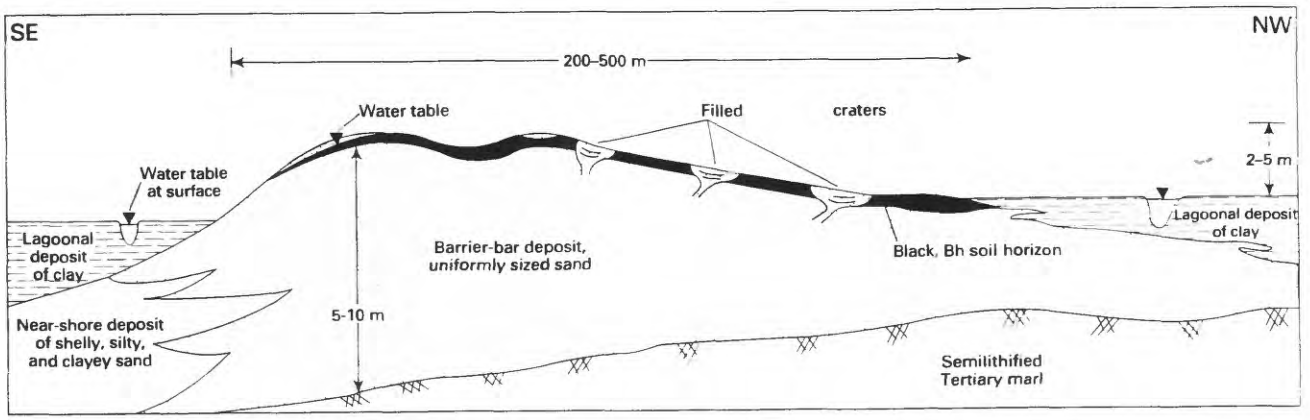

Figure 14. Schematic vertical section of filled liquefaction crater that forms a bowl in three dimensions. Letters correspond to soil horizons. The filled crater in this figure long predates the 1886 Charleston earthquake, on the basis of thickness of Bh horizon in the filled crater. Insert shows zonation within the crater.

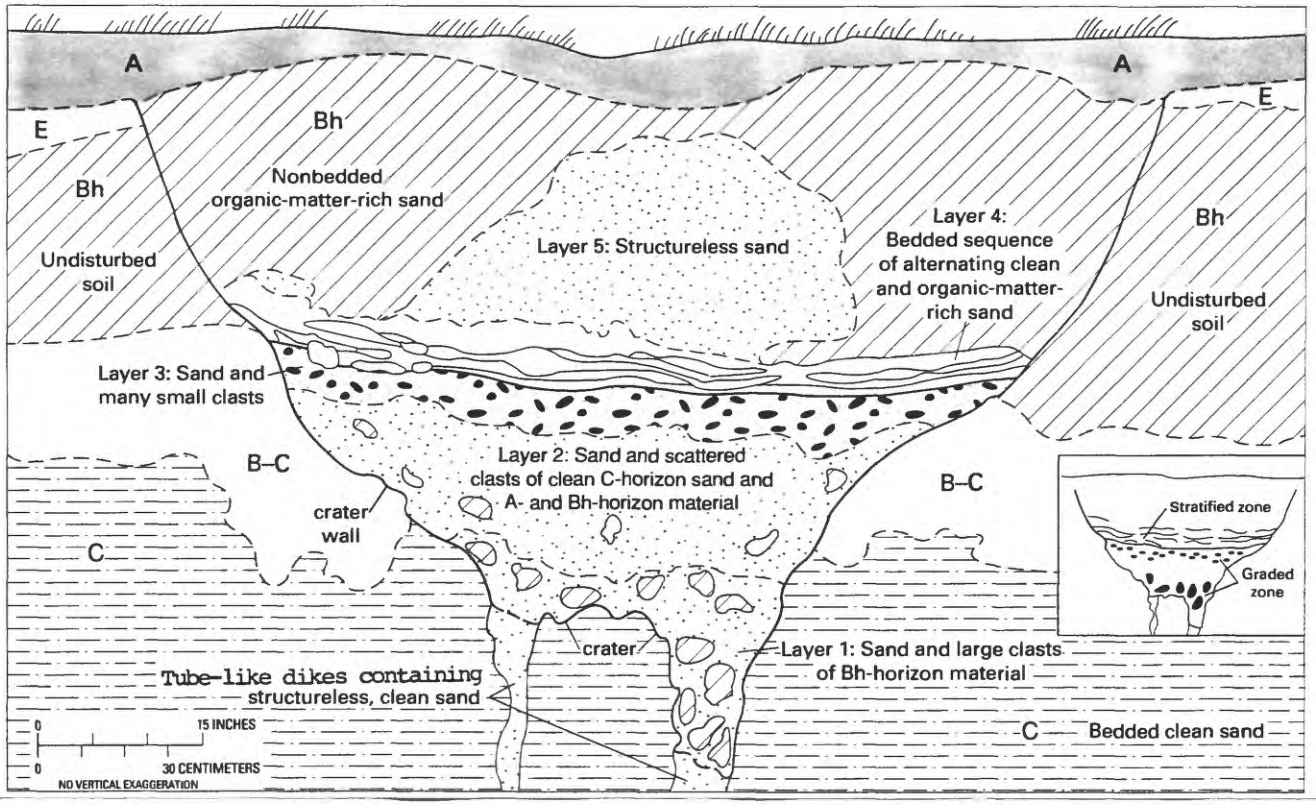

Figure 15. Schematic vertical section showing V-shaped, sand-filled fissures interpreted as resulting from liquefaction during the 1886 Charleston earthquake. Sand in the fissures came from a depth of 6 m, on the basis of grain size and mineralogy. Fissure cuts soil horizon developed on filled crater predating 1886.

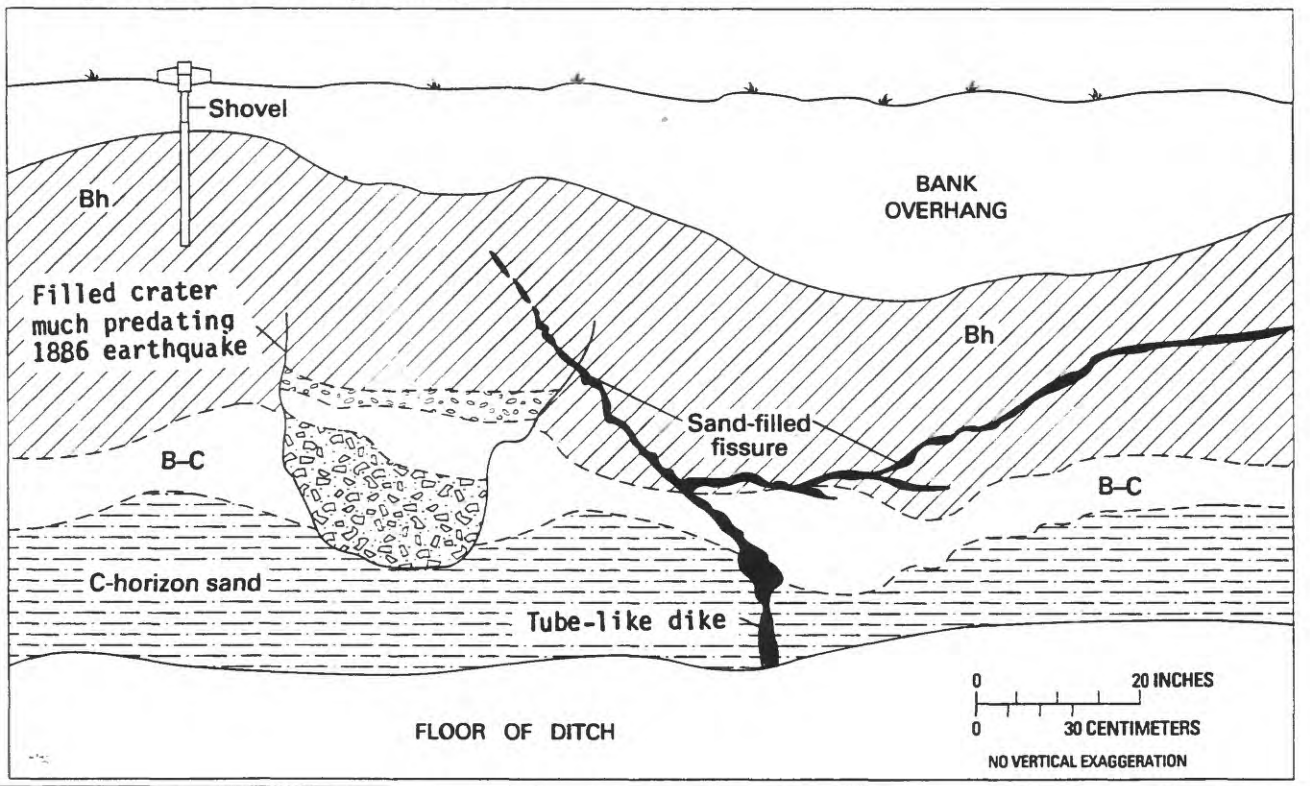

Figure 16. Approximate limits of New Madrid Seismic Zone and Wabash Valley Seismic Zone. New Madrid Seismic Zone is the source area of 1811-12 earthquakes and continues to have many small earthquakes and a few slightly damaging earthquakes. Wabash Valley Seismic Zone is a weakly defined zone of seismicity having infrequent small to slightly damaging earthquakes.

Figure 17. Regions having abundant vented sand, excluding modern flood plains, in the New Madrid Seismic Zone. (From Obermeier et al., 1990.) Sand was presumably vented in response to 1811-12 earthquakes. Severe liquefaction also occurred locally beyond the areas shown on the map, especially along streams west of the Crowleys Ridge (Fuller, 1912). Also shown are the approximate epicenters for the three strongest 1811-12 earthquakes and major faults and fault zones.

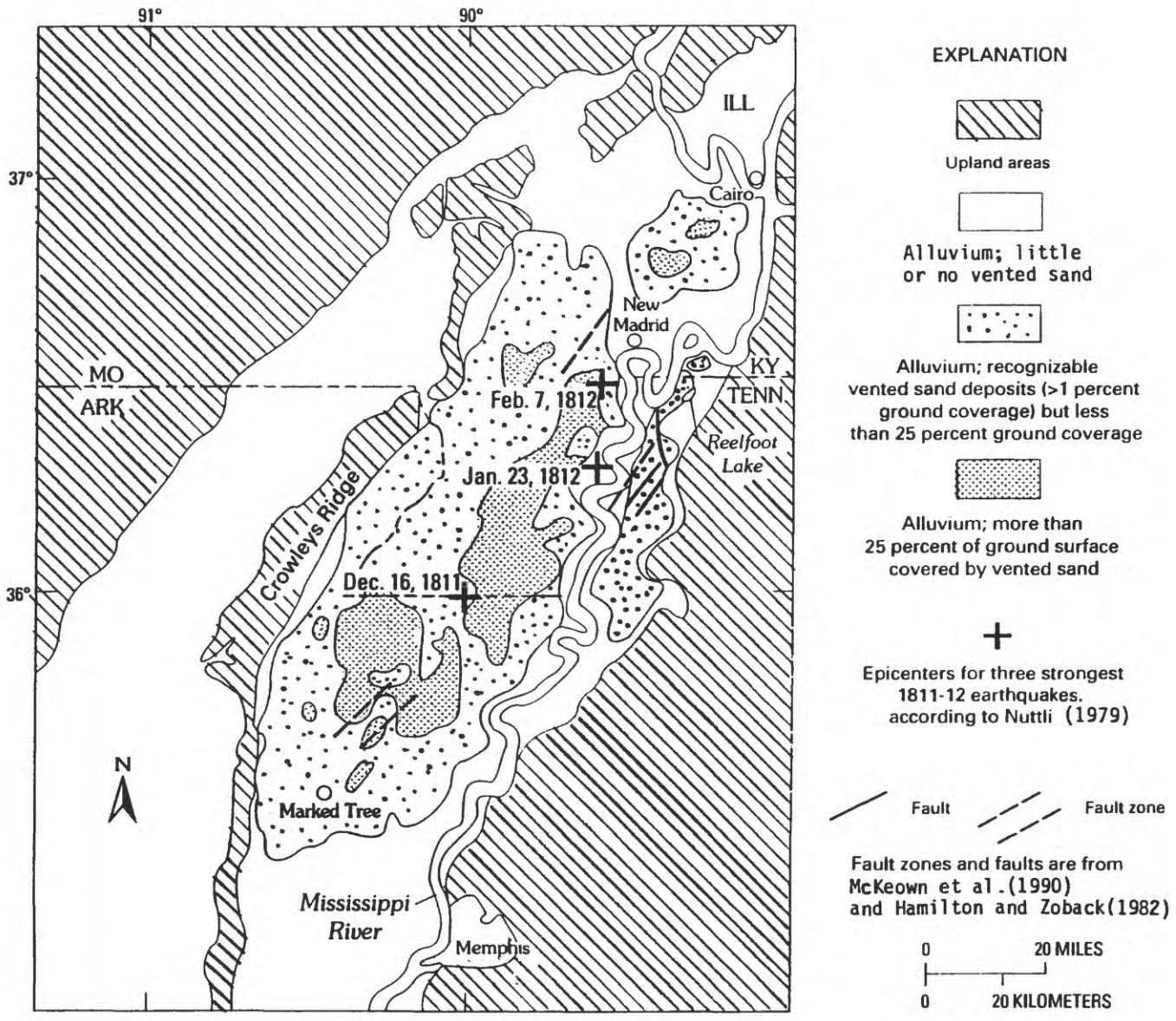

Figure 18. Aerial photographs that show long fissures through which sand vented (light-colored linear features) and also show individual sand blows (light-colored spots) formed by liquefaction during the 1811-12 New Madrid earthquakes. A, A portion of the Manila, Arkansas, 7.5-minute orthophotographic quadrangle. Fissuring and venting in braid-bar deposits of latest Pleistocene age and in younger Holocene point-bar sediments. Note how fissures formed parallel to the scrolls of point-bar deposits. Note also the abundance of fissures in the upper part of the right side of the photograph. These fissures have formed near a break in slope, where the terrace that is underlain by braid-bar deposits is adjacent to the slightly lower floodplain level of point-bar deposits. B, Aerial photograph taken about 40 km north of A. Extensive fissuring and venting in braid-bar deposits of latest Pleistocene age. Cap thickness (about 6 m) is relatively unifirm. Topographic relief is only on the order of 1 m throughout the region of extensive fissuring. Note severe fissuring over a width of at least 3 km.

(Figures on next two pages.)

Figure 18A.--Continued

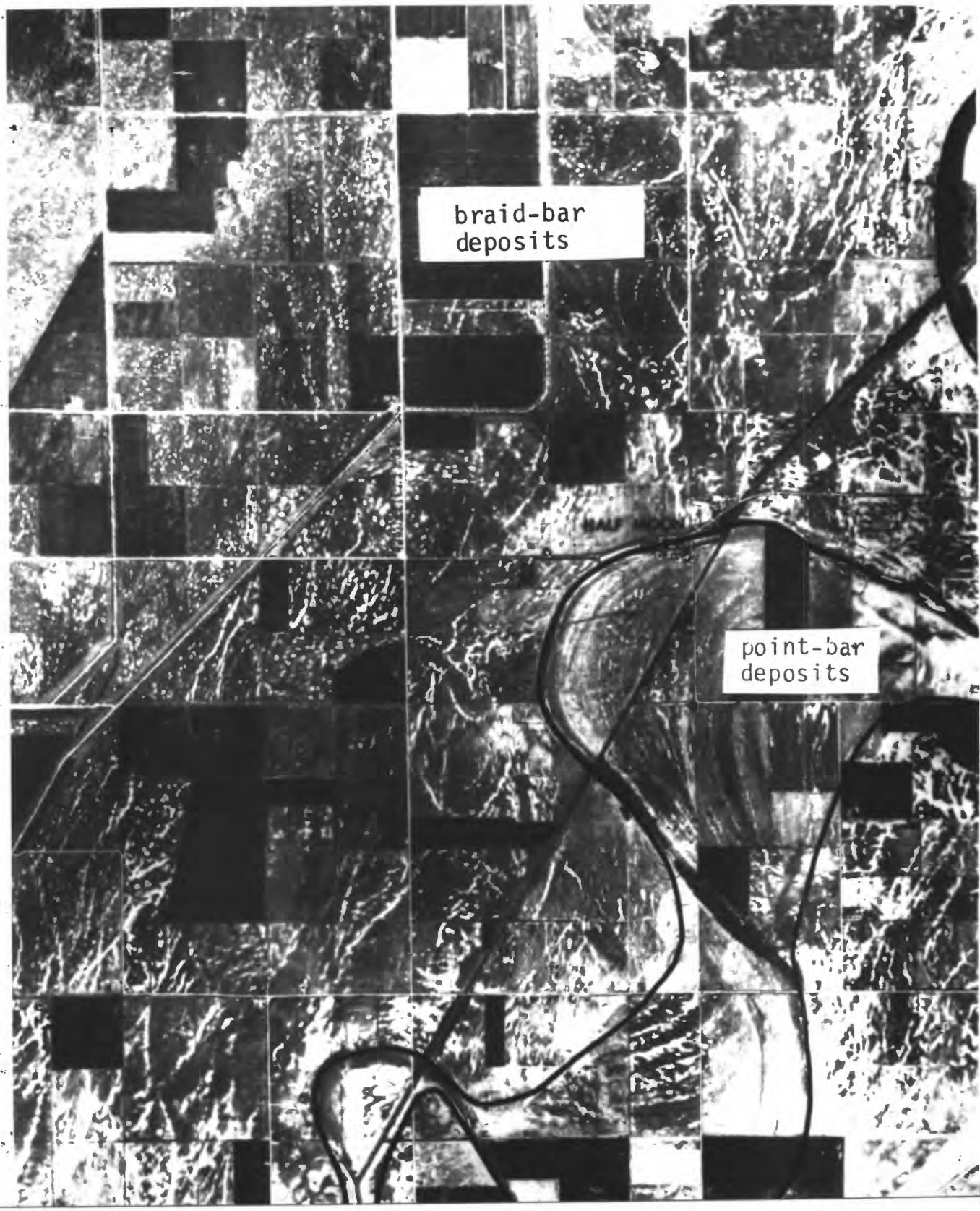

0 1 MILE

0 1 KILOMETER

73A

Location

Figure 18B.--Continued

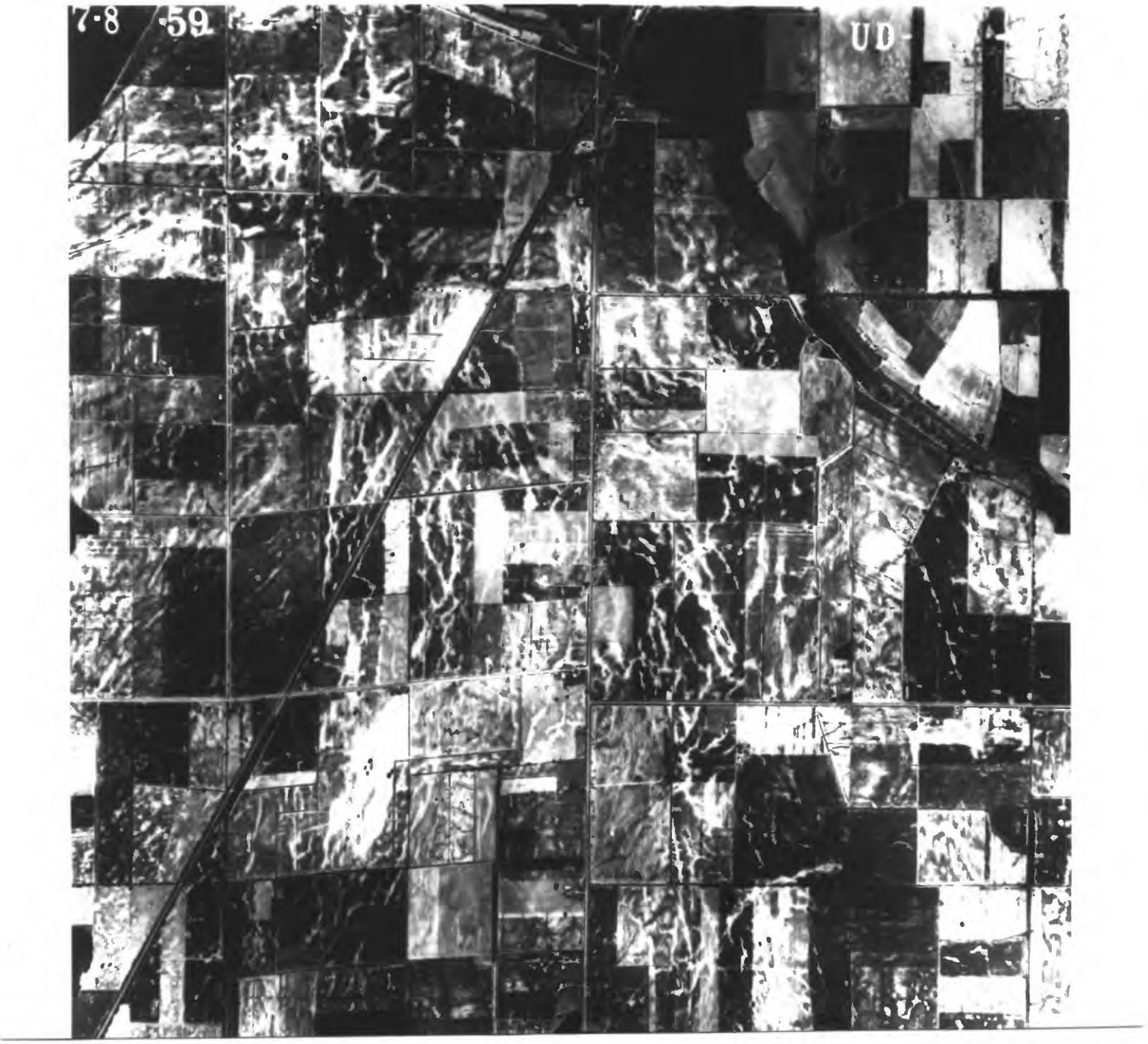

0 1 MILE

0 1 KILOMETER

74A

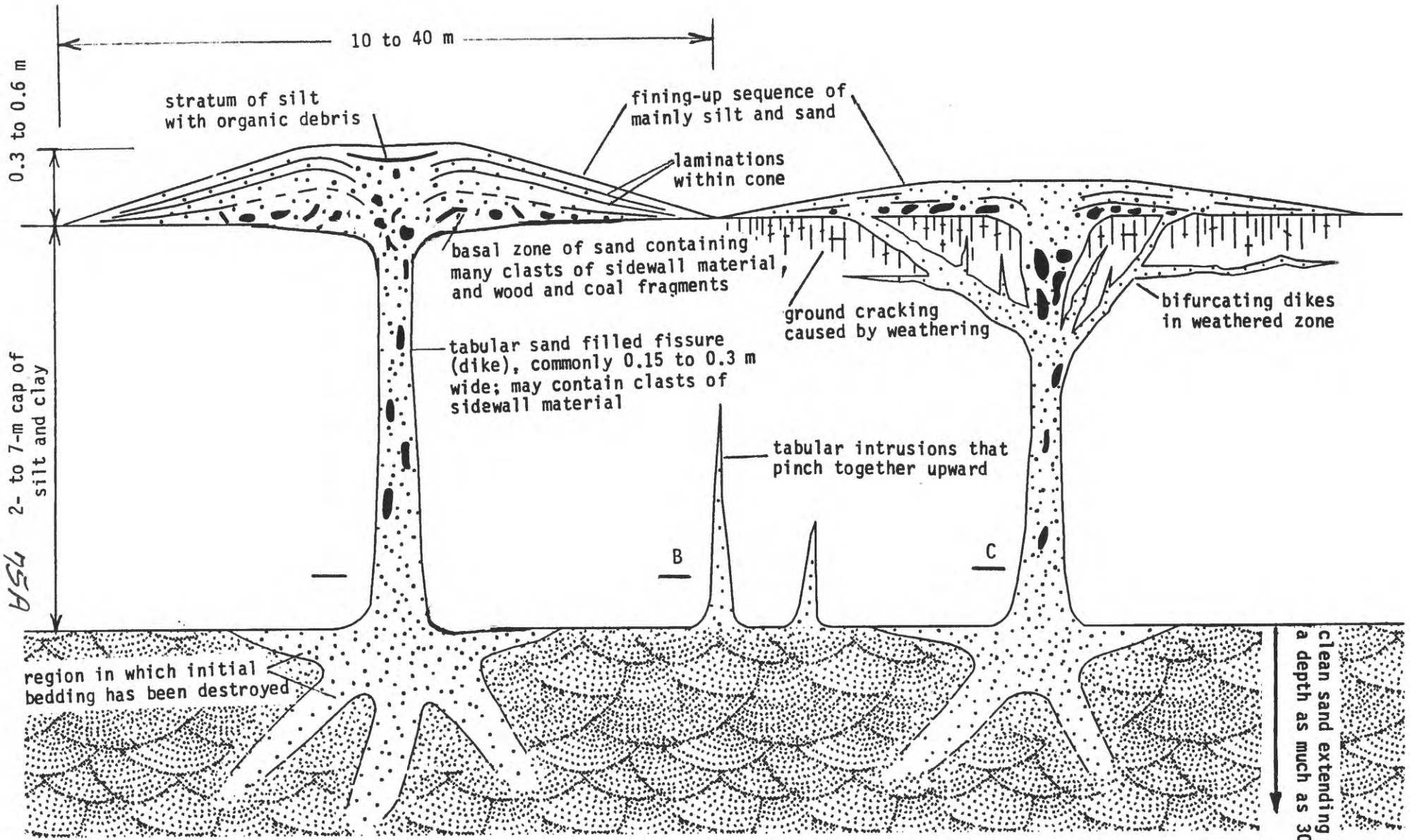

Figure 19. Schematic vertical section showing dikes cutting through overbank silt and clay strata and the overlying sand-blow deposits. A, Stratigraphic details of sediment vented to the surface. B, Dikes that pinch together as they ascend. C, Characteristics of dikes in fractured zone of weathering, in highly plastic clays. Situations shown are encountered in many places in meisoseismal zone of the 1811-12 New Madrid earthquakes.

Figure 20. Sketch and photograph of vertical exposure in a ditch in the meisoseismal zone of the 1811-12 New Madrid earthquakes showing evidence for about 1.5 m of lateral spreading. The S1 sand was emplaced during lateral spreading. The lignitic silty clay layer next was laid down on S1 sand. Later, S2 sand was vented to the surface, burying the lignitic silty clay and S1 sand. Note that the sidewalls are approximately parallel. Numbers in photograph are spacing in meters. (From Wesnousky and Leffler, 1992.)

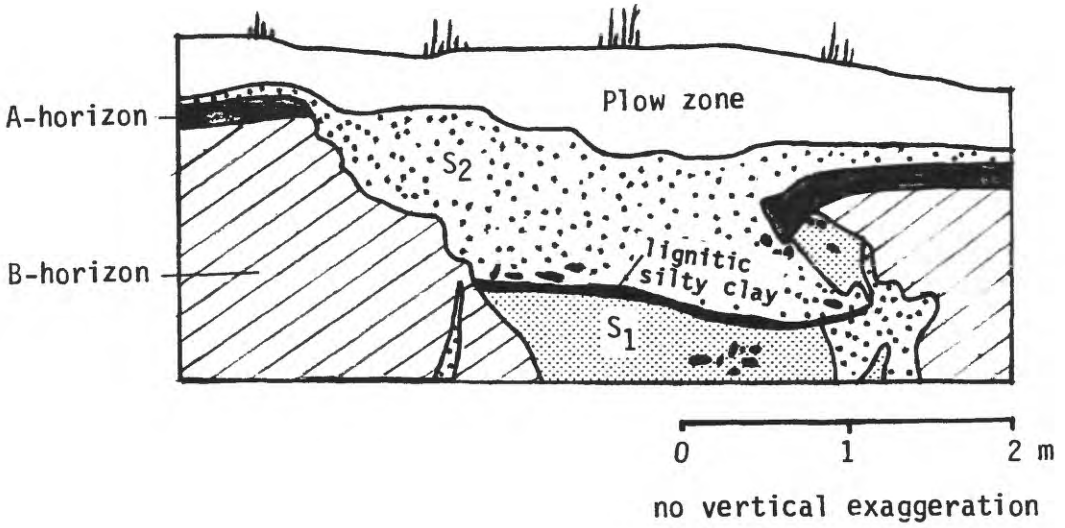

Figure 21. Schematic vertical section showing where sills preferentially form. Note that thin sills can extend great distances horizontally, especially where the overlying cap is thin.

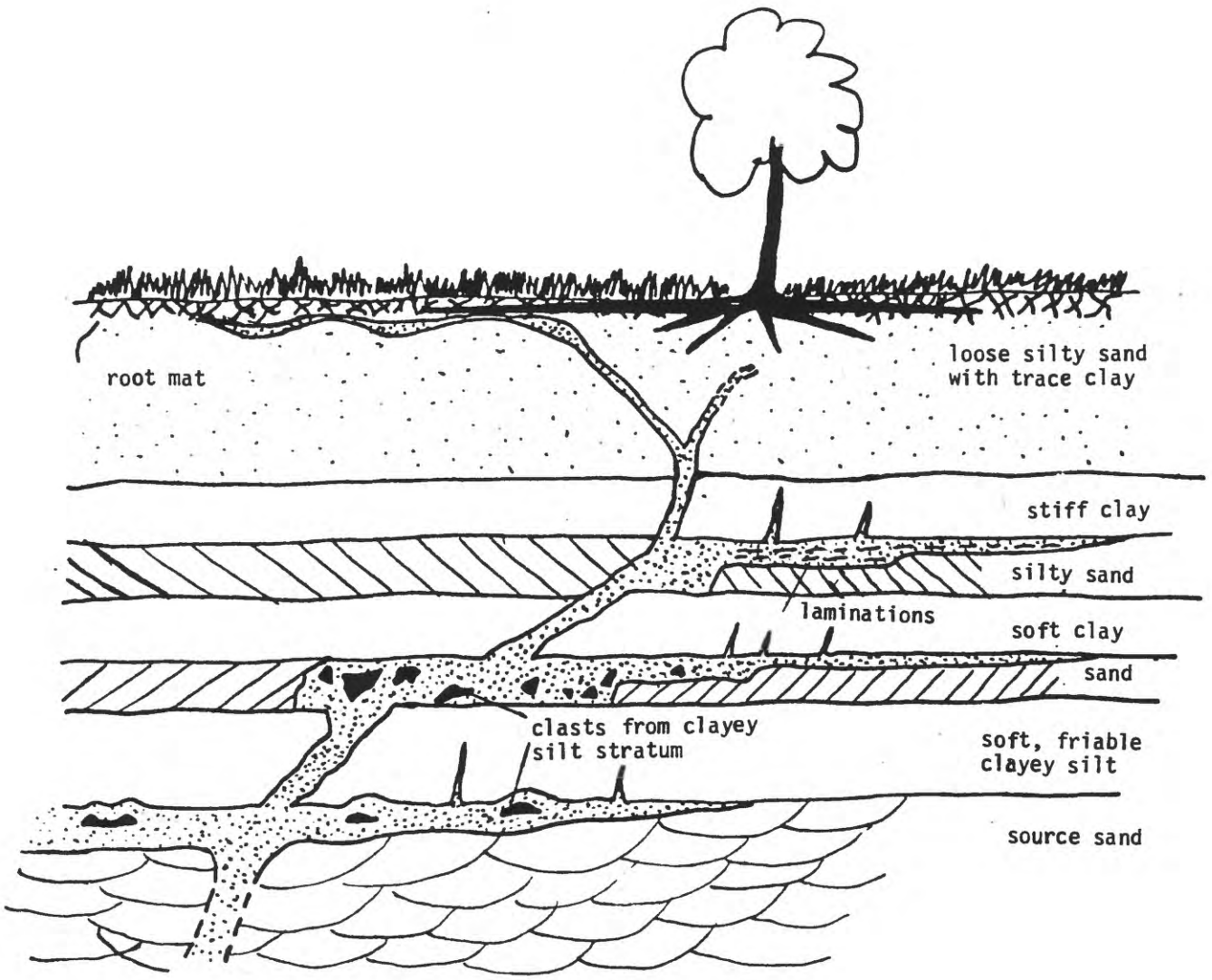

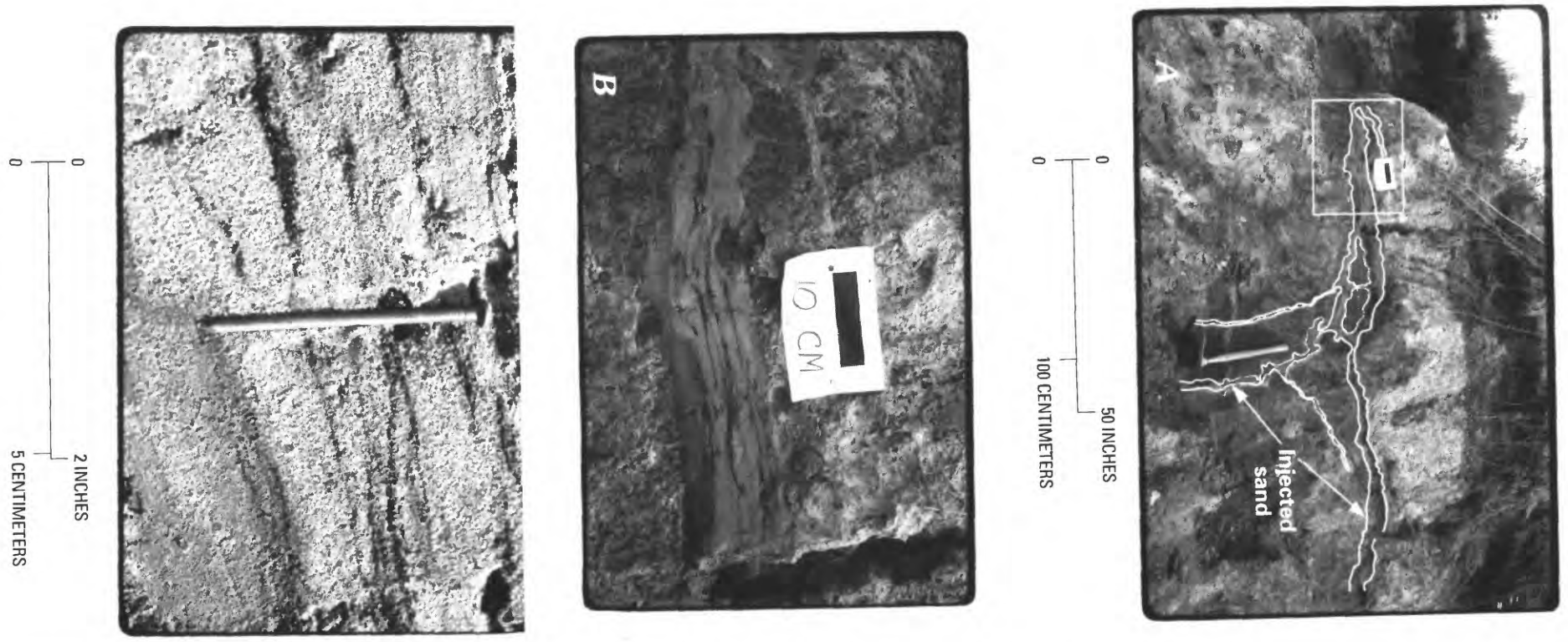

Figure 22. Sand dikes and sills exposed in a nonliquefiable cap of silt and clay; the dikes and sills are interpreted as having originated by liquefaction during the 1811-12 New Madrid earthquakes. Outcrop is a ditch bank in the meisoseismal area of the 1811-12 earthquakes. A, Overview and line drawing of typical small dikes and small sills. The sill extends far beyond the photograph and is at least 25 m long. Rectangle shows area of Figure 16B. B, View showing details of layering in sills. C, Very close view showing details of layering in sill. Sill is made up of fine- and medium-grained sand with some silt- and sand-sized lignite. Black bands are lamina of small pieces of lignite.

Figure 23. Schematic vertical section showing Holocene sediments (nonliquefiable cap) and underlying Wisconsinan age source sand that liquefied. Exposure is in a ditch in the meisoseismal region of the 1811-12 New Madrid earthquakes. Earthquake-induced intrusions cut section at many places. A, Schematic diagram of stratigraphic relations and liquefaction-induced features (numbered 1-5). Feature 1--Dikes of medium-grained sand that cut cap and source sand. Features 2 and 3--Intruded dikes and sills of massive, clean, medium-grained sand. Feature 4--Dike and flame structures of medium-grained sand containing and large clasts from bed G. Feature 5--Dikes of medium-grained sand, truncated unconformably. Feature 6--Pseudonodules collapsed in bed D. B, Photograph of beds A-D showing sand intrusion (feature 3). Knife is 12 cm long (B-E). C, Photograph of dikes (feature 1) cutting source (bed A) and bed B. D, Photograph of plan view of bed B showing intrusion structures caused by feature 1; the plan view is in the area of the knife that is oriented vertically in Figure 16B. E, Photograph of part of feature 4, showing clay clasts in sand matrix intruded into bed H.

(Figures on next two pages.)

Figure 23A.--continued

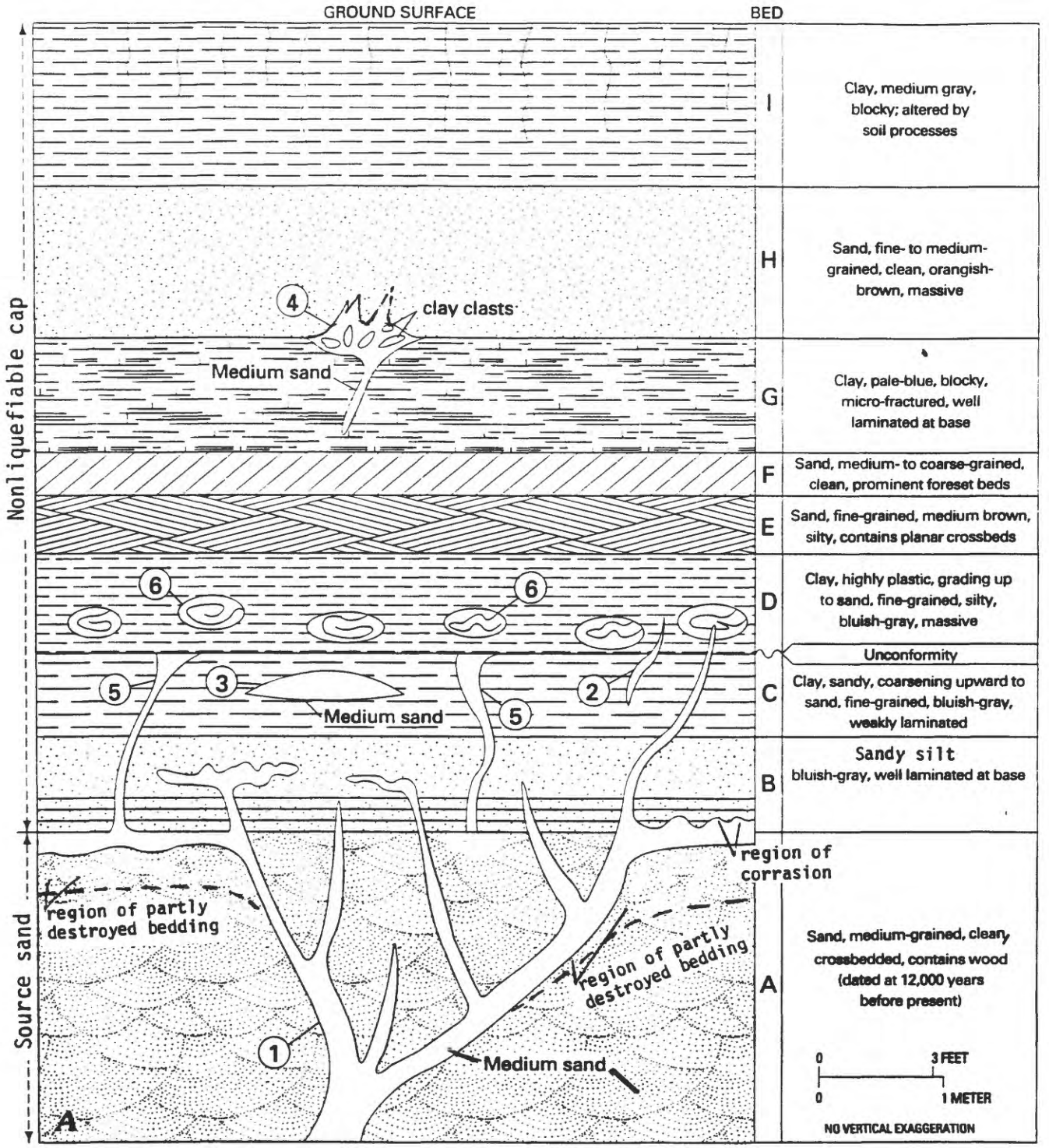

Figures 23B through 23E.--continued

B

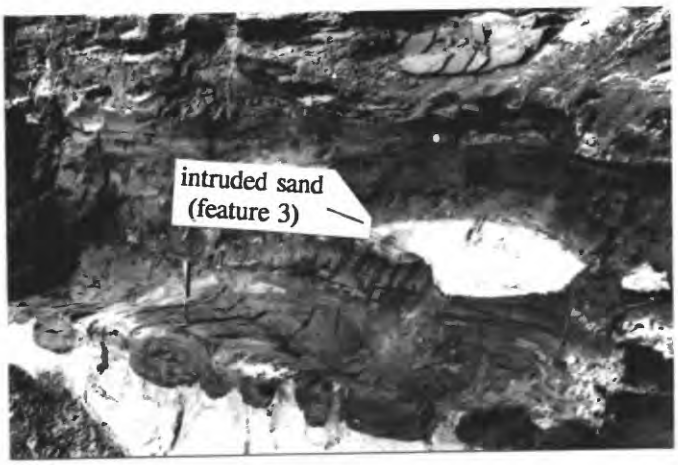

C

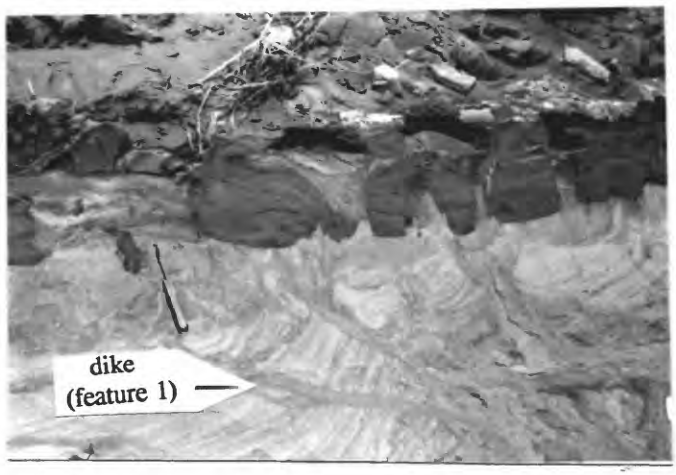

D

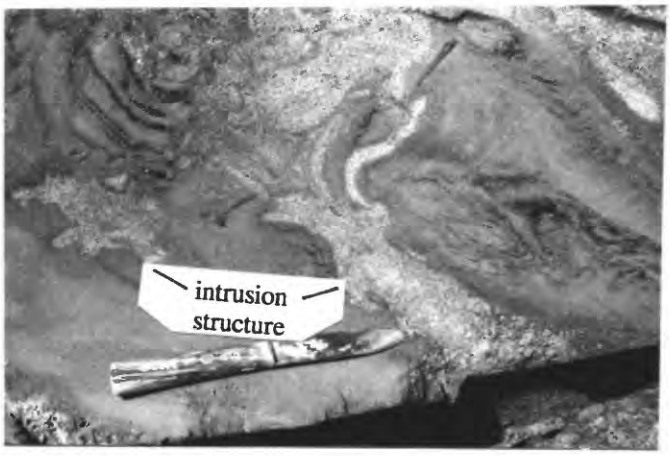

E

Figure 24. Map showing area searched for liquefaction features, showing sites where paleoliquefaction features (mainly dikes) were discovered, and showing regional limits of liquefaction for different earthquakes. About 10 percent of the length of the rivers searched has freshly eroded exposures. Only exceptionally are there no fresh exposures of mid-Holocene or older sediments within a 20 km length of river; no suitable exposures are in the region of shallow bedrock on the map. Liquefaction sites on the map generally denote exposures with numerous dikes. Some sites in the southern part of the study area have unweathered dikes near the surface, probably induced by the 1811-12 New Madrid earthquakes. Dike widths on the figure were measured at least 1 m above the base of the dike. Sites with dikes having a width > 0.7 m are shown for the 6100 yr BP earthquake. Note the core region of exceptionally large dikes around Vincennes. (Modified from Munson et al. (1994) and Obermeier et al. (1993).)

(Figure on next page.)

Figure 24.--Continued

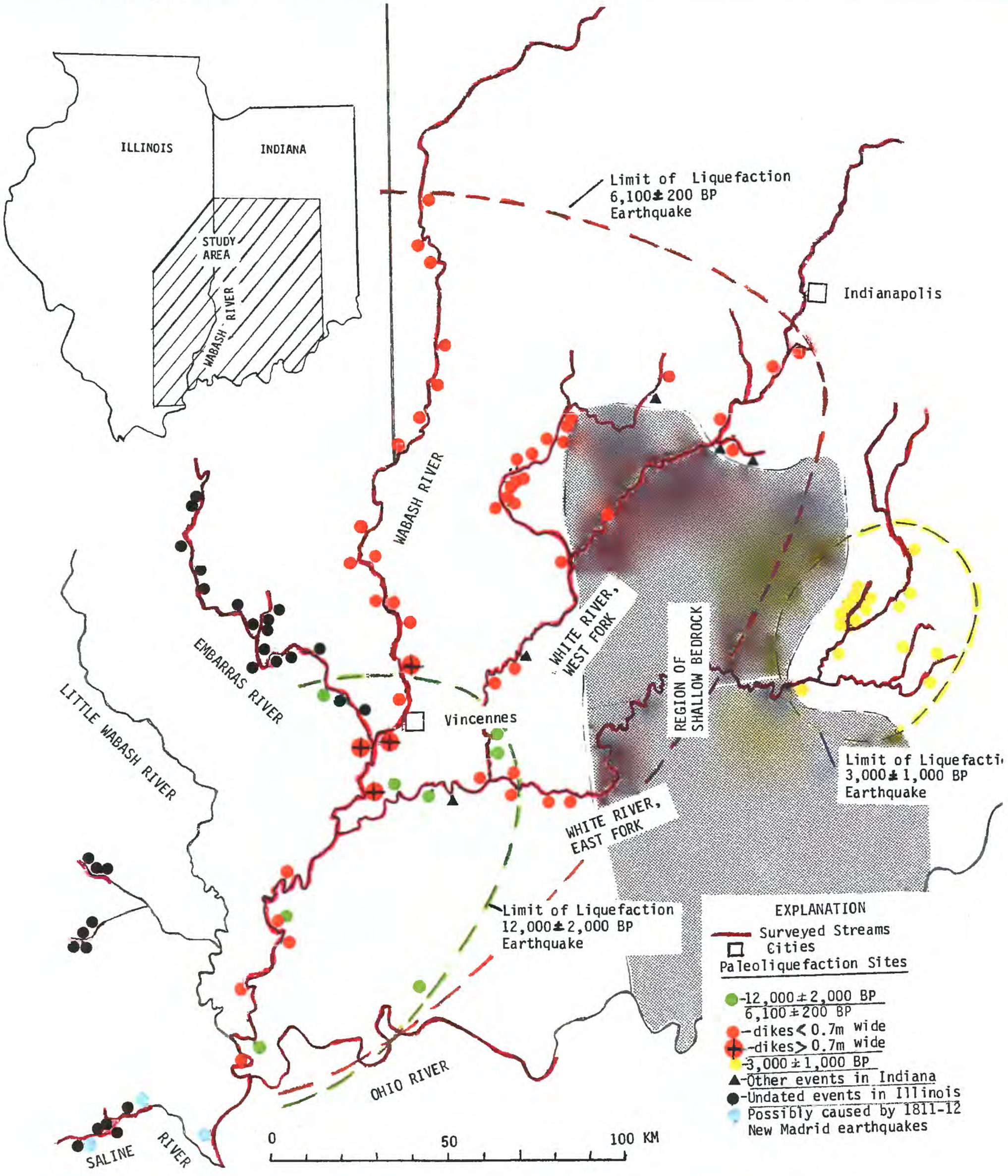

Figure 25. Diagrammatic vertical section showing general characteristics of buried sand- and gravel-filled dikes along the Wabash River. Source beds are Holocene point-bar deposits or late Wisconsinan age braid-bar deposits overlain by much finer overbank sediment. Sediment in source beds beneath dikes shows evidence of flow into dikes. Gravel content and size decrease upward in dikes at many places. The column on right side of the figure contains pedological descriptions of host materials.

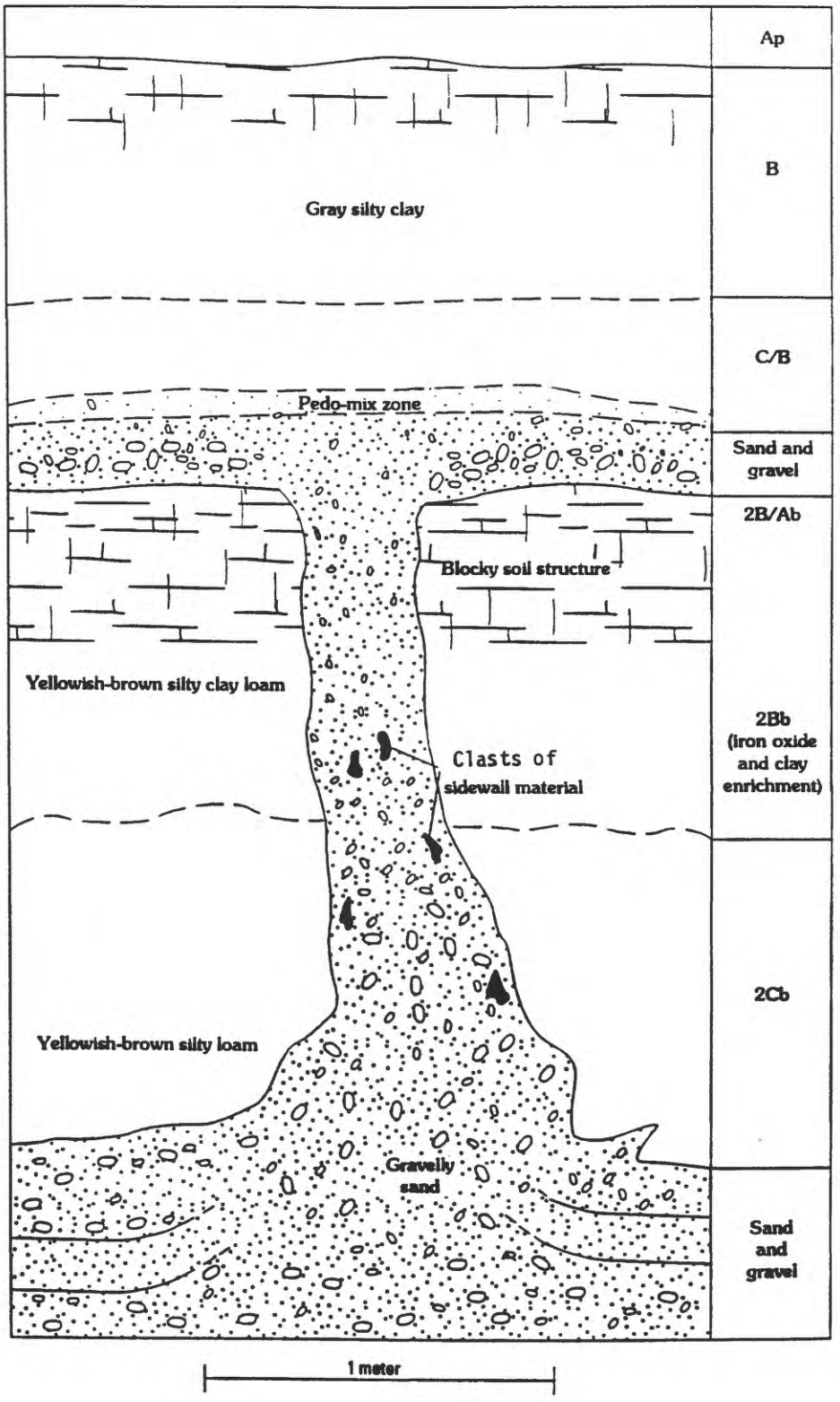

84A

Figure 26. Map showing that part of the Columbia River where banks of islands were searched for paleoliquefaction features. These searched islands have ages between 600 and 1,000 years at most places. Sands beneath islands are fine to medium grained and generally are at least moderately susceptible to liquefaction. Maximum dike width is measured at least 1 m above the base of the dike. Inset shows seaward edge of Cascadia subduction zone.

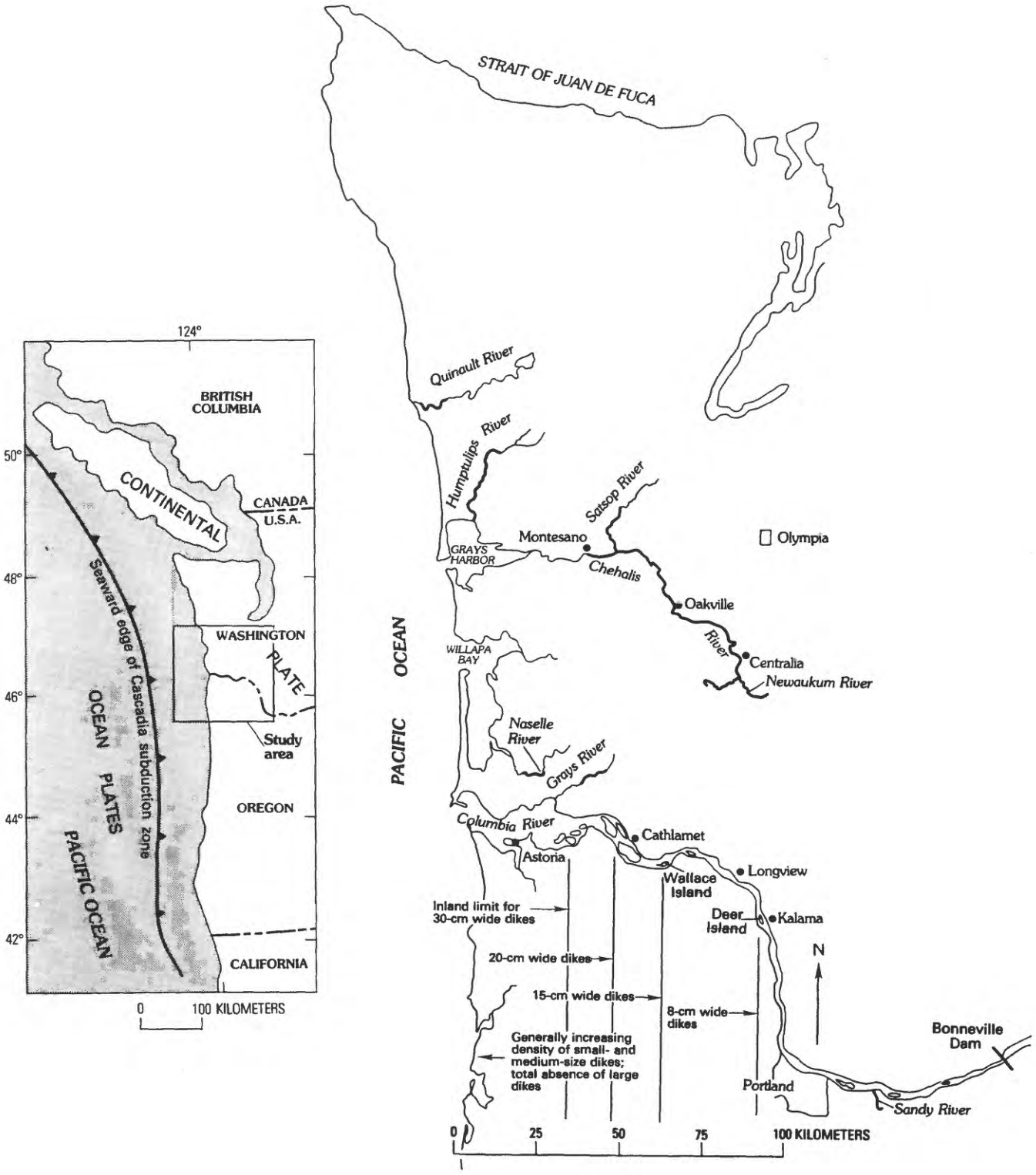

85A

Figure 27. Block diagram showing typical field relations at liquefaction sites in Columbia River islands. A sand-filled dike cuts through a 1- to 2-m thickness of soft silt and clay with a weakly developed soil at the top. The dike connects to a thin sand sheet on the soil horizon that is buried by a 1-m thickness of silt and clay. Tubers at widespread sites collected in their growth position near the base of the stratum cut by dikes have radiocarbon ages ranging between 600 and 1,000 years. Widths of top of dikes are typically only several millimeters.

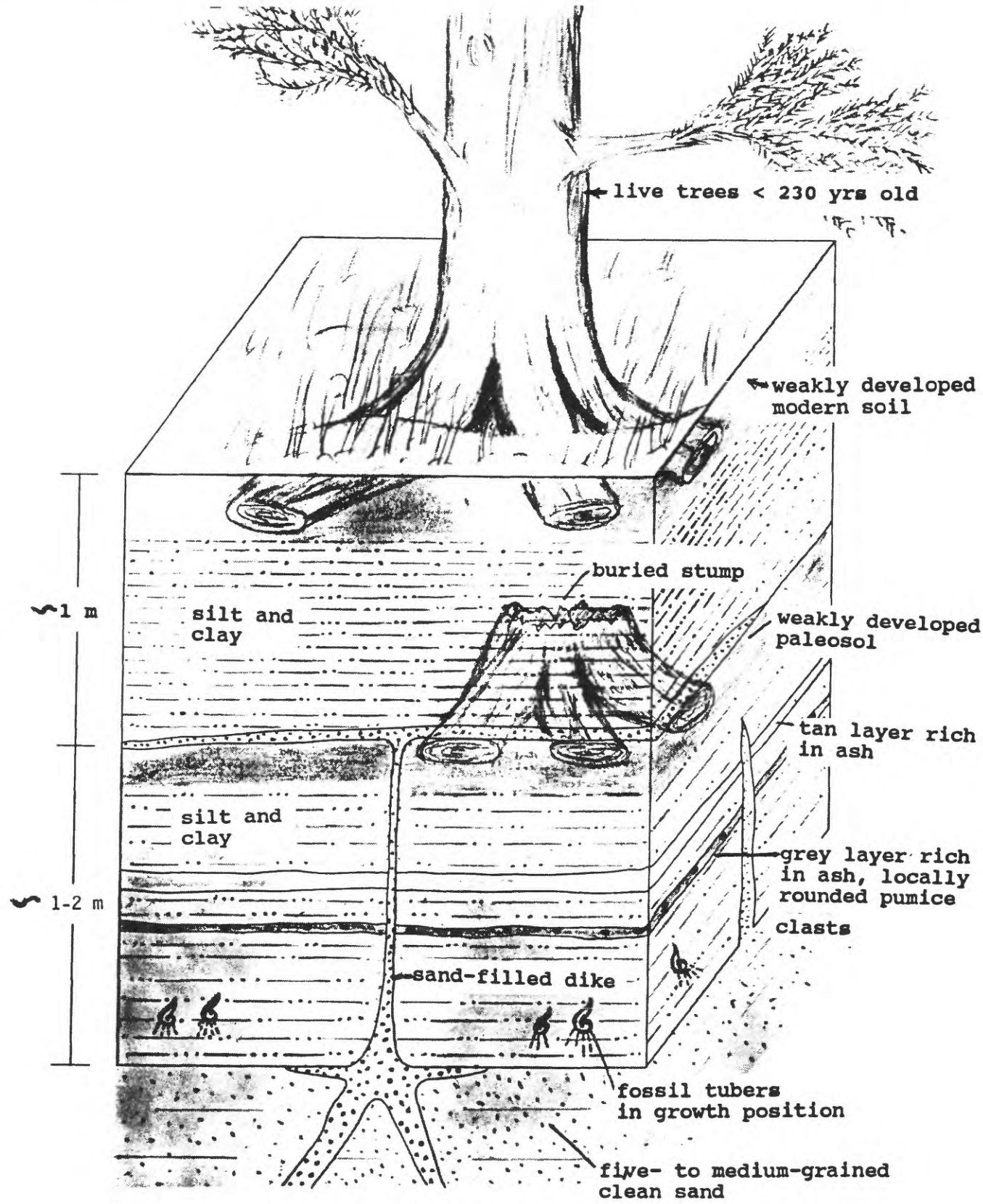

Figure 28. Aerial photograph of mima mounds (white circular spots) in northern portion of meisoseismal area of 1811-12 New Madrid earthquakes. Note regularity of spacing and alignment of mounds.

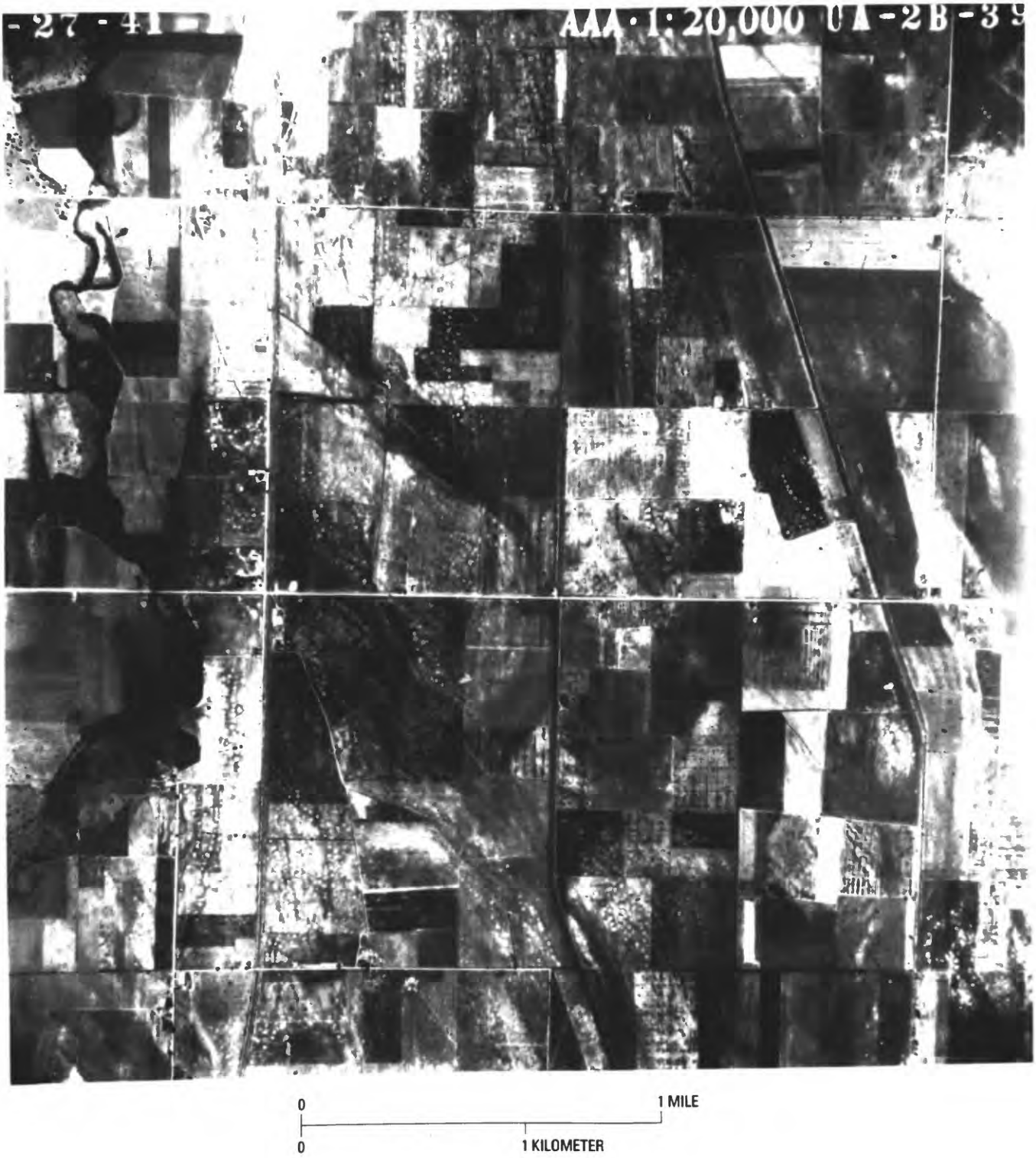

Figure 29. Schematic vertical section showing pseudonodules formed by shaking (From Kuenen, 1958). A layer of sand (unit 1) overlies very soft clay (unit 2) in A. With shaking, pseudonodules developed (B and C and became completely enclosed in clay (D and E). Note the destruction of layering from C to D. This deformation is due to sinking of the entire sand layer into the very soft clay and also to localized sinking caused by uneven loading.

Figure 30. Schematic vertical section showing development of load-casted ripples, caused by ripple crests sinking into soft mud. Note the progressive tilt of the internal cross-lamination, which causes the downflow portion to be more steeply inclined than the upflow portion (modified from Dzulynski and Kotlarczyk, 1962). Load-casted ripples can also have an opposite sense of rotation (upflow more steeply inclined than downflow), as observed in the meisoseismal region of the 1811-12 New Madrid earthquakes.

Figure 29

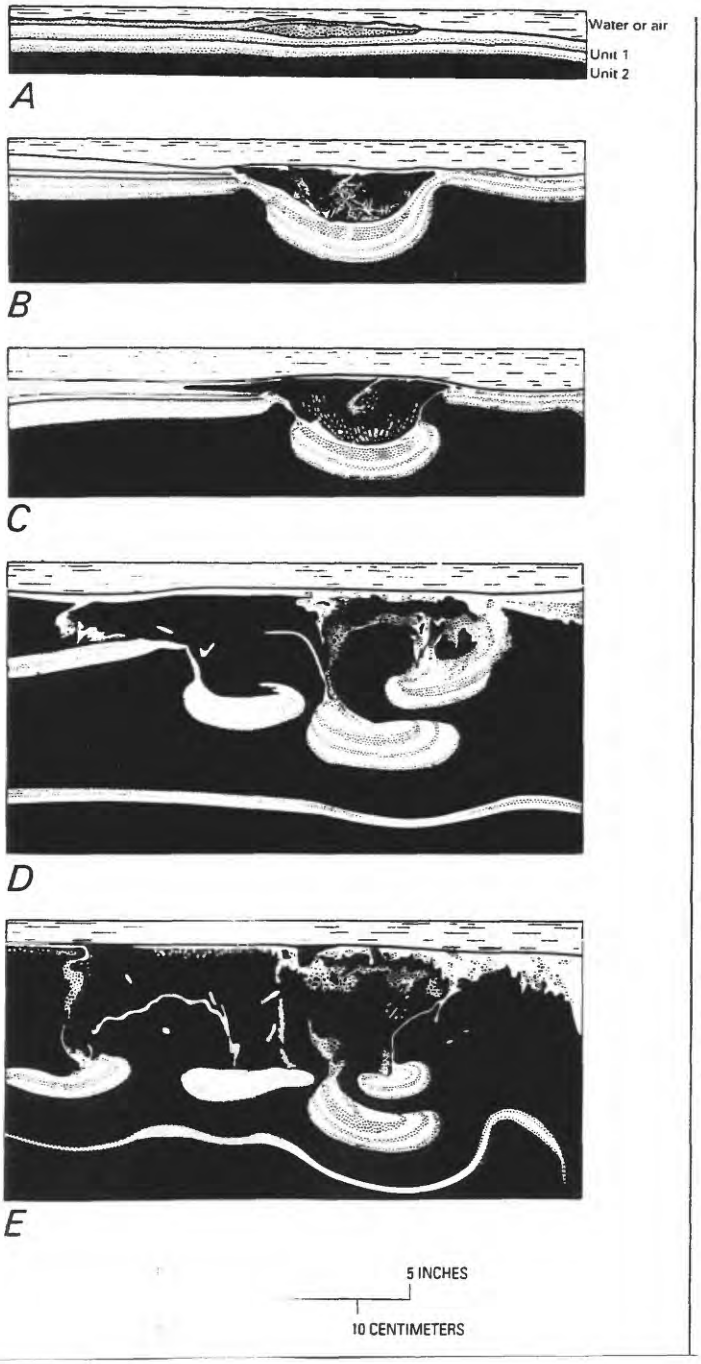

Figure 30

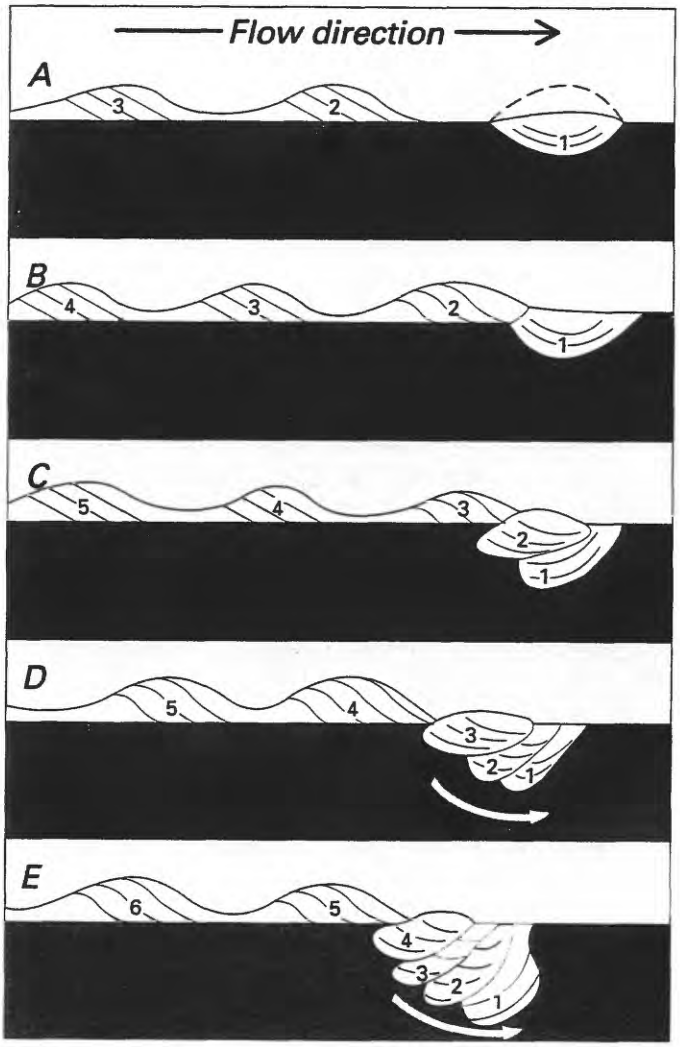

88A

Figure 31. Schematic drawing of spatial relations inferred for crevasse deltas (arrows) extending into a shallow water-filled swale, in the meisoseismal zone of the 1811-12 New Madrid earthquakes. The deltas form convex-up lenses having ripple cross-laminations (white, with diagonal lines). The edges of the delta are rippled sands that completely foundered into the soft clay, forming pseudonodules (detached white bodies with diagonal lines), whereas the main body only exhibits local load-casted ripples and a broad sagging. Arrows indicate direction of paleocurrents.

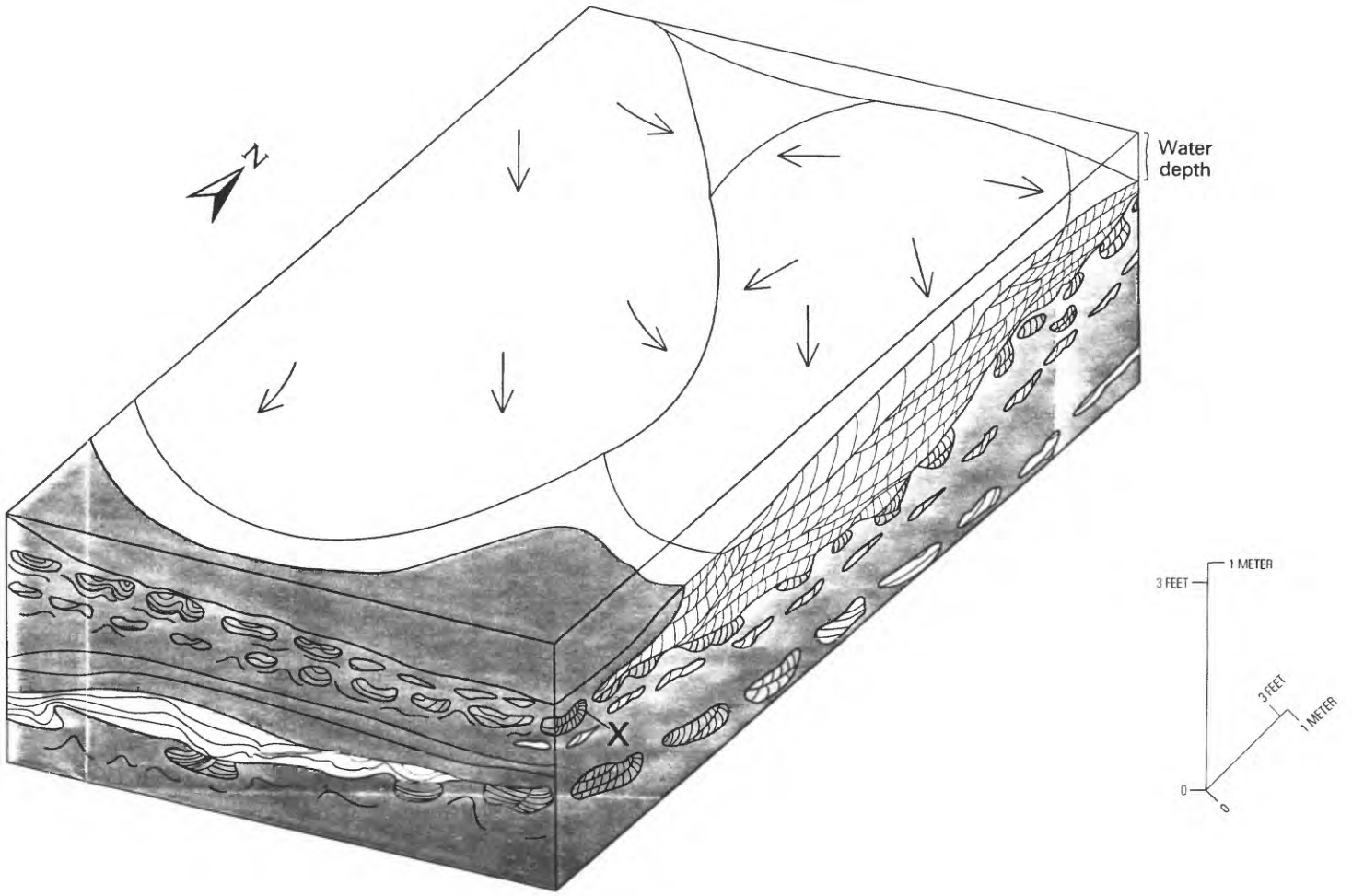

Figure 32. Photograph showing strong development of dish structure in fine-grained sandstone. Dish structures are the very thin laminations. Two generations of dish structures are present. Older dishes (1) are strongly concave, discontinuous, and have commonly been blurred by the upward flow of fluidized sediment. Dikes formed later (2) are flatter, more continuous, and separated vertically by sand showing a well defined substructure--the dark dish lamination, an underlying zone of white clay-poor sand, and an underlying zone of gray argillaceous sand. (From Lowe and LoPiccolo, 1974). I have observed such strong development of dish structures in sediments exposed in banks of the Edisto River (Fig. 11) near the meisoseismal zone of the 1886 earthquake of Charleston.

Figure 33. Photograph of pillar structure in fine-grained sandstone. Pillars are light-colored washed sand between the upturned margins of strongly concave dishes (From Lowe and LoPiccolo, 1974.)

Figure 32

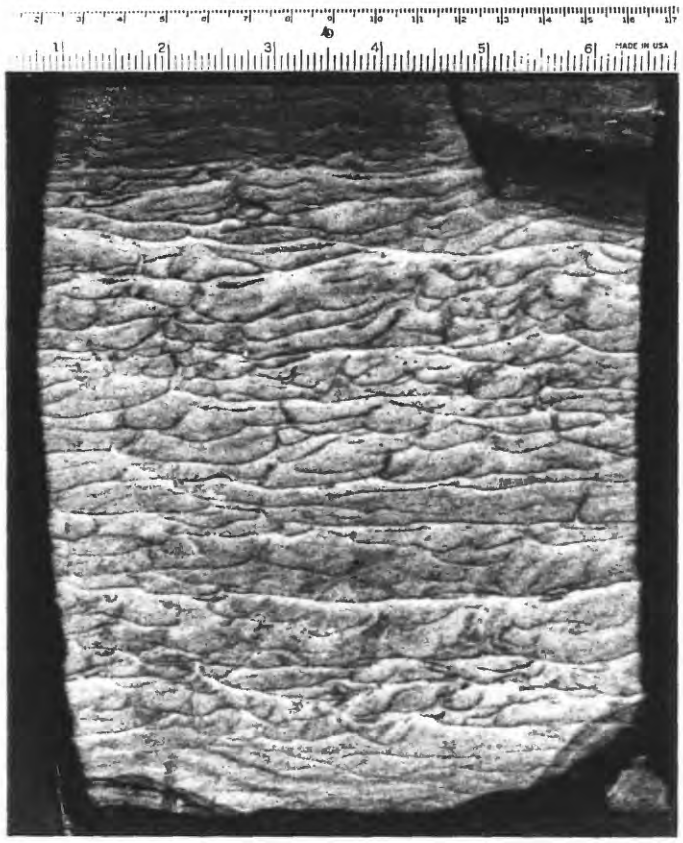

Figure 33

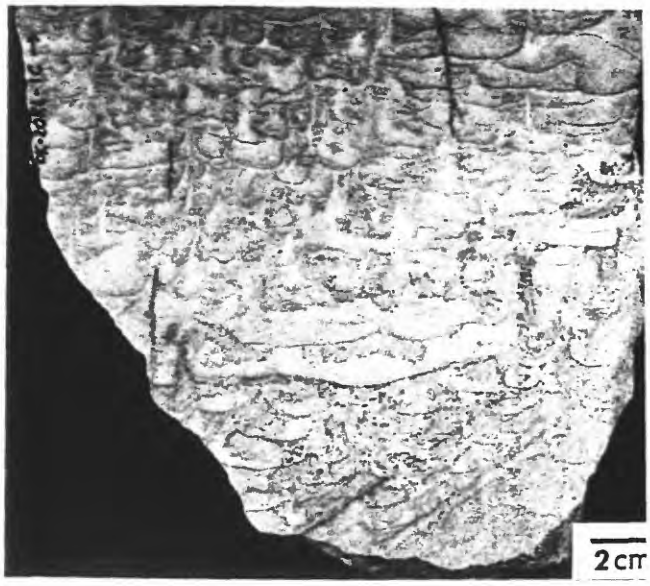

Figure 34. Schematic vertical section showing commonly observed vertical sequence of the sedimentary structures of convolute bedding, pillars, and dishes. Example shown is in thick sandstone beds. (From Lowe and LoPiccolo, 1974.) I have observed this sequence of structures in sediments exposed in banks of the Edisto River (Fig. 11), near the meisoseismal zone of the 1886 earthquake of Charleston.

Figure 35. Schematic depiction of sediment deformation structures observed by Ringrose (1989) in late Quaternary lake sediments. Sediment consist of laminated silts and sands (stippled). A through D represent change from most severe deformations to slightly distinguishable deformations.

Figure 34

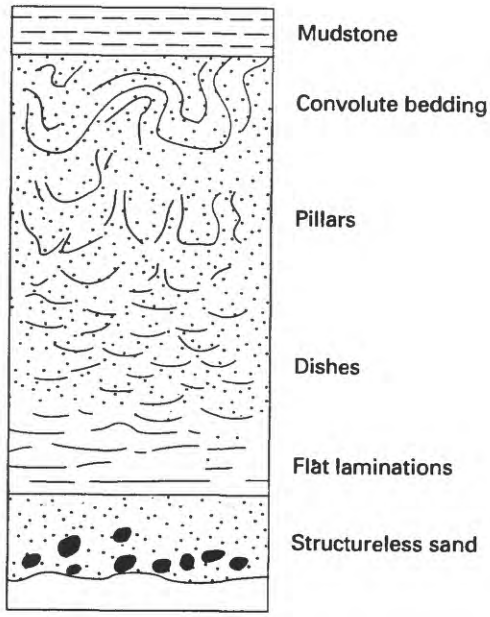

Figure 35

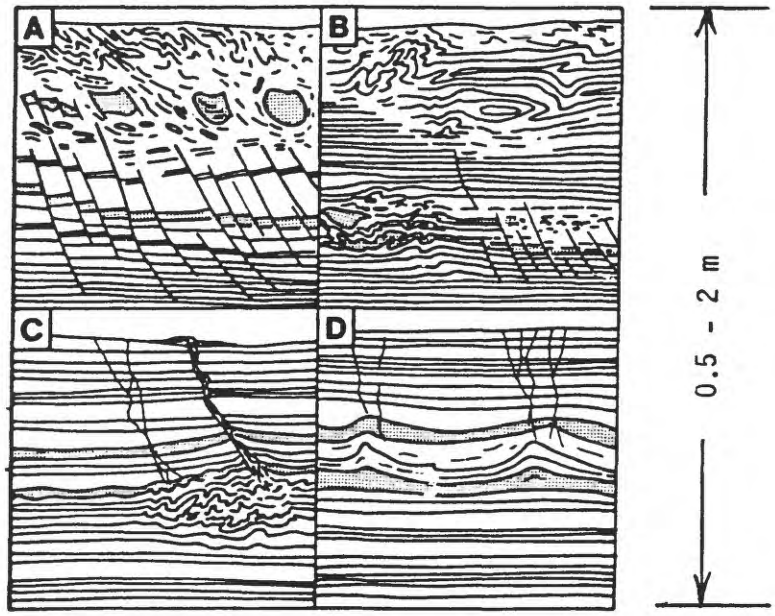

Figure 36. Schematic vertical section through a white, pedogenic sand tongue from an exposure in a drainage ditch near Charleston, South Carolina. Prime designations on E and Bh horizons indicate the lower horizons of a bisequal (vertically repeated) weathering profile. Bhir is iron-enriched Bh horizon. Note that the E horizon tongue dips in the same direction as the ground surface.

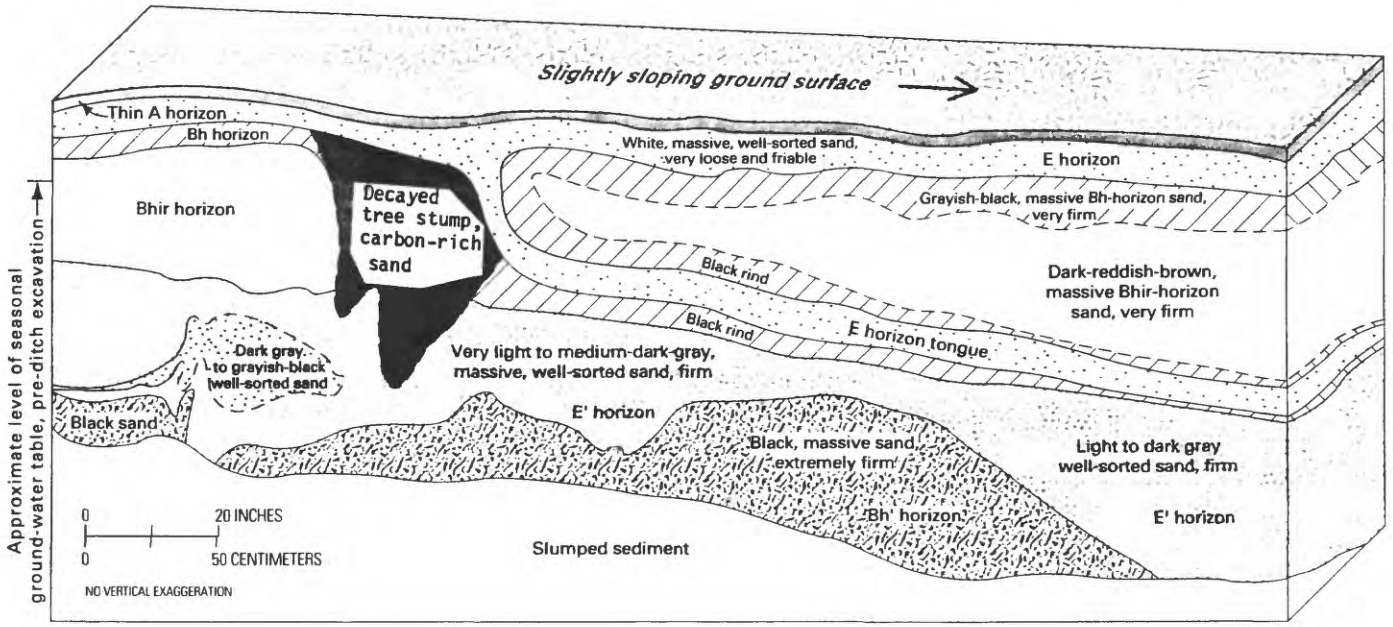

Figure 37. Schematic vertical section through BE' weathering horizon at a site near Charleston, South Carolina. White, structureless, well-sorted sand is interpreted to have had clays removed by chemical weathering.

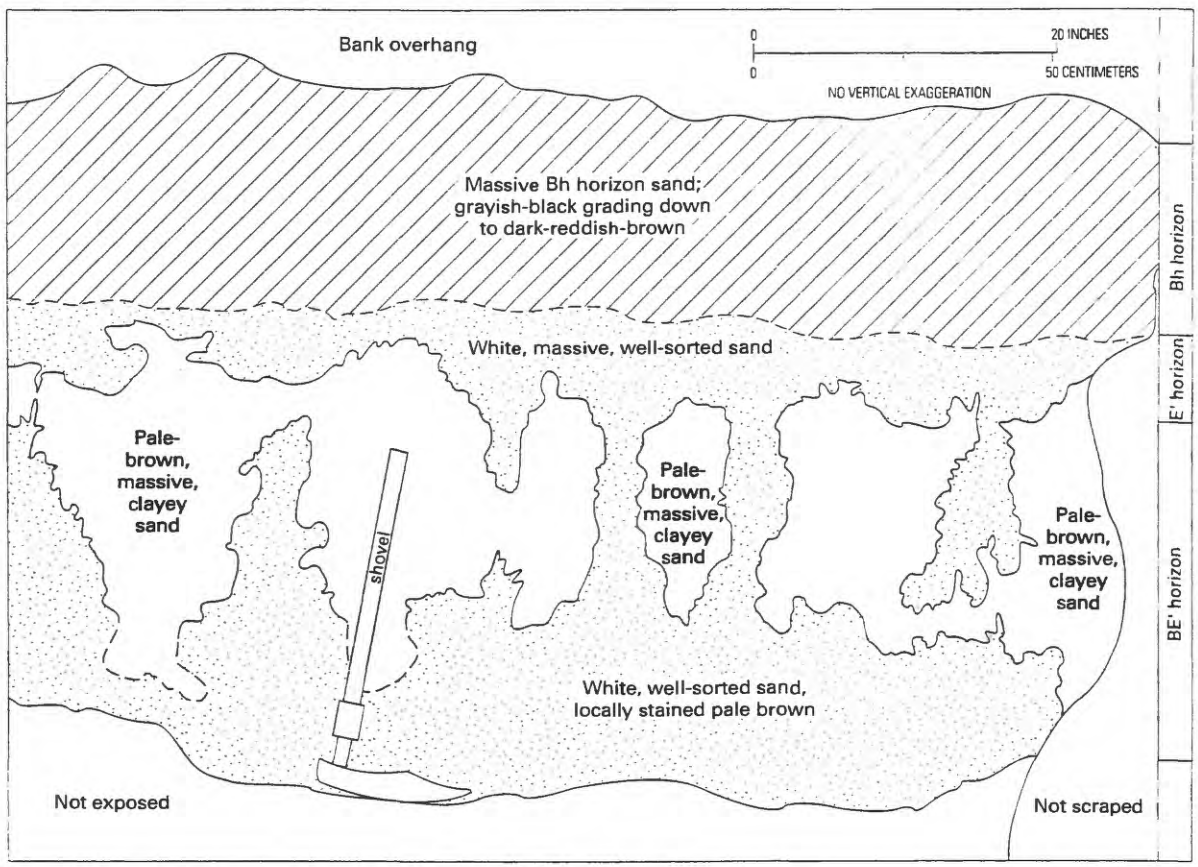

Figure 38. Examples from northeastern United States of ground disturbances associated with involutions. A, Photograph of very large involution of aeolian sand penetrating down into glaciofluvial gravel. Involution extends about 1 m in depth. B, Fluidized sand and gravel penetrating upward into aeolian silty sand. Shovel handle is 50 cm long. (Photographs courtesy of B. D. Stone.)

A

B

Figure 39. Sectional view sketch of an ice-wedge cast showing upturned strata in the upper portion of the host. Downturned strata occur at greater depth. Within the cast are clasts from the sidewalls, and strata sag toward the middle. Small normal faults border the walls of the host. Schematic drawing represents relations commonly observed in northeastern United States. (From Stone and Ashley, 1992.)

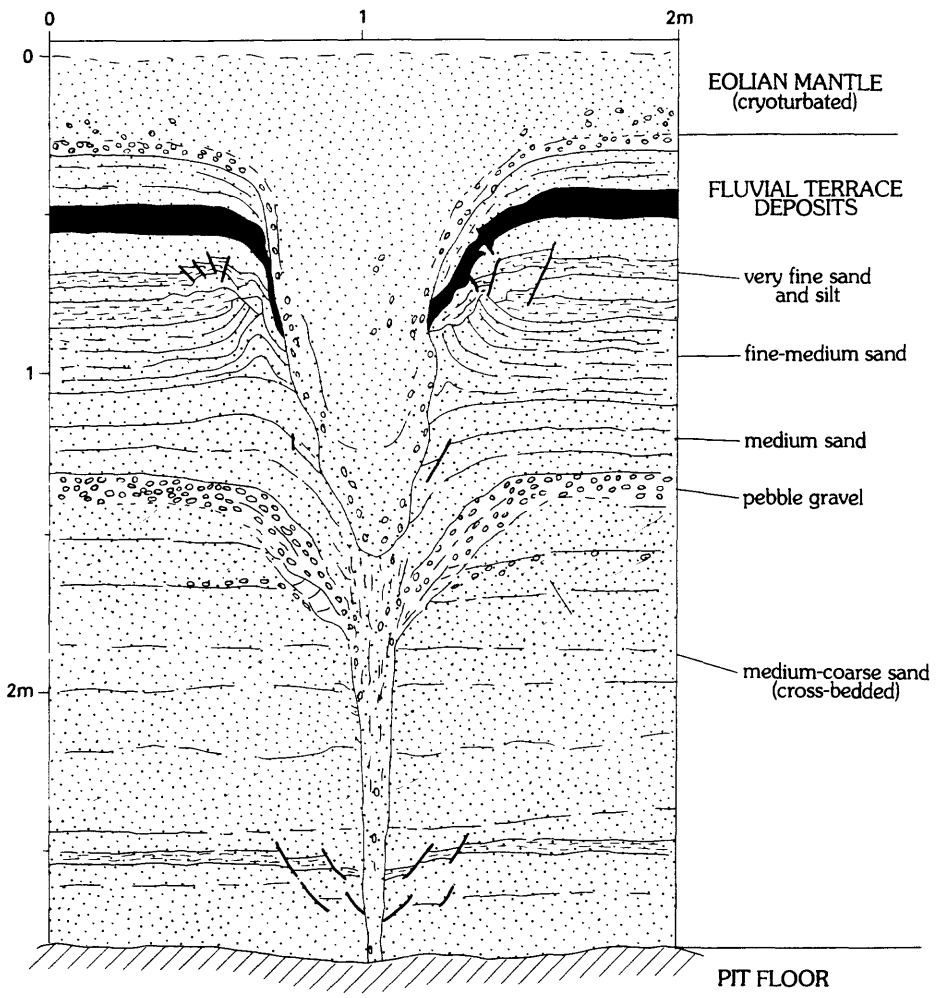

Figure 40. Pseudo-ice-wedge cast of Black (1976), probably caused by tension fracturing of ground.

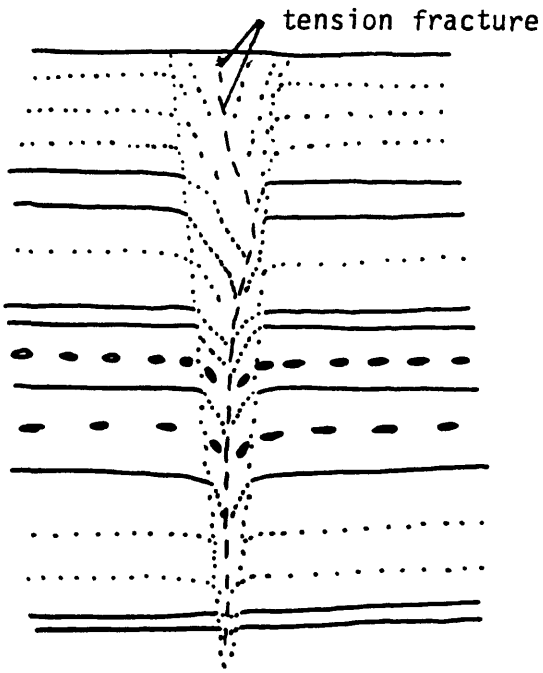

Figure 41. Relationship between earthquake moment magnitude (Mw) and distance from earthquake epicenter to the farthest liquefaction effect (venting to the surface or ground fracturing), with bound suggested by Ambraseys (1988). Curve separates data from earthquakes worldwide that had focal depths <50 km from depths >50 km..

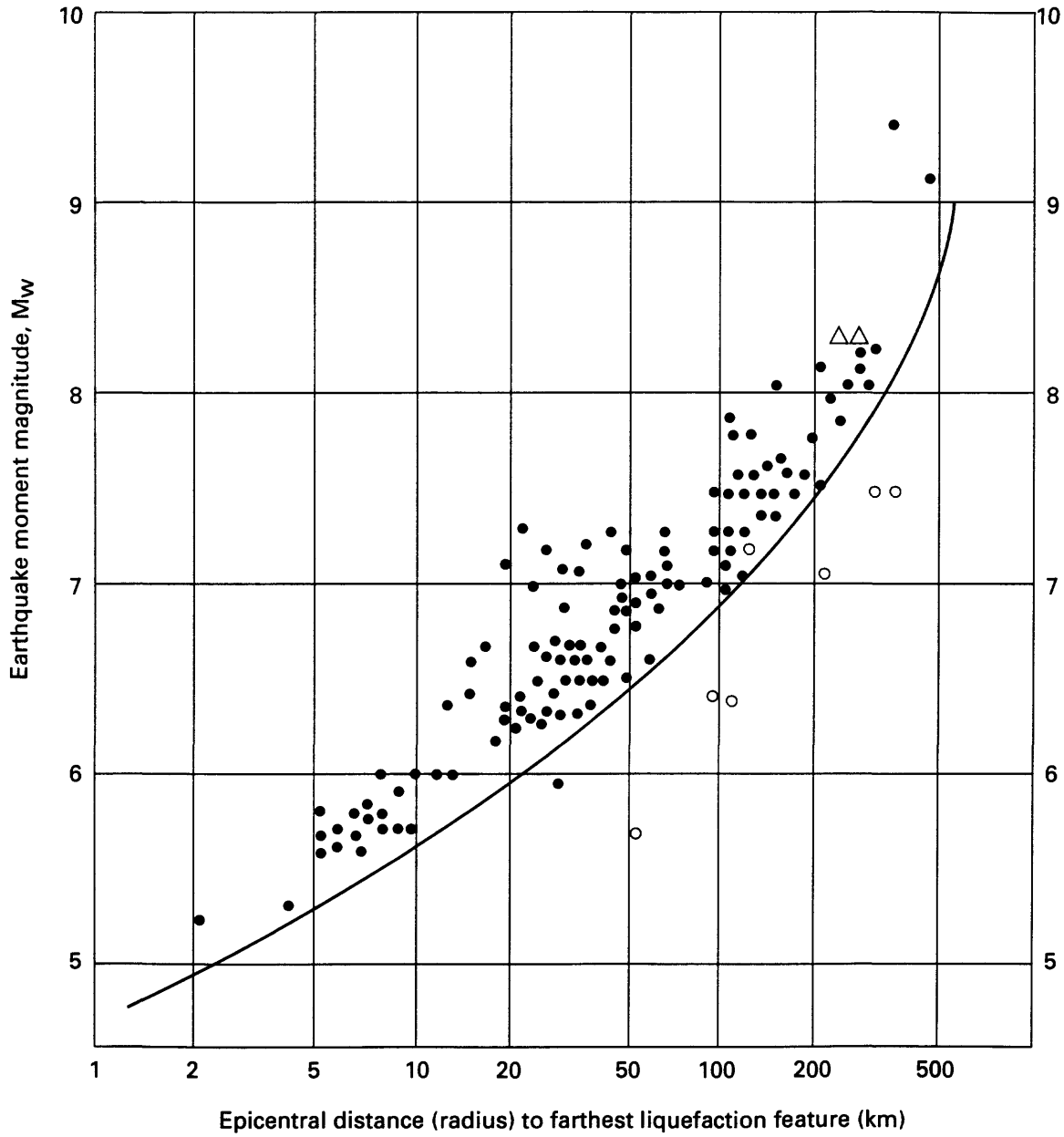

Figure 42. Curves for the method of Seed et al. (1983) used to evaluate the potential occurrence of liquefaction with accompanying venting of sand on appreciable ground cracks at a site on level ground. Curves are for clean sand deposits (average diameter >0.25 mm) and for different earthquake magnitudes (5.25 to 8.5). Points above and to the left of curves show conditions having high potential for liquefaction.

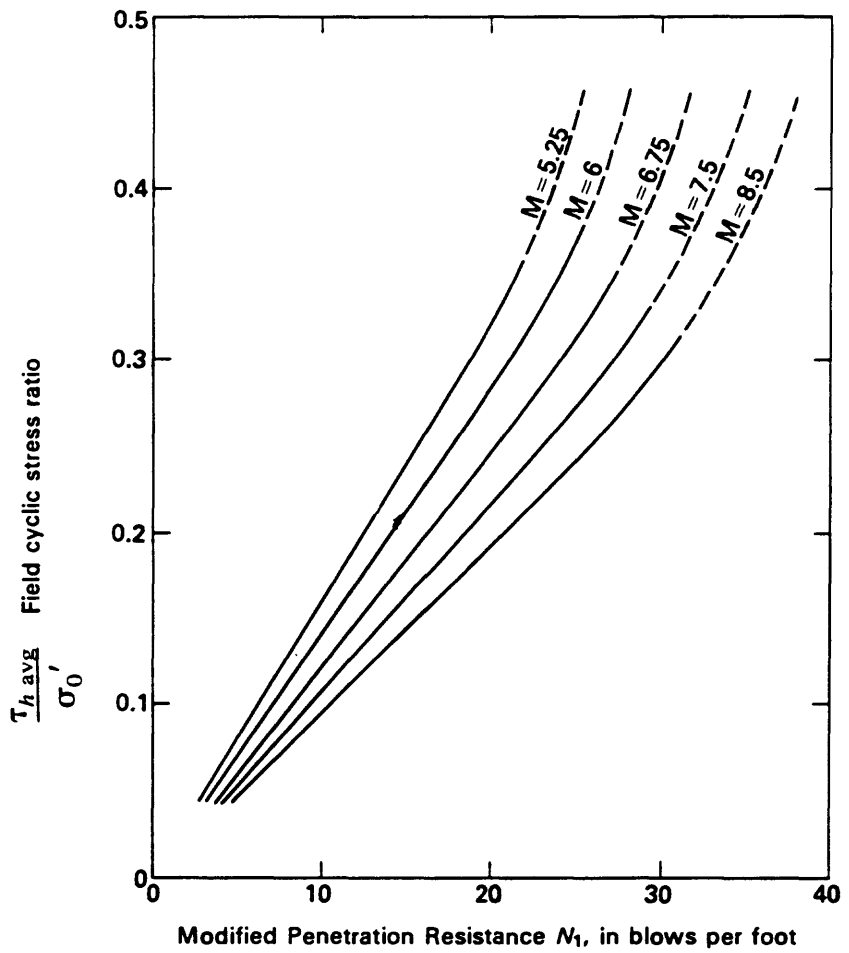

EXPLANATION

$\tau_{h\,avg}$	Average earthquake-induced horizontal cyclic shear stress
σ_0'	Vertical effective stress
N_1	Standard Penetration Test blow count measured in field, modified to blow count resistance at vertical effective stress of 1 ton/ft^2

Figure 43. Probability of liquefaction with accompanying venting or appreciable ground cracking, normalized to blow count value, magnitude, and field cyclic stress ratio. A, curves for silt and clay content ≤5 percent. B, curves for silt and clay contents of 15 and 35 percent. (From Liao et al., 1988.)

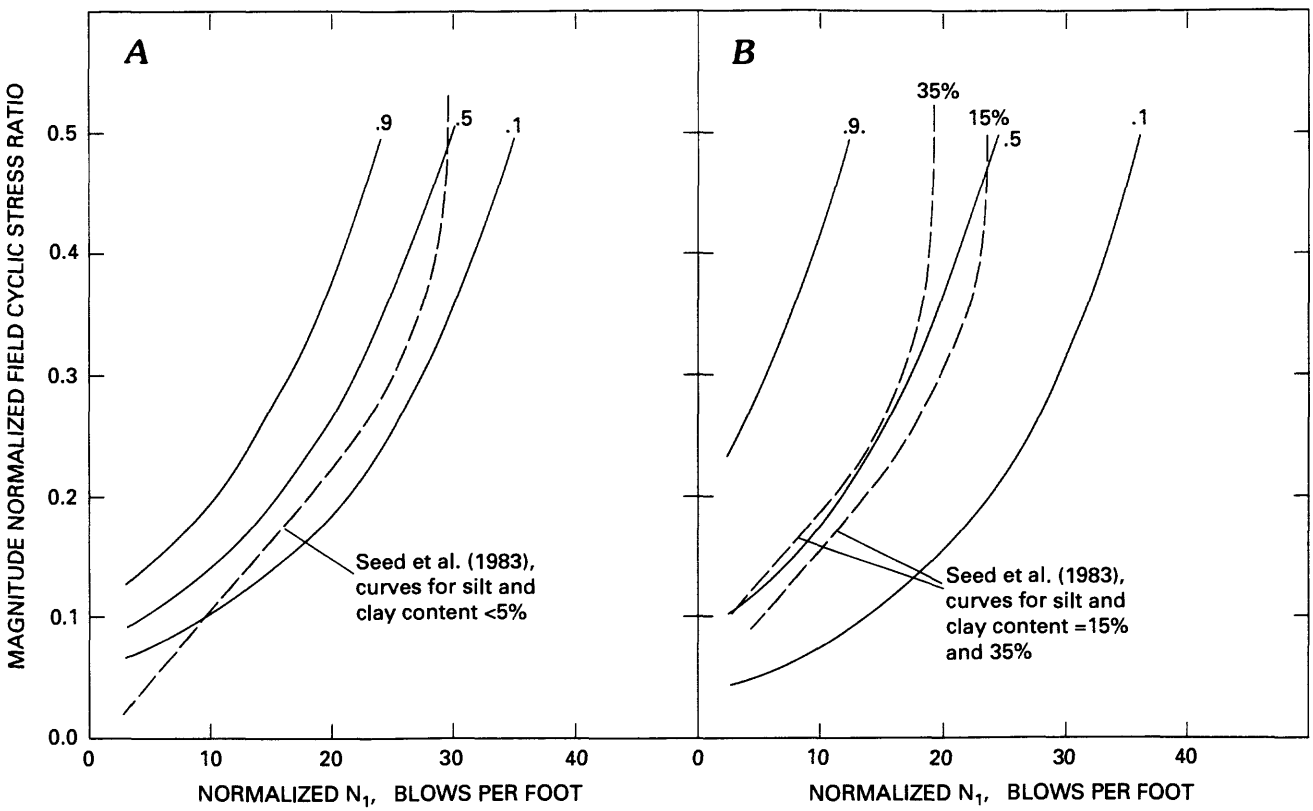

CHAPTER B

USING LANDSLIDES FOR PALEOSEISMIC ANALYSIS

RANDALL W. JIBSON

U.S. GEOLOGICAL SURVEY

OPEN-FILE REPORT 94-663

CHAPTER B CONTENTS

CHAPTER B

USING LANDSLIDES FOR PALEOSEISMIC ANALYSIS

RANDALL W. JIBSON

U.S. Geological Survey
Box 25046, MS 966, Denver Federal Center
Denver, Colorado 80225

ABSTRACT

In many environments, landslides preserved in the geologic record can be analyzed to determine the liklihood of seismic triggering. If evidence indicates that a seismic origin is likely for a landslide or group of landslides, and if the landslides can be dated, then a paleo-earthquake can be inferred and some of its characteristics estimated. Such paleoseismic landslide studies thus can help reconstruct the seismic history of a site or region. In regions that contain multiple seismic sources and in regions where surface faulting is absent, paleoseismic ground-failure studies are valuable tools in hazard and risk studies that are more concerned with shaking hazards than with interpretation of the movement histories of individual faults. Paleoseismic landslide analysis involves three steps: (1) identifying a feature as a landslide, (2) dating the landslide, and (3) showing that the landslide was triggered by earthquake shaking. This paper addresses each of these steps and discusses methods for interpreting the results of such studies by reviewing the current state of knowledge of paleoseismic landslide analysis.

1. INTRODUCTION

Most moderate to large earthquakes trigger landslides. In many environments, landslides preserved in the geologic record can be analyzed to determine the likelihood of seismic triggering. If evidence indicates that a seismic origin is likely for a landslide or group of landslides, and if the landslides can be dated, then a paleo-earthquake can be inferred and some its characteristics can be estimated. Such paleoseismic landslide studies thus can help reconstruct the seismic shaking history of a site or region.

Paleoseismic landslide studies differ fundamentally from paleoseismic fault studies. Whereas fault studies seek to characterize the movement history of a specific fault, landslide studies characterize the shaking history of a site or region irrespective of the earthquake source. In regions that contain multiple seismic sources and in regions where surface faulting

is absent, paleoseismic ground-failure studies thus can be valuable tools in hazard and risk studies that are more concerned with shaking hazards than with interpretation of the movement histories of individual faults.

As will be discussed in this chapter, the practical lower-bound earthquake that can be interpreted from paleoseismic landslide investigations is about magnitude 5-6. This range is comparable or perhaps slightly lower than that for paleoseismic fault studies. Obviously, however, larger earthquakes tend to leave much more abundant and widespread evidence of landsliding than smaller earthquakes; thus, available evidence and confidence in interpretation increase with earthquake size.

Paleoseismic landslide analysis involves three steps: (1) identify a feature as a landslide, (2) date the landslide, and (3) show that the landslide was triggered by earthquake shaking. This chapter addresses each of these steps and discusses methods for interpreting the results of such studies by reviewing the current state of knowledge of paleoseismic landslide analysis.

2. IDENTIFYING LANDSLIDES

Landslides include many types of movement of earth materials. In this chapter, the classification system of Varnes (1978) is used, which categorizes landslides by the type of material involved (soil or rock) and by the type of movement (falls, topples, slides, slumps, flows, or spreads). Other modifiers commonly are used to indicate velocity of movement, degree of internal disruption, state of activity, and moisture content (Varnes, 1978).

Identifying surface features as landslides can be relatively easy for fairly recent, well developed, simple landslides. Older, more degraded landslides or slides having complex or unusual morphologies are more difficult to identify. Several excellent summaries of approaches to landslide identification and investigation have been published (Schuster and Krizek, 1978; Záruba and Mencl, 1982; Brunsden and Prior, 1984; McCalpin, 1984), and the details need not be repeated here. In general, landslides are identified by anomalous topography, including arcuate or linear scarps, backward rotated masses, benched or hummocky topography, bulging toes, and ponded or deranged drainage. Abnormal vegetation type or age also are common. Submarine landslides can be identified with the aid of marine remote-sensing techniques (Field and others, 1982).

Earthquakes can trigger all types of landslides, and all types of landslides triggered by earthquakes also can occur without seismic triggering. Therefore, an earthquake origin cannot be determined solely on the basis of landslide type. However, some types of landslides tend to be much more abundant in earthquakes than other types. For example, Solonenko (1977) described some common characteristics of landslides triggered by earthquakes in the former Soviet Union. In a more comprehensive study, Keefer (1984) ranked the relative abundance of various types of landslides from 40 major earthquakes throughout the world (Table 1). Overall, the more disrupted types of landslides are much more abundant than the more coherent types of landslides. The relative rarity of subaqueous landslides stems, in part, from difficulties in observation. Keefer (1984) also observed that most earthquake-induced landslides occur in intact materials rather than in preexisting landslide deposits; thus, the number of reactivated landslides is small compared to the total number of landslides triggered by earthquakes. Keefer (1984) described typical properties of

source areas of various types of earthquake-triggered landslides. In general, slope materials that are weathered, sheared, intensely fractured or jointed, or saturated are particularly susceptible to landsliding during earthquakes.

Sackungen (ridge-crest troughs) are a somewhat controversial type of ground failure that some investigators claim may be related to seismic shaking. Sackungen are identified by one or more of the following: (1) grabens or troughs near and parallel to ridge crests of high mountains, (2) uphill-facing scarps a few meters high that parallel the topography, (3) double-crested ridges, and (4) bulging lower parts of slopes (Varnes and others, 1989).

3. DETERMINING LANDSLIDE AGES

Paleoseismic interpretation requires establishing the numerical age of a paleo-earthquake. In the case of earthquake-triggered landslides, this means that dating landslide movement is required. Several methods for dating landslide movement can be used; some are similar or identical to those used for dating fault scarps (as discussed in other chapters), while others are unique to landslides. Most of the methods discussed below are simply applications of numerical dating techniques discussed in detail in Chapter 3, which contains more detailed descriptions of the sampling and testing procedures.

Different types of landslides may be datable by different methods, depending on a variety of factors such as distance of movement, degree of internal disruption, landslide geometry, type of landslide material, type and density of vegetation, and local climate. Ideally, multiple, independent dating methods should be used to increase the level of certainty of the age of landslide movement (Johnson, 1987).

3.1 Historical Methods

Some old landslides may have been noted by local inhabitants or may have damaged or destroyed human works or natural features (e.g., Whitehouse and Griffiths, 1983). In some parts of the world, potentially useful historical records or human works may extend back several hundreds or thousands of years. For example, a prehistoric encampment at Mam Tor, in Derbyshire, England, was partly destroyed by a landslide (Johnson, 1987). The encampment was first occupied about 3,000 yr b.p. according to archeological studies (Jones and Thompson, 1965); this date provides an approximate maximum age of the landslide. In the United States, few historical records exceed 200 yr in length, but some of these may still be useful. In a paleoseismic investigation of landslides possibly triggered by the 1811-12 New Madrid earthquakes, Jibson and Keefer (1988) reported that oral accounts of local inhabitants helped establish minimum landslide ages in the 1850's, which helped bracket absolute ages. Also, grave markers on landslide masses, datable roads and trails whose locations clearly show that they either postdated or predated landslide movement, disturbed stone fences or other property markers, and other human works can potentially bracket or definitively date landslide movement (e.g., Jibson and Keefer, 1988).

For fairly recent events, comparing successive generations of topographic maps or aerial photographs can bracket the time period in which mappable landslides first appeared.

3.2 Dendrochronology

Dendrochronology can be applied to date landslide movement in several ways (Hupp and others, 1987). At the simplest level, the oldest undisturbed trees on disrupted or rotated parts of landslides should yield reasonable minimum ages for movement (Jibson and Keefer, 1988; Logan and Schuster, 1991; Williams and others, 1992). On rotational slides that remained fairly coherent, preexisting trees that survived the sliding will have been tilted because of headward rotation of the ground surface; if both tilted and straight trees are present on such landslides, the age of slide movement is bracketed between the age of the oldest straight trees and the youngest tilted trees (Fuller, 1912). Using this simple application of dendrochronology to date coherent translational slides is more difficult because trees can remain upright and intact even after landslide movement. On all types of landslides, trees growing from the surface of the scarp will yield minimum ages of scarp formation, from which the age of slide movement can be interpreted.

In some cases, trees killed by landslide movement will be preserved and can thus yield the exact date of movement. For example, Jacoby and others (1992) dated trees beneath the surface of Lake Washington near Seattle that were drowned by landsliding into the lake. They were able to date the landslide movement from the preserved tree-ring records and from radiocarbon dating of the outermost wood.

A more sophisticated application of dendrochronology involves quantitative analysis of growth rings. For trees that have survived one or more episodes of landslide movement, such analysis can be used to identify and date reaction wood (eccentric growth rings), growth suppression, and corrosion scars, which may be evidence of landslide movement (Hupp and others, 1987). Reconstruction of movement histories by such dendrochronologic analysis has been documented successfully in several areas (e.g., Terasmae, 1975; Reeder, 1979; Jensen, 1983; Bégin and Filion, 1985; Hupp and others, 1987; Osterkamp and Hupp, 1987).

Some landslides block stream drainages and form dams that impound ponds or lakes. Inundation of areas upstream from landslide dams can drown trees that can be dated dendrochronologically (Logan and Schuster, 1991).

3.3 Radiocarbon Dating

Radiocarbon dating can be used in a variety of ways to date organic material buried by landslide movement, as discussed by Stout (1977). Landslide scarps degrade similarly to fault scarps, so colluvial wedges at the bases of landslide scarps may contain organic material that can be retrieved by trenching or coring and dated radiometrically. Fissures on the body of a landslide, particularly near the head where extension may take place, also may trap and preserve organic matter. If the landslide mass is highly disrupted, as in rock or soil falls or avalanches, then some vegetation from the original ground surface may have become mixed with the slide debris; such organic material excavated from slide debris can be dated radiometrically (Burrows, 1975; Whitehouse and Griffiths, 1983; McCalpin, 1989, 1992). At the toes of landslides, slide material commonly is deposited onto undisturbed ground; if this original ground surface can be excavated beneath the toe of a slide, buried organic material from this surface can be dated to indicate the age of initial movement.

Sag ponds commonly form on landslides, and organic material deposited in such ponds can be dated radiometrically. Organics at the base of the pond deposits should yield

reliable dates of pond formation (Stout, 1969, 1977; McCalpin, 1989).

Vegetation submerged from inundation of areas upstream from landslide dams also can be dated radiometrically. Schuster and others (1992) dated the emplacement of rock-avalanche dams by radiocarbon dating the outer few rings of drowned trees protruding from landslide-dammed lakes and detrital wood and charcoal in lacustrine deposits that formed behind a landslide dam. Similarly, landslides into lakes can submerge and kill vegetation that can be dated radiometrically (Jacoby and others, 1992).

3.4 Lichenometry

Lichenometry—analysis of the age of lichens based on their size—has been used successfully to date rock-fall and rock-avalanche deposits (Nikonov and Shebalina, 1979; Oelefke and Butler, 1985; Nikonov, 1988; Smirnova and Nikonov, 1990; Bull and others, 1991). By measuring lichen diameters on rock faces freshly exposed at the time of failure, numerical ages can be roughly estimated by assuming that lichens colonized the rock face in the first year after exposure. Because rock-fall and rock-avalanche deposits typically include abundant rocks having freshly exposed faces, numerous samples generally can be taken to create a database for the statistical analysis required by lichenometry. Lichenometric ages must be calibrated at sites of known historical age or by comparison with other numerical dating techniques. Lichenometric dating is subject to considerable uncertainty, however, because a several decades may elapse before lichens colonize a fresh rock exposure, and lichens may never colonize unstable landslide deposits on very steep slopes (Oelefke and Butler, 1985).

3.5 Weathering Rinds

For a given climate and rock type, measuring the thickness of weathering rinds can be used to date when rocks were first exposed at the ground surface (Chinn, 1981; Knuepfer, 1988). For rock falls and rock avalanches and for other landslides whose movement exposed rock fragments at the ground surface, measuring the thickness of weathering rinds can be used to date landslide movement (Whitehouse and Griffiths, 1983; McCalpin, 1989, 1992). Determining which rock surfaces were initially exposed at the time of landsliding can be difficult, but if a sufficiently large number of samples can be measured, consistent statistical results of predominant ages that relate to landslide movement can be obtained.

3.6 Pollen Analysis

Analysis of pollen in deposits filling depressions on landslides can yield both an estimated age of initial movement and, in some cases, a movement history through time (Franks and Johnson, 1964; Adam, 1975; Tallis and Johnson, 1980; Dietrich and Dorn, 1984; Johnson, 1987). Such analyses assume that sediment deposition and incorporation of pollen occur immediately following landslide movement and that local climatic and vegetation variation can be accounted for. Pollen samples from the buried ground surface beneath the toes of landslides also have the potential for use in dating landslide movement.

3.7 Geomorphic Analysis

Landslides are disequilibrium landforms that will change through time more rapidly than surrounding terrain. By analyzing the degree of degradation of landslide features such as scarps, ridges, sags, and toes, relative ages can be assigned to various landslides (Schroder, 1970; McCalpin, 1986; Crozier, 1992). For example, McCalpin and Rice (1987) analyzed 1,200 landslides in the Rocky Mountains and assigned each of them to one of four relative age groups based on morphology. Numerical age ranges for these groups were estimated based on correlation with other landslides in the Rocky Mountains that have similar morphologies and surface-clast weathering and for which ^{14}C dates were available. Although the classification scheme of McCalpin and Rice (1987) was developed for the Rocky Mountains, similar schemes could be developed for other areas (Wieczorek, 1984).

Another example of relative dating by geomorphic analysis was developed in New Zealand by Crozier (1992), who identified distinct age groups of landslides based on degree of definition of landslide features, soil development, tephra cover, stream dissection, preservation of vegetation killed by movement, and drainage integration. Ranges of numerical ages for these groups were estimated by dating organic material retrieved from representative landslides from each group.

Jibson and Keefer (1988) concluded that since a large group of landslides in the New Madrid seismic zone all appeared to have the same degree of geomorphic degradation, these landslides were contemporaneous. Other types of evidence (Jibson and Keefer, 1988, 1989, 1993) were then used to link the synchronous ages of these landslides to triggering by the 1811-12 New Madrid earthquakes.

Models of fault-scarp degradation also have potential application in landslide dating because landslide scarps should behave similarly to fault scarps. Several approaches to morphologic fault-scarp dating have been proposed (e.g., Bucknam and Anderson, 1979; Nash, 1980; Mayer, 1984), all of which require calibration for various parameters such as climate and scarp material. Scarp degradation commonly is modeled as a diffusion process (Colman and Watson, 1983; Andrews and Hanks, 1985; Andrews and Bucknam, 1987), in which degradation rate varies in time and is a function of slope angle, which represents the degree to which the scarp is out of equilibrium with the surrounding landscape.

Christiansen (1983) used sedimentation rates to date landslide age. An ancient landslide moved over alluvium deposited by the North Saskatchewan River, Canada, and part of the landslide was buried by continued deposition. The rate of alluvial deposition was determined by radiocarbon dating to be fairly uniform at about 2.4 mm/yr. By measuring the depth of the landslide shear zone below the present surface of the alluvium, an age of about 4,000 yr b.p. was estimated.

Johnson (1987) discusses some other geomorphic methods to date landslide movement, including correlation of landsliding with specific periods of fluvial downcutting or aggradation and correlation with known limits of ice sheets.

Analysis of soil-profile development also is a potential tool for dating landslides. New soil profiles will begin to develop on disrupted landslide surfaces. If such surfaces can be identified, dating the newly developed soil profile will indicate the age of movement (Small and Clark, 1982; Birkeland, 1984; Knuepfer, 1988; Birkeland and others, 1991).

4. INTERPRETING AN EARTHQUAKE ORIGIN FOR LANDSLIDES

Interpreting an earthquake origin for a landslide or group of landslides is by far the most difficult step in the process, and methods and levels of confidence in the resulting interpretation vary widely. Because paleoseismology is a relatively new field of study, analysis of landslides within that field is, in many respects, embryonic. Only a handful of studies have been published to date that explicitly use landslides to identify and date paleo-earthquakes, although several others develop methods that can be applied in paleoseismic investigations. This section summarizes several basic approaches that have been documented to interpret the seismic origin of landslides.

4.1 Regional Analysis of Landslides

Most paleoseismic landslide studies involve analysis of large groups of landslides rather than individual features. The premise of these regional analyses is that a group of landslides of the same age that are scattered across a discrete area were triggered by a single event of regional extent. In an active seismic zone, that event commonly is inferred to be an earthquake. Such an interpretation may be justified in areas where landslide types and distribution from historical earthquakes have been documented and can be used as a standard. In areas where such historical observations are absent, assuming an earthquake origin for landslides of synchronous age is much more tenuous, primarily because large storms can trigger widespread landslides having identical ages and spatial distribution.

Crozier (1992) cited six criteria to support a seismic origin for some landslides in New Zealand; these criteria can be applied generally: (1) ongoing seismicity in the region, which has triggered landslides, (2) coincidence of landslide distribution with an active fault or seismic zone, (3) geotechnical slope-stability analyses showing that earthquake shaking would have been required to induce slope failure, (4) large size of landslides, (5) presence of liquefaction features associated with the landslides, and (6) landslide distribution that cannot be explained solely on the basis of geological or geomorphic conditions. Obviously, the more of these criteria that are satisfied, the stronger the case for seismic origin.

Russian scientists were the first to analyze the distribution and ages of landslides in seismic zones for paleoseismic analysis. Several papers in Russian deal with the development and application of such studies in Central Asia, but these papers are not readily available outside Russia. A few papers by Russian authors written in English that reference this body of Russian literature are discussed below.

Nikonov (1988) estimated that analysis of landslides in a region can detect earthquakes having magnitudes greater than 6.5 and that epicentral zones can be located within about 10 km. Analysis of fault features is considered preferable for epicentral location and magnitude estimates; analysis of landslides is preferable for age determination (Nikonov, 1988). The method developed by the Russians (Nikonov, 1988) involves complementary studies of fault-related features and shaking-induced features in a known seismic zone. The premise of the approach is that large earthquakes in mountainous areas trigger many landslides, and that the number, size, and areal extent of the landslides are proportional to the size of the earthquake (Solonenko, 1977). Many landslides in a seismic zone are dated either by radiocarbon or lichenometry; if one or more groups of landslides cluster in both space and time, then an earthquake origin is inferred (Nikonov, 1988). Each age cluster is interpreted

to define a different paleo-earthquake. Generally, no criteria other than synchronous age are used, so the seismic origin of these landslides is, to a great degree, simply assumed. An earthquake origin is more certain in cases where landslide ages match ages of local fault features and where the types of landslides correspond to those documented in previous earthquakes (Solonenko, 1977). Based on historical observations that large, deep-seated landslides are triggered only within Modified Mercalli Intensity (MMI) isoseismals VII-IX, only large earthquakes that triggered large, well-preserved landslides have been interpreted from such landslide studies (Nikonov, 1988). This method was applied to rock-avalanche deposits in the epicentral region of the 1907 Karatog and 1949 Khait earthquakes (both $M \approx 7.4$) in Tadjikistan (Nikonov and Shebalina, 1979). Lichenometric ages from young-looking deposits near the epicenter of these two earthquakes correlate with the 1907 and 1949 earthquakes, respectively. Lichenometric dates from the older parts of the deposits suggest an earlier earthquake about 200 yr before the study.

Bull and others (1991) also used lichenometry to date numerous rock-fall deposits and rock-fall scarps near the Hope fault on South Island, New Zealand. Recent ages of deposits were linked to historical earthquakes, and older deposits were interpreted to have been triggered by previous earthquakes.

Adams (1981a) used landslide-dammed lakes in New Zealand to identify paleo-earthquakes. He examined 17 historical landslide-dammed lakes and found that 15 of them formed during earthquakes; he therefore concluded that a seismic origin reasonably can be inferred if several synchronous prehistoric landslide dams cluster in an area. Perrin and Hancox (1992) later confirmed that most landslide dams in parts of New Zealand were, indeed, seismically triggered. Adams (1981a) estimated magnitudes of prehistoric earthquakes by comparing the areal extents of landslide dams of a given age with areal extents of landslide dams in historical earthquakes. He dated a group of prehistoric landslide-dammed lakes on South Island, New Zealand, using three types of samples: (1) woody detritus in the debris of the landslide dams, (2) standing trees drowned by the lakes, and (3) submerged soil horizons cored beneath lake sediment. His results indicate an earthquake of magnitude 7.4 in about A.D. 1650. Adams (1981a) indicated that such analyses could identify earthquakes of $M \geq 6.75$ that occurred within the past few hundred or thousand years.

Schuster and others (1992) used a similar approach to date prehistoric rock avalanches that dammed streams in the Olympic Mountains in the State of Washington. Synchronous dates for several such avalanches indicate a common triggering event at about 1,100 yr b.p., which they argued was a large earthquake. Several lines of evidence for seismic triggering were cited: (1) the rock that failed is not known to have failed historically either during large storms or in moderate earthquakes; (2) more than 40 percent of a recent inventory of worldwide rock avalanches that formed landslide dams were formed by earthquake shaking (Costa and Schuster, 1991); and (3) in New Zealand, the distribution of landslide-dammed lakes approximates the distribution of shallow earthquakes having magnitudes 6.5 or greater (Perrin and Hancox, 1992).

Jacoby and others (1992) used dendrochronology to date prehistoric landslides that moved into Lake Washington near Seattle. They were able to correlate the tree-ring records from these landslides directly with a tree buried in a tsunami deposit elsewhere in the region.

Thus, they inferred an earthquake origin for the Lake Washington landsliding since it was synchronous with a deposit of more certain seismic origin.

Jibson and Keefer (1989) used a regional analysis based on both spatial distribution and synchronous age. They used discriminant analysis and multivariate regression to analyze the geographic distribution of three distinct types of landslides along bluffs that extend more than 300 km through the New Madrid seismic zone. Field evidence indicated that landslides of two of the three types (old coherent slides and earth flows) were synchronous and could have ages consistent with triggering in the 1811-12 earthquakes there; landslides of the third type (young rotational slumps) appeared much younger and unrelated to seismic activity. The bluffs were divided into segments 762 m (2,500 ft) long, and the percentage of the length of each segment covered by landslides of the three types was measured for use as the dependent variable in the statistical analyses. Independent variables measured for each segment included slope height, slope angle, stratigraphic thicknesses of various units, slope aspect, and proximity to the estimated hypocenters of the 1811-12 New Madrid earthquakes. Discriminant analysis showed that bluffs having old coherent slides and earth flows are significantly closer to the estimated hypocenters of the 1811-12 earthquakes than bluffs without these types of slides (Jibson and Keefer, 1989). Bluffs having young slumps showed no such correlation. Multiple regression analysis, which simultaneously combined all factors, showed that the distribution of old coherent slides and earth flows correlates strongly with proximity to the hypocenters of the 1811-12 earthquakes, as well as with slope height and aspect (Jibson and Keefer, 1989). Again, young slumps showed no such correlation with earthquake-related independent variables. The results of these statistical analyses thus showed that old coherent slides and earth flows in the New Madrid seismic zone are spatially related to the 1811-12 earthquake hypocenters and thus probably formed in those earthquakes. This type of analysis can be used only in areas where landslide locations can be correlated with well-defined seismic source zones.

4.2 Submarine Landslides and Turbidites

The classic paper by Heezen and Ewing (1952) demonstrated that large offshore earthquakes can trigger huge turbidity currents having regional extent. They described the Grand Banks turbidity current, which was triggered in the epicentral area of a magnitude 7.2 earthquake on 28 November 1929. The Grand Banks turbidity current involved detachment and downslope movement of submarine sediment along 240 km of the continental shelf; after traveling 650 km from its source, the turbidity current still was moving faster than 20 km/hr and therefore probably continued to move for additional hundreds of kilometers. Heezen and Ewing (1952) postulated that the earthquake triggered submarine slumps along an extensive length of the continental shelf corresponding to the epicentral zone of the earthquake and that these slumps transformed into turbidity currents that moved as rapidly as 100 km/hr down slopes averaging only about 1.5°.

More recently, several studies have confirmed the triggering of large submarine landslides and turbidity currents by earthquakes. Perissoratis and others (1984) documented a slump covering 15-20 km^2 in the eastern Korintiakos Gulf along the coast of Greece triggered by a series of earthquakes (M=6.4-6.7) from 24 February to 4 March 1981. Field and others (1982) documented a sediment flow/lateral spread on a 0.25° slope on the submarine

Klamath River delta off the coast of northern California; the feature extends along 20 km of the delta front and is about 1 km long (from scarp to toe). The very low slope and the presence of liquefaction features on the surface both suggest seismic triggering, and repeated bottom surveys before and after the M=6.5-7.2 offshore earthquake of 8 November 1980 conclusively linked the landslide to the earthquake. Lee and Edwards (1986) analyzed the stability of four submarine landslides off the coasts of California and Alaska and concluded that three of them required seismic shaking to have triggered failure. These studies provide the basis for interpreting older submarine landslides and turbidite deposits in terms of seismic triggering.

Several investigators have studied turbidites for paleoseismic interpretation. Kastens (1984) studied submarine debris flows and turbidites from the Calabrian Ridge off the coast of Italy and was able to temporally correlate deposits across several basins. This correlation is inconsistent with a mechanism of gradual oversteepening and slope failure from long-term sedimentation, which would produce temporally independent deposits in different basins. Thus, a seismic origin is postulated because of regional extent and proximity to the seismically active Aegean and Appenine-Sicily arcs. Kastens (1984) identified four debris-flow/turbidite events between 8,000 and 14,000 yr b.p. and thus estimated a 1,500-yr recurrence interval between postulated seismic triggering events during that period. She also compared estimates of peak ground accelerations having return periods of 1,500 yr in the region with estimated ground accelerations required to trigger the submarine debris flows to show that seismic triggering is a reasonable interpretation.

Adams (1990) conducted a similar study along the Cascadia subduction zone off the coast of Washington and Oregon. He collected bottom core samples over a broad region and documented deposits from 13 turbidity currents having regional extent. He postulated triggering by very large earthquakes because each of these deposits originated in multiple independent channels 50-150 km apart and merged to form one large turbidity current. Synchronous, independent triggering by local endogenic processes (such as local oversteepening from long-term sedimentation) is highly unlikely. The relatively regular time interval between deposits likewise implies triggering by earthquakes having regular recurrence intervals. The mean recurrence interval between the 13 turbidites was 590 ± 50 yr, and the very broad regional extent suggests triggering earthquakes in the magnitude-9 range. Using current sedimentation rates, Adams (1990) argued that the most recent turbidite likely occurred about 300 yr b.p., which agrees with independent paleoseismic evidence of a great Cascadia earthquake at about that time (Atwater, 1987).

Analysis of turbidites also provides an opportunity to make paleoseismic interpretations much farther back in the geologic record. Mutti and others (1984) studied Cretaceous and Tertiary flysch sequences in Italy for paleoseismic interpretation. They used the term "seismoturbidite" for turbidites interpreted as being triggered by earthquake shaking. Primary criteria for this interpretation include (1) exceptional volumes (~ 100 km^3) and thicknesses ($\geq$100 m) that are 1-2 orders of magnitude greater than the largest "normal" turbidites in the region; (2) basinwide extent of distinct, synchronous, sheet-like deposits that are easily mappable over large areas; (3) lack of vertical and lateral facies associations with long-lived channel-lobe turbidite systems; and (4) proximity to seismic source zones. Additional criteria include irregular vertical spacing (indicating erratic occurrence), ages and

repeat times proportional to the volume of the deposit, and inability to explain the deposits in terms of meteorological or eustatic processes. Using these criteria, Mutti and others (1984) interpreted repeat intervals for large earthquakes triggering seismoturbidites in ancient rock sequences: an Upper Cretaceous sequence yielded repeat times of about 200,000 yr, an Eocene sequence repeat times of 500,000-1,000,000 yr, and a Miocene sequence repeat times of 2,000-45,000 yr. Obviously, such interpretations are of little use for modern seismic hazard assessment, but they do provide potentially valuable tools for reconstructing the paleoseismic history of a region.

Seguret and others (1984) used a similar approach to interpret Eocene turbidite sequences of the South Pyrenean basin in Spain. They used the term "megaturbidite" in the same sense as seismoturbidite was defined above. Using diagnostic criteria similar to those of Mutti and others (1984), they interpreted several megaturbidite deposits to have been seismically triggered. Based on the size and regional extent of these deposits, they postulated triggering earthquakes having magnitudes of 7.0-7.5. Average recurrence intervals for these Eocene events is about 500,000 yr.

4.3 Landslide Morphology

Some landslides have morphologies that strongly suggest triggering by earthquake shaking. For example, stability analyses of landslides on low-angle basal shear surfaces show that they generally form much more readily under the influence of earthquake shaking than in other conditions (Hansen, 1965; Jibson and Keefer, 1988, 1993). Landslides that formed as a result of liquefaction of subsurface layers also are much more likely to have formed seismically than aseismically (Seed, 1968). Perrin and Hancox (1992) indicated that slides that form as a result of intense rainfall are more fluid and tend to spread out more across a depositional area, whereas seismically induced landslides may have a blockier appearance and a more limited depositional extent in some cases. None of these criteria are definitive, but the types and characteristics of landslides described above do suggest seismic triggering and can be used as corroborative evidence of earthquake triggering.

Solonenko (1977) described several types of earthquake-triggered landslides documented in the Soviet Union, some of which have morphologies that he argued may be unique to seismic origin. His descriptions of such landslides can be condensed into six types: (1) subsidence of areas tens of square kilometers in extent by the opening of fracture systems in very large ($M > 8$) earthquakes; (2) collapse of slopes and mountain spurs crossed by active faults; (3) toppling of steep mountain peaks; (4) translational or rotational sliding of topographic benches covering several square kilometers; (5) rock falls and rock avalanches having abnormally long runout distances, including extreme runout events that may have moved on an air cushion; and (6) "ground avalanches and flows," where thick deposits of weak sediment such as loess collapse and flow large distances even on nearly level ground.

Landslide size also is cited widely as evidence of seismic triggering (for example, Whitehouse and Griffiths, 1983; Nikonov, 1988; Crozier, 1992). In the case of turbidites, large size is a definitive factor because of the criteria of multiple, independently triggered sources over a large area. For terrestrial landslides, use of size to demonstrate seismic origin is more tenuous. Size commonly is inferred to be a factor because of observations of large landslides in past earthquakes (Solonenko, 1977; Whitehouse and Griffiths, 1983; Nikonov,

1988). In areas where large landslides have been documented in historical time to occur only during earthquakes, large size of prehistoric landslides may suggest seismic origin and may even be used to infer the relative size of the triggering earthquake (Nikonov, 1988). It must be remembered, however, that landslides of all sizes form in the absence of earthquake shaking in a wide variety of environments. And Naumann and Savigny (1992) reached an opposite conclusion from their analysis of the stability of several rock avalanches in British Columbia, Canada. They showed that the larger slides analyzed were more susceptible to failure from increased pore-water pressure than from earthquake shaking and that earthquakes are more likely to trigger smaller rock falls (Naumann and Savigny, 1992).

In summary, landslide morphology and size can, in some circumstances, be used as corroborative evidence for seismic triggering, but only when a clear link between a specific morphology or size and earthquake triggering is observed.

4.4 Sackungen

Several different interpretations of the origin of sackungen have been proposed. Clearly, topography controls the ridge-parallel geometry of sackungen, and gravity is the principal driving force. But whether initiation of movement is by long-term creep, faulting, strong shaking, or a combination of factors has been debated. Bovis (1982) and Varnes and others (1987), who studied sackungen in western North America, argued that movement stems from long-term, gravity-driven creep, although both studies mention tectonism as a possible contributor in some cases. On the other hand, Beck's (1968) investigations of sackungen in New Zealand concluded that earthquake shaking was the most likely trigger of movement, primarily because the sackung topography appeared stable over long periods of seismic quiescence and because sackung were abundant in seismically active areas there. Jahn (1964) likewise surmised that sackungen in the Tatra Mountains of Czechoslovakia were triggered by earthquakes. Tabor (1971) indicated that earthquake shaking might play a minor role in sackung formation in the Olympic Mountains of Washington. Using sackungen for paleoseismic analysis appears tenuous, at best, and requires independent evidence of seismic triggering. To date, no criteria for establishing the seismic origin of sackungen have been published.

4.5 Interpretation of Sedimentary Structures

Some sedimentary structures have been interpreted as being seismically generated and thus could be used for paleoseismic interpretation. Although such structures are not landslides, they do involve seismic disturbance of surficial earth material. Among the first such studies was that by Seilacher (1969), in which he describes "fault-graded" bedding and argues that seismic shaking is the most likely origin of this type of structure. Fault-graded bedding consists of a sequence, perhaps several decimeters thick, that includes (from top down) (1) a liquefied zone, (2) a rubble zone, and (3) a step-faulted zone, all in gradational contact. His observation of three such sequences in a 10-m-thick section of Miocene Monterey Shale in coastal California led him to conclude that such structures result from very rare, very strong earthquakes. A subsequent study (Seilacher, 1984) identified pleated lamination, convex-down stacking of bowl-shaped shells, and current orientation in starved shell ripples as additional sedimentary structures that may have seismic origin.

Spalletta and Vai (1984) examined Upper Devonian turbidites in the Carnic region of northern Italy and interpreted a seismic origin on the basis of sedimentologic structures as well as the geometries of the deposits. Their diagnostic sedimentologic criteria for seismic triggering is the presence of "intraclast parabreccias," described as being caused by "shallow earthquakes generat[ing] in-situ (autoclastic) brecciation of the early lithified, centimeters-thick, surficial pelagic carbonate layer" (Spalletta and Vai, 1984, p. 135). This brecciation is followed within seconds to hours by a sandy turbidity current triggered upslope by the same earthquake. Repeated sections containing such structures were discovered, but no recurrence intervals were estimated.

Large rock avalanches commonly are triggered by large earthquakes (Keefer, 1984). Sedimentologic criteria for identifying rock-avalanche deposits in the geologic record have been developed (Yarnold and Lombard, 1989) and could potentially be applied to paleoseismic studies if diagnostic criteria for seismic triggering were developed.

Studies of in-place deformation of lake-bottom sediment by seismically induced liquefaction have identified criteria by which lacustrine sedimentary structures can be attributed to earthquake shaking (Sims, 1973, 1975; Hempton and Dewey, 1983). Such liquefaction structures are discussed in Chapter 7.

4.6 Lacustrine Sediment Pulses Caused by Landslides

Adams (1980) measured sediment loads of rivers in New Zealand immediately following earthquakes and observed an order-of-magnitude increase in load for a period of several months. He correlated increases in load in different areas with the density of earthquake-triggered landslides in those areas and concluded that seismically induced landslides cause large increases in fluvial sediment load, which, in turn, cause increases in sedimentation rates in lakes and oceans. These observations have been corroborated with published observations from earthquakes elsewhere (Adams, 1981b).

On the premise of these observations, Doig (1986) analyzed organic-free silt layers 0.3-2.0 cm thick in otherwise organic-rich lake sediment in eastern Canada. Using sedimentation rates and radiometric methods, three of these layers were correlated with known earthquakes of A.D. 1663, 1791, and 1860+1870 (two events combined). Two older silt layers were likewise dated and attributed to paleo-earthquakes in A.D. 1060 and 600. Doig (1986) stated that cores from deep lakes likely will yield the best cores for this type of analysis because of lack of bioturbation. He also warned that dating young (a few hundred years) silt layers characterized by lack of organic material can be difficult; he suggested that lead-210 and cesium-137 are the ideal radiometric methods for this type of analysis (see details of dating techniques in Chapter 3).

4.7 Landslides that Straddle Faults

In some areas, landslides have formed on slopes immediately above fault traces, and the slide mass has extended across the trace (Hunt, 1975; Morton and Sadler, 1989). Subsequent surface movement of such a fault would offset the landslide mass and allow estimation of fault slip rates if the slide could be dated. This approach does not require that the landslide be seismically triggered, because the paleoseismic interpretation is based on post-landslide fault offset of the landslide mass. However, landslides triggered in the immediate vicinity of active faults commonly are seismically triggered (Burrows, 1975).

4.8 Speleothems

Forti and Postpischl (1984) detailed a method for analyzing the toppling of stalagmites for paleoseismic interpretation. By measuring and dating tilting and collapse of many stalagmites in a region, they differentiated sudden (seismic) versus gradual movements and local versus regional causes. Tilting and collapse events are dated by analysis of radiometrically determined speleothem growth rates, which allows interpretation for about the last 100,000 yr. Because stalagmites are inverted pendulums, the minimum ground shaking necessary to cause collapse can be estimated fairly easily by pseudostatic engineering analysis. Although the method has some promise, it has not, thus far, been applied successfully to identify and date specific paleo-earthquakes.

4.9 Summary

A wide variety of methods for interpreting the seismic origin of landslides has been developed and, in some cases, successfully applied to paleoseismic analysis. Virtually all of the methods summarized in this section have one aspect in common, which is stated explicitly in most papers: the seismic origin of the features being interpreted remains tentative and cannot be proven, because in each case a nonseismic process could have produced the observed features. Circumstantial evidence for seismic triggering ranges from very strong to extremely tenuous. Indeed, on the latter end of the spectrum, the reasoning can be rather circular: an earthquake origin for a feature is assumed and then an earthquake origin is interpreted and concluded from analysis of that feature. Any paleoseismic interpretation of a feature is limited primarily by the certainty with which seismic triggering can be established. The following section addresses this dilemma by describing an approach to directly assess the conditions leading to failure of individual landslides.

5. ANALYSIS OF THE SEISMIC ORIGIN OF A LANDSLIDE

The most direct way to assess the relative likelihood of seismic versus aseismic triggering of an individual landslide is to apply established methods of static and dynamic slope-stability analysis (Lee and Edwards, 1986; Crozier, 1992; Jibson and Keefer, 1993). The first step in such an analysis involves constructing a detailed slope-stability model of static conditions to determine if failure is likely to have occurred in any reasonable set of ground-water and shear-strength conditions in the absence of earthquake shaking. All potential nonseismic factors must be considered; these might include processes such as fluvial or coastal erosion that oversteepens the slope or undrained failure resulting from rapid drawdown (for slopes subject to submersion). If aseismic failure can reasonably be excluded even in worst-case conditions (minimum shear strength, maximum piezometric head), then an earthquake origin can be inferred. Dynamic slope-stability analyses can then be used to estimate the minimum shaking conditions that would have been required to cause failure. In the sections that follow, a method for conducting such an analysis is described using an example from the New Madrid seismic zone summarized from Jibson and Keefer (1993).

5.1 Physical Setting of Landslides in the New Madrid Seismic Zone

The New Madrid earthquakes of 1811-12 (Fuller, 1912) triggered many large landslides along the bluffs that form the eastern edge of the Mississippi River alluvial plain in Tennessee and Kentucky (Figure 1). Many landslide features currently are visible along these bluffs, and one of these landslides is analyzed below to determine if a seismic versus nonseismic origin can be established with a reasonable level of confidence.

The bluffs in the study area are not, for the most part, active river banks and thus are subject to landsliding from fluvial erosion in only a few locations. The bluffs stand as high as 70 m above the alluvial plain of the Mississippi River and therefore are not subject to landsliding from conditions such as rapid drawdown because the bluff is never inundated by flooding to a significant height. The average height of the bluffs in this area is 35 m, and slope angles range from a few degrees to almost vertical, but typically are 15-25°.

The base of the bluffs throughout most of the area is formed by as much as 45 m of shallow-marine clays and silts of the Eocene Jackson Formation (Conrad, 1856). Lying unconformably on the Jackson Formation is as much as 20 m of Pliocene alluvial gravel and sand of the Lafayette Gravel (McGee, 1891; Potter, 1955). The bluffs are capped by 5-50 m of Pleistocene loess lying unconformably on the Jackson Formation and Lafayette Gravel. The average thickness of the loess in the area is about 15 m.

A translational block slide about 11 km north of Dyersburg, Tenn., referred to as the Stewart landslide, was chosen for detailed analysis (Figure 1). This landslide is representative of coherent block slides in the area, which previous research (Jibson and Keefer, 1988, 1989) indicated were probably triggered by the 1811-12 earthquakes. Figure 2 shows a profile of the Stewart slide; subsurface data is from drilling along the line of profile.

5.2 Geotechnical Investigation

Four rotary drill holes were placed along the line of profile to determine the bluff stratigraphy and to procure soil samples for geotechnical testing (Figure 2). Standard-Penetration testing (SPT) yielded split-spoon samples, which typically were heavily disturbed by the sampling process and were used primarily for determining index properties, such as grain size, plasticity, water content, and color. Several 13-cm-diameter undisturbed piston cores were procured to measure soil unit weight and shear strength, both needed for limit-equilibrium stability analysis. Jibson (1985) described the sampling methods in detail.

Drained shear strengths, for use in static stability analyses, were measured using two methods: (1) direct shear in which the rate of strain was slow enough to allow full drainage and (2) consolidated-undrained triaxial (CUTX) shear in which pore pressures were measured to allow modeling of drained conditions (Jibson, 1985). Undrained shear strengths, for use in dynamic analysis, were measured primarily by CUTX tests. CUTX test results were supplemented by vane-shear and penetrometer data and correlation with SPT blow counts where undisturbed samples were unavailable.

5.3 Static (Aseismic) Slope-Stability Analysis

Figure 3 shows an idealized model of the pre-landslide bluff in drained conditions, appropriate for modeling static (aseismic) stability. The bluff is 45 m high as measured from the profile (Figure 2). Undisturbed bluffs adjacent to the Stewart slide have slopes of about 20° and have simple, uniformly sloping faces. Geotechnical properties of the stratigraphic layers in the model were assigned using the results of the shear-strength tests; layers where no shear-strength tests were performed were assigned strengths based on stratigraphic and index-property correlation with layers where strengths were measured (Jibson, 1985).

Lack of published data made modeling ground-water conditions along the bluffs difficult. Therefore, several potential ground-water conditions were modeled (Figure 4) that effectively bracket the most and least critical conditions that are physically possible. Because of the local topography and hydraulic properties of the bluff materials, the most critical condition modeled (Figure 4, condition 1) is a more critical situation than can realistically exist in the bluffs and thus provides a worst-case bounding condition. The most likely ground-water condition also was modeled: a water table sloping upward from the base of the bluffs to the top of the Jackson Formation, and a second water table perched on the relatively impermeable Jackson that saturates the Lafayette Gravel.

The STABL computer program (Siegel, 1978) was used to determine the stability of the modeled bluff in aseismic conditions. STABL searches for the most critical failure surface by randomly generating circular, wedge, and irregular slip surfaces and calculating the factor of safety[1] for each generated surface. The program plots the ten most critical surfaces of each type and their factors of safety. The geometry of the actual failure surface (shown diagrammatically in Figure 2) was determined by locating weak or disturbed layers by drilling and by analysis of the surface geometry of the landslide. The safety factor for this surface was calculated using the simplified Janbu method (Siegel, 1978) for each ground-water condition.

Determining the stability of the bluffs from the factor of safety requires judgment. Gedney and Weber (1978) recommended that engineered slopes have safety factors between 1.25 and 1.50 for the type of analysis used. Because of the high density of good-quality geotechnical data, this range is used as the criterion to evaluate slope stability: between FS 1.00 and 1.25, slopes are considered to be marginally stable; between FS 1.25 and 1.50, slopes are considered to be stable; and above FS 1.50, slopes are considered to be very stable.

The results of the stability analyses are summarized in Table 2. The lowest factor of safety in the most critical ground-water condition is 1.32, which indicates that the bluff at the Stewart site is stable in aseismic conditions even in the most critical ground-water condition. In the most likely ground-water condition (sloped and perched), the minimum factor of safety is 1.82, indicating a very stable bluff. The factor of safety of the actual failure surface in the most likely ground-water condition is 1.88.

---

[1]The factor of safety (FS) is the ratio of the sum of the resisting forces that act to inhibit slope movement to the sum of the driving forces that tend to cause movement. Slopes having factors of safety greater than 1.0 are thus stable; those having factors of safety less than 1.0 should move.

Our analysis shows that an artesian piezometric surface tens of meters above ground level at the top of the bluff would be needed to reduce the factor of safety to 1.0. Such an artesian condition is impossible because (1) the regional geology and topography preclude such a condition because the top of the bluff is 30-70 m above the alluvial plain, and no topographically higher artesian recharge area exists, and (2) a piezometric surface high above the bluff-top that dips steeply to the base of the bluff is physically unrealistic.

Figure 5 shows the locations of the most critical slip surfaces of various shapes and of the actual slip surface. All the surfaces have grossly similar shapes, but the most critical computer-generated surfaces all lie well above the actual failure surface. This disparity suggests that the sliding did not take place under drained, static conditions.

The rather high factors of safety, even in unrealistically high ground-water conditions, and the disparity between the most critical computer-generated slip surfaces and the actual surface indicate that it is extremely unlikely that the existing landslide at the Stewart site formed in aseismic, drained conditions.

5.4 Dynamic (Seismic) Slope-Stability Analysis

Jibson and Keefer (1993) used the dynamic displacement analysis developed by Newmark (1965), now used widely in engineering practice (Seed, 1979), to evaluate the seismic stability of the bluff. In the Newmark method a landslide is modeled as a rigid friction block that begins to move when a given critical acceleration is exceeded; critical acceleration is defined as the acceleration required to overcome frictional resistance and initiate sliding on an inclined plane. The analysis calculates the cumulative permanent displacement of the block as it is subjected to the effects of an earthquake acceleration-time (strong-motion) history, and the user judges the significance of the displacement. Laboratory model tests (Goodman and Seed, 1966) and analysis of actual earthquake-induced landslides (Wilson and Keefer, 1983) have confirmed that Newmark's method can fairly accurately predict landslide displacements if slope geometry and soil properties are known accurately and if earthquake ground accelerations can be estimated using real or artificial acceleration-time histories.

Newmark (1965) showed that the critical acceleration is a simple function of the static factor of safety and the landslide geometry; it can be expressed as

$$a_c = (FS - 1)\text{g} \sin \alpha, \tag{1}$$

where a_c is the critical acceleration in terms of a ratio to g, the acceleration of Earth's gravity; FS is the static factor of safety; and α is the angle from the horizontal (hereafter called the thrust angle) that the center of mass of the potential landslide block first moves.

The algorithm developed by Wilson and Keefer (1983) is used to apply Newmark's method, which simply consists of double-integrating the portions of the selected acceleration-time history that lie above the critical acceleration of the landslide block. This double integration of the acceleration record yields the cumulative permanent displacement of the block.

Conducting a Newmark analysis requires three pieces of information: (1) the static factor of safety and (2) the thrust angle of the potential landslide (both needed to calculate the critical acceleration), and (3) an earthquake acceleration-time history.

5.4.1 *Static Factor of Safety*

During earthquakes, soils behave in a so-called undrained manner because excess pore pressures induced by the transient ground deformation cannot dissipate during the brief duration of the shaking; therefore, a layered model of the bluff in undrained conditions was constructed (Figure 6). Undrained shear strength is treated as a single numerical quantity that is represented in the analysis as cohesion, and the friction angle is taken to be zero (Lambe and Whitman, 1969). Undrained shear strengths used in the model (Figure 6) were measured directly in the laboratory, as described previously. Because undrained strength depends in large part on consolidation stress, layers of roughly similar thickness were constructed that reflect the increase in shear strength with depth even for relatively homogeneous materials.

STABL was used to generate potential failure surfaces and to determine the most critical failure surface in the same manner as described above for the aseismic stability analysis in drained conditions. Table 2 summarizes the results of the undrained slope stability analyses using this model. The lowest factor of safety is 1.53, which shows that the bluff is statically stable in undrained conditions. Figure 7 shows the locations of the most critical slip surfaces for the most likely ground-water condition. All the slip surfaces, including the actual failure surface, plot very close to one another and have similar factors of safety. Both circular surfaces have large radii and approximate planar basal shear surfaces, as is expected from the shape of the actual shear surface (Figure 2). The fact that the most critical computer-generated surfaces closely parallel the actual failure surface indicates that the model of the bluffs is reasonable and that slope failure is more likely to have occurred in undrained conditions than in drained conditions.

5.4.2 *Thrust Angle*

The thrust angle (α) is the direction the center of gravity of the slide mass moves when displacement first occurs. For a planar slip surface parallel to the slope face (an infinite slope), the thrust angle is the slope angle. For rotational movement on a circular surface, Newmark (1965) showed that the thrust angle is the angle between the vertical and a line segment connecting the center of gravity of the landslide mass and the center of the slip circle.

Figure 7 shows geometric constructions of the thrust angles for the two circular failure surfaces and the circular approximation of the irregular surface. Thrust angles for these surfaces all are 15-16°. The thrust angle of the actual surface is difficult to estimate because of its irregular shape and consequent complex movement. An average inclination of the actual failure surface can be calculated by weighting the inclinations of the line segments forming the actual surface by their relative lengths. This yields an average inclination of 16°, consistent with the other generated surfaces.

5.4.3 *Earthquake Acceleration-Time History*

The hypothesis being tested is that the Stewart landslide was triggered by the 1811-12 earthquakes; therefore, earthquake acceleration-time histories must be selected to approximate the shaking conditions from the 1811-12 earthquakes at the Stewart site. Choosing strong-motion records to represent the ground motions from the 1811-12 earthquakes is difficult because most available records are from California earthquakes, which probably differ in many respects from large earthquakes in the central United States (e.g., Nuttli, 1983). Differences in the propagation of strong ground motion due to regional differences in attenuation, however, may not be as great as previously believed, and they appear to be significant only at great epicentral distance (> 150 km) for very large earthquakes (Hanks and Johnston, 1992). The Stewart site is only 20-70 km from the three estimated epicenters of the 1811-12 earthquakes.

Estimating various ground-motion characteristics of the 1811-12 earthquakes at the Stewart site and comparing these estimated characteristics with those of existing earthquake records provides a basis for choosing an input ground motion. Peak ground acceleration (*PGA*), duration, and shaking intensity are used for this comparison, and these parameters can be estimated by several methods, as described by Jibson and Keefer (1993). Although *PGA* is the most commonly used index of strong shaking, it is a rather crude single measure of earthquake shaking intensity because it measures only a single point in an acceleration-time history. A more quantitative measure of total shaking intensity developed by Arias (1970) is useful in seismic hazard analysis and correlates well with distributions of earthquake-induced landslides (Harp and Wilson, 1989). Arias intensity is the integral over time of the square of the acceleration, expressed as

$$I_a = \pi/2g \int [a(t)]^2 dt, \qquad (2)$$

where I_a is the Arias intensity, expressed in units of velocity, and $a(t)$ is the ground acceleration as a function of time. Arias intensity is used as the primary characteristic for comparison in selecting strong-motion records.

Although strong motion has not been recorded for earthquakes in the magnitude range of the 1811-12 events, several existing strong-motion records have shaking characteristics similar enough to the estimated shaking characteristics of the 1811-12 events to be useful. An extensive catalog of digitized strong-motion records was examined, primarily from California earthquakes, and two records for each of the three 1811-12 earthquakes were selected. Records were chosen to match, as closely as possible, the estimated range of Arias intensities and *PGA*'s from the 1811-12 events so as to bracket the likely ranges of shaking conditions that actually occurred. None of the available strong-motion records have Arias intensities greater than 10 m/s; therefore, where estimated Arias intensities exceeded this level, the available record having the greatest Arias intensity was used. Table 3 shows the records selected and compares some of their characteristics with those estimated by Jibson and Keefer (1993) for the Stewart site from the 1811-12 earthquakes.

5.4.4 *Calculation of the Newmark Landslide Displacement*

Critical accelerations were calculated based on a thrust angle of 16° and on the factors of safety (FS 1.62, 1.64) of the two circular slip surfaces in the perched and sloped ground-water conditions. These slip surfaces most closely coincide with the actual surface and have the lowest factors of safety. Equation 1 yields critical accelerations of 0.17-0.18 g for these input values. These critical accelerations are specified in the computer program that double integrates the strong-motion record to calculate the Newmark displacement.

The significance of the Newmark displacements must be judged in terms of the probable effect on the potential landslide mass. For example, Wieczorek and others (1985) used 5 cm as the critical displacement leading to failure of landslides in San Mateo County, Calif.; Keefer and Wilson (1989) used 10 cm as the critical displacement for coherent slides in southern California. When displacements in this range occur, previously undisturbed soils can lose some of their strength and be in a residual-strength condition. Static factors of safety using residual shear strengths can then be calculated to determine the stability of the landslide after earthquake shaking (and consequent inertial landslide displacement) ceases.

Table 3 shows Newmark displacements calculated for the two critical accelerations using the six strong-motion records listed. Displacements are 6-55 cm and thus fall on both sides of the critical 5-10 cm range. Displacements generated by the model earthquakes of the 16 December 1811 event are 6-8 cm; in this range, the likelihood of catastrophic failure is uncertain. The soils sampled and tested at the Stewart site all showed significant strength reductions during strain in both drained and undrained conditions (Jibson, 1985); residual strength generally was reached after shear displacements of about 0.5 cm (for silts and sands) to 6 cm (for clayey silts). Therefore, even modest displacements would have at least partially reduced the soil shear strength and thus would have reduced the critical acceleration of the landslide in future earthquakes. The model earthquakes for the 23 January and 7 February 1812 events generated Newmark displacements of 23-55 cm, which undoubtedly would have reduced soil shear strengths to residual levels.

For all ground-water conditions, static factors of safety for the Stewart slide calculated using residual shear strengths in both drained and undrained conditions (Jibson, 1985) all were less than 0.8 and in most cases were less than 0.4. Therefore, if the bluff materials reach residual strength, catastrophic failure almost certainly will occur. Displacements of 20-50 cm thus would reduce the shear strength of the bluff materials to a residual-strength condition and probably would lead to catastrophic failure. The repeated shaking of the bluffs by three large earthquakes (and the far more numerous moderate earthquakes) and the reduction of the critical acceleration of the partially failed landslide mass leave little doubt that very large displacements of the Stewart slide would have occurred during the entire 1811-12 earthquake sequence.

5.4.5 *Summary*

In summary, static stability analyses of drained conditions indicate that failure of the Stewart landslide in aseismic conditions is extremely unlikely. Dynamic analysis shows that shaking conditions similar to those in 1811-12 would have induced large displacements that probably would lead to catastrophic failure. Further analysis (Jibson and Keefer, 1993) showed that no earthquakes since 1812 could have triggered the observed landslide

movement. The results of these analyses are consistent with results from field and regional studies (Jibson and Keefer, 1988, 1989), which indicated that the ages and regional distribution of landslides similar to the Stewart slide are consistent with triggering in 1811-12. Datable material needed to determine a precise age of landsliding at the Stewart site could not be recovered, so the analytical approach outlined above was crucial in linking the landslide to the 1811-12 earthquakes. Considered together, these studies strongly support such a conclusion.

5.5 Analysis of Unknown Seismic Conditions

The procedure described above was used to test the hypothesis that an individual landslide was triggered by a historical earthquake whose magnitude and location have already been estimated. The goal of most paleoseismic investigations, by contrast, is to detect and characterize prehistoric or undocumented earthquakes whose effects are recorded in the geologic record. Therefore, a more general procedure for paleoseismic landslide analysis is required.

If static stability analyses clearly indicate that failure in aseismic conditions is highly unlikely, then an earthquake origin can be hypothesized on that basis alone. A dynamic analysis can then be used to estimate the minimum shaking intensities necessary to have caused failure. Such an approach requires a general relationship between critical acceleration, shaking intensity, and Newmark displacement; a relationship developed by Jibson and Keefer (1993) is reiterated here.

Jibson and Keefer (1993) selected 11 strong-motion records having Arias intensities between 0.2 and 10.0 m/s, which span the range between the smallest shaking intensities that might cause landslide movement and the largest shaking intensities ever recorded. For each strong-motion record, they calculated the Newmark displacement for several critical accelerations between 0.02 and 0.40 g, the range of practical interest for most earthquake-induced landslides. Analysis of the resulting data set indicated that a multivariate model of the following form would fit the data well:

$$\log D_N = A\log I_a + Ba_c + C \pm \sigma, \tag{3}$$

where D_N is Newmark displacement in centimeters; I_a is Arias Intensity in meters per second; a_c is critical acceleration in g's; σ is the estimated standard deviation of the model; and A, B, and C are the regression coefficients. The resulting model has an R^2 of 0.87, and the coefficients all are significant above the 99.9 percent confidence level:

$$\log D_N = 1.460\log I_a - 6.642a_c + 1.546 \pm 0.409. \tag{4}$$

This model yields the mean value of Newmark displacement when σ is ignored; the variation about this mean represented by σ results from the stochastic nature of earthquake ground shaking. Thus, even two strong-motion records having identical Arias intensities can produce significantly different Newmark displacements for slopes having identical critical accelerations. Therefore, Equation 4 yields a range of displacement values that must be interpreted with considerable judgment. Figure 8 shows critical acceleration lines defined by

Equation 4. The model underestimates Newmark displacement at low levels of Arias intensity (less than 0.5 m/s) for very small critical accelerations (0.02 g), but otherwise, the data are well fit by the model.

In the case of the Stewart landslide, if we knew nothing of the shaking history of the site, the minimum earthquake shaking intensity could be estimated using Equation 4. This requires judging the amount of Newmark displacement (the critical displacement) that would reduce shear strength on the failure surface to residual levels and lead to catastrophic failure. As discussed previously, critical displacements of about 10 cm are probably realistic for this type of slide, based on previous studies (Wieczorek and others, 1985; Wilson and Keefer, 1985; Keefer and Wilson, 1989), laboratory shear-strength testing of soil samples from the site (Jibson, 1985), and field studies of landslides in the region (Jibson and Keefer, 1988). Inserting a displacement value of 10 cm and the range of critical accelerations of the Stewart landslide (0.17-0.18 g) into Equation 4 yields a lower-bound Arias intensity of about 2.6 m/s to trigger the Stewart slide.

Wilson and Keefer (1985) developed an empirical relationship between Arias intensity, earthquake magnitude, and source distance:

$$\log I_a = M - 2\log R - 4.1, \quad (5)$$

where I_a is Arias intensity in meters per second, M is moment magnitude, and R is earthquake source distance in kilometers. For a minimum source distance of 5 km (focal depth at the epicenter), the Arias intensity of 2.6 m/s estimated above yields M=5.9 as the minimum threshold earthquake magnitude required to have caused slope failure. Although this magnitude is considerably lower than those estimated to have been generated by the 1811-12 earthquakes, it provides a reasonable lower bound in the absence of any other information. If more than one landslide of identical age were similarly analyzed in an area, magnitude and location estimates can be optimized by using the larger required source distances between two or more separate sites.

6. INTERPRETING RESULTS OF PALEOSEISMIC LANDSLIDE STUDIES

Once a landslide or group of landslides has been identified, dated, and linked to earthquake shaking, what can we learn about the magnitude and location of the triggering earthquake? Several approaches to this last level of paleoseismic interpretation are possible, and, in most cases, multiple lines of evidence will be required to reasonably estimate magnitude and location. Perhaps the most important aspect of such interpretation is a thorough understanding of the characteristics of landslides triggered by recent, well-documented earthquakes.

6.1 Some Characteristics of Landslides Triggered by Earthquakes

Keefer (1984) conducted by far the most comprehensive study of landslides caused by historical earthquakes. He documented minimum earthquake magnitudes and intensities that have triggered landslides of various types, average and maximum areas affected by landslides as a function of magnitude, and maximum distances of landslides from earthquake sources as a function of magnitude. For these comparisons, he grouped different types of landslides into

three categories: disrupted slides and falls (defined as falls, slides, and avalanches in rock and soil); coherent slides (defined as slumps and block slides in rock and soil and slow earth flows); and lateral spreads and flows (defined as lateral spreads and rapid flows in soil and subaqueous landslides).

6.1.1 *Minimum Earthquake Magnitudes That Trigger Landslides*

In a review of intensity reports from 300 earthquakes, Keefer (1984) found that the smallest earthquake reported to have caused landslides had a magnitude of 4.0. Landslides of various types have threshold magnitudes ranging from 4.0 to 6.5 (Table 4); disrupted landslides have lower threshold magnitudes than coherent slides. Although smaller earthquakes could conceivably trigger landslides, such triggering by very weak shaking probably would occur on slopes where failure was imminent before the earthquake.

6.1.2 *Minimum Shaking Intensities That Trigger Landslides*

Keefer (1984) also compared landslide initiation to Modified Mercalli Intensity (MMI). Table 5 shows the lowest MMI values and the predominant minimum MMI values reported where the three categories of landslides were occurred. Keefer's (1984) data show that landslides of various types are triggered one to five levels lower than indicated in the current language of the MMI scale.

Nikonov (1988) and Solonenko (1977) correlated landslide initiation with threshold shaking levels using the Russian MSK intensity scale. Their observations indicated that small landslides are initiated at intensities IV-VII, large landslide at intensities VIII-IX, and "large landslides in basement rocks" at intensities of IX or greater.

6.1.3 *Areas Affected by Earthquake-Triggered Landslides*

For 30 historical earthquakes, Keefer (1984) drew boundaries around all reported landslide locations and calculated the areas enclosed. His plot of area versus earthquake magnitude (Figure 9) shows a well-defined upper bound curve representing the maximum area that can be affected for a given magnitude. Also shown is a regression line showing average area, the equation of which is

$$\log A = M_S - 3.46, \tag{6}$$

where A is area affected by landslides in square kilometers and M_S is surface-wave magnitude (Keefer and Wilson, 1989).

Keefer (1984) noted that the area affected by landslides will be influenced, in part, by the geologic conditions that control the distribution of susceptible slopes. Also, he noted that earthquakes having focal depths greater than about 30 km plot on or near the upper bound (Figure 9), which indicates that deeper earthquakes can trigger landslides over larger areas. Surprisingly, he found no differences in the areas affected by landsliding that could be attributed to regional differences in seismic attenuation.

6.1.4 *Maximum Distance of Landslides From Earthquake Sources*

Keefer (1984) related earthquake magnitude to the maximum distance of the three categories of landslides from the earthquake epicenter and from the closest point on the fault-rupture surface (Figure 10). Again, upper bound curves are well defined and are constrained to pass through the minimum threshold magnitudes shown in Table 4 as distance approaches zero.

Figure 10 indicates that disrupted slides and falls have the lowest shaking threshold and that lateral spreads and flows have the highest shaking threshold. As with area, earthquakes having focal depths greater than 30 km generally triggered landslides at greater distances than shallower earthquakes of similar magnitude.

6.2 Interpreting Earthquake Magnitude and Location

Keefer's (1984) results allow interpretation of earthquake magnitude and location in a variety of ways. If a single landslide is identified as being seismically triggered, then a minimum magnitude and MMI can be estimated based on the landslide type. For example, Schuster and others (1992) used Keefer's (1984) magnitude of 6.5 as a lower bound estimate for triggering of rock avalanches that formed dams. If several landslides in an area are identified as being seismically induced, then application of Keefer's (1984) magnitude-area and magnitude-distance relationships can yield minimum magnitude estimates. As the area in which landslides documented to have been triggered by the same earthquake increases, the estimated magnitude will increase toward the actual magnitude of the triggering earthquake. Therefore, documentation and analysis of landslides over a large area will produce more accurate magnitude estimates. If seismic source zones are well documented, then the distance from the closest source zone to the farthest landslide will yield a reasonable minimum magnitude estimate. The observation that greater source depth relates to greater areas affected and source distances for landslides of all types (Keefer, 1984) further complicates estimation of earthquake magnitude.

For a specific region, earthquake magnitude can be estimated based on comparison of paleoseismic landslide distribution with landslide distributions from recent, well-documented earthquakes in the region. This approach has been applied to landslide dams in New Zealand (Adams, 1981a) and to landslides in central Asia (Nikonov, 1988).

Several types of interpretations from seismically triggered turbidites are possible. The linear extent of synchronous turbidites triggered from the edges of continental shelves can be used to estimate fault rupture length and, hence, earthquake magnitude (Adams, 1990). The extreme size and very long recurrence intervals (10^4-10^6 yr) for lithified turbidites preserved in the older geologic record argue that they formed in very rare, large-magnitude earthquakes (Mutti and others, 1984; Spalletta and Vai, 1984). The paucity of seismically induced sedimentary structures in some older, lithified deposits likewise suggests long recurrence intervals and consequent large earthquake magnitudes (Seilacher, 1969).

Static and dynamic slope-stability analyses facilitate direct estimation of the minimum ground shaking, and hence magnitude, required to have caused failure of individual landslides (Jibson and Keefer, 1992, 1993), as described in detail previously. If the critical acceleration of a landslide can be determined by stability analysis, and if a reasonable amount of displacement (such as 10 cm) leading to catastrophic failure can be estimated, then Equation

4 can be used to estimate the threshold Arias intensity required to initiate failure. Equation 5 (from Wilson and Keefer, 1985) can then be used to estimate the minimum magnitude of the triggering earthquake.

A similar approach for estimating earthquake magnitude from the results of slope-stability analyses was outlined by Crozier (1992) and is based on the work of Wilson and Keefer (1985). They defined a quantity referred to as $(A_c)_{10}$, which is the critical acceleration of a landslide that will yield 10 cm of displacement (the estimated critical displacement leading to catastrophic failure) in a given level of earthquake shaking. They selected 10 strong motion records that spanned a range of Arias intensities and iteratively determined $(A_c)_{10}$ for each record. From these values, they developed a regression model relating Arias intensity to $(A_c)_{10}$:

$$\log(A_c)_{10} = 0.79\log I_a - 1.095, \tag{7}$$

where $(A_c)_{10}$ is in g's and I_a is in meters per second. If the critical acceleration of a landslide can be determined, then this value can be used as the threshold value of $(A_c)_{10}$ in Equation 7, and the Arias intensity that would trigger the critical displacement of 10 cm can be calculated. Magnitude can then be estimated from Equation 5.

Stability analysis also could possibly be applied to speleothemes, whose dynamic stability can easily be modeled, to estimate the ground shaking required to cause failure.

Earthquake locations generally are estimated based on the distribution of synchronous landslides attributed to a single seismic event. In a broad area of roughly similar susceptibility to landsliding, the earthquake epicenter probably will coincide fairly closely with the centroid of the landslide distribution. In areas of highly variable or asymmetrical landslide susceptibility, epicenter estimation is much more difficult and subject to error. In areas where seismic source zones are well defined, the epicentral location is best defined as the point in a known seismic source zone (or along a known seismogenic fault) closest to the centroid of the landslide distribution.

7. SOME FINAL COMMENTS

The use of landslides as paleoseismic indicators is a fairly recent development that is beginning to expand in scope and complexity. A few final comments on the advantages and limitations of paleoseismic landslide analysis are in order.

The primary limitation of paleoseismic analysis of landslides is the inherent uncertainty in interpreting a seismic origin. Unlike liquefaction, which can occur aseismically only in relatively rare conditions, landslides of all types form readily in the absence of earthquake shaking as a result of many different triggering mechanisms. In many cases, ruling out aseismic triggering will be impossible, and the level of confidence in any resulting paleoseismic interpretation will be limited. For this reason, paleoseismic landslide analysis should include, so far as possible, multiple lines of evidence to constrain a seismic origin. In this way, a strong case can be built for seismic triggering of one or more landslides, even if no single line of evidence is unequivocal. Where independent paleoseismic evidence from fault or liquefaction studies is available, paleoseismic landslide evidence can provide useful corroboration.

Detailed slope-stability analysis generally can be performed only on certain types of landslides. Failure conditions of falls, avalanches, and disrupted slides cannot easily be modeled using Newmark's (1965) method, and even static stability analyses of these types of slides can be very problematic. Also, the pre-landslide geometry of slides in very steep terrain can be difficult or impossible to reconstruct. Thus, the analytical method described herein generally can be applied only to fairly coherent landslides where pre-landslide geometry can be reconstructed with confidence, where ground-water conditions can be modeled reasonably, and where the geotechnical properties of the materials can be accurately measured.

Even allowing for these limitations, paleoseismic landslide studies have been extremely useful where applied successfully, and they hold great potential in the field of paleoseismology. Dating landslide deposits is, in many cases, easier than dating movement along faults because many different dating methods can be used on the same slide to produce redundant results. In addition, landslides have the potential for preserving large amounts of datable material in the various parts of the slide (scarp, body, toe, etc.). In areas containing multiple or poorly defined seismic sources, paleoseismic ground-failure analysis may be preferable to fault studies because landslides preserve a record of the shaking history of a site or region from all seismic sources. Knowing the frequency of strong shaking events may, in many cases, be more critical than knowing the behavior of any individual fault.

Paleoseismic landslide analysis may have greatest utility in assessing earthquake hazards in stable continental interiors, such as the eastern and central United States, where fault exposures are rare or absent but where earthquakes are known to have occurred. In such areas, analysis of earthquake-triggered ground failure, both landslides and liquefaction, may be one of the few paleoseismic tools available.

Another advantage of paleoseismic landslide analysis is that it gets directly at the effects of the earthquakes being studied. Ultimately, most paleoseismic studies are aimed at assessing earthquake hazards. Fault studies can be used to estimate slip rates, recurrence intervals, and, indirectly, magnitudes. From these findings, we extrapolate the effects of a possible earthquake on such a fault. In paleoseismic landslide studies, we observe the effects directly. Thus, if a seismic origin can be established, a landslide shows directly what the effects of some previous earthquake were. Even if magnitude and location are poorly constrained, at least we have a partial picture of the actual effects of seismic shaking in a locale or region. Thus, for example, a map of the distribution of landslides triggered by the 1811-12 earthquakes in the New Madrid seismic zone (Jibson and Keefer, 1988) yields a very useful picture of the likely distribution of landslides in future earthquakes there.

In conclusion, paleoseismic landslide analysis can be applied in a variety of ways and can yield many different types of results. Although interpretations are limited by the certainty with which a seismic origin can be established, paleoseismic landslide studies can play a vital role in the paleoseismic interpretation of many areas, particularly those lacking fault exposures.

REFERENCES

Adam, D.P., 1975, A late Holocene pollen record from Pearson's Pond, Weeks Creek landslides, San Francisco Peninsula, California: U.S. Geological Survey Journal of Research, v. 3, p. 721-731.

Adams, J., 1980, Contemporary uplift and erosion of the Southern Alps, New Zealand: Summary: Geological Society of America Bulletin, Part I, v. 91, p. 2-4.

Adams, J., 1981a, Earthquake-dammed lakes in New Zealand: Geology, v. 9, p. 215-219.

Adams, J., 1981b, Earthquakes, landslides, and large dams in New Zealand: Bulletin of the New Zealand National Society for Earthquake Engineering, v. 14, no. 2, p. 93-95.

Adams, J., 1990, Paleoseismicity of the Cascadia subduction zone: Evidence from turbidites off the Oregon-Washington margin: Tectonics, v. 9, p. 569-583.

Andrews, D.J., and Bucknam, R.C., 1987, Fitting degradation of shoreline scarps by a model with nonlinear diffusion: Journal of Geophysical Research, v. 92, p. 12,857-12,867.

Andrews, D.J., and Hanks, T.C., 1985, Scarps degraded by linear diffusion: inverse solution for age: Journal of Geophysical Research, v. 90, p. 10,193-10,208.

Arias, A., 1970, A measure of earthquake intensity, *in* Hansen, R.J., ed., Seismic design for nuclear power plants: Cambridge, Massachusetts Institute of Technology Press, p. 438-483.

Atwater, B.F., 1987, Evidence of great Holocene earthquakes along the outer coast of Washington State: Science, v. 236, p. 942-944.

Beck, A.C., 1968, Gravity faulting as a mechanism of topographic adjustment: New Zealand Journal of Geology and Geophysics: v. 11, p. 191-199.

Bégin, C., and Filion, L., 1985, Analyse dendrochronologique d'un glissement de terrain de la région du Lac à l'Eau Claire (Québec nordique): Canadian Journal of Earth Sciences, v. 22, p. 175-182 [in French].

Birkeland, P.W., 1984, Soils and geomorphology: Oxford University Press, 372 p.

Birkeland, P.W., Machette, M.N., and Haller, K.M., 1991, Soils as a tool for applied Quaternary geology: Utah Geological and Mineral Survey Miscellaneous Publication 91-3, 63 p.

Bovis, M.J., 1982, Uphill-facing (antislope) scarps in the Coast Mountains, southwest British Columbia: Geological Society of America Bulletin, v. 93, p. 804-812.

Brunsden, D., and Prior, D.B., 1984, Slope instability: New York, John Wiley and Sons, 620 p.

Bucknam, R.C., and Anderson, R.E., 1979, Estimation of fault-scarp ages from a scarp-height–slope-angle relationship: Geology, v. 7, p. 11-14.

Bull, W.B., Cowan, H.A., and Pettinga, J.R., 1991, New ways of dating earthquakes on two segments of the oblique-slip Hope fault, New Zealand: Geological Society of America, Abstracts with Programs, v. 23, no. 5, p. A431.

Burrows, C.J., 1975, A 500-year-old landslide in the Acheron River valley, Canterbury (Note): New Zealand Journal of Geology and Geophysics, v. 18, p. 357-360.

Chinn, T.J.H., 1981, Use of rock weathering-rind thickness for Holocene absolute age-dating in New Zealand: Arctic and Alpine Research, v. 13, p. 33-45.

Christiansen, E.A., 1983, The Denholm landslide, Saskatchewan. Part I: Geology: Canadian

Geotechnical Journal, v. 20, p. 197-207.
Colman, S.M., and Watson, K., 1983, Ages estimated from a diffusion equation model for scarp degradation: Science, v. 221, p. 263-265.
Conrad, T.A., 1856, Observations of the Eocene deposit of Jackson, Miss., with descriptions of 34 new species of shells and corals: Philadelphia Academy of Natural Sciences, Proceedings, 1855, 1st ser., v. 7, p. 257-258.
Costa, J.E., and Schuster, R.L., 1991, Documented historical landslide dams from around the world: U.S. Geological Survey Open-File Report 91-239, 486 p.
Crozier, M.J., 1992, Determination of paleoseismicity from landslides, *in* Bell, D.H., ed., Landslides (Glissements de terrain), International Symposium, 6th, Christchurch, New Zealand, 1992, Proceedings: Rotterdam, A.A. Balkema, v. 2, p. 1173-1180.
Dietrich, W.E., and Dorn, R., 1984, Significance of thick deposits of colluvium on hillslopes: A case study involving the use of pollen analysis in the coastal mountains of northern California: Journal of Geology, v. 92, p. 147-158.
Dobry, R., Idriss, I.M., and Ng, E., 1978, Duration characteristics of horizontal components of strong-motion earthquake records: Bulletin of Seismological Society of America, v. 68, p. 1487-1520.
Doig, R., 1986, A method for determining the frequency of large-magnitude earthquakes using lake sediments: Canadian Journal of Earth Sciences, v. 23, p. 930-937.
Field, M.E., Gardner, J.V., Jennings, A.E., and Edwards, B.D., 1982, Earthquake-induced sediment failures on a 0.25° slope, Klamath River delta, California: Geology, v. 10, p. 542-546.
Forti, P., and Postpischl, D., 1984, Seismotectonic and paleoseismic analyses using karst sediments: Marine Geology, v. 55, p. 145-161.
Franks, J.W., and Johnson, R.H., 1964, Pollen analytical dating of a Derbyshire landslide: New Phytologist, v. 63, p. 209-216.
Fuller, M.L., 1912, The New Madrid earthquake: U.S. Geological Survey Bulletin 494, 120 p.
Gedney, D.S., and Weber, W.G., Jr., 1978, Design and construction of soil slopes, *in* Schuster, R.L., and Krizek, R.J., eds., Landslides–Analysis and control: Transportation Research Board, National Academy of Sciences, Washington, D.C., Special Report 176, p. 172-191.
Goodman, R.E., and Seed, H.B., 1966, Earthquake-induced displacements in sand embankments: American Society of Civil Engineers, Journal of the Soil Mechanics and Foundations Division, v. 92, no. SM2, p. 125-146.
Hadley, D.M., Hawkins, H.G., and Benuska, K.L., 1983, Strong ground motion record of the 16 September 1978 Tabas, Iran, earthquake: Bulletin of the Seismological Society of America, v. 73, no. 1, p. 315-320.
Hamilton, R.M., and Johnston, A.C., 1990, Tecumseh's prophecy–Preparing for the next New Madrid earthquake: U.S. Geological Survey Circular 1066, 30 p.
Hansen, W.R., 1965, Effects of the earthquake of March 27, 1964, at Anchorage, Alaska: U.S. Geological Survey Professional Paper 542-A, 68 p.
Hanks, T.C., and Johnston, A.C., 1992, Common features of the excitation and propagation of strong ground motion for North American earthquakes: Bulletin of the

Seismological Society of America, v. 82, p. 1-23.
Harp, E.L., and Wilson, R.C., 1989, Shaking intensity thresholds for seismically induced landslides: Geological Society of America Abstracts with Programs, v. 21, no, 5, p. 90.
Heezen, B.C., and Ewing, M., 1952, Turbidity currents and submarine slumps, and the 1929 Grand Banks earthquake: American Journal of Science, v. 250, p. 849-873.
Hempton, M.R., and Dewey, J.F., 1983, Earthquake-induced deformational structures in young lacustrine sediments, East Anatolian Fault, southeast Turkey: Tectonophysics, v. 98, p. T7-T14.
Hunt, C.B., 1975, Death Valley: Geology, Ecology, and Archeology: Berkeley, University of California Press, 234 p.
Hupp, C.R., Osterkamp, W.R., and Thornton, J.L., 1987, Dendrogeomorphic evidence and dating of recent debris flows on Mount Shasta, northern California: U.S. Geological Survey Professional Paper 1396-B, 39 p.
Jacoby, G.C., Williams, P.L., and Buckley, B.M., 1992, Tree ring correlation between prehistoric landslides and abrupt tectonic events in Seattle, Washington: Science, v. 258, p. 1621-1623.
Jahn, A., 1964, Slopes morphological features resulting from gravitation: Zeitschrift für Geomorphologie, supplement 5, p. 59-72.
Jensen, J.M., 1983, The Upper Gros Ventre landslide of Wyoming: A dendrochronology of landslide events and the possible mechanics of failure: Geological Society of America, Abstracts with Programs, v. 15, no. 5, p. 387.
Jibson, R.W., 1985, Landslides caused by the 1811-12 New Madrid earthquakes: Stanford, Calif., Stanford University, Ph.D. dissertation, 232 p.
Jibson, R.W., and Keefer, D.K., 1988, Landslides triggered by earthquakes in the central Mississippi Valley, Tennessee and Kentucky: U.S. Geological Survey Professional Paper 1336-C, 24 p.
Jibson, R.W., and Keefer, D.K., 1989, Statistical analysis of factors affecting landslide distribution in the New Madrid seismic zone, Tennessee and Kentucky: Engineering Geology, v. 27, p. 509-542.
Jibson, R.W., and Keefer, D.K., 1992, Analysis of the seismic origin of a landslide in the New Madrid seismic zone: Seismological Research Letters, v. 63, p. 427-437.
Jibson, R.W., and Keefer, D.K., 1993, Analysis of the seismic origin of landslides–Examples from the New Madrid seismic zone: Geological Society of America Bulletin, v. 105, p. 421-436.
Johnson, R.H., 1987, Dating of ancient, deep-seated landslides in temperate regions, *in* Anderson, M.G., and Richards, K.S., eds., Slope Stability: New York, John Wiley and Sons, p. 561-600.
Jones, G.D.B., and Thompson, F.H., 1965, Excavations at Mam Tor and Brough-en-Noe: Derbyshire Archeological Journal, v. 85, p. 89-93.
Kastens, K.A., 1984, Earthquakes as a triggering mechanism for debris flows and turbidites on the Calabrian ridge: Marine Geology, v. 55, p. 13-33.
Keefer, D.K., 1984, Landslides caused by earthquakes: Geological Society of America Bulletin, v. 95, p. 406-421.

Keefer, D.K., and Wilson, R.C., 1989, Predicting earthquake-induced landslides, with emphasis on arid and semi-arid environments, *in* Sadler, P.M., and Morton, D.M., eds., Landslides in a Semi-Arid Environment: Riverside, Calif., Inland Geological Society, v. 2, p. 118-149.

Knuepfer, P.L.K., 1988, Estimating ages of late Quaternary stream terraces from analysis of weathering rinds and soils: Geological Society of America Bulletin, v. 100, p. 1224-1236.

Lambe, T.W., and Whitman, R.V., 1969, Soil mechanics: New York, John Wiley and Sons, 553 p.

Lee, H.J., and Edwards, B.D., 1986, Regional method to assess offshore slope stability: Journal of Geotechnical Engineering, v. 112, p. 489-509.

Logan, R.L., and Schuster, R.L., 1991, Lakes divided: The origin of Lake Crescent and Lake Sutherland, Clallam County, Washington: Washington Division of Geology and Earth Resources, Washington Geology, v. 19, no. 1, p. 38-42.

Mayer, L., 1984, Dating Quaternary fault scarps in alluvium using morphological parameters: Quaternary Research, v. 22, p. 300-313.

McCalpin, J.P., 1984, Preliminary age classification of landslides for inventory mapping: Engineering Geology and Soils Engineering Symposium, 21st, University of Idaho, Moscow, Idaho, 1984, Proceedings, p. 99-120.

McCalpin, J.P., 1986, Relative dating and age classification of landslides: Association of Engineering Geologists, Abstracts and Program, 29th Annual Meeting, San Francisco, p. 56.

McCalpin, J.P., 1989, Prehistoric earthquake-induced landslides along the Awatere fault, South Island, New Zealand: Association of Engineering Geologists, Abstract and Program, 32nd Annual Meeting, Vail, Colorado, p. 94.

McCalpin, J.P., 1992, Glacial and postglacial geology near Lake Tennyson, Clarence River, New Zealand: New Zealand Journal of Geology and Geophysics, v. 35, p. 201-210.

McCalpin, J.P., and Rice, J.B., Jr., 1987, Spatial and temporal analysis of 1200 landslides in a 900 km^2 area, middle Rocky Mountains: *in* International Conference and Field Workshop on Landslides, 5th, Christchurch, New Zealand, 1987, Proceedings, p. 137-146.

McGee, W.J., 1891, The Lafayette Formation: U.S. Geological Survey 12th Annual Report, pt. 1, p. 387-521.

Morton, D.M., and Sadler, P.M., 1989, Landslides flanking the northeastern Peninsular Ranges and in the San Gorgonio Pass area of southern California, *in* Sadler, P.M., and Morton, D.M., eds., Landslides in a semi-arid environment: Riverside, Calif., Inland Geological Society, v. 2., p. 338-355.

Mutti, E., Lucchi, F.R., Seguret, M., and Zanzucchi, G., 1984, Seismoturbidites: A new group of resedimented deposits: Marine Geology, v. 55, p. 103-116.

Nash, D.B., 1980, Morphological dating of degraded normal fault scarps: Journal of Geology, v. 88, p. 353-360.

Naumann, C.M., and Savigny, K.W., 1992, Large rock avalanches and seismicity in southwestern British Columbia, Canada, *in* Bell, D.H., ed., Landslides (Glissements de terrain), International Symposium, 6th, Christchurch, New Zealand, 1992,

Proceedings: Rotterdam, A.A. Balkema, v. 2, p. 1187-1192.
Newmark, N.M., 1965, Effects of earthquakes on dams and embankments: Geotechnique, v. 15, no. 2, p. 139-160.
Nikonov, A.A., 1988, Reconstruction of the main parameters of old large earthquakes in Soviet Central Asia using the paleoseismogeological method: Tectonophysics, v. 147, p. 297-312.
Nikonov, A.A., and Shebalina, T.Y., 1979, Lichenometry and earthquake age determination in central Asia: Nature, v. 280, p. 675-677.
Nuttli, O.W., 1973, The Mississippi Valley earthquakes of 1811 and 1812: Intensities, ground motion, and magnitudes: Seismological Society of America Bulletin, v. 63, p. 227-248.
Nuttli, O.W., 1983, Average seismic source-parameter relations for mid-plate earthquakes: Bulletin of the Seismological Society of America, v. 73, no. 2, p. 519-535.
Oelfke, J.G., and Butler, D.R., 1985, Lichenometric dating of calcareous landslide deposits, Glacier National Park, Montana: Northwest Geology, v. 17, p. 7-10.
Osterkamp, W.R., and Hupp, C.R., 1987, Dating and interpretation of debris flows by geologic and botanical methods at Whitney Creek Gorge, Mount Shasta, California, *in* Costa, J.E., and Wieczorek, G.F., eds., Debris flows/avalanches: Process, recognition, and mitigation: Geological Society of America, Reviews in Engineering Geology, v. 7, p. 157-164.
Perissoratis, C., Mitropoulos, D., and Angelopoulos, I., 1984, The role of earthquakes in inducing sediment mass movements in the eastern Korinthiakos Gulf. An example from the February 24-March 4, 1981 activity: Marine Geology, v. 55, p. 35-45.
Perrin, N.D., and Hancox, G.T., 1992, Landslide-dammed lakes in New Zealand–Preliminary studies on their distribution, causes and effects, *in* Bell, D.H., ed., Landslides (Glissements de terrain), International Symposium, 6th, Christchurch, New Zealand, 1992, Proceedings: Rotterdam, A.A. Balkema, v. 2, p. 1457-1466.
Potter, P.E., 1955, The petrology and origin of the Lafayette Gravel, part II, geomorphic history: Journal of Geology, v. 63, no. 2, p. 115-132.
Reeder, J.W., 1979, The dating of landslides in Anchorage, Alaska–A case for earthquake-triggered movements: Geological Society of America, Abstracts with Programs, v. 11, no. 7, p. 501.
Schroder, J.F., Jr., 1970, Landslide landforms and the concept of geomorphic age applied to landslides: International Geographic Congress, Commun. no. 21, Selected Papers, v. 1, Physical Geography, p. 124-126.
Schuster, R.L., and Krizek, R.J., eds., 1978, Landslides–Analysis and control: Transportation Research Board, National Academy of Sciences, Washington, D.C., Special Report 176, 234 p.
Schuster, R.L., Logan, R.L., and Pringle, P.T., 1992, Prehistoric rock avalanches in the Olympic Mountains, Washington: Science, v. 258, p. 1620-1621.
Seed, H.B., 1968, Landslides during earthquakes due to soil liquefaction: American Society of Civil Engineers Journal of the Soil Mechanics and Foundations Division, v. 94, p. 1055-1122.
Seed, H.B., 1979, Considerations in the earthquake-resistant design of earth and rockfill

dams: Geotechnique, v. 29, no. 3, p. 215-263.
Seguret, M., Labaume, P., and Madariaga, R., 1984, Eocene seismicity in the Pyrenees from megaturbidites on the South Pyrenean Basin, Spain: Marine Geology, v. 55, p. 117-131.
Seilacher, A., 1969, Fault-graded beds interpreted as seismites: Sedimentology, v. 13, p. 155-159.
Seilacher, A., 1984, Sedimentary structures tentatively attributed to seismic events: Marine Geology, v. 55, p. 1-12.
Siegel, R.A., 1978, STABL user manual: West Lafayette, Indiana, Purdue University, 104 p.
Sims, J.D., 1973, Earthquake-induced structures in sediments of Van Norman Lake, San Fernando, California: Science, v. 182, p. 161-163.
Sims, J.D., 1975, Determining earthquake recurrence intervals from deformational structures in young lacustrine sediments: Tectonophysics, v. 29, p. 141-152.
Small, R.J., and Clark, M.J., 1982, Slopes and weathering: Cambridge, Great Britain, Cambridge University Press, 112 p.
Smirnova, T.Y., and Nikonov, A.A., 1990, A revised lichenometric method and its application dating great past earthquakes: Arctic and Alpine Research, v. 22, p. 375-388.
Solonenko, V.P., 1977, Landslides and collapses in seismic zones and their prediction: Bulletin of the International Association of Engineering Geology, no. 15, p. 4-8.
Spalletta, C., and Vai, G.B., 1984, Upper Devonian intraclast parabreccias interpreted as seismites: Marine Geology, v. 55, p. 133-144.
Stout, M.L., 1969, Radiocarbon dating of landslides in southern California and engineering geology implications, *in* Schumm, S.A., and Bradley, W.C., eds., United States contributions to Quaternary research: Geological Society of America Special Paper 123, p. 167-179.
Stout, M.L., 1977, Radiocarbon dating of landslides in southern California: California Division of Mines and Geology, California Geology, May 1977, p. 99-105.
Tabor, R.W., 1971, Origin of ridge-top depressions by large-scale creep in the Olympic Mountains, Washington: Geological Society of America Bulletin, v. 82, p. 1811-1822.
Tallis, J.H., and Johnson, R.H., 1980, The dating of landslides in Longdendale, north Derbyshire, using pollen-analytical techniques, *in* Cullingford, R.A., Davidson, D.A., and Lewin, J., eds., Timescales in geomorphology: New York, John Wiley and Sons, p. 189-205.
Terasmae, J., 1975, Dating of landslides in the Ottawa River valley by dendrochronology—A brief comment, *in* Yatsu, E., Ward, A.J., and Adams, F., eds., Mass Wasting: Proceedings of the 4th Guelph Symposium on Geomorphology: Norwich, England, GeoAbstracts, p. 153-158.
Varnes, D.J., 1978, Slope movement types and processes, *in* Schuster, R.L., and Krizek, R.J., eds., Landslides—Analysis and control: Transportation Research Board, National Academy of Sciences, Washington, D.C., Special Report 176, p. 11-33.
Varnes, D.J., Radbruch-Hall, D.H., and Savage, W.Z., 1989, Topographic and structural

conditions in areas f gravitational spreading of ridges in the western United States: U.S. Geological Survey Professional Paper 1496, 28 p.

Whitehouse, I.E., and Griffiths, G.A., 1893, Frequency and hazard of large rock avalanches in the central Southern Alps, New Zealand: Geology, v. 11, p. 331-334.

Wieczorek, G.F., 1984, Preparing a detailed landslide-inventory map for hazard evaluation and reduction: Bulletin of the Association of Engineering Geologists, v. 21, p. 337-342.

Wieczorek, G.F., Wilson, R.C., and Harp, E.L., 1985, Map showing slope stability during earthquakes of San Mateo County, California: U.S. Geological Survey Miscellaneous Geologic Investigations Map I-1257E, scale 1:62,500.

Williams, P.L., Jacoby, G.C., and Buckley, B., 1992, Coincident ages of large landslides in Seattle's Lake Washington: Geological Society of America, Abstracts with Programs, v. 24, no. 5, p. 90.

Wilson, R.C., and Keefer, D.K., 1983, Dynamic analysis of a slope failure from the 6 August 1979 Coyote Lake, California, earthquake: Seismological Society of America Bulletin, v. 73, no. 3, p. 863-877.

Wilson, R.C., and Keefer, D.K., 1985, Predicting areal limits of earthquake-induced landsliding, *in* Ziony, J.I., ed., Evaluating earthquake hazards in the Los Angeles region—An earth-science perspective: U.S. Geological Survey Professional Paper 1360, p. 316-345.

Yarnold, J.C., and Lombard, J.P., 1989, A facies model for large rock-avalanche deposits formed in dry climates, *in* Colburn, I.P., Abbott, P.L., and Minch, J., eds., Conglomerates in Basin Analysis: A Symposium Dedicated to A.O. Woodford: Pacific Section, Society of Economic Paleontologists and Mineralogists, v. 62, p. 9-31.

Záruba, Q., and Mencl, V., 1982, Landslides and their control (2d ed.): Amsterdam, Elsevier, 324 p.

TABLE 1. RELATIVE ABUNDANCE OF EARTHQUAKE-INDUCED LANDSLIDES

Abundance	Landslide type
Very abundant	Rock falls
	Disrupted soil slides
	Rock slides
Abundant	Soil lateral spreads
	Soil slumps
	Soil block slides
	Soil avalanches
Moderately common	Soil falls
	Rapid soil flows
	Rock slumps
Uncommon	Subaqueous landslides
	Slow earth flows
	Rock block slides
	Rock avalanches

Note: Data from Keefer (1984). Landslide types use nomenclature of Varnes (1978) and are listed in decreasing order of abundance.

TABLE 2. STATIC FACTORS OF SAFETY FROM STABILITY ANALYSES OF THE STEWART LANDSLIDE IN DRAINED AND UNDRAINED CONDITIONS

Type of Failure Surface	Location of Piezometric Surface: Base of Bluff [1]	Top of Jackson[2] Formation	Top of Lafayette[3] Gravel	Top of Bluff [4]	Most Likely[5]
		Drained Stability Analyses			
Circular	**1.90**	**1.66**	**1.61**	1.35	**1.82**
Irregular	1.95	1.69	1.64	**1.32**	1.87
Wedge, Layer 5	4.06	3.98	3.76	2.83	4.03
Wedge, Layer 6	4.24	4.03	3.80	2.79	4.23
Wedge, Layer 7	2.46	2.28	2.14	1.47	2.45
Wedge, Layer 8	3.81	3.39	3.23	2.51	3.72
Wedge, Layer 9	2.83	2.48	2.38	1.88	2.71
Wedge, Layer 10	2.40	2.10	2.03	1.68	2.25
Actual Surface	1.96	1.73	1.67	1.40	1.88
		Undrained Stability Analyses			
Circular	1.72	1.72	1.64	**1.99**	1.62
Irregular	**1.64**	**1.64**	**1.55**	2.16	**1.53**
Wedge, Layer 5	2.81	2.81	2.50	3.59	2.49
Wedge, Layer 6	3.23	3.23	2.96	3.84	2.93
Wedge, Layer 7	2.19	2.19	1.99	2.81	1.97
Wedge, Layer 8	3.18	3.18	3.05	3.57	3.02
Wedge, Layer 9	2.00	2.00	1.89	2.41	1.87
Wedge, Layer 10	1.99	1.99	1.88	2.25	1.87
Actual Surface	1.74	1.74	1.66	2.12	1.65

Note: Most critical surface for each ground-water condition shown in **bold** type.

[1] Figure 4B, piezometric surface 4
[2] Figure 4B, piezometric surface 3
[3] Figure 4B, piezometric surface 2
[4] Figure 4B, piezometric surface 1
[5] Figure 4A

TABLE 3. STRONG-MOTION RECORDS USED TO MODEL GROUND SHAKING FROM THE 1811-12 EARTHQUAKES AT THE STEWART LANDSLIDE

Earthquake Recording site, component	M	R (km)	$\hat{a}$ (g)	T (s)	$I_a D_N$ (m/s)(cm)
16 Dec 1881 New Madrid, Mo., Stewart landslide site (estimated)	8.2	68	0.39	20-40	2.7* 2.7-5.5†
•15 Oct 1979 Imperial Valley, Calif., El Centro differential array, 360°	6.5	7	0.49	6.6	2.16-8
•24 Nov 1987 Superstition Hills, Calif., Superstition Mountain site 8, 135°	6.5	6	0.90	12.2	6.823-25
23 January 1812 New Madrid, Mo., Stewart landslide site (estimated)	8.1	24	0.74	18-40	17.4* 8.9-19.7†
•9 Feb 1971 San Fernando, Calif., Pacoima Dam, 164°	6.6	3	1.22	6.7	9.150-55
•16 Sep 1978 Tabas, Iran, 74°	7.4	3	0.71	16.1	10.039-44
7 Feb 1812 New Madrid, Mo., Stewart landslide site (estimated)	8.3	44	0.71	25-40	8.2* 11.3-18.1†
•24 Nov 1987 Superstition Hills, Calif., Superstition Mountain site 8, 135°	6.5	6	0.90	12.2	6.823-25
•16 Sep 1978 Tabas, Iran, 74°	7.4	3	0.71	16.1	10.039-44

Note: Characteristics of the 1811-12 earthquakes estimated as described in text. All strong-motion records are from U.S. Geological Survey recording stations except for the Tabas, Iran, record (Hadley and others 1983). **M** is moment magnitude (estimates for the 1811-12 earthquakes from Hamilton and Johnston, 1990); R is earthquake source distance; $\hat{a}$ is peak ground acceleration; T is duration of strong shaking as defined by Dobry and others (1978); I_a is Arias (1970) intensity; D_N is Newmark (1965) displacement (range shown covers range of critical accelerations discussed in text).

*Estimated using Equation 4 of Jibson and Keefer (1992).
†Estimated using Equation 5 of Jibson and Keefer (1992).

TABLE 4. MINIMUM EARTHQUAKE MAGNITUDES REQUIRED TO TRIGGER LANDSLIDES

Earthquake Magnitude	Type of landslide
4.0	Rock falls, rock slides, soil falls, disrupted soil slides
4.5	Soil slumps, soil block slides
5.0	Rock slumps, rock block slides, slow earth flows, soil lateral spreads, rapid soil flows, subaqueous landslides
6.0	Rock avalanches
6.5	Soil avalanches

Note: Data from Keefer (1984).

TABLE 5. MINIMUM MODIFIED MERCALLI INTENSITY REQUIRED TO TRIGGER LANDSLIDES

Landslide Type	Lowest Modified Mercalli Intensity	Predominant Modified Mercalli Intensity
Disrupted slides and falls	IV	VI
Coherent slides	V	VII
Lateral spreads and flows	V	VII

Note: Data from Keefer (1984).

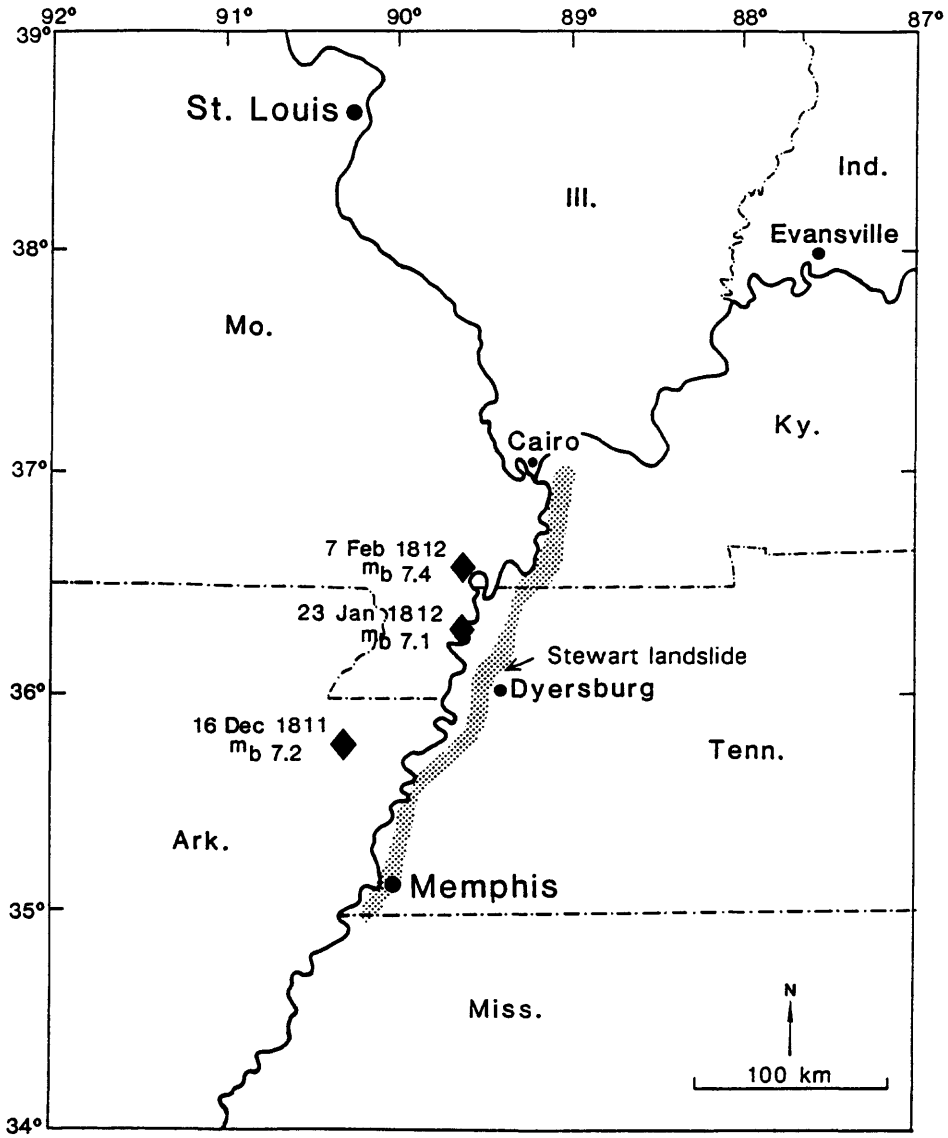

Figure 1. Map showing estimated epicenters (diamonds), dates, and body-wave magnitudes (m_b) of the three largest earthquakes in the 1811-12 New Madrid sequence (from Nuttli, 1973); bluffs (shaded) containing landslides triggered in 1811-12; and the location of the Stewart landslide.

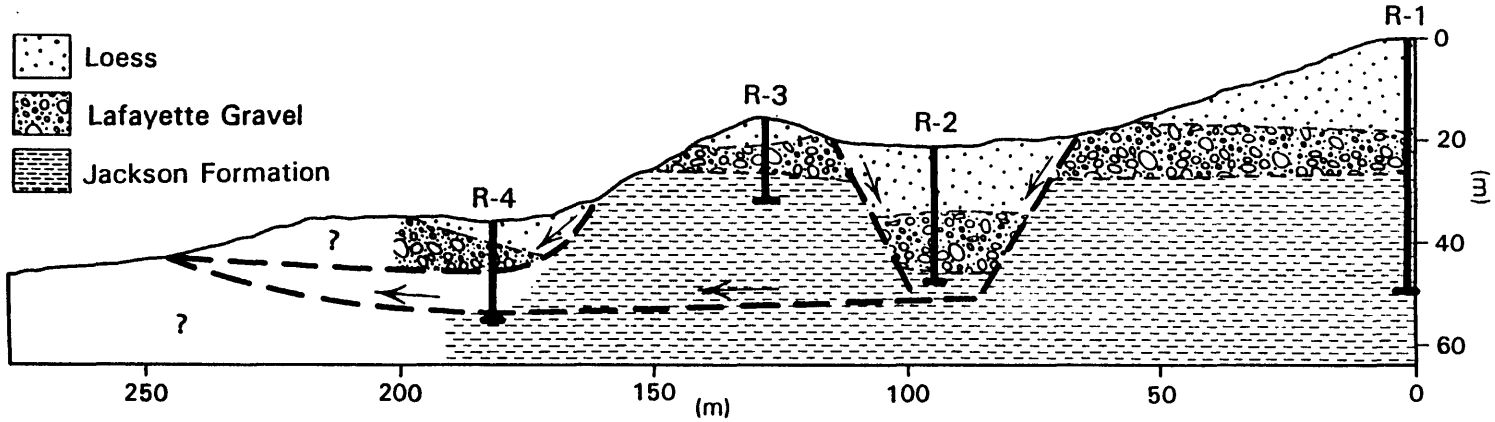

Figure 2. Cross section of Stewart landslide showing subsurface stratigraphy (identified from drill holes designated R-1 through R-4) and diagrammatic representation of failure surfaces. Undisturbed stratigraphy is shown at R-1.

Layer	Unit Weight (kN/m^3)	Drained Friction Angle	Drained Cohesion (kPa)
1	19.3	34°	0.25
2	19.6	35°	0.50
3	19.8	30°	0.43
4	22.0	32°	0.32
5	18.1	15°	2.06
6	18.1	20°	1.81
7	17.3	12°	0.71
8	18.1	20°	2.27
9	18.1	15°	2.06
10	18.1	12°	2.52

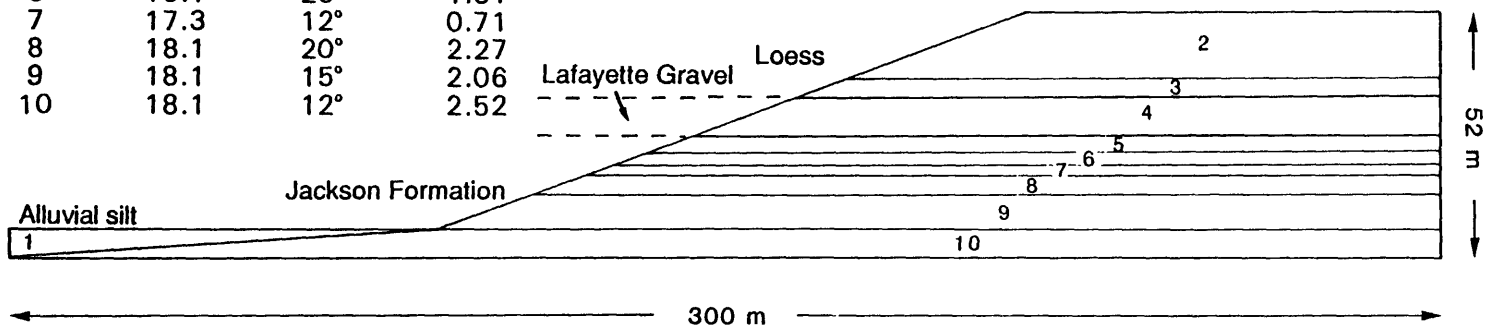

Figure 3. Idealized model of pre-landslide bluff at Stewart site in drained conditions. Soil properties are shown for each designated layer in the computer model.

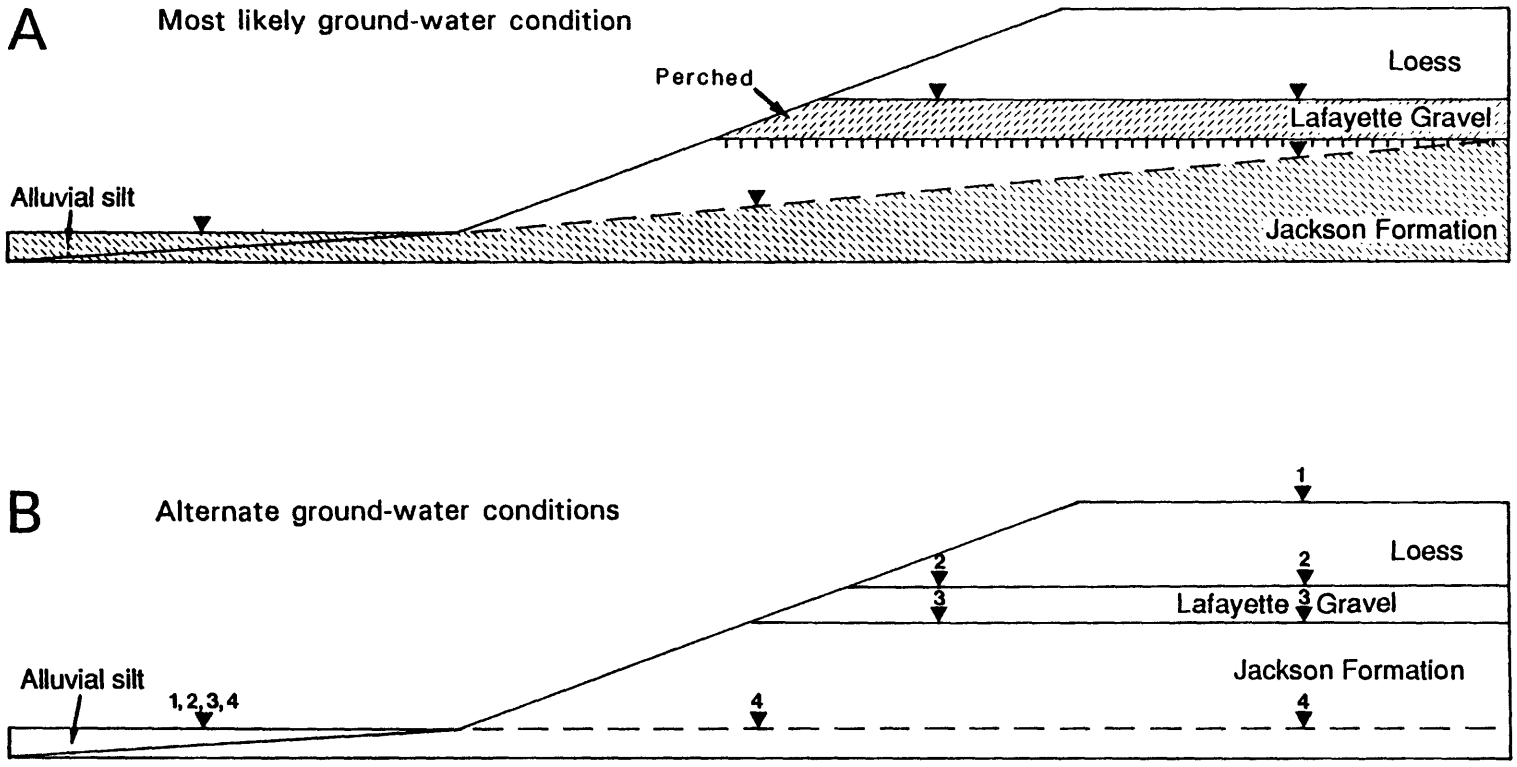

Figure 4. Ground-water conditions modeled in the slope-stability analyses. (A) Most likely ground-water condition; saturated zones are shown by cross-hatched pattern. (B) Piezometric surfaces of four alternate ground-water conditions are shown by inverted triangles numbered 1-4.

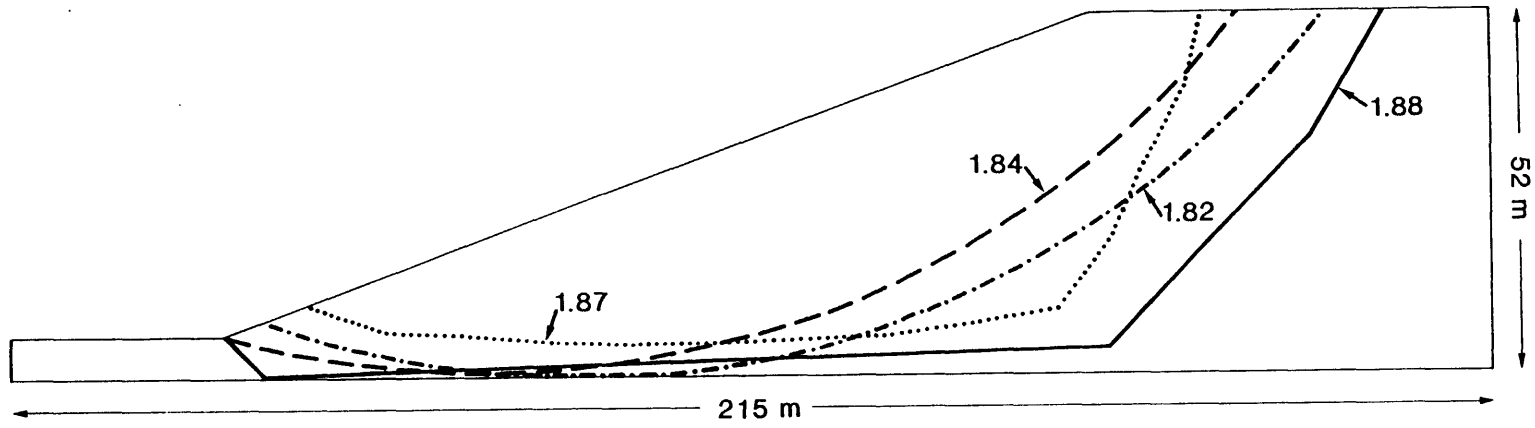

Figure 5. The three most critical slip surfaces and their factors of safety (FS=1.82, 1.84, 1.87) for static, drained conditions at the Stewart site in the most likely ground-water condition. Heavy, solid line shows location of actual failure surface (FS=1.88).

Layer	Unit Weight (kN/m^3)	Undrained Shear Strength (kPa)
1	19.3	8.41
2	19.6	4.63
3	19.6	16.01
4	19.6	4.63
5	22.0	3.93
6	22.0	4.46
7	18.1	2.54
8	18.1	3.58
9	17.3	2.42
10	18.1	5.04
11	18.1	3.17
12	18.1	3.78
13	18.1	4.38

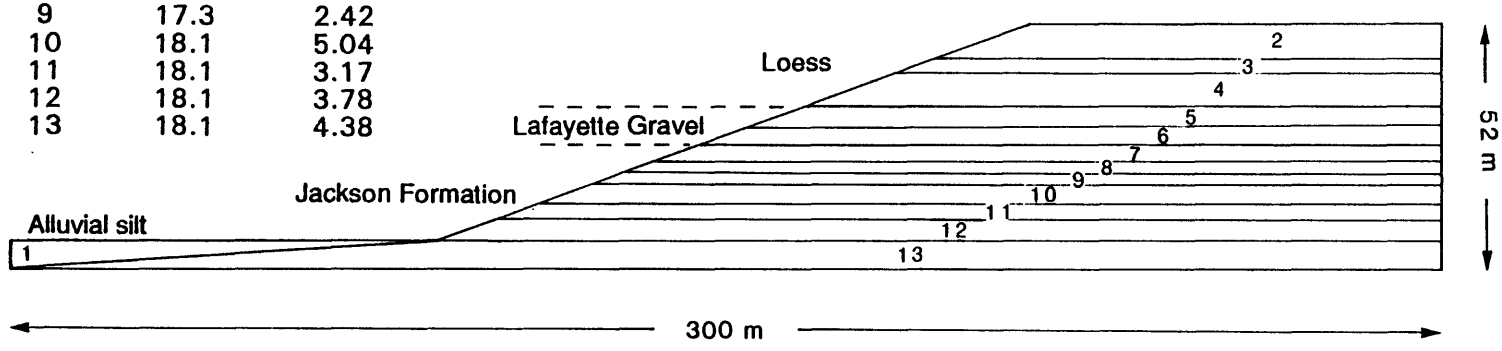

Figure 6. Idealized model of pre-landslide bluff at Stewart site in undrained conditions. Soil properties are shown for each designated layer in the computer model.

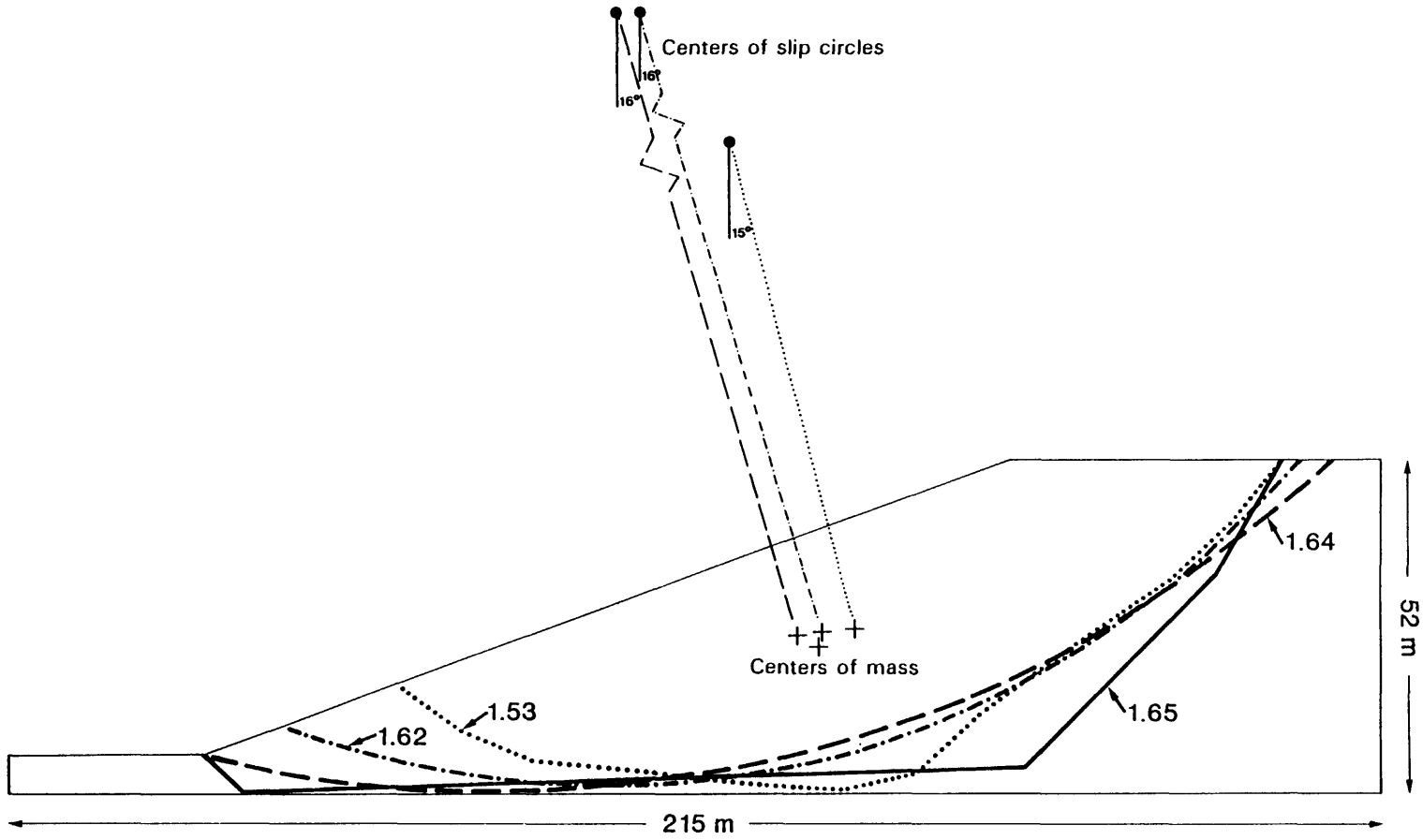

Figure 7. The three most critical slip surfaces and their factors of safety (FS=1.53, 1.62, 1.64) for static, undrained conditions at the Stewart site in the most likely ground-water condition. Heavy, solid line shows location of actual failure surface (FS=1.65). Geometric construction to determine thrust angle also shown.

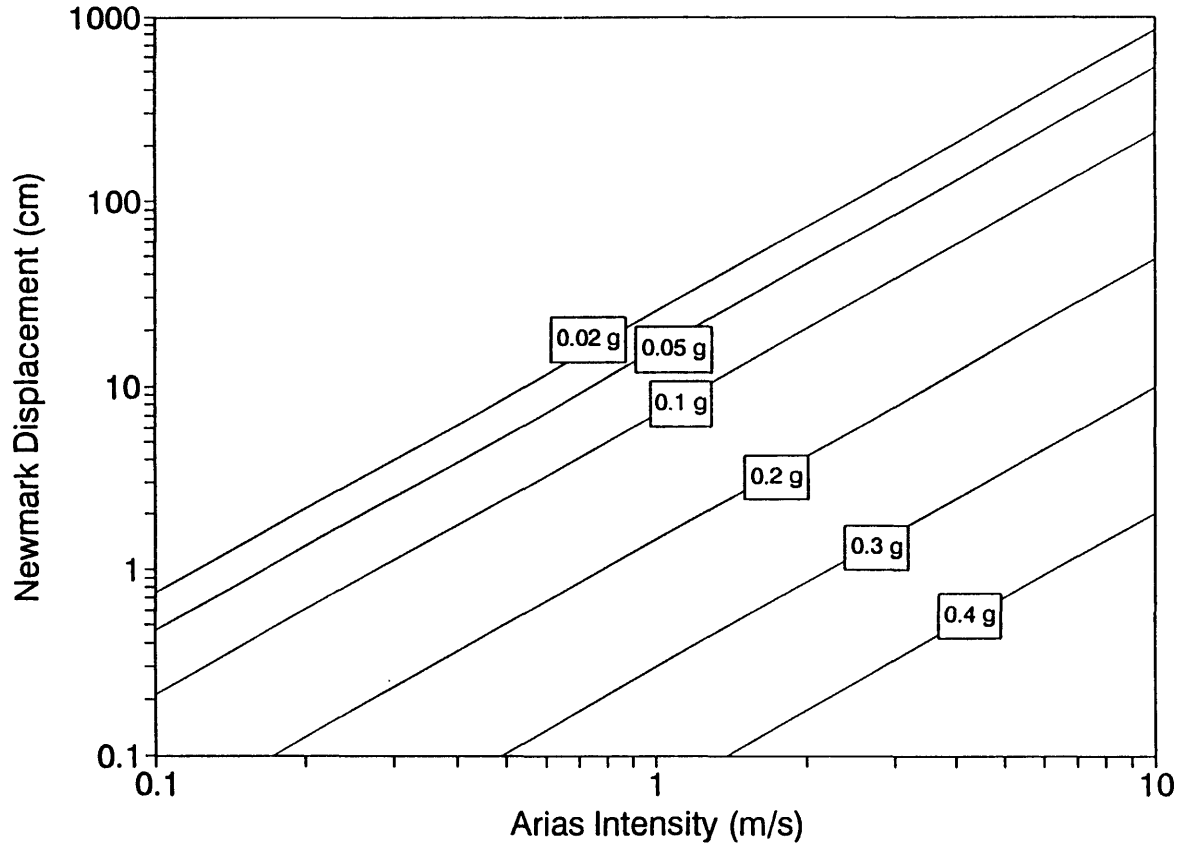

Figure 8. Newmark displacement as a function of Arias intensity for several values of critical acceleration, as predicted by Equation 4.

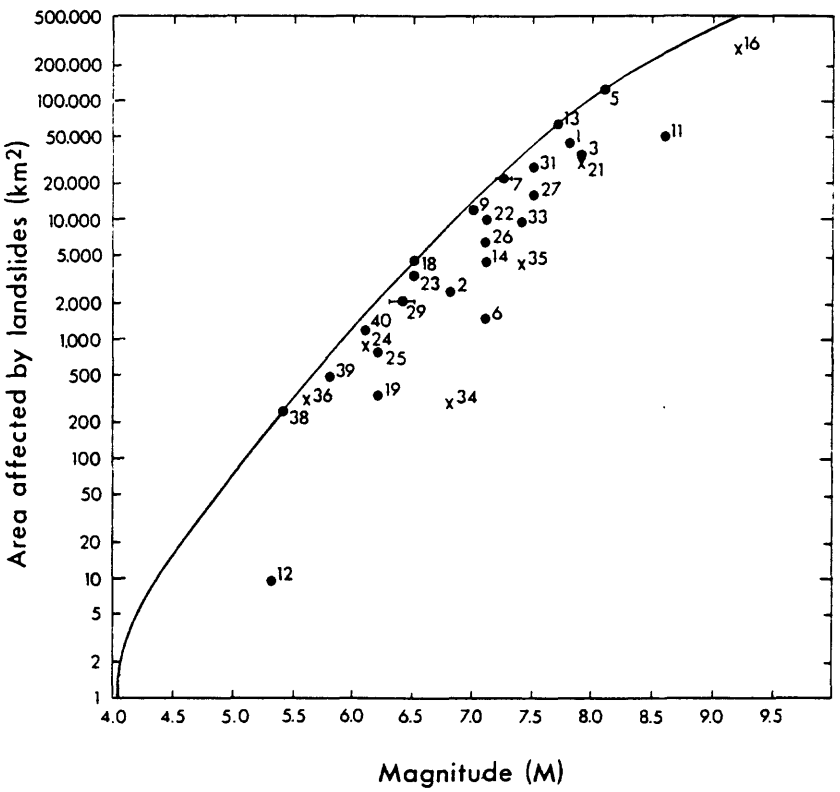

Figure 9. Area affected by landslides in earthquakes having different (generally M_S) magnitudes (from Keefer, 1984). Solid line is upper bound; dashed line is best-fit regression line; numbers beside data points refer to earthquakes analyzed by Keefer (1984); dot denotes onshore earthquake; × denotes offshore earthquake.

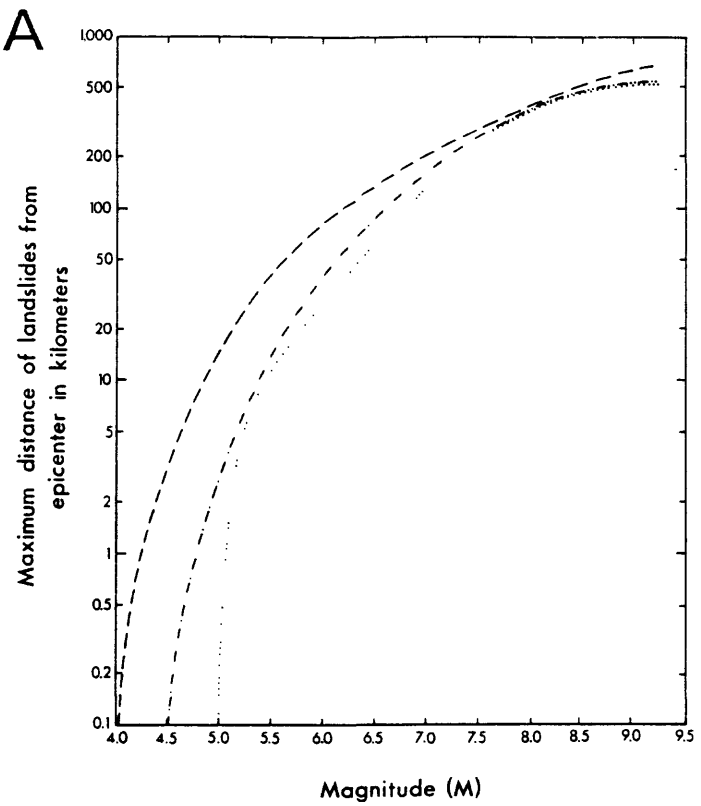

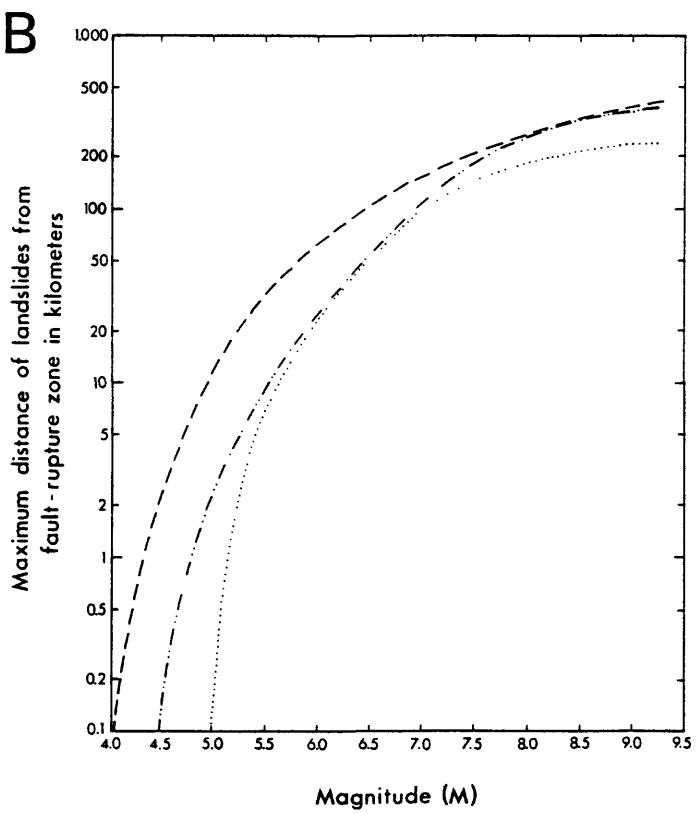

Figure 10. Maximum distance to landslides from (A) epicenter and (B) fault-rupture zone for earthquakes of different magnitudes (from Keefer, 1984). Dashed line is upper bound for disrupted slides and falls; dash-double-dot line is upper bound for coherent slides; and dotted line is upper bound for lateral spreads and flows.